uOttawa

L'Université canadienne
Canada's university

FACULTÉ DES ÉTUDES SUPÉRIEURES ET POSTOCTORALES

uOttawa

L'Université canadienne
Canada's university

FACULTY OF GRADUATE AND POSDOCTORAL STUDIES

Nathalie Lavoie

AUTEUR DE LA THÈSE / AUTHOR OF THESIS

Ph.D. (Chemistry)

GRADE / DEGREE

Department of Chemistry

FACULTÉ, ÉCOLE, DÉPARTEMENT / FACULTY, SCHOOL, DEPARTMENT

Didubstituted 1,8 – Diaminonaphthalene as Supporting Ligands for High Oxidation State Early Transition Metal and Lanthanide Complexes

TITRE DE LA THÈSE / TITLE OF THESIS

Darrin Richeson

DIRECTEUR (DIRECTRICE) DE LA THÈSE / THESIS SUPERVISOR

CO-DIRECTEUR (CO-DIRECTRICE) DE LA THÈSE / THESIS CO-SUPERVISOR

Sean Barry	Sandro Gambarotta
Muralee Muguresu	John Protasiewicz (Case Western Reserve Uuniverity)

Gary W. Slater

Le Doyen de la Faculté des études supérieures et postdoctorales / Dean of the Faculty of Graduate and Postdoctoral Studies

Disubstituted 1,8-Diaminonaphthalene as Supporting Ligands For High Oxidation State Early Transition Metal and Lanthanide Complexes

Nathalie Lavoie

Thesis submitted to the

Faculty of Graduate and Postdoctoral Studies

In partial fulfillment of the requirements for the degree of

Doctorate in Philosophy

In

Chemistry

Ottawa-Carleton Chemistry Institute

University Of Ottawa

Candidate

Nathalie Lavoie

Supervisor

Professor Darrin Richeson

Your file Votre référence
ISBN: 978-0-494-65578-8
Our file Notre référence
ISBN: 978-0-494-65578-8

Dédié à mes parents

Pour votre support constant tout au long de ma vie.

Pour m'avoir transmit les valeurs importantes pour réussir dans la vie

Vous avez toujours été la pour moi et pour cela je vous serais toujours reconnaissante.

Acknowledgements

First and foremost I would like to acknowledge my supervisor for all of his support and encouragement. Darrin's positive attitude is always contagious and makes working in is lab enjoyable. Without your support and many discussions over the last few years this work would not be what it is.

I would also like to thank all the professors that I have taught me the basics of science during my stay at the University of Ottawa. The administration team and supporting staff who have also been very helpful when I had questions.

I would also like to acknowledge all the crystallographers I have had a chance to work with; Ilia Krobokov, Tara Kell and Glen Yap. Glenn Facey has also been a great help with all the NMR questions I have had over the last few years. Serge Gorelsky for his help with all the computational work.

I would also like to thank all the past people from the Richeson group, Heather Spinney, Gan Ong and Patrick Bazinet you have shown me a lot during the time we worked together. I would also like to thank all other members of the Richeson lab that I had a chance to work with over the past few years. Ian and Jess for all your help in mounting crystals. Titel, Dominique, Ahmed and all undergraduate students that have worked in our lab it was a pleasure to work with you.

To all my friends and family that have always been there to support me and encourage me when times got difficult. The times we have spent together during the past few years has been very important to me.

Last but not least I would like to thank my fiancé Francois your presence in my life has been very important to me. You have been there for me during the good times and the hard ones. Without your support and encouragement this work would have been more difficult to complete.

Abstract

This work was launched to study the chemistry of disubstituted 1,8-diaminonaphthalene (R_2DAN) as a supporting framework for carbene centers, high oxidation state early transition metals and lanthanide centers. R_2DAN ligands are dianionic bidentate groups making them good candidates to stabilize high oxidation state complexes. This work focuses on the preparation of early transition metal (Ti, Zr, Hf, Ta, W) and lanthanide complexes. This framework for the preparation of bridging carbenes is also presented.

Chapter 1 gives an introduction on ligands found in the literatutre and the importance on amido ligands in catalysis. The second chapter focusses on the use of the disubstituted 1, 8-damiononaphthalene framework in the preparation of bridging carbenes. A dimerization study of a mono carbene is also presented. The third chapter explores the use of the R_2DAN ligand to support lanthanide centers. The synthesis of these species and their structural features these complexes are discussed. In the fourth chapter the preparation of group IV complexes bearing R_2DAN ligands is presented. A few different approaches to introduce the ligand to a metal centers are outlined and discussed. The influence of the nitrogen substituent on the structure of the complexes is also disscused. Chapter 5 presents the synthesis of tantalum complexes bearing R_2DAN ligands along with a structural study of these compounds. A computational study of the structural features of these complexes is presented. The last section of chapter 5 describes the reactivity of the tantalum complexes towards $LiNMe_2$ and MeLi. In Chapter 6 the synthesis of tungsten bis(imido) complexes bearing R_2DAN ligands is presented. The fold of the ligands in these complexes is explored using computational chemistry. The reactivity of the tungsten complexes with heterocumelenes and trimethyl aluminum is discussed. The final section of chapter 6 shows the potential of the tungsten complexes as catalysts for cyclotrimerization of isocyanates. Chapter 7 summarizes the work presented in this thesis.

Contents

List of Common Abbreviation

1. Chemicals and Ligands

Ar	Aromatic group
Cp	Cyclopentadienyl, C_5H_5
Cp*	Pentamethyl Cyclopentadienyl, C_5Me_5
R_2DAN or DAN	1,8-diaminonaphthalene, 1,8-$(NH_2)_2C_{10}H_6$
DAB	Diaminobenzene
E	Element
Et	Ethyl
^{i}Pr	*iso*-propyl
L	Ligand
Ln	Lanthanide
M	Central atom (usually a metal) in compound
Me	Methyl
NHC	N-heterocyclic carbene
BuLi	Butyl lithium
PDA	o-phenylenediamine, 1,2-$(NH_2)_2C_6H_4$
Ph	Phenyl, C_6H_5
py	pyridine
R	alkyl or aryl group
^{t}Bu	t-butyl
THF	tetrahydrofuran
X	Halogen

2. Miscellaneous

Å	Angstrom unit, 10^{-10}m
Hz	Hertz
NMR	Nuclear magnetic resonance
ppm	Parts per million

List of Figures

List of Tables

Chapter 1

Introduction

Catalysis is one of the most important field in chemistry. With all the concerns in today's world about energy usage and protection of the environment the reduction of waste and conservation of energy have become major concerns for industry. For these reasons considerable efforts have been put into designing new catalysts that will facilitate atom economical transformations in a short amount of time and with the smallest possible amount of energy. Metal based catalysts have become very important to attain these goals. Early and late transition metals complexes have become commonly used for organic transformations and in polymerization reactions.

Ligands

One of the important components of a catalyst is the ancillary ligand. These ligands support the catalyst center during the catalytic transformation and they can become very important in determining the product that will be obtained. Ancillary ligands need to be sturdy and must provide appropriate steric protection to the metal center. The role of the ligand in catalysis is not always clear and the reason why one ligand is better than another is sometimes not obvious. For these reasons ligand design is still a very active area of research. No ligand is the best for every reaction and this is why the design of ligands with different structural and electronic properties is necessary.

A good ligand needs to be a good Lewis base to allow the donation of electrons to the metal center to form strong bonds. A ligand must be unreactive towards reagents to minimize side reactions during catalysis. Variability in a ligand can also be important for tuning of a catalyst. Some ligands that are common in the literature are: carbon monoxide (CO), olefins and phosphines. CO is an intermediate σ donor but a great π acceptor making it a great ligand for lower oxidation state metals. One of the down falls of the CO ligand is a lack of variability thus it can't be tuned to improve a catalyst.

Phosphines have also been used extensively as ligands. Phosphines are Lewis bases and can also be strong π acids depending on the R group in the PR_3 ligand. The main features that make phosphine attractive as a ligand is the fact that the sterics and electronic properties of phosphine ligands can be changed by varying the R groups. Phosphines can also be part of more elaborate ligand by linking the phosphine to other moiety.

Olefins are also important ligands they can be σ donor and π acids like CO but like phosphines they can be part of a more elaborate ligand. The most common olefin ligands are probably dienes such as 1,5-cyclooctadiene (COD) and cyclopentadienyl anion (Cp). The cyclopentadiene ligand can form π complexes when more than one of the carbons is bound to the metal or σ complexes when only one of the carbons binds to the metal. Cp ligand can be tuned by replacing the hydrogen on the ring with other substituents such as methyl groups the give the well established Cp*. Cp ligands can also be bridged to give more elaborate ligands.[1]

Amido ligands

During the last decade the use of non cyclopentadiene ligands has dramatically increased. One of the common replacements for the Cp ligands are amido ligands. Amido ligands are widespread in the literature.[2] Figure1.1 shows just a few examples of ligands that have appeared in the literature in the last decade. The variability of amido ligands is tremendous due to their nitrogen substituents.

Figure 1.1 Bis(Amido) ligands

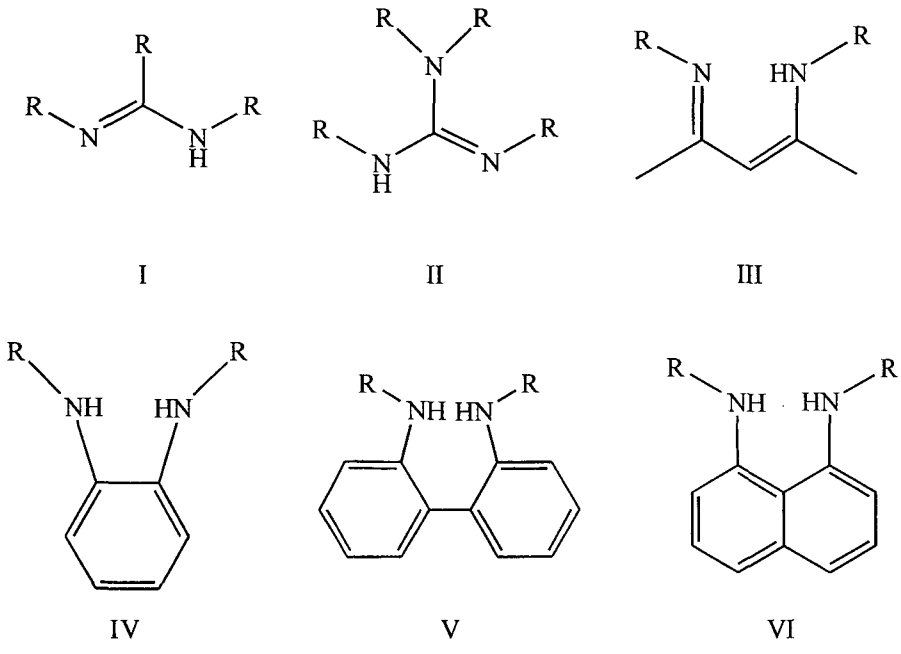

The nitrogen substituents can give steric protection and can also give different electronic properties. The amido substituents can be bridging units that make the ligands bidentate. The bridging unit can also make the ligands versatile by making them rigid or flexible depending on what is needed. The degree of influence of the nitrogen substituents can also depend on the ring size that is formed when bridging ligands coordinate to a metal center. Amido ligands are strong σ and π electron donors (Figure 1.2) consequently they can make strong bonds to the metal.

Figure 1.2 Sigma and pi Orbitals for Amido Ligands

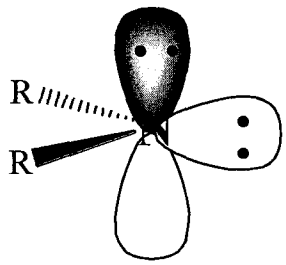

Ligands I, II and III are monoionic ligands just like Cp ligands while IV, V and VI are all dianionic and can replace the Cp ligands in a bis(Cp) systems. The dianionic system can also be more practical to access higher oxidation state metal complexes. The amido ligands presented in Figure 1.1 are all chelating ligands which means they have a greater potential to form strong ligand metal interaction than simple CO and phosphine ligands due to the chelate effect. These ligand all have a π-delocalized system in their backbone making them more stable ligands. The sterics and electronics of all of these ligands can be tuned by changing the R substituents on the nitrogen. One of the main differences between the ligands is the ring size that is form when they are chelating a metal. The size of the ring varies from four membered ring for ligands I and II up to seven membered ring for V. Increasing the ring size will bring the nitrogen substituents closer the metal increasing their steric impact.

Amidinate (I) and guanidate (II) ligands have been extensively studied by our group, Hessen, Jones, Lawrence and many other groups.[3] Both ligands form four-membered rings when chelating a metal and have been employed in main group and transition metal chemistry. β-Diketiminate ligands (III) (NacNac) have received tremendous attention in the last decade replacing its better know predecessor β-diketonato

ligands (Figure 1.3 (**A**)) that is less versatile due to the lack of substituents on the oxygen. These species have been studied by a number of groups as supporting ligands for early transition metals.[4] Lappert and Shen have used them as a supporting ligand for lanthanide complexes.[5] This monoanionic ligand forms a six-membered ring when chelating a metal.

Figure 1.3 β-diketonato (A) and β-diketiminate (B) ligands

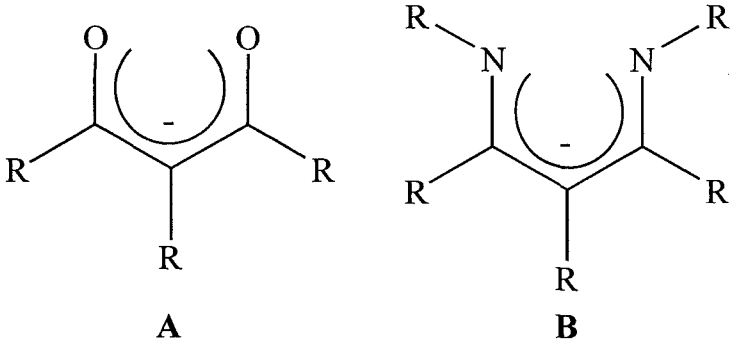

Bis(triisopropylsilyl)-*o*-phenylenediamido (IV) ligands have been employed in group 4[6]and 5[6,7] chemistry by Tilley and others. The diamino benzene ligand (DAB) is dianionic and processes silyl groups as nitrogen substituents making them less variable than the alkyl and aryl groups found in other ligands. This ligand forms a five-membered ring when chelating to a metal center and is often distorted in complexes.

Ligand V has been extensively explored by the Tilley in the stabilization of lanthanide and transition metal complexes.[8] This dianionic ligand forms a seven-membered ring when chelating a metal center bringing the nitrogen substituents close to the metal center leading to a increased steric impact. This ligand once again processes silyl groups as nitrogen substituents making it less tunable than other ligands such as are 1,8-disubstituted diaminonaphthalene (VI) ligand.

Naphthalene Based igands

N,N'-disilylated 1,8-diaminonaphthalene ligands (Figure 1.4) have also been employed as a supporting ligand.[9] This ligand resembles are 1,8-disubstituted diaminonaphthalene (R_2DAN) but is slightly less versatile.

Figure 1.4. N,N'-disilylated 1,8-diaminonaphthalene ligands

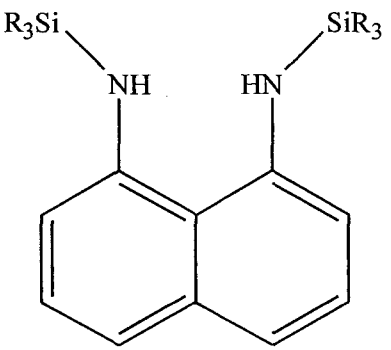

R= Me, ^{i}Pr, ^{t}BuMe$_2$

It possesses the same rigid backbone and is dianionic just like our R_2DAN ligand. The nitrogen substituents are alkylsilyl groups consequently the electronics and sterics can not be tuned as well as with the aryl and alkyl group in the R_2DAN ligands. The limitation with the nitrogen substituents means that the structural features of this ligand in metal complexes might not be the same as in R_2DAN complexes.

Among the goals of this thesis was the stabilization of high oxidation state early transition metals and lanthanide complexes and to study their structures. Ligand VI is a 1,8-disubstituted diaminonaphthalene ligand that has been prepared in the Richeson[10] lab. This ligand possesses a rigid backbone with a delocalized π-system. The nitrogen substituents

can be varied to change the electronic but most of all the sterics of the ligand. The rigid backbone is used in hopes of obtaining specific structures to give more control for the steric impact of the nitrogen subtituents. The increased steric protection provided by the nitrogen substituents can become important for the protection of the chelated metal center. The 1,8-disubstituted diaminonaphthalene structure resembles the β-diketiminate ligands. When chelating to a metal center both ligands form a six-membered ring but the naphthalene rigid backbones eliminates the potential reactivity that has been reported in β-diketiminate ligands.[11] But the most important difference between these two ligands is the anionic charge, the R_2DAN ligands are dianionic this makes them better candidates to support high oxidation state complexes.

The success that has been achieved with β-diketiminate ligands is one of the motivations the lead use to the design of the disubstituted diaminonaphthalene ligands. Their similarity motivated us to use computational methods to compare the topology/shape and relative energies of the ligand orbitals. The frontier molecular orbitals for the R_2DAN^{2-} ligand shown on the left in Figure 1.5, are very similar to the β-diketiminate orbitals shown on the right. The major difference between these ligands is the occupancy of the orbitals. The diaminonaphthalene ligand being a dianionic ligand means that an additional MO is filled and the HOMO of the R_2DAN system correlates with the LUMO of the β-diketiminate ligand. The increase charge for the R_2DAN ligands will make them a stronger donor hopefully leading to a better stabilizer of high oxidation state complexes. In the NacNac ligand we can see that the LUMO and the HOMO are π-type orbitals this is also true for the HOMO and HOMO-1 for the R_2DAN ligand. The HOMO-1 and HOMO-2 for the NacNac ligand and the HOMO-2 and HOMO-3 for the R_2DAN ligand represent σ

oribtals. The similarity of these orbitals lead us to believe that the R_2DAN ligand might interact with metal centers in a similar way as the NacNac ligands.

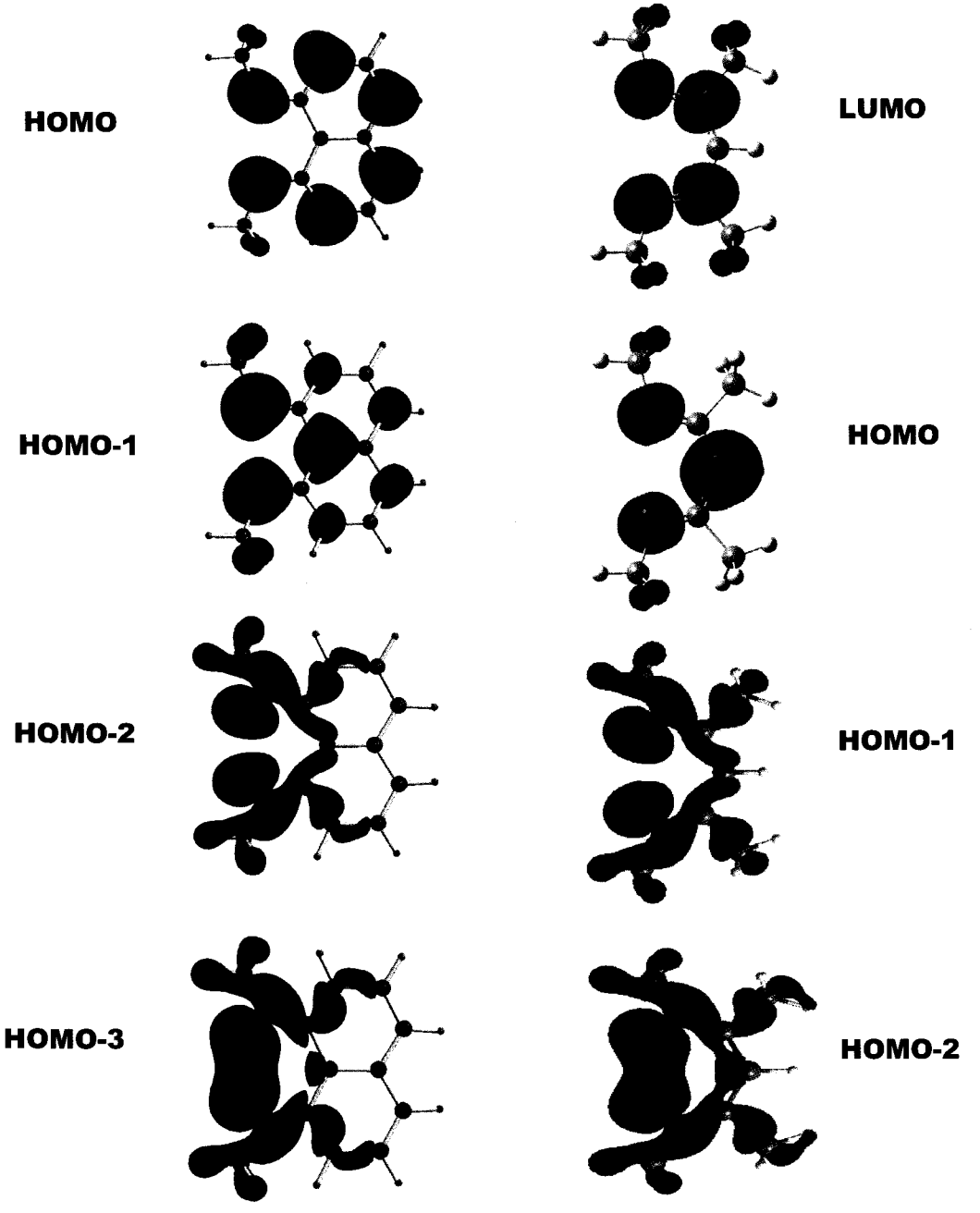

Figure 1.5 Frontier Orbitals of R_2DAN and β-diketiminate

Metal complexes

High oxidation state complexes are important in catalysis and for small molecule transformations. The structures of a catalyst can dictate the products obtained during catalytic transformations. The structure of a complex is dictated by its interaction with the ligands. R_2DAN ligands and other dianionic ligands have been known to distort from their typical planar configuration to modify the donation from the ligand to the metal. NacNac ligands are known to fold along the axis defined by the two nitrogens to permit the interaction if the NacNac backbone with the metal center (Figure 1.6)[5a] giving a η^5 ligand instead of the expected η^2.

Figure 1.6 Bent β-diketiminate complex

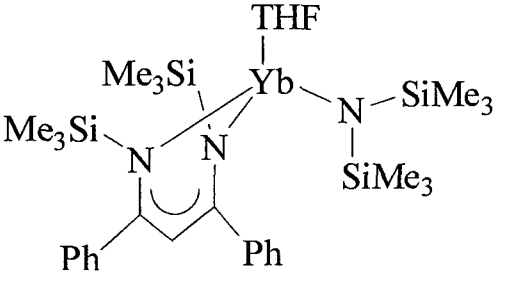

Other example of bent NacNac complexes describe the ligand as being a shallow boat configuration[12] but no detailed explanation of the cause of this distortion has been given in the literature.

Similar distortions have also been observed for diamino benzene ligands. Two examples are shown in Figure 1.7.[13] A rational for the observed orientation of the diamidobenzene ligand in the tungsten imido complex (**A**) is that the folding permits a weak coordination of the phenyl ring of the ligand to the metal center.[13] The second

example is a molybdenum complex (**B**) bearing the same ligand.[14] In this example the folding of the ligands occurs because the π donation of the diamide ligands into the metal d_{xy} orbital is not possible because it is already occupied. The folding reduces the repulsion between the electrons in the metal's orbital and the diamide lone pairs.

Figure 1.7 Bent Diamino Benzene Ligand

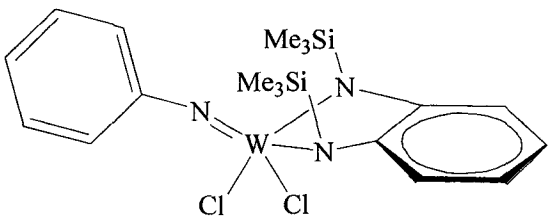

A

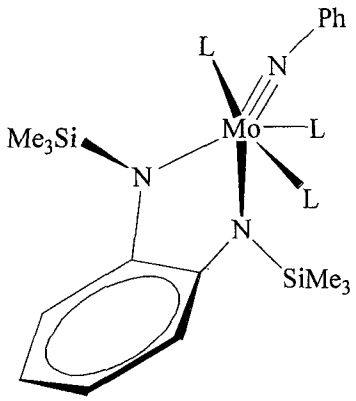

B

The disubstituted 1,8-diaminonaphthalene ligands have also shown some flexibility and Figure 1.8[15] shows a few examples of complexes synthesized in our lab. The germylene and carbene species both have very planar ligands but the ligand in the stannylene is distorted with the Sn(II) center laying out of the backbone plane. This distortion was attributed to the intermolecular interaction between the Sn center and the π-electron of a adjacent naphthalene ring.

Figure 1. 8 Complexes bearing 1,8-disubstituted diaminonaphthalene ligands

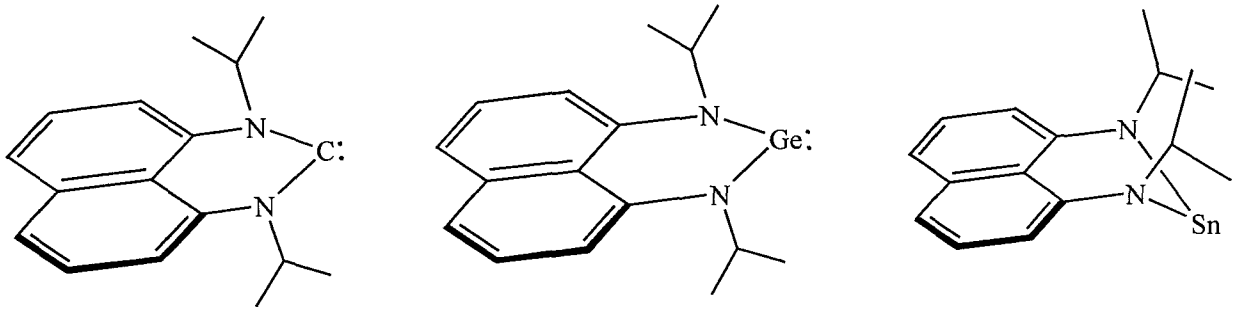

Although many examples of distorted diamido ligands exist, explanations for the distortion are often not given or are very vague. One of our goals was to determine and study the reason for the distortions in such ligands. We did this using DFT calculations with the help of Dr. Serge Gorelsky.

Ligand Preparation

Disubstituted 1,8-diaminonaphthalene ligands can be prepared using methods developed in our lab.[10] The first method is summarized in Scheme 1.1 and begins with the reaction of 1,8-diaminonaphthalene with a ketone to obtain **I**. This compound can then be reduced with $LiAlH_4$ to give the monoalkyl-1,8-DAN. The first two steps can then be repeated to introduce a second alkyl group to give the desired ligand (IV).

Scheme 1.1

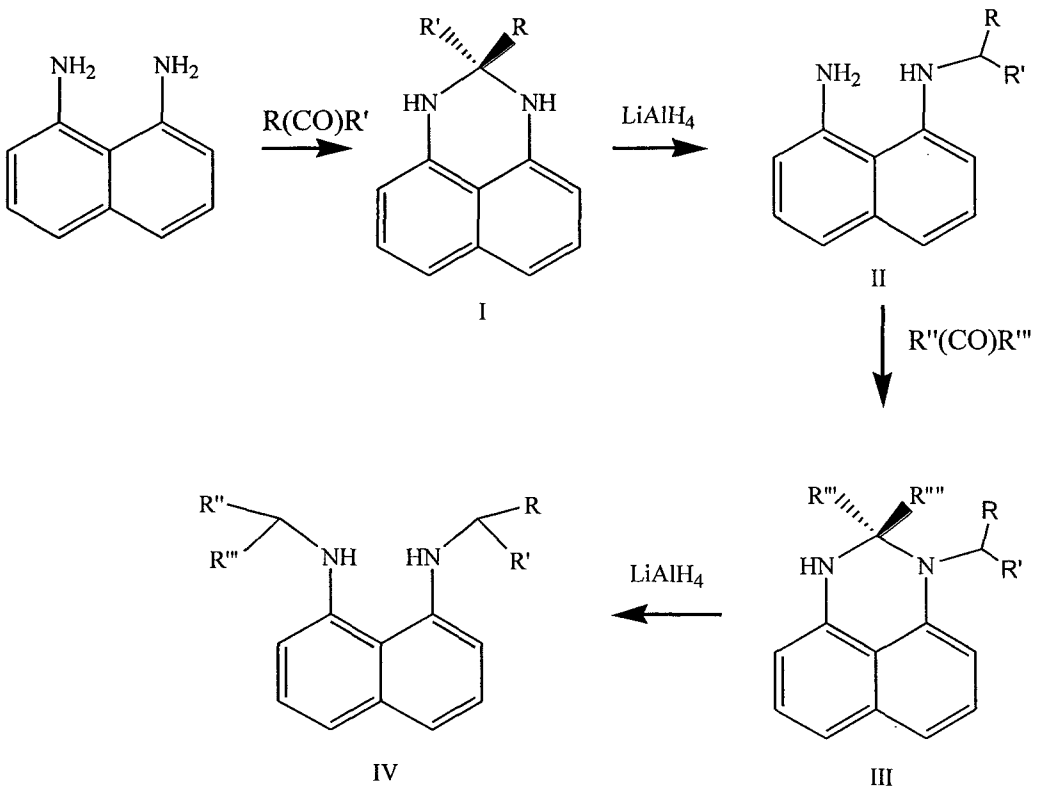

A different method used to introduce aromatic nitrogen substituents was also developed in our lab.[10] The first step of this synthesis is the reaction of 1,8-diaminonaphthalene with diphenylcarbonate to produce 1H,3H-perimidin-2-one. Subsequent reaction of the perimidinone with an aryl iodide was carried out in diphenylether in the presence of a catalyst mixture of CuI, K_2CO_3, N,N'-dicyclohexylethane-1,2-diamine to introduce the aryl groups. This product was then allowed to react with 4 equiv of $NaNH_2$ to produce the desired ligand.

Scheme 1.2

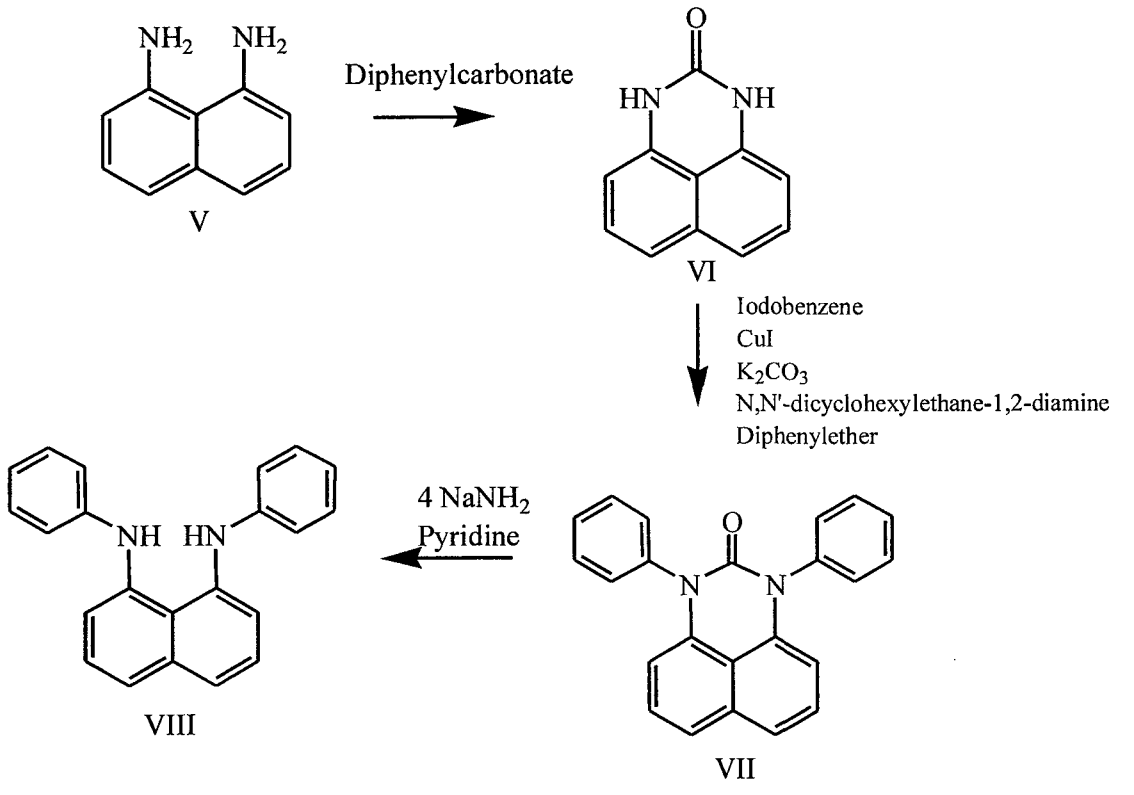

In this thesis the use of 1,8-disubstituted diaminonaphthalene ligands as a supporting framework for carbenes and in the synthesis of high oxidation state early transition metal and lanthanide complexes will be presented.

Chapter 2 focuses on the use of the R_2DAN ligand in the formation of carbenes and bis carbenes and the study of the dimerization of these carbenes. The formation of a gold complex with a R_2DAN carbene is also presented.

In Chapter 3 we describe the use of R_2DAN ligands in the synthesis of lanthanide complexes. The different structures obtained are discussed.

Chapter 4 describes the synthesis and structure of high oxidation state group IV complexes using different approaches. The structural features of the complexes and the effects of nitrogen substituents are discussed.

In Chapter 5 the reaction of the parent ligand and of the dilithium salt with different tantalum starting materials and the reactivity of these complexes is presented. The flexibility of the R_2DAN ligands is presented in the different crystal structures and a computational study helps explain the distortion we see in these complexes.

Chapter 6 describes the synthesis of bis(imido) tungsten complexes with the disubstituted 1,8- diaminonaphthalene ligands. The reactivity of these complexes with heterocumulenes and Lewis acids are presented. This chapter also includes a computational section that presents a study on the distortion of the R_2DAN ligands in the tungsten complexes. And finally the last part presents the results from the cyclotrimerization of isocyanates with the tungsten complexes.

References

[1] (a) Hanaoka, H.; Hino, T,; Souda, H.; Yanagi, K.; Oda, Y.; Imai, A. *J Organomet Chem*, **2007**, 692, 4059. (b) Bredeau, S.; Altenhoff, G.; Kunz, K.; Döring, S.; Grimme, S.; Kehr, G.; Erker. G. *Organometallics,* **2004**, *23,* 1836. (c) Cho, D. J.; Wu, J. W.; Sujith S, S.; Han, W. S.; Kang, S. O.; Lee, B. Y. *Organometallics,* **2006,** *25,* 2133.

[2] (a) Gade, L. H. *Chem. Commun.* **2000**, 173–181. (b) Kempe, R.; *Angew. Chem. Int. Ed.* **2000**, 39, 468, 493.

[3] Edelmann, F.T. *Adv. Organomet. Chem.*, **2008**, 57, 183.

[4] (a) Basuli, F.; Huffman, J. C.; Mindiola, D. J. *Inorg. Chem.* **2003**, *42,* 8003. (b) Basuli, F.; Bailey, B. C.; Tomaszewski, J.; Huffman, J. C.; Mindiola, D. J. *J. Am. Chem. Soc.* **2003**, *125*, 6052. (c) Basuli, F.; Bailey, B. C.; Huffman, J. C.; Mindiola, D. J. *Chem. Commun.* **2003**,1554. (d) Kakaliou, L.; Scanlon, W. J.; Qian, B.; Baek, S. W.; Smith, M. R. *Inorg. Chem.* **1999**, *38,* 5964. (e) Budzelaar, P. H. M.; Van Oort, A. B.; Orpen, A. G. *Eur. J. Inorg. Chem.* **1998**, 1485.

[5] (a) Hitchcock, P. B.; Khvostov, A. V.; Lappert, M. F.; Protchenko. A. V. *Dalton Trans.* **2009**, 2383. (b) Wei. X.; Cheng, Y.; Hitchcock. P. B.; Lappert, M. F. *Dalton Trans.* **2008**, 5235. (c) Yao, Y.; Zhang, Z.; Peng, H.; Zhang, Y.; Shen, Q.; Jun, L. J. *Inorg Chem*, **2006,** 45, 5, 2175. (d) Xue, M.; Yao. Y.; Shen. Q.; Zhang. Y. *J. Organomet. Chem,* **2005,** 690, 4685. (e) Zhang. Z. Q.; Yao, Y. M.; Zhang. Y.; Shen, Q.; Wong. W. T. *Inorganica Chimica Acta,* **2004**, 357, 3173.

[6] Aoyagi, K.; Gantzel, P. K.; Kalai, K.; Tilley, T. D. *Organometallics* **1996**, *15,* 923.

[7] (a) Pindado, J. G.; Thornton-Pett. M.; Bochmann. M. *J. Chem. Soc., Dalton Trans. 1998, 393.*

[8] (a) Gountchev, T. I.; Tilley, D. T. *Inorganica Chimica Acta,* **2003**, 345, 81. (b) Gountchev. T. I.; Tilley. T. D. *J. Am. Chem. Soc.* **1997**, *119.* (c) Gountchev, T. I.; Tilley, T. D. *Organometallics* **1999**, *18,* 5661. (d) Gountchev. T. I.; Tilley. T. D. *Organometallics,* **1999**, *18,* 2896.

[9] (a) Decams. J. M.; Daniele, S.; Hubert-Pfalzgraf, L. G.; Vaissermanm, J.; Lecocq. S. *Polyhedron,* **2001**, 20, 2405. (b) Galka, C. H.; Trolsch, D. J. M.; Ruldenauer, I.; Gade, L. H.; Scowen, I.; McPartlin, M. *Inorg. Chem.* **2000**, *39,* 4615. (c) Nomura. K.; Naga, N.; Takaoki, K.; Imai, A.; *Journal of Molecular Catalysis, A: Chemical*, **1998**, 130, L209. (d) Lee, C. H.; La, Y. H.; Park, S. J.; Park, J. W. *Organometallics* **1998**, *17,* 3648.

[10] Bazinet, P.; Ong, T. G.; O'Brien, J. S.; Lavoie, N.; Bell, E.; Yap, G. P. A.; Korobkov, I.; Richeson, D. S. *Organometallics,* **2007**, *26,* 2885.

[11](a) Basuli, F.; Huffman, J. C,; Mindiola, D. J. *Inorganic Chemistry*, **2003**, 42, 24, 8003. (b) Hitchcock, P.B.; Lappert, M. F.; Nycz, J. E. *Chem. Commun.* **2003**, 1142. (c)

Ragogna, P. J.; Burford, N.; D'eon, M.; McDonald, R. *Chem. Commun.* **2003**, 1052, (d) Radzewich, C. E.; Coles, M. P.; Jordan, R. F. *J. Am. Chem. Soc.* **1998**, *120,* 9384.

[12] Liddle, S. T.; Arnold, P. L. *Dalton Trans.* **2007**, 3305.

[13] VanderLende, D. D.; Abboud, K. A.; Boncella, J. M. *Organometallics* **1994**, *13,* 3378.

[14] Ison, E. A.; Ortiz, C. O.; Abboud, K.; Boncella, J. M. *Organometallics* **2005,** *24,* 6310.

[15] (a) Bazinet, P.; Yap, G. P. A.; Richeson, D. S. *J. Am. Chem. Soc.,* **2003**, 125, 13314. (b) Bazinet, P.; Yap, G. P. A.; Richeson, D. S. *J. Am. Chem. Soc.* **2001**, *123,* 11162. (c) Bazinet, P.; Yap, G. P. A.; DiLabio, G. A.; Richeson, D. S. *Inorganic Chemistry,* **2005**, 44, 13.

Chapter 2

Stable Free Carbenes and Enetetramines

I. Introduction

Access to stable carbenes and their success in stabilizing transition metal complexes has resulted in carbenes becoming very important ligands. Several studies indicate that the strong σ-donor strength with negligible π-accepting ability engenders nucleophilic carbenes with similar properties to electron-rich trialkylphosphines.[1] Carbenes have a divalent carbon atom with only six valence shell electrons while remaining neutral. The carbene center bonds with the two substituents account for four of these electrons leaving two non-

bonding electrons on the carbene center. In general, carbenes can be linear or bent. The linear geometry has an sp-hybridized carbene center giving two degenerate p-type orbital labeled p_x and p_y (Figure 2.1). Each of these two orbitals can have an unpaired electron resulting in a triplet state carbene. In contrast, the bent geometry has a sp^2-hybridized carbene center causing the two orbitals, known as the σ and p_π, to adopt different orientations and energies and resulting a singlet carbene with both electrons in the same orbital as the ground electronic state. For bent carbenes the energy gap between the σ and p_π orbitals determines if the singlet or triplet state is adopted. If the pairing energy for the doubly occupied orbital is smaller than the energy gap the singlet state is favored. A singlet-triplet gap of 7.6×10^{-23}Kcal or more usually leads to a singlet gound state and a gap less than 5.7×10^{-23}Kcal leads to a triplet ground state.[2] Two factors are important in the formation of free carbenes. The first is the size of the nitrogen substituents, when very large nitrogen substituents are employed they prevent the formation of dimers. The other important factor is the triplet-singlet gap. The smaller the singlet-triplet energy gap ($\Delta E_{s/t}$= $E_{triplet}$-$E_{singlet}$) the more likely the carbene will dimerize. For the first reason our choice of nitrogen substituents was very important in our attempts to prepare free carbenes.

Figure 2.1 The ground state orbital picture for linear and bent carbenes

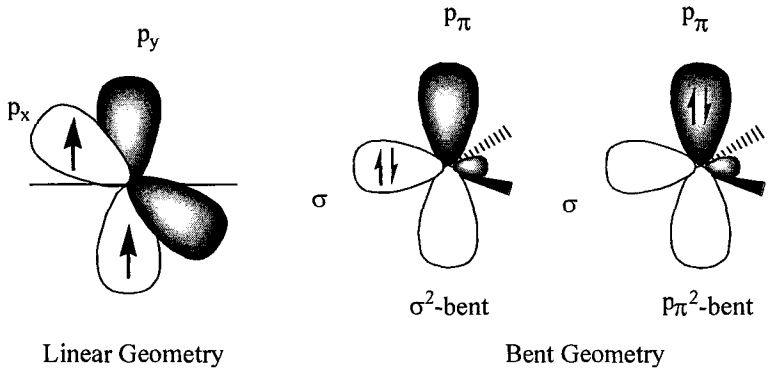

The first room temperature stable carbene was reported by Arduengo in 1991.[3] It had the framework represented by **A** with R being adamantyl groups. After this account many other five membered N-heterocyclic ring carbenes (NHCs) were reported. They have become widespread ligands and are now commercially available. The unsaturated species (**A**) are much more stable than the saturated species (**B**) due to the fact that the unsaturated species possess a 6π electron aromatic system. Type **B** carbenes are less stable and tend to exist as dimers.

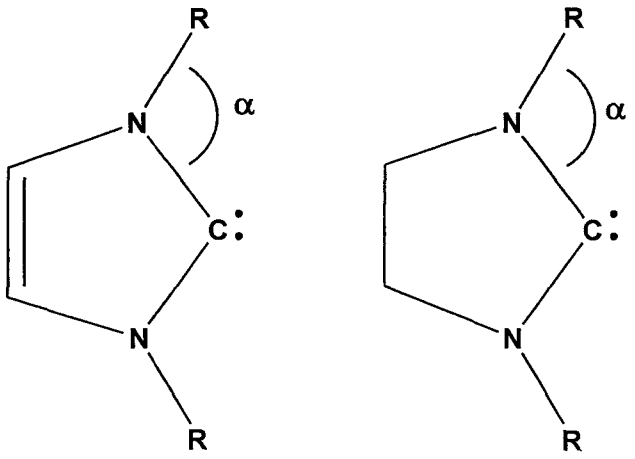

Efforts to expand on the structural and electronic diversity of carbene ligands have lead to the design of many stable carbenes such as **C**[4], **D**[5], **E**[6],**F**[7]and **G**[8]. One of the major differences between all of these scaffolds is the α angle, the larger the ring size the closer the nitrogen substituents are to the carbene center increasing the steric protection. In our lab we have developed carbenes with the **F** framework. In this particular framework the carbene sits in a six-membered ring decreasing the α angle and bringing the R substituents closer to the carbene carbon increasing the steric protection. The other important feature for this framework is the naphthalene backbone. The extended aromatic system of the naphthalene backbone places the carbene center in a formally seven π-electron heterocycle[9]. This could make this type of carbene more donating than others.

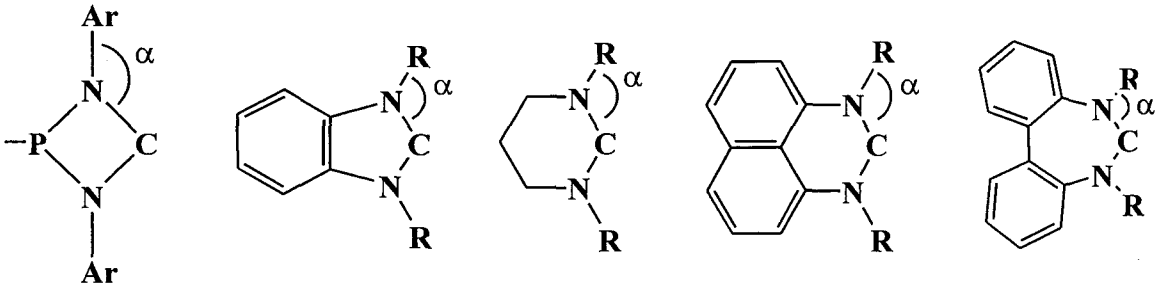

C D E F G

II. Results and Discussion

Carbenes with Perimidine Scaffold

Efforts in our lab over the last few years have focused on the design of sterically demanding and electron rich carbenes and their application as ligands in transition metal complexes.[10] We have focused on the perimidine scaffold with a naphthalene backbone, this scaffold leads to an electron rich system and nitrogen substituents can be sterically demanding. A series of free stable carbenes and enetetramines have been prepared in our lab by deprotonation of the perimidinium salts with lithium hexamethylsilylamide (Scheme 2.1). From theses results we can see that depending on the identity of the N-substituents we obtained free carbenes or enetetramines.

Scheme 2.1

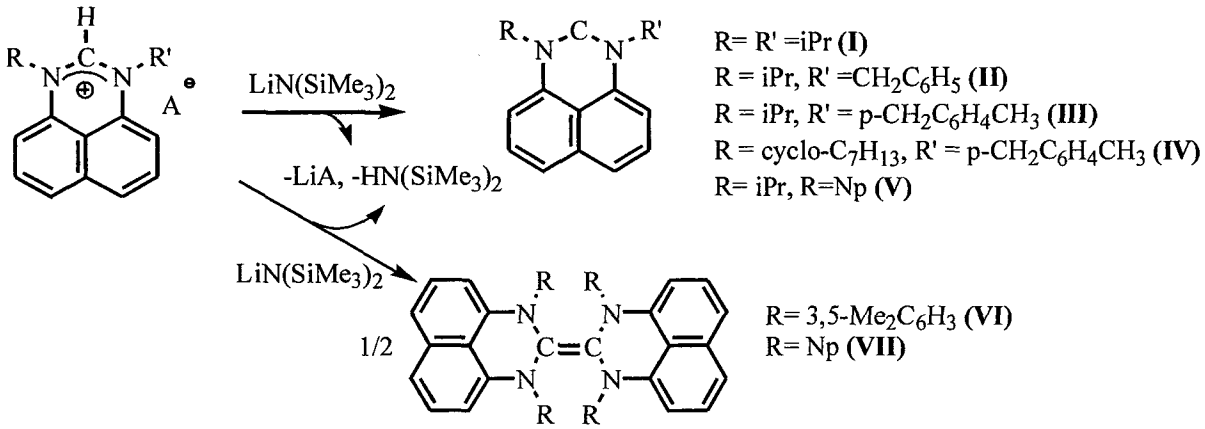

One of theses carbenes **(IV)** has shown a interesting transformation when left in solution. The ^{1}H NMR spectra of carbene **(IV)** taken after a period of time displayed new resonances indicating its transformation into a new compound. In particular, the appearance of doublets instead of a singlet associated with the benzylic CH_2 groups, a feature the was previously observed in a enetetramine with neopentyl subtituents **(VII)** suggested that this free carbene was slowly undergoing dimerization (Scheme 2.2). This transformation was monitored by dissolving a sample of **(IV)** in C_6D_6 and observing the time evolution of its NMR spectra. The initially observed ^{1}H NMR spectrum exhibited only the signals for the free carbene. This sample was then heated to 80°C for 24 hours. At the end of this period, the ^{1}H NMR spectrum of this sample displayed a diminished intensity for the singlet arising from the methylene group of the starting material at 5.29 ppm; concomitant with this observation was the appearance of four new doublets centered at 5.51, 5.22, 4.98 and 4.48 ppm consistent with diastereotopic protons for the benzyl CH_2 moieties and corresponding to the formal dimerization of **IV**. The appearance of four doublets suggested the formation

of both *cis* and *trans* isomers of the product enetetramines. This sample was further heated to 80°C for 24 hours after which time the methylene singlet for **IV** in the ^{1}H NMR spectrum had completely disappeared and was replaced by the four doublets. Heating at 80°C for an additional 24 hours did not result in any further change in the ^{1}H NMR spectrum. Furthermore, the NMR spectrum did not display any additional changes over the next 13 days at room temperature leading use to believe that the dimerization of this particular carbene was not reversible. Similar experiments with carbene **I** was attempted but no formation of enentramine was observed even at elevated temperature. The carbene appeared to decompose before dimerization could be observed.

Scheme 2.2

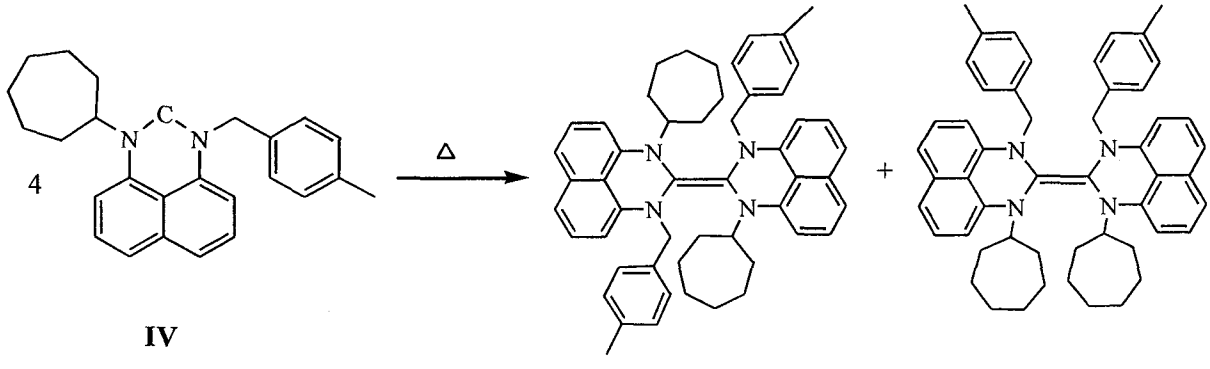

IV trans-$(2.1)_2$ cis-$(2.1)_2$

We were fortunate to be able to obtain crystals of both isomers of the dimer **2.1** and were able to confirm their structural features using single crystal X-ray diffraction (Table 2.1). The structural diagrams obtained from these analyses are shown in Figure 2.2 and 2.3 and selected bond distances and angles are provided in Table 2.2. The structure of ***trans-***

(2.1)$_2$ has a C=C bond length of 1.348(4) Å this is very similar to what is observed in **(VII)**.[10] The C=C bond lies on an inversion center with the two halves of the molecule slightly twisted along this axis [N1-C1-C(1A)-N(2A)= 9.9(2)°]. Similarly, C1 deviates from the naphthyl plane by approximately 0.5 Å and the non-planar nature of the heterocyclic ring is further demonstrated by the torsion angles C(10)-N(1)-C(1)-N(2) [46.5(2)°] and C(16)-N(2)-C(1)-N(1) [-49.6(2)°]. The two nitrogen centers in ***trans*-(2.1)$_2$** exhibit different geometries: one with a planar environment [$\sum$ angles for N1 = 359.8(2)°] and one that is pyramidal ($\sum$ angles for N2 = 347.8(2)°). An effect of this distortion is the projection of the cycloheptyl group on N2 out of the plane of the C_2N_4 core. Other than the obvious difference in substituent orientation, there are only slight differences between the ***cis*-(2.1)$_2$** and ***trans*-(2.1)$_2$** isomers. The C=C bond length of the *cis* isomer (1.340(5)Å) is identical to the *trans* isomer within experimental error, there is a similar twist along this bond and the olefinic carbons again deviate from the heterocyclic planes by approximately 0.5 Å. As with both **VI** and the *trans* isomer, the nitrogen centers of ***cis*-(2.1)$_2$** are a combination of planar (N2 and N3) and pyramidal (N1 and N4) centers. Interestingly, the two pyramidal nitrogen centers of ***cis*-(2.1)$_2$** bear the cycloheptyl groups as was observed in ***trans*-(2.1)$_2$**.

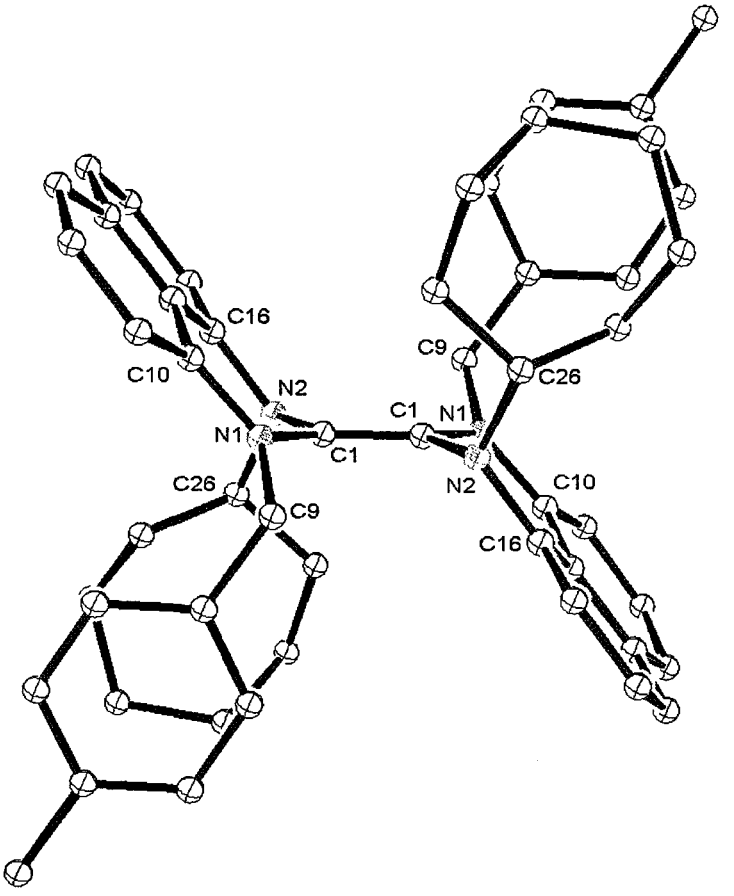

Figure 2.2. Molecular structure and atom-numbering scheme for the trans isomers of enetetramine $\{C_{10}H_6(cyclo\text{-}C_7H_{13}N)(p\text{-}MeC_6H_4CH_2N)C\}_2$, (***trans*-(2.1)$_2$**). Only one of the two molecules in the asymmetric unit is shown. Thermal ellipsoids are drawn at 20% probability. Hydrogen atoms have been omitted for clarity.

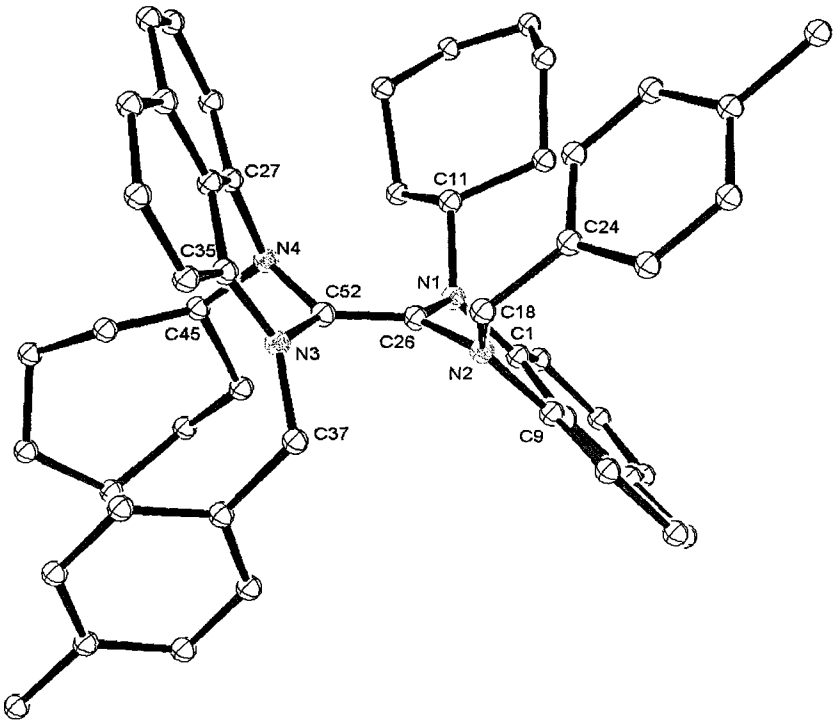

Figure 2.3. Molecular structure and atom-numbering scheme for cisisomers of enetetramine $\{C_{10}H_6(cyclo\text{-}C_7H_{13}N)(p\text{-}MeC_6H_4CH_2N)C\}_2$ (***cis*-(2.1)$_2$**). Thermal ellipsoids are drawn at 20% probability. Hydrogen atoms have been omitted for clarity.

Table 2.1. Selected Crystal Data and Structure Refinement Parameters for the *cis* and *trans* Isomers of $(C_{10}H_6(cyclo\text{-}C_7H_{13}N)(p\text{-}MeC_6H_4CH_2N)C\}_2$, *trans*-$(2.1)_2$ and *cis*-$(2.1)_2$.

Empirical formula	$C_{104}H_{112}N_8$	$C_{52}H_5N_4$
Formula weight	1474.02	737.01
Temperature (K)	207(2)	207(2)
Wavelength (Å)	0.71073	0.71073
Crystal system	triclinic	triclinic
Space group	P-1	P-1
a (Å)	8.6140(13)	10.964(3)
b (Å)	13.555(2)	11.591(4)
c (Å)	17.067(3)	17.429(5)
α(deg)	93.690(3)	91.921(6)
β(deg)	97.561(3)	97.232(6)
γ(deg)	97.573(3)	113.765(6)
V ($Å^3$)	1951.5(5)	2002.4(1)
Z	1	2
ρ (calc) (Mg/m^3)	1.254	1.222
μ (mm^{-1})	0.073	0.071
Absorption correction	Semi-empirical from equivalents	
Final R indices [I>2σ(I)]		
R1[a]	0.0727	0.0721
***w*R2**[b]	0.1822	0.1452

[a] $\boldsymbol{R1} = \Sigma \| F_o | - | F_c \| / \Sigma | F_o |$

[b] $\boldsymbol{wR2} = (w(| F_o | - | F_c |)^2 / \Sigma w | F_o |^2)^{1/2}$

Table 2.2. Selected bond lengths (Å) and angles (°) for the *cis* and *trans* isomers of $\{C_{10}H_6(cyclo\text{-}C_7H_{13}N)(p\text{-}MeC_6H_4CH_2N)C\}_2$ *trans*-$(2.1)_2$ and *cis*-$(2.1)_2$.

***trans*-(2.1)$_2$**			***cis*-(2.1)$_2$**		
		Bond Lengths (Å)			
N(1)-C(10)	1.393(3)	N(1)-C(1)	1.388(5)	N(3)-C(52)	1.422(4)
N(1)-C(1)	1.424(3)	N(1)-C(26)	1.419(4)	N(3)-C(37)	1.475(5)
N(1)-C(9)	1.469(3)	N(1)-C(11)	1.504(5)	N(4)-C(52)	1.434(5)
N(2)-C(16)	1.417(3)	N(2)-C(9)	1.397(5)	N(4)-C(27)	1.427(5)
N(2)-C(1)	1.431(3)	N(2)-C(26)	1.417(5)	N(4)-C(45)	1.489(5)
N(2)-C(26)	1.500(3)	N(2)-C(18)	1.464(5)	C(26)-C(52)	1.340(5)
C(1)-C(1)#1	1.348(4)	N(3)-C(35)	1.386(5)		
		Angles (°)			
C(10)-N(1)-C(1)	116.31(17)	C(1)-N(1)-C(26)	116.5(3)	C(52)-N(4)-C(27)	109.5(3)
C(10)-N(1)-C(9)	121.53(18)	C(1)-N(1)-C(11)	120.7(3)	C(52)-N(4)-C(45)	119.7(3)
C(1)-N(1)-C(9)	121.96(17)	C(26)-N(1)-C(11)	117.6(3)	C(27)-N(4)-C(45)	115.0(3)
C(16)-N(2)-C(1)	112.43(17)	C(9)-N(2)-C(26)	118.7(3)	C(52)-C(26)-N(1)	122.1(4)
C(16)-N(2)-C(26)	116.01(17)	C(9)-N(2)-C(18)	120.7(3)	C(52)-C(26)-N(2)	122.2(3)
C(1)-N(2)-C(26)	119.38(17)	C(26)-N(2)-C(18)	120.2(3)	N(1)-C(26)-N(2)	115.4(3)
C(1)#1-C(1)-N(1)	123.6(2)	C(35)-N(3)-C(52)	116.7(3)	C(26)-C(52)-N(3)	123.2(4)
C(1)#1-C(1)-N(2)	120.5(2)	C(35)-N(3)-C(37)	122.0(3)	C(26)-C(52)-N(4)	120.2(3)
N(1)-C(1)-N(2)	115.31(17)	C(52)-N(3)-C(37)	120.8(3)	N(3)-C(52)-N(4)	114.9(3)

A distinguishing feature differentiating carbenes of type **A** and **B** is their propensity to form enetetramines, the formal C=C dimers of the free carbenes.[11] The more stable, unsaturated species **A** only dimerize under very specific circumstances.[12] On the other hand, the saturated carbene analogues readily form enetetramines. In fact, stable type **B** carbenes can only be accessed by shielding the carbene center with sufficiently large N-substituents to kinetically inhibit the formation of the enetetramine.[13,14,15] Similarly, the

dimerization behavior of benzimidazole-based carbenes is highly dependant on the steric bulk of the N-substituents.[16, 11] Small N-substituents, such as methyl groups, allow the formation of the enetetramine **(H)$_2$**, whereas bulkier neopentyl groups stabilize the free carbene **I**. Intermediate sized isobutyl substituents are reported to allow for an equilibrium between the free carbene **J**, and the dimer **(J)$_2$** at room temperature.

Observations have been justified through an examination of the calculated singlet-triplet energy gaps ($\Delta E_{s/t} = E_{triplet}-E_{singlet}$) for each of these species.[17, 18, 19] The magnitude of $\Delta E_{s/t}$ for type **A** carbenes has been calculated to be approximately 82 kcal/mol[18] and, using general C=C double bond energy of 172 kcal/mol, the estimated $\Delta H_{dimerization}$ of imidazol-2-ylidenes **A** is close to zero.[20] On the other hand, type **B** carbenes are calculated to have $\Delta E_{s/t}$ values that are smaller by approximately 12 kcal/mol; these species dimerize unless sterically protected with bulky N-substituents.[18] Calculation of $\Delta E_{s/t}$ for the benzannulated analogues of **A** (e.g. **H**, **I** and **J**) gave a value of approximately 78 kcal/mol. This value is consistent with the -13.7±0.6 kcal/mol for the enthalpy of dimerization for N,N'-diethylbenzimidazol-2-ylidene and the ability to modulate the dimerization of these compounds with small steric changes to the N substituents.[15, 21] Our DFT calculation of the singlet-triplet gap of compound **I**, with the B3LYP functional using a 6-31+G(d) basis set, provided a value of $\Delta E_{s/t}$ = 65 kcal/mol.[22]

Figure 2.4 Benzimidazole-based carbenes

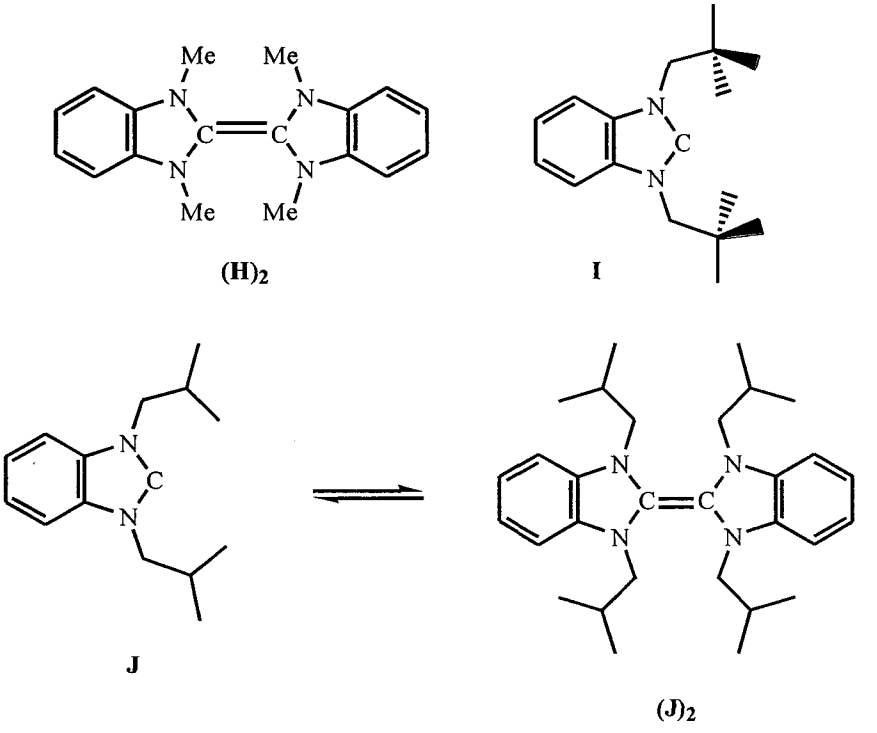

This suggests that perimidine carbenes should have a thermodynamic preference toward dimerization. Of course kinetic stabilization is not taken into account in this indirect approach to estimating propensity for dimerization. Our observations of compounds **I-VII** suggest that kinetic stability provided by the steric impact of the N-substituents plays a significant role in the isolation of free carbenes with a perimidine framework.

Bridged carbenes

Bridged carbene appeared in the literature shortly after the report of stable free carbenes. They combine the great ligand potential of carbenes with the advantage of having a chelating ligand. We have used xylyl groups as bridging units in our attempt to synthesize bis(carbenes). The first step was the synthesis of bridged bis(perimidinium) salts. This was

achieved by reacting two equivalents of 1-isopropylperimidine with α,α'-dibromo xylenes at elevated temperature to give the corresponding perimidinium salts, the products from these reactions have very low solubility in the reaction solvent indicating the synthesis of a double salt. Generation of a free carbene required the deprotonation of the salt using two equivilants of lithium bis(trimethyl)silylamide (LiHMDS). Previous work in our lab gave indications that the free bis(carbene) **(K)** had been formed using the para xylyl but this free carbene could not be purified for further characterization or further use. The use of the ortho xylyl positioned the potential carbene units closer together and lead to the formation of the corresponding enetetranine **(L)**.

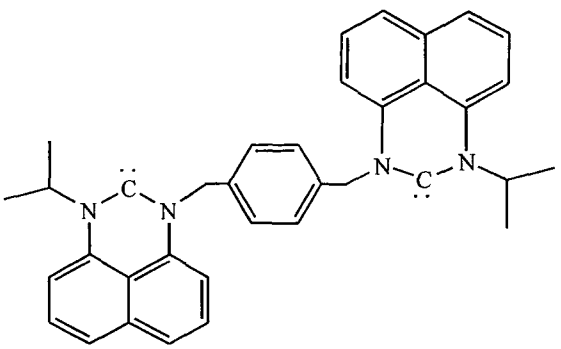

K

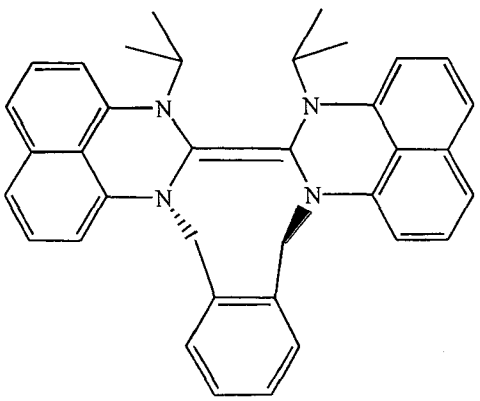

L

With this information in hand we continued the investigation with an intermediate bridging unit; the meta xylyl isomer. Reaction of α,α'-dibromo-meta-xylene with two equivalents of isopropylperimidine generated a yellow solid (Scheme 2.3). The salt was

characterized by ^{1}H and ^{13}C NMR spectroscopy. The presence of a downfield signal at 9.41ppm integrating for two hydrogen centers was characteristic of the NC(**H**)N signal. The rest of the ^{1}H

Scheme 2.3

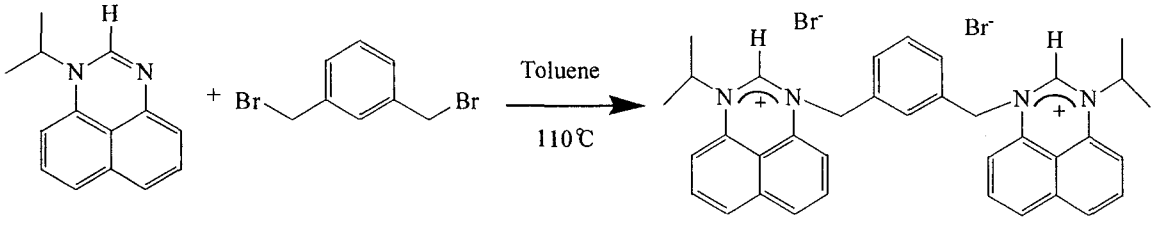

2.2

spectrum is consistent with the two perimidinium units bridged by a xylyl group. The ^{13}C spectrum also has a downfield signal at 151.2 ppm for the NCN carbon. In analogy to the mono perimidene species, the salt could be deprotonated using LiHMDS (Scheme 2.4). When the salt is added to the base in chlorobenzene the yellow color disappeared to give a clear solution. A beige solid was obtained after drying the reaction mixture and extracting the product with toluene. A downfield signal at 245.3 ppm in the ^{13}C NMR spectrum was the first indication that the product obtained was the free bis(carbene) (**2.3**).

Scheme 2.4

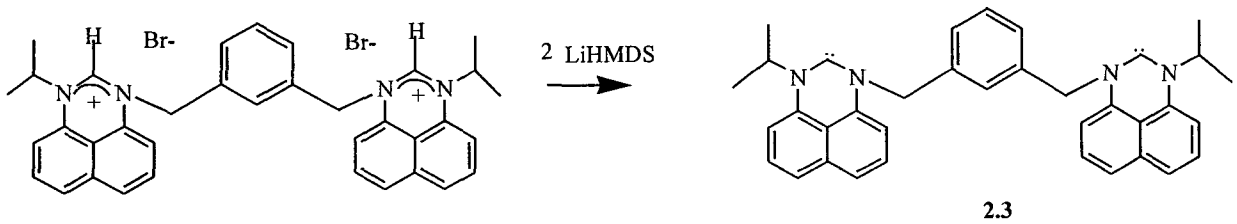

2.3

Crystal of the product were obtained from toluene and this allowed confirmation of the structure of **2.3** by an X-ray crystallography study. Figure 2.5 shows the structure and Table 2.4 gives selected bond distances and angles data. The average N-$C_{carbene}$ bond length was 1.359(6)Å which is typical of carbenes with this framework. The N-C_{ring} bond length average was 1.418(6)Å suggesting that the nitrogen lone pair is more involved in bonding in the N-$C_{carbene}$ bond than in the N-C_{ring} bond. The average of the α angle in this bis(carbene) was 115.5° this is as expected smaller than the typical values for structure of type **A** and **B** which typically have α angles of 122-123°. [12, 23] The N-$C_{carbene}$-N angle is on average 114.7° which is larger than in the **A/B** carbene that typically have a 100-110° angles but very similar to the other carbenes synthesized in our lab. All four nitrogen centers in **2.3** are planar permitting the donation of the nitrogen lone pair to the electron deficient carbene center. Both carbene units are approximately 90° from the xylyl ring both point in opposite directions.

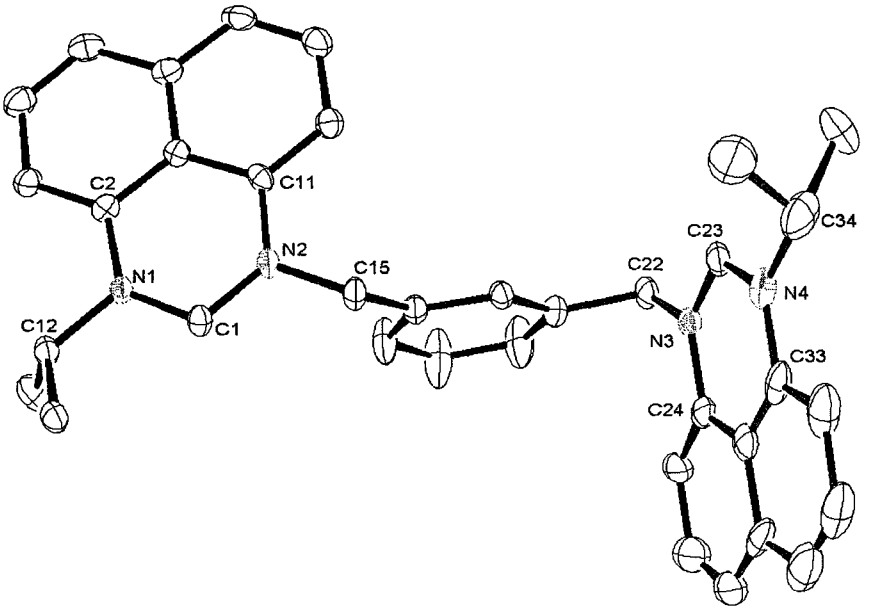

Figure 2.5. Molecular structure and atom-numbering scheme showing the bis-carbene **2.3**. Thermal ellipsoids are drawn at 20% probability. The co-crystallized solvent (toluene) and hydrogen atoms have been omitted for clarity.

Table 2.3 Selected Crystal Data and Structure Refinement Parameters for **2.3**

Empirical formula	$C_{39.50}H_{38}N_4$
Formula weight	568.74
Temperature (K)	211(2)
Wavelength (Å)	0.71073
Crystal system	Triclinic
Space group	P-1
a (Å)	9.099(2)
b (Å)	12.276(3)
c (Å)	14.835(3)
α(deg)	106.354(4)
β(deg)	97.052(4)
γ(deg)	97.25(4)
V ($Å^3$)	1551.8(6)
Z	2
ρ(calc) (Mg/m^3)	1.217
μ (mm^{-1})	0.072
Absortion correction	Semi-empirical from equivalents
Final R indices [I>2σ(I)]	
R1[a]	0.0803
***w*R2**[b]	0.1826

[a] $R1 = \Sigma \| F_o | - | F_c \| / \Sigma | F_o |$

[b] $wR2 = (w(| F_o | - | F_c |)^2 / \Sigma w | F_o |^2)^{1/2}$

Table 2.4 Selected bond lengths (Å) and angles (°)for **2.3**.

2.3			
Bond lengths (Å)			
N(1)-C(1)	1.354(5)	N(3)-C(24)	1.435(7)
N(2)-C(1)	1.364(5)	N(4)-C(33)	1.459(8)
N(3)-C(23)	1.350(6)	N(1)-C(12)	1.484(5)
N(4)-C(23)	1.362(7)	N(2)-C(15)	1.464(5)
N(1)-C(2)	1.417(6)	N(3)-C(22)	1.467(6)
N(2)-C(11)	1.419(6)	N(4)-C(34)	1.486(8)
Angles(°)			
C(1)-N(1)-C(12)	115.8(4)	N(3)-C(23)-N(4)	114.3(5)
C(12)-N(1)-C(2)	118.5(4)	C(34)-N(4)-C(33)	121.0(6)
C(2)-N(1)-C(1)	125.8(4)	C(33)-N(4)-C(23)	123.9(5)
C(1)-N(2)-C(15)	115.7(4)	C(23)-N(3)-C(22)	115.7(4)
C(15)-N(2)-C(11)	118.5(4)	C(22)-N(3)-C(24)	117.5(5)
C(11)-N(2)-C(1)	125.8(4)	C(24)-N(3)-C(23)	126.7(5)
C(23)-N(4)-C(34)	115.1(5)	N(1)-C(1)-N(2)	115.1(4)

To further expand the bis(carbene) chemistry we decided to bridge two different carbene precursors with the same xylyl group. In particular, we targeted a species that would possess one perimidene-based carbene and one imidazole-based species of type **A**. This was attempted using two methods. The first approach was the introduction of one perimidinium unit to the meta dibromoxylene. This unfortunately lead to a mixture of mono and disubstituted xylenes even when the reaction was done at room temperature. The second approach involved the initial introduction of the mesityl imidazole unit as shown in Scheme 2.5. By mixing the mesityl imidazole with the meta-xylene at room temperature and stirring for a long period of time the mono substituted product would be obtained. A

white product precipitated from the reaction mixture indicating the formation of a salt. A down field peak was found in the proton NMR at 10.28 ppm which intergrated for one proton which confirmed the presence of a NCHN proton. The ^{13}C spectrum also supports the formation of a salt with a peak at 140.68 ppm for the $C^{+}H$ carbon.

Scheme 2.5

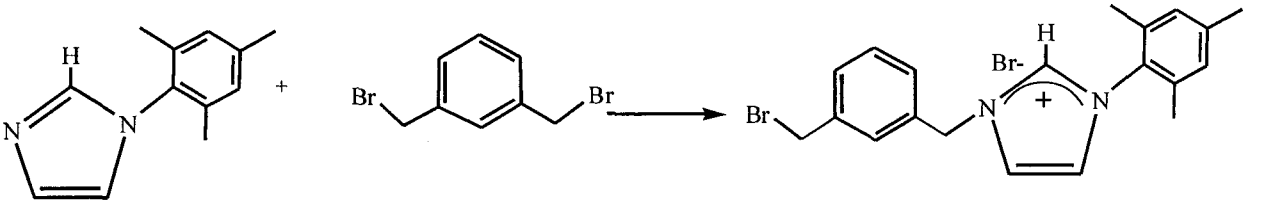

2.4

Similar reaction conditions were applied with the ortho xylene (Scheme 2.6) and once again a white powder identified as **2.5** was obtained. The ^{1}H NMR spectrum of the product shows one singlet at 10.28 ppm for the NCHN proton, the rest of the spectrum correlated with the desired product. The ^{13}C NMR displayed a peak at 141.0 ppm corresponding to the $C^{+}H$ signal. The connectivity of the product **2.5** was definitively established by X-ray diffraction experiment (Figure 2.6).

Scheme 2.6

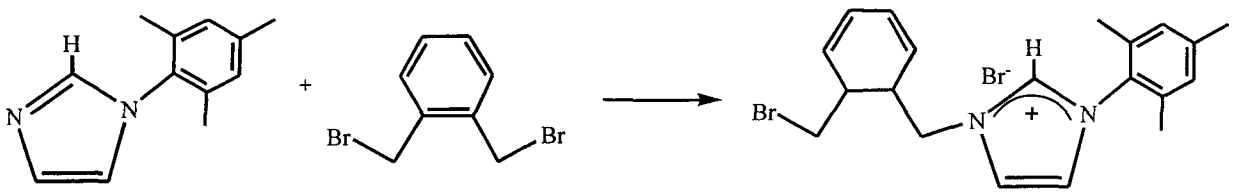

2.5

Crystal data and bond distances and angles for **2.5** are reported in Tables 2.5 and 2.6. The data showed that both nitrogens centers were planar with the sum of the angles around them being 360.0 and 359.7° for N(1) and N(2) respectively. The α angle in the salts are of 125.9(3) and 125.5(3)° for N(1) and N(2) respectively and the N(1)-C(12)-C(2) angle in this salt is of 108.5(4)°.

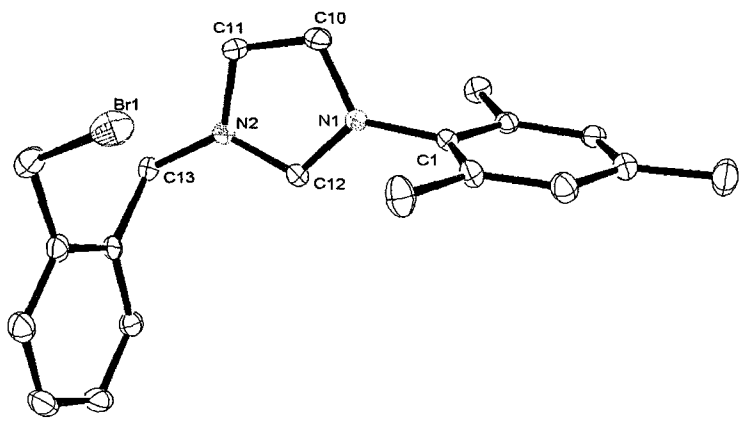

Figure 2.6. Molecular structure and atom-numbering scheme showing the imidozolium salt **2.5**. Thermal ellipsoids are drawn at 20% probability. Hydrogen atoms and the bromide anion have been omitted for clarity.

With these salts in hand we then proceded to the introduction of the perimidinium carbene precursor. This was done by heating **2.4** and **2.5** with one equivalent of isopropylperimidine (Scheme 2.7 and 2.8) at 80°C for two days. Bright yellow solids where isolated from the reaction mixtures. In both cases the proton NMR spectra of the resulting products showed two downfield peaks at 10.28 and at 9.90 ppm for **2.6** and at 10.31 and 9.90 ppm for **2.7**, these peaks correspond to two different the NCHN protons. The ^{13}C spectrum indicates the presence of two salts with two peaks at 150.7 ppm and 141.1 ppm for **2.6** and at 150.8 and 141.1 ppm for **2.7** representing the $C^{+}H$ signals. These observations were a good indication that the desired products were obtained but this was further confirmed by X-ray crystallography experiments. Tables 2.5 and 2.6 give selected parameters and bond lengths and angles for the structures of **2.6** and **2.7**. The structure of **2.6** showed the incorporation of the two salt units that have their rings perpendicular to the xylyl ring bridge and which are oriented to minimize electrostatic repulsion by pointing in opposite direction. The average $N\text{-}C^{+}$ is 1.332 Å for the perimidium unit and 1.334 Å for the imidazolium unit. The α angle are in average 118.4° for the perimidium unit and 125.7° for the imidalozium unit. The $N\text{-}C^{+}$ bond lengths for the perimidium salt are very similar to those observed in **2.2** with an average bond distance of 1.32Å. The average for the imidazolium salt is the same as in salt **2.2** (1.334Å). The average α angles in this compound are 119.4° for the perimidium unit and 124.7° for the imidazolium unit these are the same within experimental errors that was observed for **2.2** and **2.5**.

Scheme 2.7

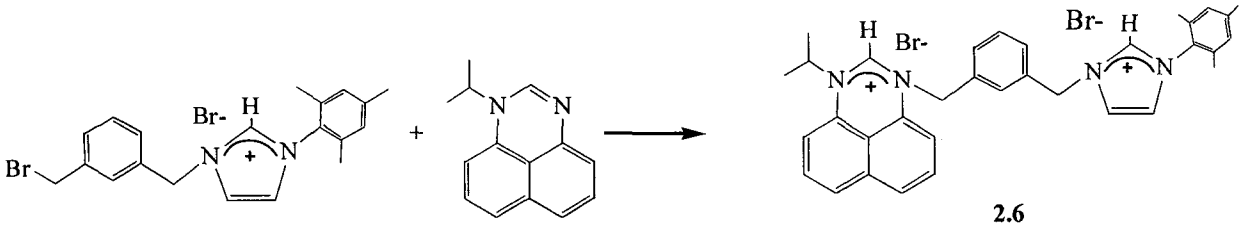

2.6

Scheme 2.8

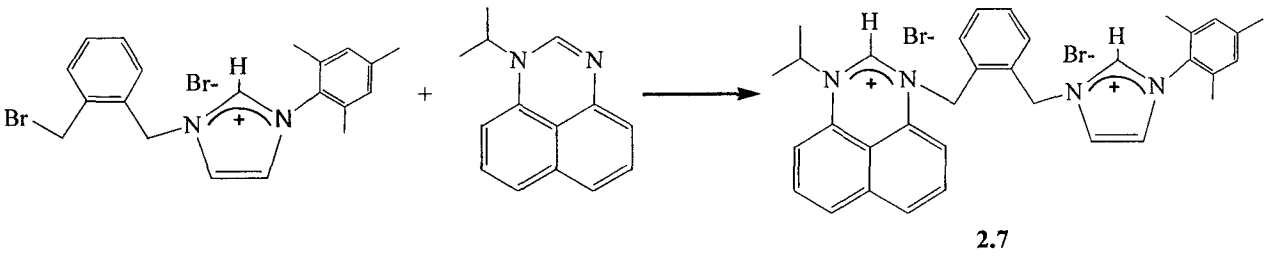

2.7

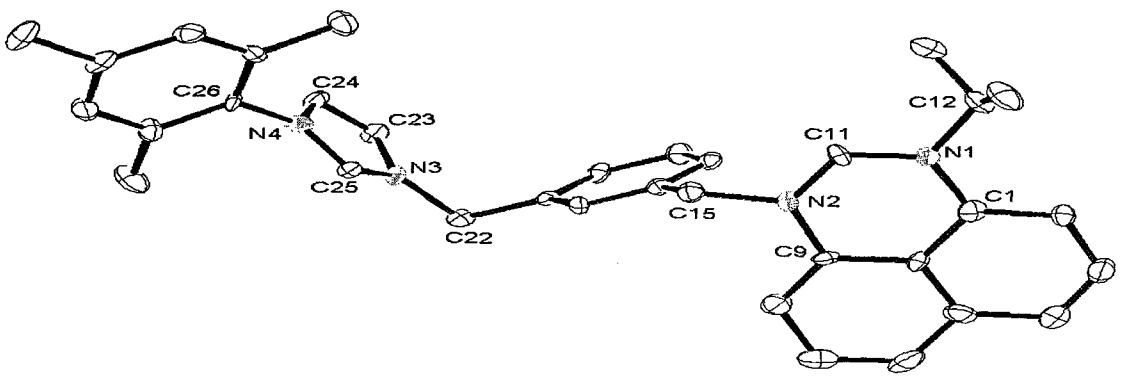

Figure 2.7. Molecular structure and atom-numbering scheme showing the bridged imidozolium and perimidinium salt **2.6**. Thermal ellipsoids are drawn at 20% probability. Hydrogen atoms and the bromide anions have been omitted for clarity.

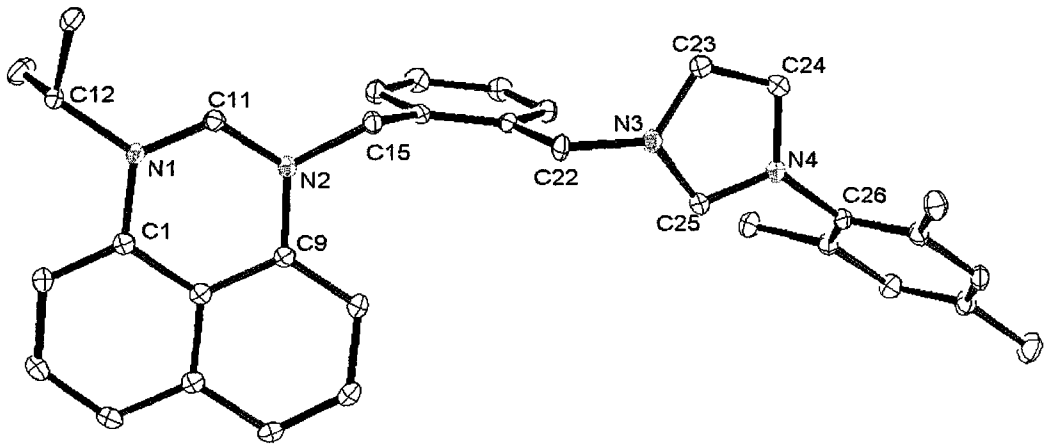

Figure 2.8. Molecular structure and atom-numbering scheme showing the bridged imidozolium and perimidinium salt **2.7.** Thermal ellipsoids are drawn at 20% probability. Hydrogen atoms and the bromide anions have been omitted for clarity.

Table 2.5 Selected Crystal Data and Structure Refinement Parameters for **2.5**, **2.6** and **2.7**.

Compound	**2.5**	**2.6**	**2.7**
Empirical formula	$C_{20}H_{21}Br_2N_2$	$C_{36}H_{42}Br_2N_4O_2$	$C_{36}H_{46}Br_2N_4O_3$
Formula weight	449.21	722.56	742.59
Temperature (K)	207(2)	207(2)	200(2)
Wavelength (Å)	0.71073	0.71073	0.71073
Crystal system	Monoclinic	Monoclinic	Triclinic
Space group	C2/c	P2(1)/n	P-1
a (Å)	25.877(6)	10.739(9)	8.883(6)
b (Å)	6.7831(15)	20.854(18)	13.257(9)
c (Å)	24.398(5)	16.559(14)	15.737(11)
α(deg)	90	90	75.522(11)
β(deg)	113.936(4)	96.063(17)	79.821(11)
γ(deg)	90	90	77.859(11)
V ($Å^3$)	3914.2(15)	3688(5)	1739(2)
Z	8	4	2
ρ(calc) (Mg/m^3)	1.525	1.301	1.418
μ (mm^{-1})	4.145	2.233	2.371
Absorption Correction	Semi-empirical from equivalents		
Final R indices [I>2σ(I)]			
R1[a]	0.0467	0.0720	0.0401
***w*R2**[b]	0.1105	0.1575	0.1057

[a] $R1 = \Sigma \| F_o | - | F_c \| / \Sigma | F_o |$

[b] $wR2 = (w(| F_o | - | F_c |)^2 / \Sigma w | F_o |^2)^{1/2}$

Table 2.6. Selected bond length (Å) and angle (°) for compound **2.5** and **2.6** and **2.7**.

Bond lengths (Å)					
2.5		**2.6**		**2.7**	
N(1)-C(10)	1.382(6)	N(1)-C(11)	1.332(12)	N(1)-C(11)	1.314(4)
N(1)-C(1)	1.447(5)	N(2)-C(11)	1.331(12)	N(2)-C(11)	1.326(4)
N(1)-C(12)	1.337(6)	N(3)-C(25)	1.321(12)	N(3)-C(25)	1.331(4)
N(2)-C(12)	1.338(5)	N(4)-C(25)	1.347(12)	N(4)-C(25)	1.337(4)
N(2)-C(13)	1.458(6)	N(1)-C(1)	1.429(13)	N(1)-C(1)	1.426(4)
N(2)-C(11)	1.379(6)	N(2)-C(9)	1.431(12)	N(2)-C(9)	1.413(4)
		N(3)-C(23)	1.379(12)	N(3)-C(23)	1.382(4)
		N(4)-C(24)	1.393(13)	N(4)-C(24)	1.383(4)
		N(1)-C(12)	1.467(13)	N(1)-C(12)	1.505(3)
		N(2)-C(15)	1.490(12)	N(2)-C(15)	1.487(4)
		N(3)-C(22)	1.494(12)	N(3)-C(22)	1.468(4)
		N(4)-C(26)	1.460(12)	N(4)-C(26)	1.455(4)
		Angles (°)			
C(12)-N(2)-C(13)	125.5(3)	C(11)-N(1)-C(12)	119.8(9)	C(11)-N(1)-C(12)	120.3(2)
C(13)-N(2)-C(11)	125.9(4)	C(12)-N(1)-C(1)	120.2(9)	C(12)-N(1)-C(1)	119.1(2)
C(11)-N(2)-C(12)	108.3(4)	C(1)-N(1)-C(11)	119.9(9)	C(1)-N(1)-C(11)	120.6(2)
C(12)-N(1)-C(1)	125.9(3)	C(11)-N(2)-C(15)	116.9(8)	C(11)-N(2)-C(15)	118.5(2)
C(1)-N(1)-C(10)	125.6(4)	C(15)-N(2)-C(9)	121.4(8)	C(15)-N(2)-C(9)	120.1(2)
C(10)-N(1)-C(12)	108.5(4)	C(9)-N(2)-C(11)	121.5(9)	C(9)-N(2)-C(11)	121.1(2)
		C(25)-N(3)-C(22)	124.9(9)	C(25)-N(3)-C(22)	125.0(3)
		C(22)-N(3)-C(23)	125.4(9)	C(22)-N(3)-C(23)	125.6(3)
		C(23)-N(3)-C(25)	109.6(9)	C(23)-N(3)-C(25)	108.9(2)
		C(25)-N(4)-C(26)	126.5(9)	C(25)-N(4)-C(26)	124.4(2)
		C(26)-N(4)-C(24)	125.4(9)	C(26)-N(4)-C(24)	126.9(2)
		C(24)-N(4)-C(25)	108.1(9)	C(24)-N(4)-C(25)	108.7(2)
N(2)-C(12)-N(1)	108.5(4)	N(1)-C(11)-N(2)	123.3(10)	N(1)-C(11)-N(2)	123.9(3)
		N(3)-C(25)-N(4)	108.1(9)	N(3)-C(25)-N(4)	108.2(3)

Deprotonation reactions for both the ortho and the meta salts **2.6** and **2.7** were attempted using lithium bis(trimethyl)silylamide. The reaction of **2.6** with two equivalents of LiHMDS lead to the isolation of a brown sticky product. The ^{1}H NMR of this sticky solid was complicated and could not be interpreted. Attempts to isolate a single pure product from the sticky solid have so far been unsuccessful. The orthoxylyl salt was deprotonated using a similar method (Scheme 2.9) and a bright orange powder was isolated after work-up. The ^{1}H NMR suggested that the product of this reaction might be the dimerized carbene due to the presence of two set of doublets for the CH_2 groups in the bridging xylyl group, a feature reminiscent of the CH_2 group in benzyl group for the dimerized carbene **2.1**.

Scheme 2.9

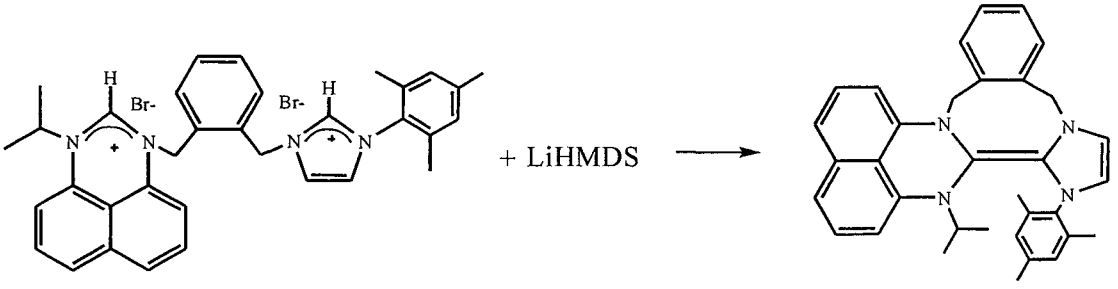

2.7 **2.8**

Our suspicions were confirmed by X-ray crystallography. Table 2.7 presents the crystal data and structure refinement parameter and Table 2.8 gives selected bond distances and angles for compound **2.8**. The structure shows that the C=C bond length is similar to

what was observed in **(2.1)$_2$** dimers with a value of 1.370(6) Å. N(2) and N(4) are planar in this enetetramine with the sum of the angles surrounding them being 359.7 and 359.9° respectively. The other two nitrogen centers deviate from planarity with N(1) having a sum of angles of 341.5° and the sum of the angles around N(3) being 350.8°. The average bond length for the N-C_{olefin} bonds is of 1.401Å this is slightly longer than what was observed in the free bis-carbene that had an average N-$C_{carbene}$ bond length of 1.359Å. The N-$C_{naphthalene}$ bond lengths where on average 1.418 Å the exact same as in the bis-carbene.

Table 2.7 Selected Crystal Data and Structure Refinement Parameters for **2.8**.

Empirical formula	**$C_{37}H_{42}N_4$**
Formula weight	542.75
Temperature (K)	207(2)
Wavelength (Å)	0.71073
Crystal system	Triclinic
Space group	P-1
a (Å)	10.527(4)
b (Å)	10.819(4)
c (Å)	15.439(5)
α(deg)	97.628(8)
β(deg)	101.604(9)
γ(deg)	96.202(7)
V (Å^3)	1690.7(10)
Z	2
ρ(calc) (Mg/m^3)	1.066
μ (mm^{-1})	0.063
Absorption correction	Semi-empirical from equivalents
Final R indices [I>2σ(I)]	
R1[a]	0.0790
***w*R2**[b]	0.1254

[a] $R1 = \Sigma \| F_o | - | F_c \| / \Sigma | F_o |$

[b] $wR2 = (w(| F_o | - | F_c |)^2 / \Sigma w | F_o |^2)^{1/2}$

Table 2.8. Selected bond length (Å) and angle (°) for compound **2.8.**

Bond lengths (Å)		Angles (°)	
N(1)-C(11)	1.397(5)	C(11)-N(1)-C(1)	110.1(4)
N(2)-C(11)	1.412(5)	C(1)-N(1)-C(12)	115.9(4)
N(3)-C(25)	1.387(5)	C(12)-N(1)-C(1)	115.5(4)
N(4)-C(25)	1.408(5)	C(11)-N(2)-C(9)	118.1(4)
N(1)-C(1)	1.453(6)	C(9)-N(2)-C(15)	120.9(4)
N(2)-C(9)	1.382(5)	C(15)-N(2)-C(11)	120.7(3)
N(3)-C(23)	1.404(5)	C(25)-N(3)-C(23)	108.3(4)
N(4)-C(24)	1.406(5)	C(23)-N(3)-C(22)	120.7(4)
N(1)-C(12)	1.486(6)	C(22)-N(3)-C(25)	121.8(4)
N(2)-C(15)	1.480(5)	C(25)-N(4)-C(24)	107.6(4)
N(3)-C(22)	1.466(6)	C(24)-N(4)-C(26)	122.7(4)
N(4)-C(26)	1.426(6)	C(26)-N(4)-C(25)	129.6(4)
C(11)-C(25)	1.370(6)	N(1)-C(11)-N(2)	117.9(4)
		N(3)-C(25)-N(4)	106.3(4)

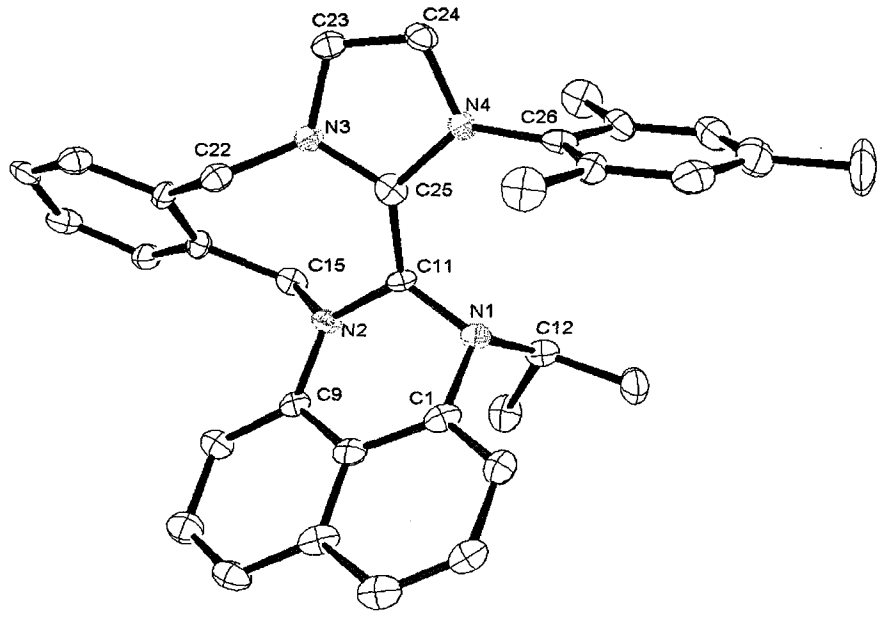

Figure 2.9. Molecular structure and atom-numbering scheme showing the enetetramine **2.8**. Thermal ellipsoids are drawn at 20% probability. Hydrogen atoms have been omitted for clarity.

A Gold Carbene Complex

Gold carbene complexes have become very widespread in the literature over the past few years and their value in catalysis is increasing. This extreme interest in gold carbene complexes has motivated us to try to isolate gold complexes with carbene (**I**). Our initial attempt to introduce carbene **I** to the $AuPPh_3Cl$ complexes involved the reaction of an equimolar ratio of **I** and $AuPPh_3Cl$ in dichloromethane. A yellow solid was isolated from this reaction mixture and analyzed by ^1H NMR. The spectrum showed two doublets for the isopropyl substituents with different integration values indicating the presence of two products. This powder was recrystallized and the X-ray experiment showed that one of the products obtained was a cationic gold complex with two carbenes and a chloride anion

(Scheme 2.10). To try to isolate the gold complex with only one carbene on the metal center the reaction was attempted with less than one equivalent of carbene and in a more dilute solution but this continued to give two products. We were able to isolate a pure sample of the cationic complex by stirring an excess of (1,3-(iPr)2-perimidin-2-ylidene) with $AuClPPh_3$ overnight. The ^1H NMR of the yellow powder obtained from this reaction show the presence of only one product. The ^{13}C NMR spectrum suggests that the carbene has coordinated to the gold center due to the downfield shift from 241.7 ppm in the free carbene to 200.0 ppm in the gold complex.

Scheme 2.10

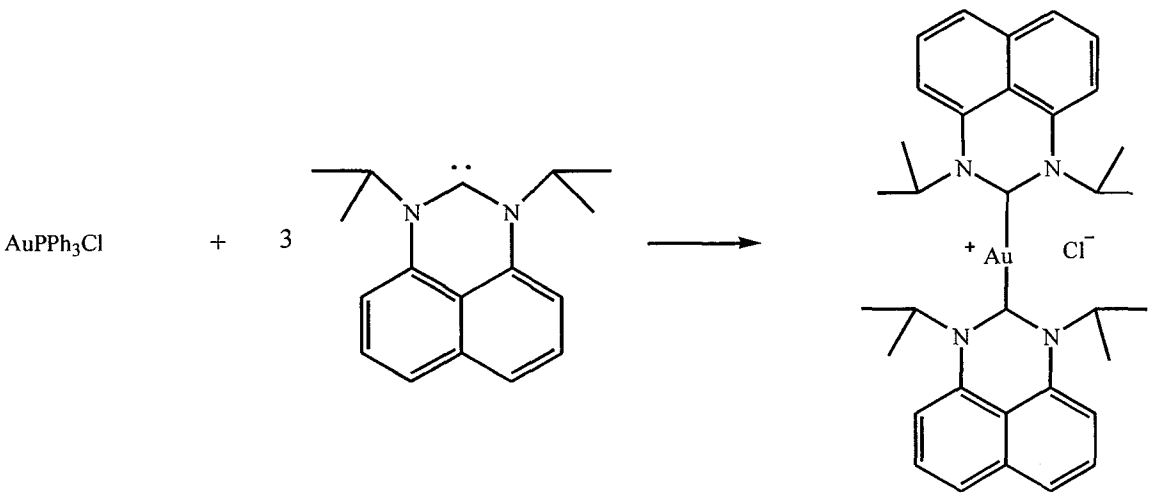

2.9

The product of this reaction was further characterized by crystallography and the molecular structure is shown in Figure 2.10. Selected bond distance and angles are provided in Table 2.10. The structure showed the presence of two carbenes with the planes of these two ligands forming a 73.7° angle. The gold $C_{carbene}$ distance for this complex is of

2.06(2)Å which is in the same range as the bond length observed for the cationic gold carbene complexes of the five membered ring carbenes **A** and **B**.[24] The average N-$C_{carbene}$ distances is 1.37 Å and the N-$C_{naphtyl}$ average distance is longer at 1.48 Å indicating that the nitrogen lone pair is more involved in bonding with the carbene center than with the naphthyl ring. Both naphthalene nitrogen are planar with the some of the angles surrounding them being 359.3 and 359.9° respectively for N(1) and N(2).

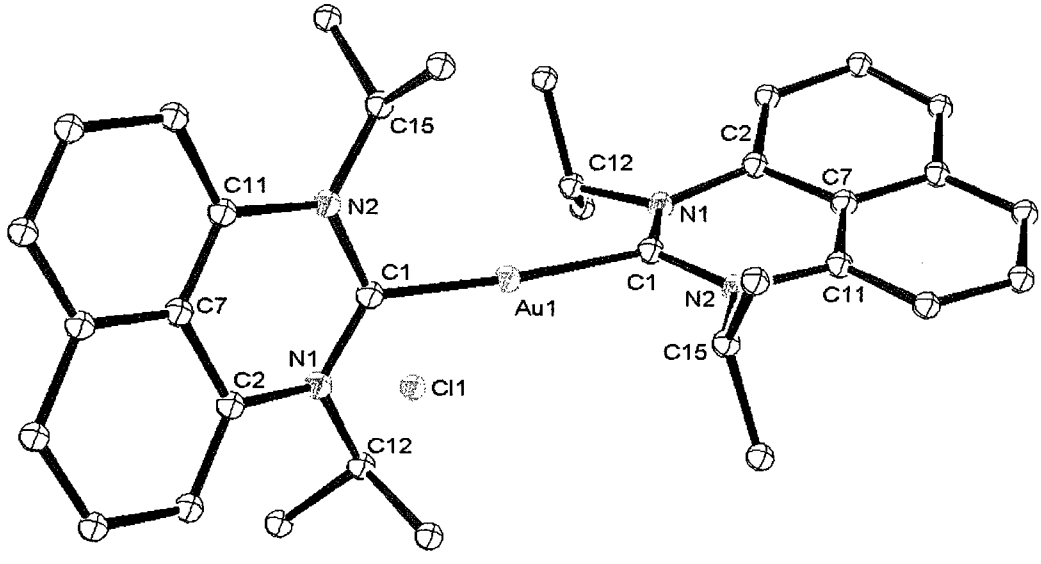

Figure 2.10. Molecular structure and atom-numbering scheme showing gold carbene complex **2.9**. Thermal ellipsoids are drawn at 20% probability. Hydrogen atoms have been omitted for clarity.

Table 2.9. Selected Crystal Data and Structure Refinement Parameters for **2.9.**

Compound	**2.9**
Empirical formula	$C_{34}H_{40}AuClN_4$
Formula weight	737.13
Temperature (K)	203(2)
Wavelength (Å)	0.71073
Crystal system	Orthorhombic
Space group	C222(1)
a (Å)	16.114(6)
b (Å)	17.840(6)
c (Å)	10.731(4)
α(deg)	90
β(deg)	90
γ(deg)	90
V (Å^3)	3084.7(19)
Z	4
ρ(calc) (Mg/m^3)	1.587
μ (mm^{-1})	4.885
Absorption correction	Semi-empirical from equivalents
Final R indices [I>2σ(I)]	
R1[a]	0.0633
***w*R2**[b]	0.1516

[a] $R1 = \Sigma \| F_o | - | F_c \| / \Sigma | F_o |$

[b] $wR2 = (w(| F_o | - | F_c |)^2 / \Sigma w | F_o |^2)^{1/2}$

Table 2.10. Selected bond Distances (Å) and Angles (°) for **2.9**

Bond lengths (Å)		Angles (°)	
Au-$C_{carbene}$	2.06(2)	N(1)-$C_{carbene}$-N(2)	122(2)
N(1)-$C_{carbene}$	1.33(3)	C(1)-N(1)-C(12)	117.1(18)
N(2)-$C_{carbene}$	1.40(3)	C(1)-N(1)-C(2)	120.0(18)
N(2)-C(11)	1.50(3)	C(12)-N(1)-C(2)	122.2(17)
N(1)-C(2)	1.45(3)	C(1)-N(2)-C(11)	118.9(18)
N(1)-C(12)	1.45(3)	C(15)-N(2)-C(11)	119(2)
N(2)-C(15)	1.41(3)	C(1)-N(2)-C(15)	122 (2)
Au-Cl	3.695	C(1)#1-Au-C(1)	168.2(14)

III. Conclusion

We have been able to prepare a series of perimidium and perimidium/imidozolium mixed salts bridged by xylyl groups. The deprotonation of these salt has lead to the isolation of free bis(carbene) in the case of the bis(perimidium) salt bridge by the metaxylyl isomer and to the isolation if an enetetramine for the ortho perimidium/imidozolium salt. Studies of one of our mono carbene showed that the dimerization of this carbene is possible when it is heated and shows no reversibility. Finally, we demonstrated that perimidine-based carbenes can function as ligands for catalytically relevant metals such as gold through the isolation of a cationic gold complex with the diisopropyl carbene.

IV. Experimental Section

General Methods. Synthesis of all salts was carried out in air and all other manipulations were carried out in either a nitrogen-filled drybox or under nitrogen using standard Schlenk line techniques. Unless otherwise noted, solvents were sparged with nitrogen and then dried by passage through column of activated alumina using an apparatus purchased from Anhydrous Engineering. Deuterated benzene and dichloromethane were dried by vacuum transfer from dried molecular sieve. $AuPPh_3Cl$ was purchased from Strem and used without further purification. Lithium bis(trimethyl)silylamide, α,α'-dibromo ortho xylene, α,α'-dibromo-meta xylene, deuterated chloroform and deuterated dimethyl sulfoxide where purchased from Aldrich and used without further purification. ^1H NMR spectra were run on either a Bruker Avance 300 MHz or a Varian INOVA 500 MHz spectrometer with deuterated benzene, methylene chloride, chloroform or dimethyl sulfoxide as a solvent and internal standard. Elemental analyses were carried out by Robertson Microlit Laboratories, Inc, Madison N.J or Midwest Microlab, LLC, Indianapolis, IN and by Guelph Chemical Laboratories Ltd., Guelph, ON. $C_{10}H_6N_2(^iPr)CH$ was prepared following a published method[25]. $C_{10}H_6(^iPrN)_2C$ and $C_{10}H_6(c\text{-}C_7H_{13}N)(CH_3C_6H_4CH_2N)C$ and 1-(mesityl)imidazole[26] where prepared using literature methods.

Spectroscopic Observation of Formation of 2.1.

In a glovebox, a sample of **IV** was dissolved in C_6D_6 and placed in a Teflon capped NMR tube. An initial ^1H NMR spectrum confirmed the sample to be carbene **IV**. The NMR sample was then heated to 80 °C for 24 h followed by further heating to 80 °C for 24 h. A

^{1}H NMR spectrum of this sample confirmed the transformation of the starting material, and the following ^{1}H NMR was obtained:

^{1}H NMR δ 7.60-6.60 (br m, 20H, CH), 5.51 (d, 1H, NCH_2), 5.22 (d, 1H, NCH_2), 4.98 (d, 1H, NCH_2), 4.48 (d, 1H, NCH_2), 3.25 (br m, 2H, NCH), 2 .04 (s, 3H, CH_3), 1.96 (s, 3H, CH_3), 1.70-0.80 (br m, 24H, CH_2).

Heating for an additional 24 h did not result in any further change in the ^{1}H NMR spectrum. We were able to isolate a sample of one of the components of this mixture and obtain the following NMR spectra.

^{1}H NMR (300 MHz, CD_2Cl_2): δ 7.37-6.87 (m, 18H, CH), 6.60 (d, 2H, CH), 5.21 (d, 2H, CH_2), 5.06 (d, 2H, CH_2), 3.19 (br, 2H, NCH), 2.22 (s, 6H, CH_3), 1.85 (br, 2H, CH_2), 1.28 (br m, 18H,CH_2) 1.01 (br m, 4H, CH_2).

^{13}C{^{1}H} NMR (75 MHz, CD_2Cl_2): δ 143.3, 143.0, 137.0, 136.7, 135.9, 132.5, 129.3, 128.2, 127.1, 126.9, 121.3, 119.9, 116.8, 115.1, 104.4, 67.4 (CH_2), 52.6 (N-CH), 37.2 (CH_2),34.5 (CH_2), 32.9 (CH_2), 28.6 (CH_2), 27.8 (CH_2), 25.3 (CH_2), 25.0(CH_3)

Preparation of [α,α'-di(1-^{i}Pr perimidinium) meta-xylene] dibromide (2.2)

In a round bottom flask equipped with a magnetic stir bar and a condenser 1-isopropylperimidine (2.0 g, 9.5 mmol) and dibromo-meta-xylene (1.28 g, 4.8 mmol) were dissolved in approximately 30 ml of toluene. The mixture was heated to reflux for 6 hours. The product, a yellow powder was isolated by filtration and dried under vacuum (3.05 g, 93%).

^{1}H NMR (DMSO-d_6, 500 MHz) : δ 1.78 (d, 12H, CH_3), 4.90 (s, 2H, CH), 6.89-8.03 (m, 16H, Ar-H), 9.41 (s, 2H, C^+H).

$^{13}C\{^1H\}$ (DMSO-d_6, 125 MHz) : δ 20.1 (s, CH_3), 52.5 (s, CH_2), 54.5 (s, CH), 108.3 (C_{Ar}), 108.7 (C_{Ar}), 121.3 (C_{Ar}), 123.5 (C_{Ar}), 123.9 (C_{Ar}), 126.0 (C_{Ar}), 127.1 (C_{Ar}), 127.7 (C_{Ar}), 128.4 (C_{Ar}), 129.5 (C_{Ar}), 131.4 (C_{Ar}), 131.8 (C_{Ar}), 133.70 (C_{Ar}), 134.37 (C_{Ar}), 151.2 (C^+H).

Preparation of bis-carbene 2.3

In a round bottom flask equipped with a magnetic stir bar a suspension of [α,α'-di(1-^{i}Pr perimidinium) meta-xylene] dibromide (1.39 g, 2.12 mmol) was suspended in approximately 30 ml of chlorobenzene. To this suspension was added LiHMDS (0.69 g, 4.12 mmol) and the reaction mixture is stirred for 4 hours. The solvent is then removed under vacuum. The product is extracted with toluene, filtered through celite, dried under vacuum, and recrystallized from toluene to give an off white powder (0.53 g, 50%). The product can be crystallized from toluene at -20°C to obtain crystal suitable for X-ray diffraction experiments.

^{1}H NMR (C_6D_6, 500MHz) δ 1.43 (d, 12H, CH_3), 3.25 (m, 2H, CH), 5.19 (s, 4H, CH_2), 6.14 (d, 2H, CH), 6.32 (d, 2H, CH), 6.80 (t, 2H, CH), 6.81-7.15 (m, 9H, CH_{Ar}), 7.37 (s, 2H, CH).

$^{13}C\{^1H\}$ NMR (C_6D_6, 125MHz) δ 22.4 (CH_3), 51.5 (CH), 60.8 (CH_2), 103.4 (C_{Ar}), 105.2 (C_{Ar}), 119.7 (C_{Ar}), 119.9(C_{Ar}) , 122.4 (C_{Ar}), 125.1 (C_{Ar}), 125.6 (C_{Ar}), 128. (C_{Ar}), 129.2 (C_{Ar}), 133.1 (C_{Ar}), 133.5(C_{Ar}) , 135.6 (C_{Ar}), 138.0 (C_{Ar}), 245.3 ($C_{carbene}$).

Preparation of meta imidozolium salt (2.4)

In a 250 mL round bottom flask, mesityl imidazole (4.4 g, 23.7 mmol) was dissolved along with m-dibromo-xylene (12.5 g, 45.5 mmol) in 150 mL of ether. The solution was stirred for 3 days to yield a white precipitate. The white precipitate was filtered through a glass frit and washed with ether to yield a white powder in 66% yield (7.02 g, 15.6 mol). The white powder can be crystallized from hot acetone to obtain crystal suitable for X-ray diffraction experiment.

^{1}H NMR ($CDCl_3$, 500 MHz): δ 1.84 (s, 6H, CH_3), 2.14-2.13 (s, 3H, CH_3), 4.30-4.29 (s, 2H, CH_2), 5.76 (s, 2H, CH_2), 6.79-6.78 (s, 2H, Ar), 7.49-7.06 (m, 4H, Ar), 7.60-7.59 (s, 1H, H), 8.01-7.99 (s, 1H, CH), 10.28 (s, 1H, NCHN).

$^{13}C\{^1H\}$ NMR ($CDCl_3$, 125 MHz): δ 17.24 ($ArCH_3$), 20.7 ($ArCH_3$), 32.4 (CH_2), 52.1 (CH_2), 123.0 (CH_{olefin}), 123.20 (CH_{olefin}), 128.7 (CH), 129.2 ($C_{Ar}H$), 129.3 ($C_{Ar}H$), 129.4 ($C_{Ar}H$), 129.5 (C_{Ar}), 130.2 (C_{Ar}), 133.7 ($C_{Ar}H$), 134.1 (C_{Ar}), 136.8 (C_{Ar}), 138.5 (C_{Ar}), 140.68 (C^+H).

Anal. Calcd: C 62.64, H 6.57, N 9.13; Found: C 62.37, H 6.30, N 9.24.

Preparation of ortho imidozolium salt (2.5)

In a 250 mL round bottom flask, mesityl imidazole (4.4 g, 23.7 mmol) was dissolved along with o-dibromo-xylene (12.5 g, 45.5 mmol) in 150 mL of ether. The solution was stirred for 3 days to yield a white precipitate. The white precipitate was

filtered through a glass frit and washed with ether to yield a white powder in 94% yield (10.1 g, 22.2 mmol). The product can be crystallized from hot acetonitrile to obtain crystal suitable for X-ray diffraction experiments.

^{1}H NMR ($CDCl_3$, 500 MHz): δ 2.01 (s, 6H, CH_3), 2.25 (s, 3H, CH_3), 4.79 (s, 2H, CH_2), 6.11 (s, 2H, CH_2), 6.90 (s, 2H, Ar), 7.15 (s, 1H, CH), 7.35-7.24 (m, 3H, Ar), 7.50-7.49 (m, 1H, Ar), 7.67 (s, 1H, CH), 10.28 (s, 1H, NCHN).

$^{13}C\{^1H\}$ NMR ($CDCl_3$, 125 MHz): δ 17.8 ($ArCH_3$), 20.9 ($ArCH_3$), 31.3 (CH_2), 50.5 (CH_2), 123.0 (CH_{olefin}), 123.0 (CH_{olefin}), 129.7 ($C_{Ar}H$, 2 overlapping), 130.2 ($C_{Ar}H$),), 130.5 (C_{Ar}), 131.12 (C_{Ar}), 131.28 (C_{Ar}), 131.6 ($C_{Ar}H$), 134.0 ($C_{Ar}H$), 137.4 (C_{Ar}), 137.6 (C_{Ar}), 141.0 (C^+H).

Anal. Calcd: C53.36, H 4.93, N 6.22; Found: C 53.70, H 4.89, N 6.30.

Preparation of meta bridged imidozolium and perimidium salt (2.6)

The meta imidozolium (**2.4**) salt (8.64 g, 19.1 mmol) was added to $C_{10}H_6N_2(^i Pr)CH$ (4.07 g, 19.4 mmol) and both were dissolved in 150 mL of acetonitrile in a 250 mL round-bottom flask. The solution was stirred and heated to 80℃ for two days. The solvent was removed under vacuum to yield an orange powder. The powder was stirred in acetone for an hour and then filtered, washed with acetone and washed with ether to yield 10.25 g (15.5 mmol, 82%) of a bright yellow powder. The yellow powder was crystallized from hot ethanol to obtain crystals suitable for X-ray experiments.

^{1}H NMR ($CDCl_3$, 500 MHz): δ 1.79 (d, 6H, CH_3), 1.86 (s, 6H, CH_3), 2.22 (s, 3H, CH_3), 4.57 (sept, 1H, CH), 5.60 (s, 2H, CH_2), 5.75 (s, 2H, CH_2), 7.68-6.82 (m, 12H, Ar), 8.23 (s, 1H, CH), 8.43 (s, 1H, CH), 9.90 (s, 1H, NCHN), 10.31 (s, H, NCHN),

$^{13}C\{^1H\}$ NMR ($CDCl_3$, 125 MHz): δ 17.7 ($ArCH_3$), 20.8 ($CH(CH_3)$), 21.1 ($ArCH_3$), 52.1 (CH_2), 54.5 ($CH(Me)_2$), 55.1 (CH_2), 108.3 (CH_{olefin}), 109.4 (CH_{olefin}), 121.9 ($C_{Ar}H$), 123.1 ($C_{Ar}H$), 124.2 ($C_{Ar}H$), 124.4 (C_{Ar}), 124.6 ($C_{Ar}H$), 128.2 (C_{Ar}), 128.4 (C_{Ar}), 128.6 (C_{Ar}), 129.3 (C_{Ar}), 129.4 ($C_{Ar}H$), 129.8 ($C_{Ar}H$), 130.2 ($C_{Ar}H$), 130.7 ($C_{Ar}H$), 131.3 (C_{Ar}), 131.6 (C_{Ar}), 133.2 (C_{Ar}), 134.1 ($C_{Ar}H$), 135.0 ($C_{Ar}H$), 135.2 ($C_{Ar}H$), 137.1 (C_{Ar}), 141.1 (C^+H), 150.7 (C^+H),

Anal. Calcd: C 61.83, H 5.49, N 8.48; Found: C 61.70, H 5.93 N 8.48

Preparation of ortho bridged imidozolium and perimidinium salt (2.7)

Imidozolium salt **2.5** (5.82 g, 27.7 mmol) and $C_{10}H_6N_2(^iPr)CH$ (8.7g ,41.6mmol) both were dissolved in 150 mL of acetonitrile in a 250 mL round-bottom flask. The solution was stirred and heated to 80℃ over two days. The solvent was removed under vacuum to yield an orange powder. The powder was stirred in acetone for an hour and then filtered, washed with acetone and washed with ether to yield 13.2 g (19.9 mmol, 72%) of a bright yellow powder. The yellow powder can be crystallized from hot methanol to obtain crystals suitable for X-ray diffraction.

^{1}H NMR ($CDCl_3$, 500 MHz): δ 1.67 (d, 6H, CH_3), 2.02 (s, 6H, CH_3), 2.22 (s, 3H, CH_3), 4.55-4.54 (sept, H, CH), 6.22 (s, 2H, CH_2), 6.33 (s, 2H, CH_2), 7.27-6.89 (m, 11H, Ar),

7.39-7.36 (s, H, CH), 7.44-7.42 (s, 1H, Ar), 8.35(s, 1H, CH), 9.90 (s, 1H, NCHN), 10.28 (s, 1H, NCHN),

$^{13}C\{^{1}H\}$ NMR ($CDCl_3$, 125 MHz): δ 17.8 ($ArCH_3$), 21.0 ($ArCH_3$), 21.1 ($CH(CH_3)_2$), 50.0 (CH_2), 52.4 (CH_2), 54.1 ($CH(Me)_2$), 108.2 (CH_{olefin}), 110.1(CH_{olefin}), 121.5 (C_{Ar}), 123.4 ($C_{Ar}H$), 124.6 ($C_{Ar}H$), 124.9 ($C_{Ar}H$), 125.0 ($C_{Ar}H$), 125.1 (C_{Ar}), 128.2 (C_{Ar}), 128.6 (C_{Ar}), 128.8 ($C_{Ar}H$), 128.9 ($C_{Ar}H$), 129.4 ($C_{Ar}H$), 129.8 ($C_{Ar}H$), 130.6 (C_{Ar}), 130.8 (C_{Ar}), 131.2 (C_{Ar}), 131.4 (C_{Ar}), 132.1 ($C_{Ar}H$), 134.1 ($C_{Ar}H$), 135.0 (C_{Ar}), 137.6 ($C_{Ar}H$), 141.1 ($C^{+}H$), 150.8 ($C^{+}H$).

Anal. Calcd: C 61.83, H 5.49, N 8.48; Found: C 61.60, H 5.86, N 8.03

Preparation of enetetramine (2.8)

The yellow powder, compound **2.7**, was dissolved in 150 mL of dichloromethane in a 250 mL round-bottom flask. Silver tosylate was added to the solution. The flask was covered with aluminum foil and allowed to stir over a period of 5 days. The solution was filtered through celite in a glass frit. The yellow filtrate was dried under vacuum to yield 19 g (27.9 mmol) of a yellow powder. The yellow tosylate salt was brought into a dry box containing a nitrogenous atmosphere. In a 250 mL round bottom flask, (5g, 5.91 mmol) of the yellow tosylate salt was added to of lithium tetramethylsilyl amide (2.18 g, 13.0 mmol) base in 100 mL of chlorobenzene. The reaction mixture was stirred overnight. The next day the chlorobenzene was removed under vacuum and the product was extracted with toluene

to afford an orange solid (1.79 g, 74%). The orange solid was crystallized from hexanes to obtain crystals suitable for X-ray diffraction experiment.

^{1}H NMR (C_6D_6, 300 MHz): δ 0.63 (d, 3H, $CH(CH_3)_2$), 0.73 (d, 3H, $CH(CH_3)_2$), 2.18 (s, 3H, $ArCH_3$), 2.22 (d, 6H, $ArCH_3$), 2.81 (sept, 1H, $CH(Me)_2$), 3.94 (dd, 2H, CH_{olefin}), 4.87 (dd, 2H, CH_2), 5.52 (dd, 2H, CH_2), 6.35 (d, 1H, CH_{Ar}), 6.67-6.72 (m, 2H, CH_{Ar}), 6.82 (s, 1H, CH_{Ar}), 6.91 (s, 1H, CH_{Ar}), 6.99-7.16 (m, 5H, CH_{Ar}), 7.28 (t, 1H, CH_{Ar}), 7.45 (d, 1H, CH_{Ar})

Preparation of $Au(C_{10}H_6(iPrN)_2C)_2Cl$ (2.9)

$AuClPPh_3$ (195 mg, 0.39 mmol) and carbene (1,3-(iPr)2-perimidin-2-ylidene) (300 mg, 1.19 mmol) were weighed in a vial and dissolved in 15 ml of toluene. The solution was stirred for 48h. The yellow precipitate that formed was filtered and dried (295 mg, 74%). Crystals suitable for X-ray diffraction were obtained from crystallization in methylene chloride at -20°C.

^{1}H NMR (CD_2Cl_2, 300 MHz): 1.85 (d, 12H, CH_3), 6.02 (br, 2H, $CH(Me)_2$), 7.11(d, 2H CH_{Ar}), 7.37-7.52 (m,4H, CH_{Ar})

$^{13}C\{^1H\}$ NMR (CD_2Cl_2, 75 MHz) 19.2 $(\mathbf{CH_3})_2CH$, 63.5 $(Me_3)_2\mathbf{CH}$, 109.3 $C_{Ar}H$, 121.8 C_{Ar}, 122.6 $C_{Ar}H$, 127.4 $C_{Ar}H$, 131.5 C_{Ar}, 135.3 C_{Ar}, 200.0 C_{carb}.

Anal. Calcd for $C_{36}H_{40}N_4AuCl$: C 55.40, H 5.47, N 7.60. Found: C 55.28, H 5.59, N 7.52

Structural determination of trans-$(2.1)_2$, cis-$(2.1)_2$, 2.3, 2.5, 2.6, 2.7, 2.8 and 2.9. Single crystals were mounted on a thin glass fibre and held using viscous oil. They were subsequently cooled to data collection temperature. Crystal data and details of the measurements are summarized in table 2.1, 2.3, 2.5, 2.7 and 2.9. Data were collected on a Bruker AX SMART 1k CCD diffractometer using 0.3° ω-scans at 0, 90, 180° in Φ. Unit-cell parameters were determined from 60 data frames collected at different sections of the Ewald sphere. Semi-empirical corrections based on equivalent reflections were applied (Blessing, R., *Acta Cryst.*, **1995**, A51, 33-38). The structures were solved by direct method, completed with difference Fourier synthesis and refined with full-matrix least-squared procedures based on F^2. All non-hydrongen atoms were refined with anisotropic displacement parameters. All hydrogen atoms were treated as idealized contributions. All scattering factors and anomalous dispersion factors are contained in the SHELXTL 5.1 program library (Sheldrick, G. M. AXS, Madison, WI, 1997).

References

[1] (a) Jafarpour, L.; Nolan, S. P. *J. Organomet.Chem.* **2001**, *617*, 17. (b) Denk, K.; Sirsch, P.; Herrmann, W. A. *J. Organomet. Chem.* **2002**, *649*, 219. (c) Weskamp, T.; Kohl, F. J.; Hieringer, W.; Gleich, D.; Herrmann, W. A. *Angew. Chem., Int. Ed.* **1999**, *38*, 2416. (d) Huang, J.; Jafarpour, L.; Hillier, A. C.; Stevens, E. D.; Nolan, S. P. *Organometallics* **2001**, *20*, 2878. (e) Chianese, A. R.; Li, X.; Janzen, M. C.; Faller, J. W.; Crabtree, R. H. *Organometallics* **2003**, *22*, 1663. (f) Huang, J.; Schanz, H.-J.; Stevens, E. D.; Nolan, S. P. *Organometallics* **1999**, *18*, 2370.

[2] Hoffmann, R. *J. Am.Chem. Soc.* **1968**, 90, 1475.

[3] Arduengo, A. J.; Harlow, R.L; Kline, M. *J. Am. Chem. Soc.* **1991**, 113, 361.

[4] Despagnet-Ayoub, E.; Grubbs, R. H. *J. Am. Chem. Soc.* **2004**, *126*, 10198.

[5] Hahn, F. E.; Wittenbecher, L.; Le Van, D.; Fröhlich, R. *Angew. Chem. Int. Ed.* **2000**, 541.

[6] (a) Guillen, F.; Winn, C. L.; Alexakis, A. *Tetrahedron: Asymmetry,* **2001**, *12*, 2083. (b) Alder, R. W.; Blake, M. E.; Bortolotti, C.; Bufali, S.; Butts, C. P.; Linehan, E.; Oliva, J. M.; Orpen, A. G.; Quayle, M. J. *Chem. Commun.* **1999**, 241.

[7] Bazinet, P.; Yap, G. P. A.; Richeson, D. S. *J. Am. Chem. Soc.* **2003**, 125, 13314.

[8] (a) Scarborough, C. C.; Grady, M. J. W.; Guzei, I. A.; Gandhi, B. A.; Stahl, S. S. *Angew. Chem., I*{^{1}H} *nt. Ed.* **2005**, *44*, 5269. (b) Scarborough, C. C.; Popp, B. V.; Guzei, I. A.; Stahl, S. S. *J. Organomet. Chem.* **2005**, *690*, 6143.

[9] Handbook of Heterocyclic Chemistry, 2nd ed.; Katritzky, A. R., Pozharskii, A. F., Eds.:Pergamon: New York, **2000.**

[10] Bazinet, P.; Ong, T. G.; O'Brien, J. S.; Lavoie, N.; Bell, E.; Yap, G. P. A.; Korobkov, I.; Richeson, D. S. *Organometallics*, **2007**, *26* (11), 2885.

[11] Cetinkaya, E.; Hitchcock, P. B.; Jasim, H. A.; Lappert, M. F.; Spyropoulos, K. *J. Chem. Soc., Perkin Trans. 1* **1992**, 561.

[12] Taton, T. A.; Chen, P. *Angew. Chem., Int. Ed. Engl.* **1996**, *35*, 1011.

[13] Denk, M. K.; Thadani, A.; Hatano, K.; Lough, A. J. *Angew. Chem., Int. Ed. Engl.* **1997**, *36*, 2607.

[14] The dimerization of N-stabilized carbenes has recently been reviewed in: (a) Alder, R. W.; Blake, M. E.; Chaker, L.; Harvey, J. N.; Paolini, F.; Schutz, J. *Angew. Chem., Int. Ed.* **2004**, *43*, 5896. (b) Graham, D. C.; Cavel, K. J.; Yates, B. F. *J. Phys. Org. Chem.* **2005**, *18*, 298

[15] Hahn, F. E.; Paas, M.; Le Van, D.; Lügger, T. *Angew. Chem., Int. Ed.* **2003**, *42*, 5243.

[16] For reports of annelated carbenes see: (a) Hahn, F. E.; Wittenbecher, L.; Le Van, D.; Fro¨hlich, R. *Angew. Chem. Int. Ed.* **2000**, *39*, 541. (b) Liu,Y.; Lindner, P. E.; Lemal, D. M. *J. Am. Chem. Soc.* **1999**, *121*, 10626.

[17] Dixon, D. A.; Arduengo, A. J. III. *J. Phys. Chem.* **1991**, *95*, 4180.

[18] Heinemann, C.; Thiel, W. *Chem. Phys. Lett.* **1994**, *217*, 11.

[19] Cheng, M. J.; Hu, C. H. *Chem. Phys. Lett.* **2001**, *349*, 477.

[20] Carter, E. A.; Goddard, W. A. III. *J. Phys. Chem.* **1986**, *90*, 998.

[21] Dynamic dimerization of benzimidazole carbenes has been recently reported: Kamplain, J. W.; Bielawski, C. W. *Chem. Commun.* **2006**, 1727.

[22] Frisch, M. J., *et al. Gaussian 03*, Revision C.02; Gaussian, Inc.: Wallingford, CT, **2004**.

[23] (a) Arduengo A. J.; Goerlich' J. R.; Marshall, W. J. *J. Am. Chem. Soc.***1995**, *117*, 11027.

[24] (a) Baker, M. V.; Barnard, J. Berners-Price,; S. J.; Brayshaw, S. K.; Hickey, J. L.; Skelton, B. W.; White, A. H. *Dalton Trans.*, **2006**, 3708. (b) de Fremont, P.; Stevens, E. D.; Fructos, M. R.; Diaz-Requejob, M. M.; Perez, P. J.; Nolan, S. P.; *Chem. Commun.*, **2006**, 2045. (c) De Fremont, P.; Marion, N., Nolan, S. P. *J. Organomet. Chem.* **2009**, 694, 551.

[25] Bazinet, P. (**2004**), Diaminonaphthalene and Guanidine as Scaffolds for π-Cojugated Amido Ligands: versatile Supporting frameworks for Transition and Main group element, Unpublished thesis (Ph.D), University of Ottawa.

[26] Gardiner, M. G.; Herrmann, W. A.; Reisinger, C-L.; Schwarz, Jurgen. *Journal of Organometallic Chemistry.* **1999**, 572, 239.

Chapter 3

Lanthanide complexes

I. Introduction

Lanthanide complexes have been extensively studied due to their ability to catalyze many organic transformations including, for example, hydroamination,[1,2] hydrosilylation[3] Diels-Alder reactions,[4] hydrogenation of alkenes,[5] polymerization of α-olefins.[6] Ligand support for these complexes has been dominated by cyclopentadienyl-derived ligands. Recently more efforts have focused on the use of alkoxide and amido ligands to support the lanthanide centers. Examples of non-cyclopentadienyl rare-earth metal catalysts that are active for hydroamination[7] are represented by the amido-supported species **A**,[8] **B**,[9] **C**.[10] Catalysts such as **A** and **C** have been shown to be effective for hydroamination giving some

enantioselectivity , while complex **B** can effectively catalyze the reaction but showed no selectivity.

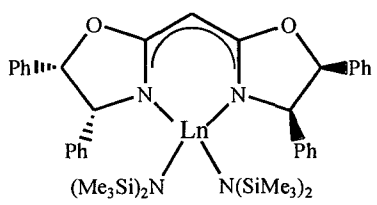

Ln= La, Nd, Sm

A

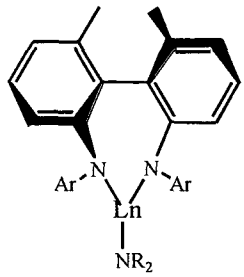

Ln= La, Sm, Y

B

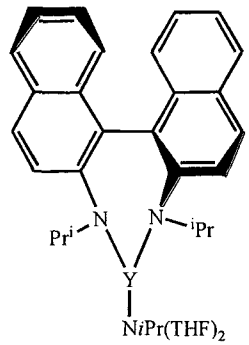

C

The introduction of amido ligands to lanthanides has not been as straightforward as one would expect. One of the major problems encountered when trying to introduce amido ligands to lanthanide centers using lithium amido reagents is the formation of "ate" complexes and retention of lithium in the product. Two general methods have been reported to minimize this problem. The first is by gentle heating of the product leading to the complete elimination of LiCl. The second has been to use heavier alkali metal salts to drive the elimination of the alkali metal halide by-product.

Examples for these two methods can be found for the introduction of β-diketiminate (NacNac) ligands that have recently been widely used in lanthanide chemistry.[11] One example for the synthesis of a β-diketiminate lanthanide complex is illustrated below[11b] (Equation 3.1). In this example the NacNac ligand reacts with lanthanide chloride to form an anionic "ate" complex that retains a lithium counter cation. Slowly heating this complex drives the elimination of LiCl and leads to the formation of the desired complex.

Equation 3.1

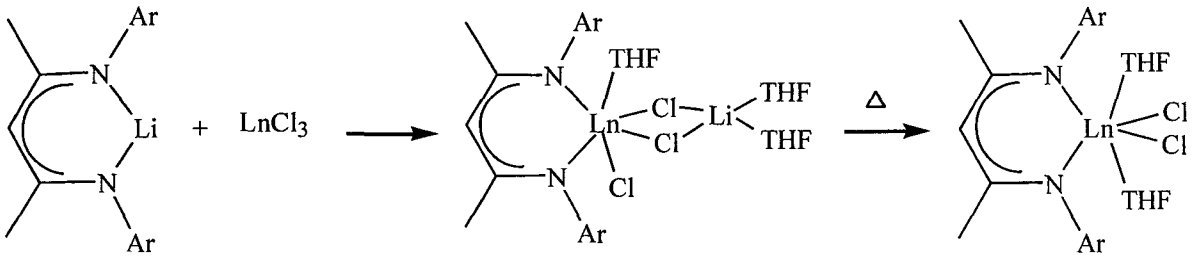

Ln= Yb,
Sm, Nd

The second strategy is represented by equation 3.2. In this case, LnI_3 is employed with potassium salts of the ligand in the synthesis of the complexes.[11f] With this approach we can see that no alkali metal is retained and one equivalent of potassium iodide is eliminated.

Equation 3.2

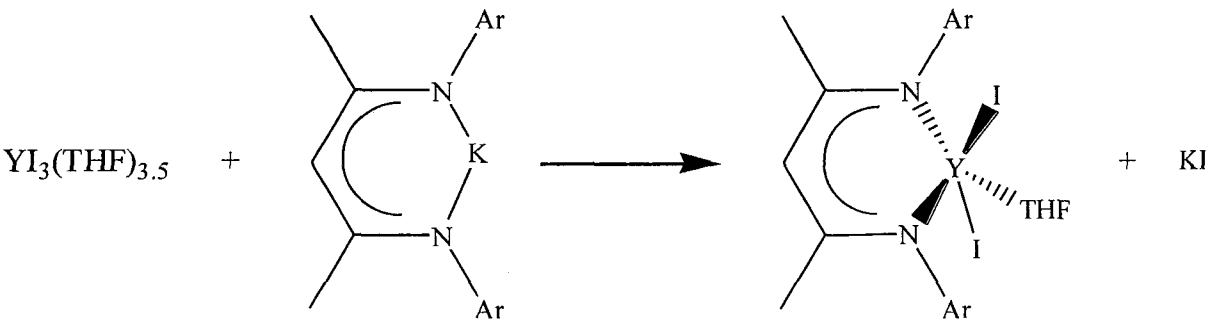

The structurally characterized β-diketiminate lanthanide complexes often display a ligand binding mode with the metallacycle in a non-planar or folded orientation. The metal center of the metallacycle often lies out of the plane of the β-diketiminate ligand to varying degree depending on the complex. The success that was observed in the synthesis of

lanthanide complexes bearing β-diketiminate ligands and these interesting structural observations motivated our efforts to employ R_2DAN ligands in the synthesis of lanthanide complexes and to study the structural features of these complexes. This chapter reports the results of these efforts

II. Results and Discussion

We first attempted the synthesis of lanthanide complexes bearing disubstituted 1,8-diaminonaphthalene ligands following the procedure outlined in Scheme 3.1. The reaction of the R_2DAN ligand with two equivalents of n-BuLi generated the dilithium dianionic species and this reaction was followed by the addition of $LnCl_3$ starting material. This process led to the formation of a range of colorful products with varying shades of green, orange and yellow. All of these reactions were attempted with both the isopropyl and aryl DAN ligands and with ligand-to-metal ratios of 1:1 and 2:1.

Scheme 3.1

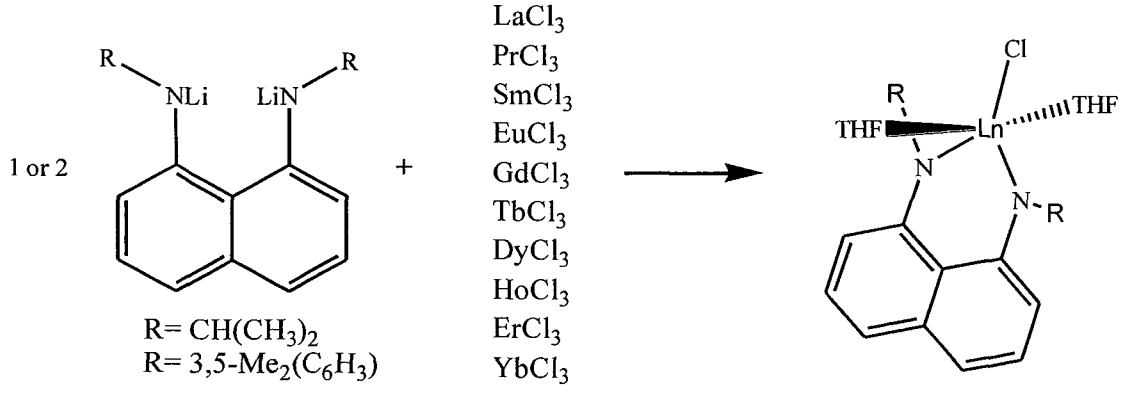

Due to the paramagnetic characteristics of the products, all of these reactions gave very broad ^{1}H NMR spectra that were not useful in product identification. Crystallization of these products was attempted. The limited solubility of the products required the use of mostly tetrahydrofuran and toluene as crystallization solvent. The first complex that was successfully crystallized was obtained from the reaction of two equivalents of the isopropyl DAN ligand with one equivalent of $YbCl_3(THF)_3$ (Scheme 3.2). This green product was crystallized from a mixture of toluene and ether to give crystals suitable for X-ray diffraction experiment.

Scheme 3.2

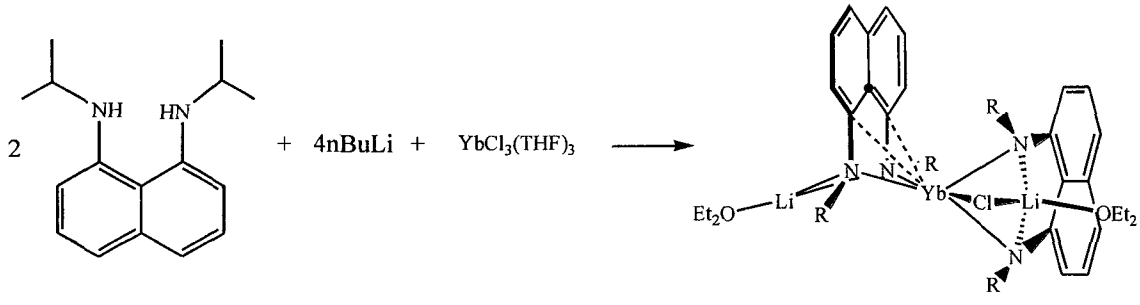

3.1

The results obtained from the X-ray crystallography experiment showed (Figure 3.1) that the product consisted of a ytterbium center coordinated by two R_2DAN ligands and one chloride. For charge balance the structure also contains two lithium atoms that are each coordinated by a R_2DAN ligand that is bridging with the ytterbium center. Each of the lithium centers is also coordinated by a diethylether from the crystallization solvent. One of the lithium centers also coordinates with the chloro group that bridges with the ytterbium. Tables 3.1 and 3.2 presents selected crystal data, structure refinement parameters and selected bond lengths and angles. The ytterbium center in this complex is in a distorted

trigonal bipyramidal geometry with the chloride and one of the N_{amido} groups in the axial position and the three remaining N_{amido} in the equatorial positions. Calculation of the τ factor can give us an idea of how distorted are complexes are (equation 3.1). When τ is close to 0 we have a complex with a square pyramidal geometry and τ closer to 1 is representative of trigonal bipyramidal geometry.

$$\tau = \frac{\theta - \Phi}{60^\circ} \quad \text{Equation 3.1}$$

θ = angle between the two axial groups

Φ= second largest angle

For complex 3.1 the τ factor 0.44 this value is smaller than expected for a trigonal bipyramydal geometry. This is due to the chelating ligand that has a small N-Yb-N angle causing the other angles to be larger and reducing the τ value. For this reason in this case and others seen later the geometry was assigned be visual observation. The N_{amido} ytterbium bond lengths in the complex had average values of 2.308Å, this is within the range of bond lengths that have been observed in β-diketiminate ligands that usually have N-Ln bond lengths varying from 2.25-2.40Å.[11b, 11e] The Yb-Cl bond length is 2.653(6)Å. The N_{amido}-Li bond lengths have average values of 2.18Å and 1.96Å for Li(1) and Li(2) respectively. The longer N_{amido}-Li bonds are observed at the lithium center that is also coordinated to the chloride atom making it more electron rich than the other lithium center therefore leading to a weaker donation of the ligand to the lithium. The bite angles for the ligands in this complex are of 77.0(7)°and 72.4(7)° , these angles are smaller than those

observed in NacNAc complexes that usually have N-Ln-N angles larger than 77°. These angles are also smaller than what we observed in early transition metal complexes bearing R_2DAN ligands.[12] The bite angle for the coordination to the Li are more similar to what we observed in the early transition metal complexes with values of 82.0(14)° and 89.3(17)°. The nitrogen atoms in this complex are in tetrahedral geometry.

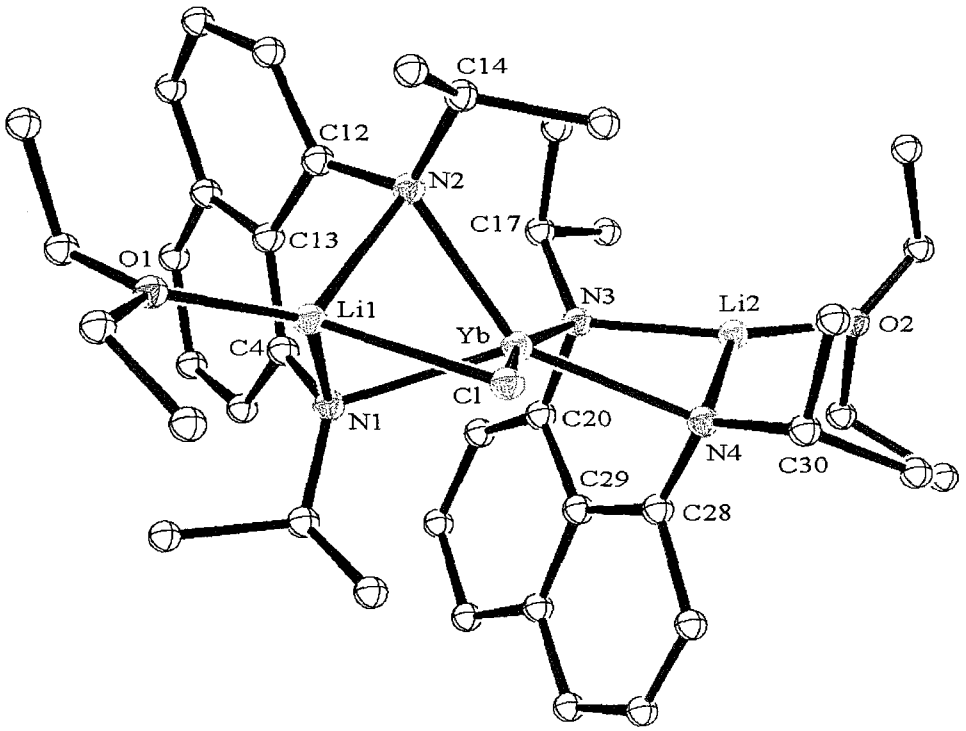

Figure 3.1. Molecular structure and partial atom-numbering schemes for **3.1**. Thermal ellipsoids are drawn at 20% probability. Hydrogen atoms have been omitted for clarity.

Table 3.1. Selected Crystal Data and Structure Refinement Parameters for **3.1**

Empirical formula	$C_{40}H_{61}ClLi_2N_4O_2Yb$
Formula weight	852.30
Temperature (K)	203(2)
Wavelength (Å)	0.7173
Crystal system	Triclinic
Space group	P-1
a (Å)	11.525(4)
b (Å)	12.302(6)
c (Å)	16.648(6)
α(deg)	81.735(7)
β(deg)	89.218(5)
γ(deg)	62.158(4)
V (Å^3)	2062.4(14)
Z	2
ρ(calc) (Mg/m^3)	1.372
μ (mm^{-1})	2.369
Absorption correction	Semi-empirical from equivalents
Final R indices [I>2σ(I)]	
R1[a]	0.1253
***w*R2**[b]	0.3339

[a] $R1 = \Sigma \| F_o | - | F_c \| / \Sigma | F_o |$

[b] $wR2 = (w(| F_o | - | F_c |)^2 / \Sigma w | F_o |^2)^{1/2}$

Table 3.2. Selected bond lengths (Å) and angles (°) for 3.1

Bond Lengths (Å)			
Yb-N(1)	2.275(17)	Yb-Li(2)	3.16(4)
Yb-N(2)	2.305(19)	N(1)-Li(1)	2.10(4)
Yb-N(3)	2.304(18)	N(2)-Li(1)	2.25(4)
Yb-N(4)	2.348(18)	N(3)-Li(2)	1.93(4)
Yb-Cl	2.653(6)	N(4)-Li(2)	1.98(5)
Yb-Li(1)	2.82(4)		
Angles (°)			
N(1)-Yb-N(2)	77.0(7)	C(14)-N(2)-Yb	118.7(15)
N(3)-Yb-N(4)	72.4(7)	Li(1)-N(2)-Yb	76.6(11)
N(1)-Li(1)-N(2)	82.0(14)	C(20)-N(3)-C(17)	112.5(18)
N(3)-Li(2)-N(4)	89.3(17)	C(20)-N(3)-Li(2)	108(2)
C(4)-N(1)-C(1)	117.0(19)	C(17)-N(3)-Li(2)	116.8(19)
C(4)-N(1)-Li(1)	112.9(18)	C(20)-N(3)-Yb	95.8(13)
C(1)-N(1)-Li(1)	113.6(17)	C(17)-N(3)-Yb	125.0(14)
C(4)-N(1)-Yb	108.0(14)	Li(2)-N(3)-Yb	96.0(15)
C(1)-N(1)-Yb	119.7(14)	C(28)-N(4)-C(30)	121(2)
Li(1)-N(1)-Yb	80.4(12)	C(28)-N(4)-Li(2)	101(2)
C(12)-N(2)-C(14)	115(2)	C(30)-N(4)-Li(2)	113.5(19)
C(12)-N(2)-Li(1)	95.6(17)	C(28)-N(4)-Yb	90.4(13)
C(14)-N(2)-Li(1)	113.2(17)	C(30)-N(4)-Yb	131.4(16)
C(12)-N(2)-Yb	124.1(16)	Li(2)-N(4)-Yb	93.3(14)
N(3)-Yb-Cl	164.1(5)	N(2)-Yb-N(4)	145.3(7)
N(1)-Yb-N(4)	137.6(7)	τ	0.44

Eliminate of the remaining LiCl in the complex was attempted by heating a toluene solution of **3.1** overnight at 60°C. The ^{1}H NMR spectrum of the isolated material remained the same as before the heating indicating that the elimination of the LiCl was probably not

achieved. Heating up to 90°C overnight gave a dark brown/green sticky solid instead of a green powder. Unfortunately, no suitable crystals for X-ray diffraction experiments where obtained from this sticky solid.

The second product we were able to characterize by X-ray crystallography came from the reaction of two equivalents of 1,8-(2,6-$Me_2C_6H_3NLi)_2C_{10}H_6$ with one equivalent of praseodymium (III) chloride (Scheme 3.3). From this reaction mixture an orange solid was isolated.

Scheme 3.3

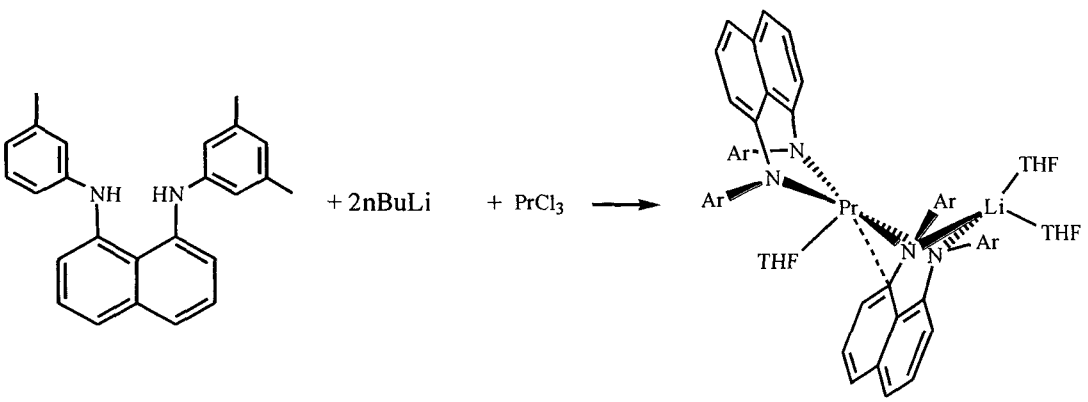

3.2

Table 3.3 and 3.4 give selected crystal data and structure refinement parameters and selected bond lengths and angles for **3.2**. As seen in Figure 3.2, the structure obtained from the X-ray experiment on this complex consisted of one praseodymium center with two ligands, one coordinated to the Pr center and the second bridging the Pr center and a lithium center. The praseodymium coordination geometry is completed by a THF solvent giving a distorted square pyramidal geometry. The Pr-N_{amido} bond lengths in this particular complex are on average 2.331Å for the terminal ligand and 2.513Å for the bridging ligand. These values are consistent with what was seen for **3.1**. The Li-N_{amido} bond lengths are on average

2.062Å and are in the same range as what was observed for **3.1**. The nitrogen centers, N(1) and N(2), of the terminal ligand are planar (Σ angles = 359.9° and 358.4°) N(3) and N(4) on the other hand are in distorted tetrahedral geometries. The bite angle of the ligand coordinated to the praseodymium center are 72.45(18)° for the terminal ligand and 66.68(17)° for the bridging ligand. These bite angles are even smaller than for complex **3.1**. Neither of the R_2DAN ligands in **3.2** coordinates to the metal centers in a planar fashion and they exhibit fold angles between the N(1)-Pr-N(2) and N(1)-C(9)-C(18)-C(17)-N(2) of 28.17° and between N(3)-Pr-N(4) and N(3)-C(35)-C(44)-C(43)-N(4) of 86.0°.

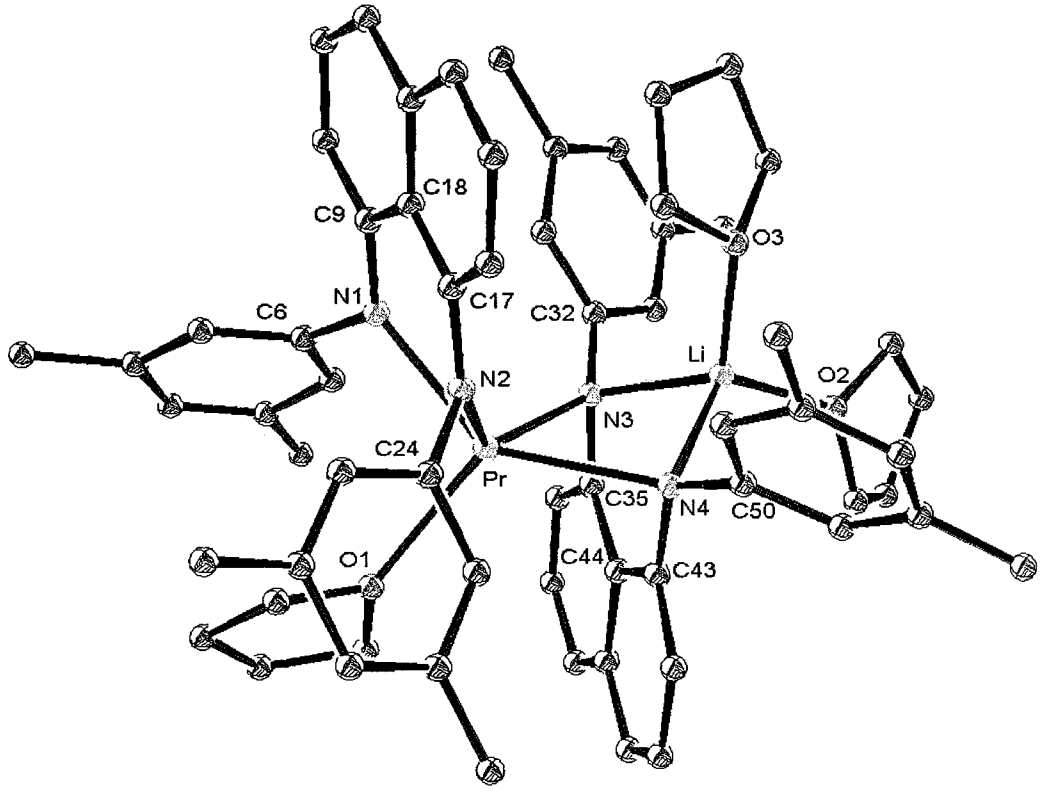

Figure 3.2. Molecular structure and partial atom-numbering schemes for **3.2**. Thermal ellipsoids are drawn at 20% probability. Co-crystallized toluene and hydrogen atoms have been omitted for clarity.

Table 3.3. Selected Crystal Data and Structure Refinement Parameters for **3.2**

Empirical formula	$C_{81.50}H_{92}LiN_4O_3Pr$
Formula weight	1323.44
Temperature (K)	202(2)
Wavelength (Å)	0.71073
Crystal system	Triclinic
Space group	P-1
a (Å)	12.718(3)
b (Å)	15.858(4)
c (Å)	17.931(4)
α(deg)	85.208(4)
β(deg)	85.629(4)
γ(deg)	74.460(4)
V ($Å^3$)	3466.6(15)
Z	2
ρ(calc) (Mg/m^3)	1.268
μ (mm^{-1})	0.754
Absorption correction	Semi-empirical with equivalents
Final R indices [I>2σ(I)]	
R1[a]	0.0725
***w*R2**[b]	0.1391

[a] $R1 = \Sigma \| |F_o| - |F_c| \| / \Sigma |F_o|$

[b] $wR2 = (w(|F_o| - |F_c|)^2 / \Sigma w |F_o|^2)^{1/2}$

Table 3.4. Selected bond lengths (Å) and angles (°) for **3.2**

Bond lengths (Å)			
Pr-N(1)	2.337(5)	Pr-N(4)	2.524(5)
Pr-N(2)	2.325(5)	N(3)-Li	2.083(12)
Pr-N(3)	2.503(5)	N(4)-Li	2.041(14)
Angles (°)			
N(1)-Pr-N(2)	72.45(18)	C(32)-N(3)-Li	98.9(5)
N(3)-Pr-N(4)	66.68(17)	C(35)-N(3)-Pr	94.2(4)
N(1)-Pr-N(3)	95.81(19)	C(35)-N(3)-Li	108.2(5)
N(2)-Pr-N(3)	93.80(17)	C(32)-N(3)-Pr	137.7(4)
N(3)-Li-N(4)	84.1(5)	Li-N(3)-Pr	97.2(4)
C(9)-N(1)-C(6)	118.8(5)	C(43)-N(4)-C(50)	118.5(5)
C(9)-N(1)-Pr	133.7(4)	C(43)-N(4)-Li	112.5(5)
C(6)-N(1)-Pr	107.4(4)	C(50)-N(4)-Li	101.1(5)
C(24)-N(2)-C(17)	119.8(5)	C(43)-N(4)-Pr	90.3(4)
C(24)-N(2)-Pr	107.1(4)	C(50)-N(4)-Pr	135.1(4)
C(17)-N(2)-Pr	131.5(4)	Li-N(4)-Pr	97.7(4)
C(35)-N(3)-C(32)	118.9(5)		

We decided to try the lanthanide and ligand reactions in a 1:1 ratio to isolate simple neutral complexes. The reaction of one equivalent of the isopropyl substituted DAN ligand with $ErCl_3$ (Scheme 3.4) lead to the isolation of orange crystals from a saturated solution of toluene. The results from an X-ray crystallography experiment presented in Figure 3.3 and summarized in Table 3.5 showed that the isolated compound contains two erbium centers. Although both Er centers are in distorted octahedral geometries, the details of environments are quite different. The first erbium center (Er1) has a bridging chloride and a THF in the axial positions [O(1)-Er(1)-Cl(2)=173.02(18)] with the four nitrogen atoms from the two different R_2DAN ligands in the equatorial positions. The second erbium center (Er2)

displayed a terminal and a bridging chloride in the axial positions [Cl(1)-Er(2)-Cl(2)=177.55(11] and the two nitrogen from one of the R_2DAN ligands in two of the equatorial positions. The two other equatorial positions are occupied by two coordinated THF molecules.

Scheme 3.4

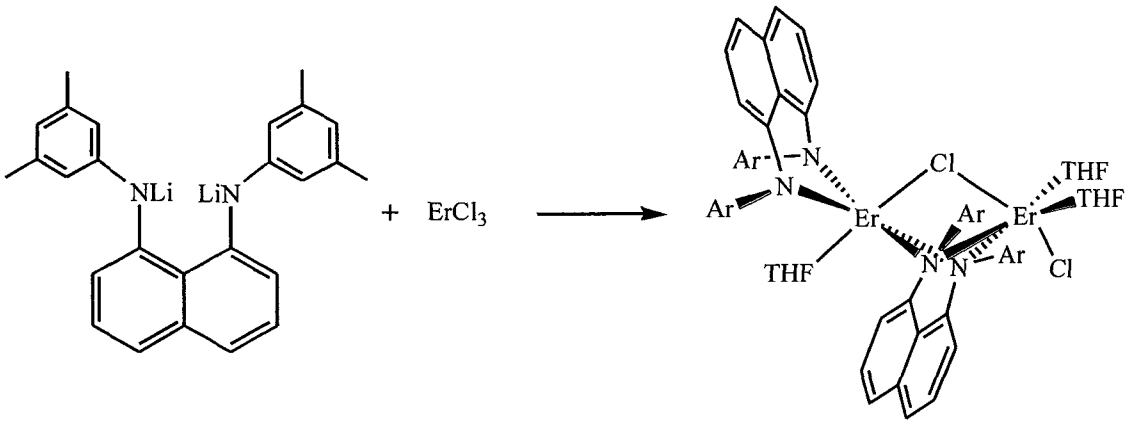

3.3

The N_{amido}-Er bond lengths for the terminal ligand are 2.244Å which is similar to what we observed in the structures of **3.1** and **3.2**. The briging ligand has as expected a longer N_{amido}-Er bond length with an average of 2.429Å. The erbium chloride bond length for the terminal chloride is 2.535(3)Å and for the bridging chlorides are Er(2)-Cl(2)= 2.592(3)Å and Er(1)-Cl(2)= 2.823(3)Å. The bridging chloride is closer to the Er(2) center a Er-Cl bond of over 0.2Å shorter than the Er(1)-Cl(2) bond lengths. The ligand bite angle in this complex vary from 67.4(3)° to 78.4(3)° these angles are smaller than what we have seen in the early transition metal complexes that usually have bite angles of over 80°. Another notable feature of the R_2DAN ligands in **3.3** is the fact that they are coordinated to the Er centers in a non-planar or "folded" fashion. The two nitrogen from the bridging

ligand both have distorted tetrahedral geometry and as expected the bridging ligand is folded to be able to chelate to both erbium centers, the angle between the N(4)-Er(2)-N(3) and N(4)-C(43)-C(44)-C(35)-N(3) planes is 48.45°. The non-bridging ligand is also folded although not as pronounced as in the other with the angle between the N(1)-Er(1)-N(2) and N(1)-C(4)-C(18)-C(17)-N(2) planes being 38.00°. The nitrogen on the non bridging ligand are both planar with the sum of the angles surrounding them being 359.8° and 359.4° respectively for N(1) and N(2).

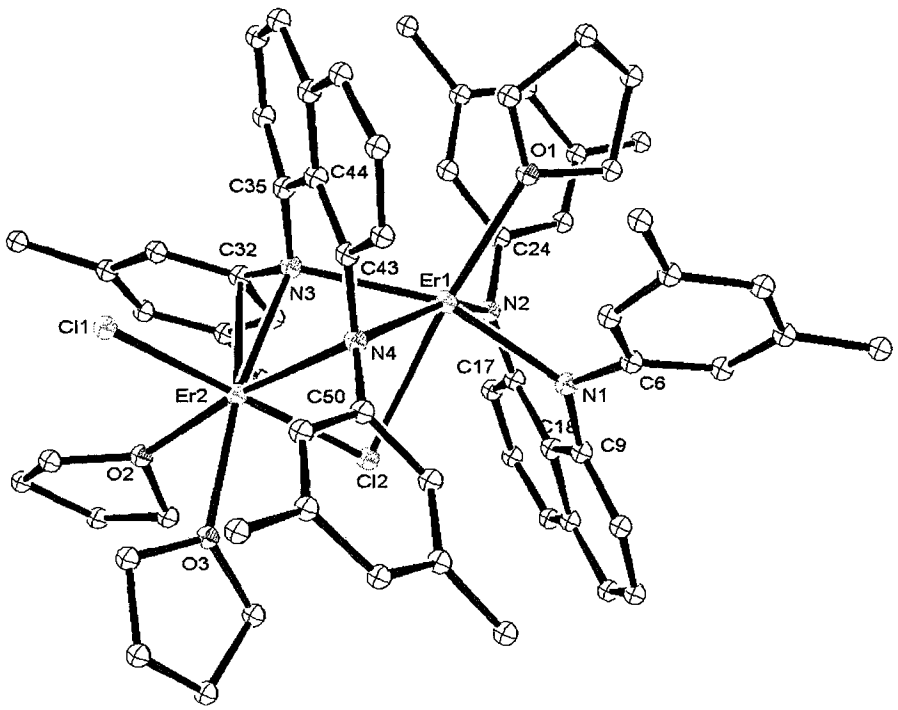

Figure 3.3. Molecular structure and partial atom-numbering schemes for **3.3**. Thermal ellipsoids are drawn at 20% probability. Hydrogen atoms have been omitted for clarity.

Table 3.5. Selected Crystal Data and Structure Refinement Parameters for **3.3.**

Empirical formula	$C_{82}H_{108}Cl_2Er_2N_4O_{7.5}$
Formula weight	1675.14
Temperature (K)	203(2)
Wavelength (Å)	0.71073
Crystal system	Triclinic
Space group	P-1
a (Å)	15.828(2)
b (Å)	17.331(3)
c (Å)	17.873(3)
α(deg)	88.847(3)
β(deg)	75.421(3)
γ(deg)	67.410(3)
V ($Å^3$)	4364.7(15)
Z	2
ρ(calc) (Mg/m^3)	1.275
μ (mm^{-1})	2.020
Absorption correction	Semi-empirical from equivalents
Final R indices [I>2σ(I)]	
R1[a]	0.0761
***w*R2**[b]	0.162

[a] $R1 = \Sigma \| F_o | - | F_c \| / \Sigma | F_o |$

[b] $wR2 = (w(| F_o | - | F_c |)^2 / \Sigma w | F_o |^2)^{1/2}$

Table 3.6. Selected bond lengths (Å) and angles (°) for **3.3**

Bond Lengths (Å)			
Er(2)-N(2)	2.240(9)	Er(2)-N(4)	2.400(9)
Er(1)-N(1)	2.248(8)	Er(1)-Cl(2)	2.823(3)
Er(1)-N(4)	2.488(9)	Er(2)-Cl(1)	2.535(3)
Er(1)-N(3)	2.489(8)	Er(2)-Cl(2)	2.592(3)
Er(2)-N(3)	2.337(9)	Er(1)-Er(2)	3.5597(9)
Angles (°)			
N(2)-Er(1)-N(1)	78.4(3)	C(35)-N(3)-Er(2)	122.1(7)
N(4)-Er(1)-N(3)	67.4(3)	C(32)-N(3)-Er(2)	92.5(7)
N(3)-Er(2)-N(4)	71.2(3)	C(35)-N(3)-Er(1)	101.4(7)
Cl(1)-Er(2)-Cl(2)	17.55(11)	C(32)-N(3)-Er(1)	130.8(7)
O(1)-Er(1)-Cl(2)	173.02(18)	Er(2)-N(3)-Er(1)	95.0(3)
C(9)-N(1)-C(6)	118.2(9)	C(50)-N(4)-C(43)	116.2(16)
C(9)-N(1)-Er(1)	123.0(7)	C(50)-N(4)-Er(2)	99.3(7)
C(6)-N(1)-Er(1)	118.6(7)	C(43)-N(4)-Er(2)	117.9(7)
C(17)-N(2)-C(24)	116.5(10)	C(50)-N(4)-Er(1)	131.1(8)
C(17)-N(2)-Er(1)	126.7(8)	C(43)-N(4)-Er(1)	98.0(6)
C(24)-N(2)-Er(1)	116.2(7)	Er(2)-N(4)-Er(1)	93.5(3)
C(35)-N(3)-C(32)	115.1(9)		

Performing the same reaction presented in Scheme 3.4 but changing the crystallization solvent from toluene to a THF/hexanes mixture led to the isolation of a different product (Scheme 3.5). The structure obtained from the X-ray experiment is presented in Figure 3.4 and summarized in Table 3.7 and 3.8. The molecular structure showed that this complex contains one erbium center with one ligand and one chloride and the coordination sphere is completed with to coordinated THF molecules.

Scheme 3.5

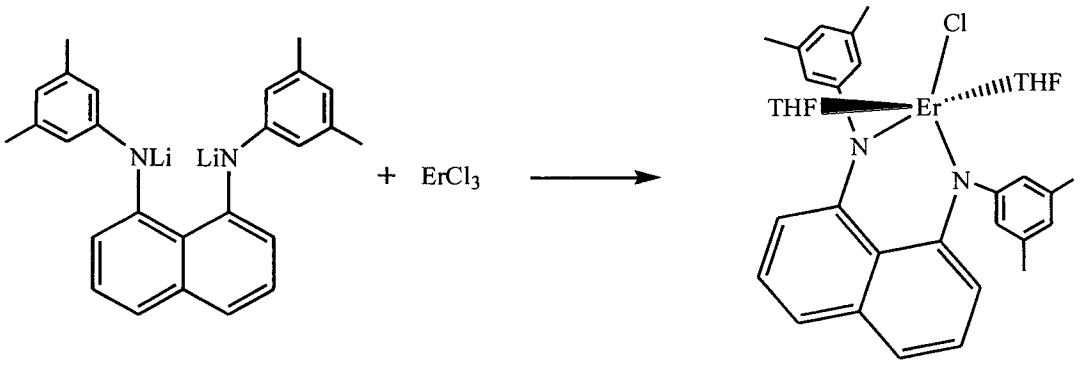

3.4

In this complex the erbium center is in a trigonal bipyramidal geometry with the two THF molecule occupying the axial positions [O(1)#1-Er-O(1)= 177.0°]. The equatorial positions are occupied by the two nitrogens of the R_2DAN ligand and a chloride. The structure is symmetric and contains a C_2 axis going through the chloride erbium bond. The Er-N_{amido} bond is 2.251(17)Å which is within experimental error comparable to what we have observed in complex **3.3**. The Er-Cl bond is in the same range as what was observed for the terminal chloride in complex **3.3** with a bond length of 2.617(8)Å. The nitrogen centers in this complex deviate slightly from planarity with the sum of the angle surrounding the nitrogen being 355.5°. The bite angle of the ligand in this complex is similar to what we have observed in are other lanthanide complexes with a value of 76.5(9)°. The one feature that is strikingly different in the lanthanide complex is the coordination geometry of the R_2DAN ligand. The R_2DAN ligand coordinates the Er center in an almost planar geometry with the angle between the N(1)-C(9)-C(14)-C(9)-C(1) and N(1)-Er-N(1) plane being 1.06°. Another interesting feature in the erbium complex is the presence of interaction between the aryl group from the ligand and the erbium center.

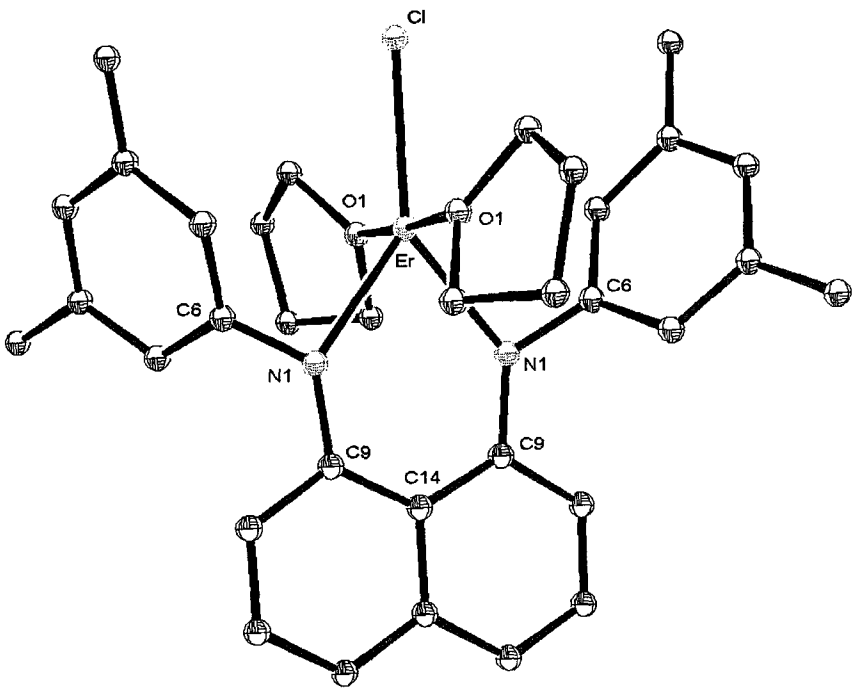

Figure 3.4. Molecular structure and partial atom-numbering schemes for **3.4**. Thermal ellipsoids are drawn at 20% probability. Hydrogen atoms have been omitted for clarity.

Table 3.7. Selected Crystal Data and Structure Refinement Parameters for **3.4.**

Empirical formula	$C_{34}H_{40}ClErN_2O_2$
Formula weight	711.39
Temperature (K)	201(2)
Wavelength (Å)	0.71073
Crystal system	Monoclinic
Space group	C2/c
a (Å)	7.850(5)
b (Å)	23.018(15)
c (Å)	17.101(11)
α(deg)	90
β(deg)	93.637(11)
γ(deg)	90
V (Å^3)	3084(3)
Z	4
ρ(calc) (Mg/m^3)	1.532
μ (mm^{-1})	2.840
Absorption correction	Semi-empirical from equivalents
Final R indices [I>2σ(I)]	
R1[a]	0.1157
***w*R2**[b]	0.2620

[a] $R1 = \Sigma \| F_o | - | F_c \| / \Sigma | F_o |$

[b] $wR2 = (w(| F_o | - | F_c |)^2 / \Sigma w | F_o |^2)^{1/2}$

Table 3.8. Selected bond lengths (Å) and angles (°) for 3.4

Bond lengths (Å)	
Er-N(1)	2.251(17)
Er-C(6)	2.75(2)
Er-C(1)	2.80(2)
Er-Cl	2.617(8)
Angles (°)	
N(1)#1-Er-N(1)	76.5(9)
N(1)-Er-Cl	141.8(5)
O(1)#1-Er-O(1)	177.0(7)
C(6)-N(1)-C(9)	124.5(17)
C(6)-N(1)-Er	94.8(12)
C(9)-N(1)-Er	136.2(16)
τ	0.59

In an effort to obtain simple lanthanide complexes that would not have lithium counterions or coordinated LiCl, reaction of the potassium salt of the R_2DAN ligand with the lanthanide iodide were investigated (Scheme 3.6).

Scheme 3.6

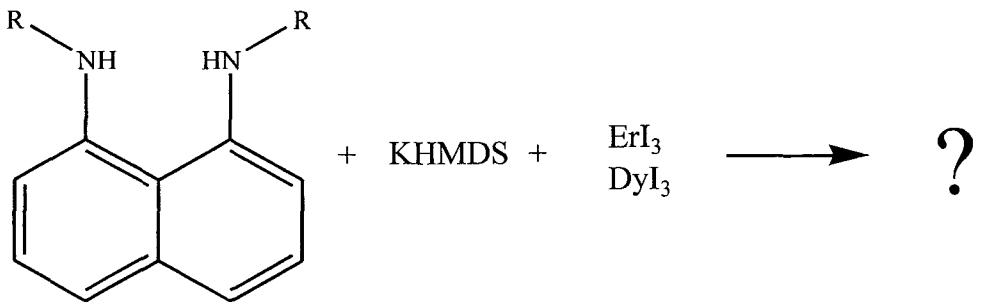

R= $CH(CH_3)_2$
R= 3,5-$Me_2(C_6H_3)$

In these reactions, similar color changes similar to what we had seen in the reaction of the lithium salts and the lanthanide chloride were observed. Unfortunately NMR spectroscopy has not been very useful in the characterization of these products and we have yet been able to isolate crystals suitable for X-ray diffraction. The difficulty encountered in the characterization of these lanthanide complexes due to crystallization problem and the uselessness of NMR spectroscopy encouraged use to move away from the lanthanides and to explore the coordination chemistry of are R_2DAN ligand in other groups of the periodic table.

III. Conclusions:

R_2DAN ligands have been shown to react with lanthanide halides to produce some colorful complexes. The characterization by X-ray crystallography of some of the complexes obtained showed that elimination of LiCl is not always complete. The importance of the solvent was demonstrated when two product were obtained when using different crystallization solvents. The complexes obtained also demonstrate the flexibility in the coordination geometry of the R_2DAN ligand. Generally, the ligands in these complexes coordinate in a non-planar or folded mode and we observed that the degree of bending depended on the remaining coordination features of the lanthanide center.

IV. Experimental Section

Preparation of of $YbClLi_2(OEt)_2[1,8\text{-}(N^iPr)_2C_{10}H_6]_2$ (3.1)

In a vial $1,8\text{-}(NH^iPr)_2C_{10}H_6$ (200 mg, 0.83 mmol) was dissolved in 10ml of THF and to this solution was added nBuLi (1.03 ml, 1.65 mmol). This reaction mixture was stirred for 1h followed by the addition of $YbCl_3(THF)_3$ (204 mg, 0.41 mmol). The reaction mixture was stirred overnight; the solvent was then removed under vacuum fallowed by extraction with toluene. Green crystals suitable for X-ray diffraction where grown at -20°C from a saturated solution of toluene/ether (104 mg, 30%).

^1H NMR (300 MHz, C_6D_6): δ -27.3 $w_{1/2}$=0.67, -14.2 $w_{1/2}$=0.44, 0.97 $w_{1/2}$=0.11, 2.03 $w_{1/2}$=0.07, 3.28 $w_{1/2}$=0.22, 5.29 $w_{1/2}$=0.23, 5.92 $w_{1/2}$=0.17, 21.4 $w_{1/2}$=0.89, 27.2 $w_{1/2}$=2.2.

Preparation of $Pr[1,8\text{-}(2,6\text{-}Me_2C_6N_3N)_2C_{10}H_6])(THF)Li(THF)_2$ (3.2)

In a vial $1,8\text{-}(2,6\text{-}Me_2C_6H_3NH)_2C_{10}H_6$ (200 mg, 0.55 mmol) was dissolved in 15ml of ether and to this solution was added nBuLi (0.68 ml, 1.09 mmol). The solution was then stirred for 30 mins followed by the addition of $PrCl_3$ (67 mg, 0.27 mmol). The reaction mixture was stirred overnight, then the solvent was removed under vacuum, and the product was extracted with toluene. The orange solid can be crystallized from a saturated THF solution at -20°C to afford crystal suitable for X-ray diffraction experiments (133 mg, 48%).

^1H NMR (300 MHz, C6D6): δ 2.04 $w_{1/2}$=0.12 ppm, 6.34 $w_{1/2}$=0.06 ppm, 0.09 pmm, 7.23 $w_{1/2}$=0.12 ppm.

Preparation of $Er_2[1,8\text{-}(2,6\text{-}Me_2C_6H_3N)_2C_{10}H_6]_2Cl_2(THF)_3$ (3.3)

In a round bottom flask equipped with a magnetic stir bar 1,8-(2,6-$Me_2C_6H_3NH)_2C_{10}H_6$ (400 mg, 1.09 mmol) was dissolved in 25 ml of THF. To this solution was added nBuLi (1.36 ml, 2.2 mmol) the reaction mixture was stirred for 30 min followed by the addition of $ErCl_3$ (299 mg,1.10 mmol). The next morning the reaction mixture was evaporated under vacuum to give a green solid that was extracted with toluene to give **3.3** (247 mg, 34%). Crystals suitable for X-ray expirement can be obtained from a saturated toluene solution at -20°C.

Preparation of $ErCl(THF)_2[1,8\text{-}(2,6\text{-}Me_2C_6H_3N)_2C_{10}H_6]$ (3.4)

In a round bottom flask equipped with a magnetic stir bar 1,8-(2,6-$Me_2C_6H_3NH)_2C_{10}H_6$ (300 mg, 0.82 mmol) was dissolved in 20 ml of THF. To this solution was added nBuLi (1.02 ml, 1.63 mmol). The reaction mixture was stirred for 45 min then $ErCl_3$ was added to the solution (224 mg 0.82 mmol).The reaction mixture was stirred overnight then the solvent was removed under vacuum, followed by extraction with toluene. The green solid obtained was crystallized from a saturated THF/hexanes solution to afford crystal suitable for X-ray diffraction experiment (217 mg, 36%).

Structural determination of 3.1, 3.2, 3.3 and 3.4.

Single crystals were mounted on a thin glass fibre and held using viscous oil. They were subsequently cooled to data collection temperature. Crystal data and details of the measurements are summarized in table 3.1, 3.3, 3.5 and 3.7. Data were collected on a

Bruker AX SMART 1k CCD diffractometer using 0.3° ω-scans at 0, 90, 180° in Φ. Unit-cell parameters were determined from 60 data frames collected at different sections of the Ewald sphere. Semi-empirical corrections based on equivalent reflections were applied (Blessing, R., *Acta Cryst.*, **1995**, A51, 33-38). The structureswere solved by direct method, completed with difference Fourier synthesis and refined with full-matrix least-squared procedures based on F^2. All non-hydrongen atoms were refined with anisotropic displacement parameters. All hydrogen atoms were treated as idealized contributions. All scattering factors and anomalous dispersion factors are contained in the SHELXTL 5.1 program library (Sheldrick, G. M. AXS, Madison, WI, 1997).

References

[1] Hultzsch, K. C. *Adv. Synth. Catal.* **2005**, 347, 367.

[2] Gagne, M.R.; Stern, C. L.; Marks T. J. *J. Am. Chem. Soc.* **1992**, 114, 275 and reference within.

[3] Trifonov, A. A.; Spaniol, T. P.; Okuda, J. *Organometallics,* **2001**, *20*, 4869.

[4] Trifonov, A. A.; Van de Weghe, P.; Collin, J.; Domingos, A.; Santos, I. *J. Organomet. Chem.* **1997**, *527*, 225.

[5] Gatti, P. M.; de Oliveira, W. *J. Alloys Compd,* **1998**, 894.

[6] (a) Schaverien, C. J. *Organometallics,* **1994**, *13*, 69. (b) Hultzsch, K. C.; Voth, P.; Beckerle, K.; Spaniol, T. P.; Okuda, J. *Organometallics,* **2000**, *19*, 228. (c) Shapiro, P. J.; Schaefer, W. P.; Labinger, J. A.; Bercaw, J. E.; Cotter, W. D. *J. Am. Chem. Soc.* **1994**, *116*, 4623. (d) Schaverien, C. J. *J. Mol. Catal.* **1994**, *90*, 177. (d) Hou, Z.; Koizumi, T.; Nishiura, M.; Wakatsuki, Y. *Organometallics,* **2001**, *20*, 3323.

[7](a) Kim, Y. K.; Livinghouse, T.; Bercaw, J. E. *Tetrahedron Lett* .**2001**, *42*, 2933. (b) Kim, Y. K.; Livinghouse, T. *Angew.Chem. Int. Ed.* **2002**, *41*, 3645. (c) Kim, Y. K.; Livinghouse, T.; Horino, Y. *J. Am. Chem. Soc.* **2003**, *125*, 9560.
(d) Kim, J. Y.; Livinghouse, T. *Org. Lett.* **2005**, *7*, 4391. (e) Hultzsch, K. C.; Hampel, F.; Wagner, T. *Organometallics* **2004**, *23*, 2601. (f) Zulys, A.; Panda, T. K.; Gamer, M. T.; Roesky, P. W. *Chem. Commun.* **2004**, 2584. (g) Panda, T. K.; Zulys, A.; Gamer, M. T.; Roesky, P. W. *J. Organomet. Chem.* **2005**, *690*, 5078. (h) Rastätter, M.; Zulys, A., Roesky, P. W. *Chem.Commun.* **2006**, 874. (i) Bambirra, S., Tsurugi, H.; van Leusen, D.; Hessen, B. *Dalton Trans.* **2006**, 1157. (j) Lauterwasser, F.; Hayes, P. G.; Bräse, S.; Piers, W. E.; Schafer, L. L. Organometallics, **2004**, 23, 2234.

[8] Hong, S.; Tian, S.; Metz, M. V.; Marks, T. J. *J. Am. Chem. Soc.*, **2003**, 125, 14768.

[9] O'Shaughnessy, P. N.; Gillespie, K. M.; Knight, P. D.; Munslow, I.; Scott, P. *Dalton Trans.* **2004,** 2251.

[10] Riegert, D.; Collin, J.; Daran, J-C.; Fillebeen, T.; Schulz, E.; Lyubov, D.; Fukin, G.; Trifonov, A. *Eur. J. Inorg. Chem.* **2007**, 1159.

[11] (a) Xue, M.; Yao, Y,; Shen, Q.; Zhang, Y. *J. Organomet. Chem.* **2005**, 690, 4685. (b) Zhang, Z-Q.; Yao, Y-M.; Zhang, Y.; Shen, Q.; Wong, W-T. *Inorganica Chimica Acta,* **2004**, 357, 3173. (c) Yao, Y.; Zhang, Z.; Peng, H.; Zhang, Y.; Shen, Q.; Lin. J. *Inorg.*

Chem. **2006,** 45, 5, 2175. (d) Hitchcock, P. B.; Khvostov, A. V.; Lappert, M. F.; Protchenko, A. V. *Dalton Trans.*, **2009**, 2383. (e) Wei, X.; Cheng, Y.; Hitchcock, P. B.; Lappert, M. F., *Dalton Trans.* **2008**, 5235. (f) Liddle, S. T.; Polly, L. Arnold. *Dalton Trans.*, **2007**, 3305.

[12] (a) Bazinet, P.; Yap, G. P. A.; Richeson, D. S. Organometallics, **2001**, 20, 4129. (b) Lavoie, N.; Ong, T-G.; Gorelsky, S.I.; Korobkov, I.; Yap G. P. A.; Richeson, D. S. *Organometallics*, **2007**, *26* (26), 6586.

Chapter 4

Group IV Complexes Bearing Disubstituted 1,8-Diaminonaphthalene Ligands

I. Introduction

An established focus for the organometallic chemistry of early transition metals has been the synthesis of catalysts for polymerization reactions. Most of the initial work in this area focused on bis(cyclopentadienyl) complexes. Zirconium complexes in the +4 oxidation state such as $[Cp_2ZrR]^+$ complexes exhibit high activity as α-olefins and ethylene

polymerization catalysts. In more recent years the interest in finding ligands with different electronics and sterics properties has lead to the use alkoxide[1] and amido ligands[2]. One important and defining feature of alkoxide and amido ligands is the presence of lone pairs of electrons on the bonding centers. The lone pairs on these centers can be donated to the metal center and thus stabilize electrophilic metal centers in high oxidation state complexes. The amido ligands are more versatile than the alkoxide ligand due to their nitrogen substituents. The sterics and electronic properties in an amido ligand can be changed by modifying the two R groups while the alkoxide ligands only have one R group making them less versatile.

Interesting contributions to the chemistry of non-cyclopentadienyl chemistry of group 4 metals are the application of diaminobenzene and β-diketiminate ligands with these early metal centers. Group 4 complexes bearing diamino benzene ligands have also been investigated as catalysts in polymerization reactions.[2p,3] β-Diketiminate ligands (so called NacNac species) have attracted considerable attention for replacement of cyclopentadienyl ligands due to their isoelectronic similarity to Cp ligands[4]. Group 4 complexes bearing NacNac ligands have been reported as good catalysts for polymerization reactions[5,6,7]

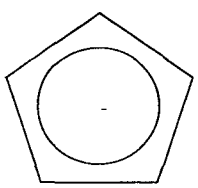

Cyclopentadienyl Anion

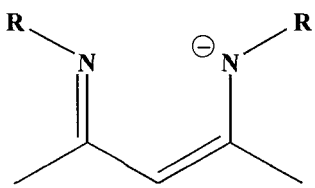

β liketiminate

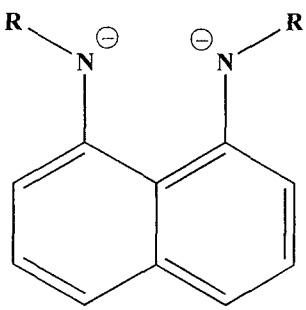

R_2DAN^{2-}

These reports attracted our attention and suggested that disubstituted 1,8-diaminonaphthlene (ligands R_2DAN) could be useful supporting ligands due to their resemblance in structure to the NacNac ligand and their similarity in electronic properties to the diaminobenzene ligands. We were also aware of the success that group 4 complexes bearing the related ligands, 1,8-$C_{10}H_6$-$(NHSiR_3)_2$, have had as polymerization catalysts. The size of the nitrogen substituent in these complexes influenced the catalytic activity[8] indicating that the nitrogen substituents are an important factor in the catalytic cycle.

The structure of a complex has an influence its ability to catalyze a reaction. For this reason structural studies of complexes are important to help improve our understanding of catalysis. The structure of a complex depends on the size of the amido groups, zirconium amido complexes often adopt either a mononuclear structure or a dinuclear one.[9] Small groups like dimethyl amido groups adopt a dinuclear structure of type **A**,[10] with two trigonal bipyramidal metal centers and two bridging amido groups. Bulkier amido group such as diphenyl amido groups lead to the formation of mononuclear tetrahedral structures (**B**).[11]

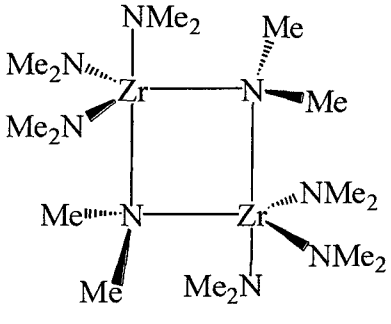

A

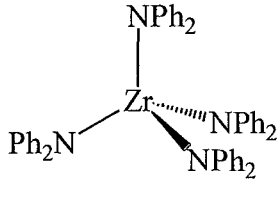

B

The tunability of bis(amido) ligands has led to many reports of bis(amido) complexes. Examples of these include dinuclear species such as **C**[12] and **E**[13] and mononuclear species such as **D**[14] and **F**[15]. These examples show different types of structures that can be obtained. **C** and **E** both have a dimeric structure with two bridging chlorides. The remaining coordination sites are occupied by the bis(amido) ligand, a chloride and the last site can be filled with a solvent molecule or another donor atom from the ligand itself to form octahedral complexes. Complex **D** is a monomeric structure that is in a tetrahedral geometry while **F** is also monomeric but has two of its coordination sites occupied by THF molecules to give an octahedral geometry. These few selected examples demonstrate that bis(amido) ligands can form different structures and that the nitrogen substituents are important in dictating what type structure will be obtained.

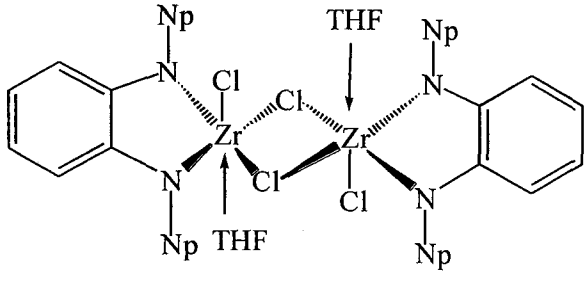

C

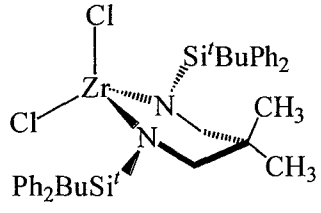

D

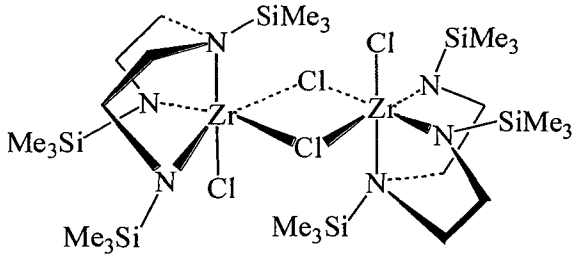

E

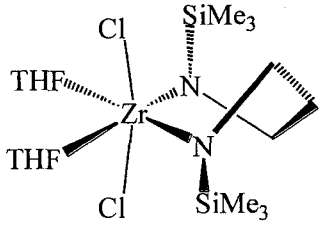

F

II. Results and discussion

Disubstituted 1-8-diaminonaphthalene (R_2DAN) ligands can be introduced to a metal center by mixing it with a metal halide followed by the addition of a base to deprotonate the coordinated ligand. This method was employed to make titanium complexes by combining the R_2DAN ligand and a solution of $TiCl_4$ followed by the addition of triethylamine (Scheme 4.1). The purple solid isolated from this reaction was characterized by NMR spectroscopy. When the reaction is performed with one equivalent of triethylamine the ^{1}H NMR shows that a significant amount of free ligand is left in the reaction. The remaining free ligand can be washed away using hexanes, but to increase the yield a large excess of NEt_3 can be used to drive the reaction towards the products. The ^{1}H NMR spectrum for complex **4.1** showed that it is very symmetric with the isopropyl group of the R_2DAN ligand giving only one doublet integrating for 12 protons at 1.42 ppm and one septet integrating for 2 protons at 5.11 ppm. The signal at 5.11 ppm for the ipso proton is indicative of a coordinated ligand versus a non-coordinated ligand that would display a septet at around 3.5 ppm. The ^{13}C NMR spectrum also indicated a symmetric structure with only one set of resonances for the isopropyl groups and 6 resonances for the naphthalene backbone.

Scheme 4.1

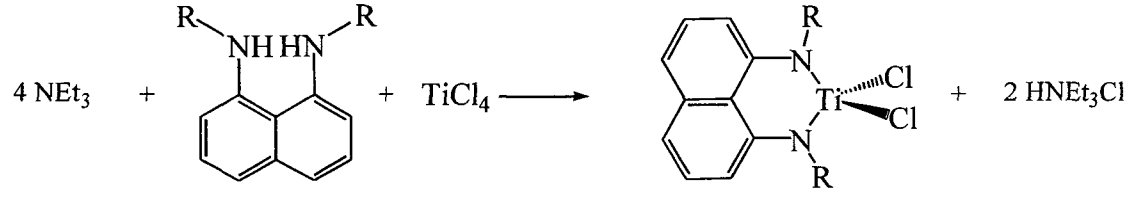

4.1 R= $CH(CH_3)_2$
4.2 R= 3,5-$Me_2C_6H_3$

Complex **4.2** is obtained by reacting one equivalent of 1,8-(2,6-$Me_2C_6H_3N)_2C_{10}H_6$ with one equivalent of $TiCl_4$ followed by the addition of an excess of triethylamine. The ^1H NMR spectrum of the crude reaction mixture indicated that the reaction does not go to completion and some ligand remains. The excess ligand could be washed away with hexanes to afford a purple solid in 29.3% yield. This purple solid can also be characterized by NMR spectroscopy. The ^1H NMR spectrum showed only one resonance for the CH_3 groups indicating a symmetric complex. The ^{13}C NMR spectrum also supports this assignment with 6 resonances for the naphthalene backbone.

An alternative means for introduction of the R_2DAN ligand into the coordination sphere of a metal is a metathesis reaction of the lithiated ligand with a metal halide. The lithiated ligand is readily accessible from the reaction of the parent ligand with two equivalents of n-BuLi. Subsequent reaction with $ZrCl_4(THF)_2$ allowed isolation of zirconium complexes bearing the R_2DAN ligand. This method was employed for the synthesis of $Zr[1,8\text{-}(N^iPr)_2C_{10}H_6]_2$, the reaction of two equivalents of $[1,8\text{-}(N^iPr)_2C_{10}H_6]Li_2$ with one equivalent of $ZrCl_4(THF)_2$ (Scheme 4.2) led to the formation of an orange powder. The ^1H NMR spectra of this product showed the isopropyl groups exhibiting one doublet at

1.24 ppm and one septet at 6.59 ppm. The single set of resonances suggested a very symmetric complex. The absence of any THF peaks in the ^{1}H NMR suggests that two ligands have coordinated to the zirconium that should be in a tetrahedral geometry.

Scheme 4.2

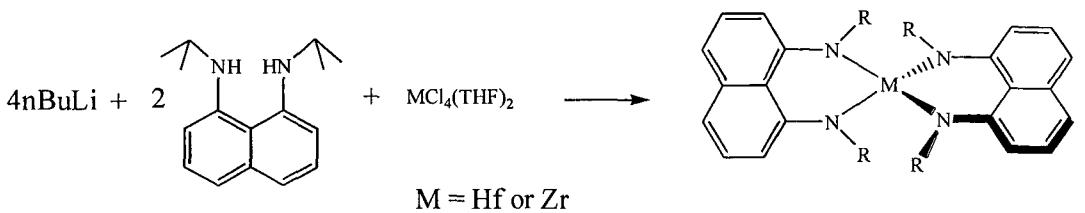

4.3 R= $C(CH_3)_2$, M= Zr
4.4 R= $C(CH_3)_2$, M= Hf

The same procedure can be employed to prepare $Hf[1,8\text{-}(N^iPr)_2C_{10}H_6]_2$. Reaction of two equivalents of $[1,8\text{-}(N^iPr)_2C_{10}H_6]Li_2$ with $Hf(Cl_4)(THF)_2$ (Scheme 4.2) led to the isolation of a yellow solid. The ^{1}H NMR spectra of **4.4** displayed a doublet at 1.23 ppm and a septet at 3.96 ppm indicating only one type of isopropyl group and a very symmetric complex. Crystals suitable for X-ray diffraction experiments were grown from a saturated solution of toluene. The result of the structure determination experiment is shown in Figure 4.1. This structure is the expected hafnium center with two R_2DAN ligands. Selected crystal data and structure refinement parameters and selected bond lengths and angles are presented in Tables 4.1 and 4.2. The structure obtained shows that the hafnium center is in a distorted tetrahedral geometry. The structure is very symmetric with all four nitrogens being equivalent. The ligands are close to 90° to each other. The four nitrogen centers are planar with the sum of the angles surrounding them being 359.7°. The Hf(1)-N(1) bond

length is of 2.060(6)Å which is comparable to what we have seen in other complexes with this ligand. The structure also shows that the R_2DAN ligand is slightly twisted, a feature that has been observed in other metal complexes.

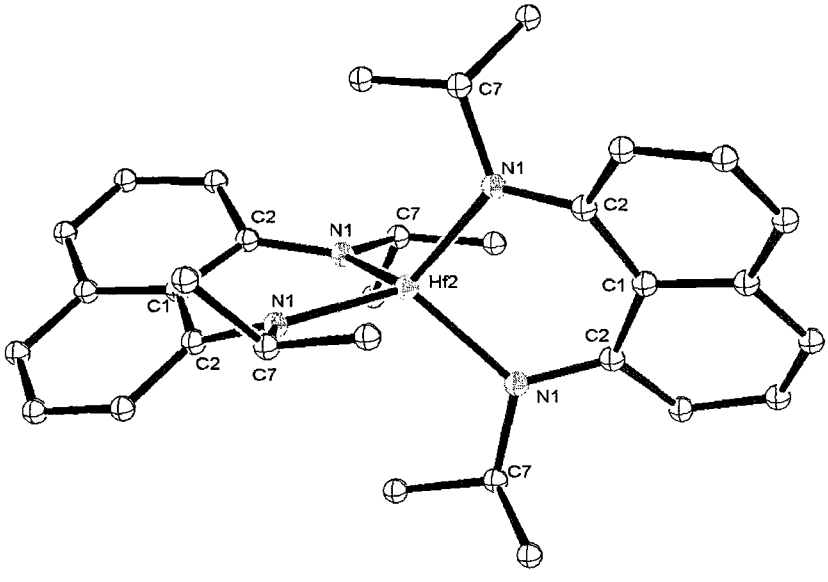

Figure 4.1. Molecular structure and partial atom-numbering schemes for **4.4**. Thermal ellipsoids are drawn at 20% probability. Hydrogen atoms have been omitted for clarity.

Table 4.1. Selected Crystal Data and Structure Refinement Parameters for Hf[1,8-$(N^iPr)_2C_{10}H_6]_2$ (**4.4**)

	4.4
Empirical formula	$C_{32}H_{40}HfN_4$
Formula weight	659.17
Temperature (K)	202(2)
Wavelength (Å)	0.71703
Crystal system	Tetragonal
Space group	$I4_1/a$
a (Å)	13.4859(9)
b (Å)	13.4859(9)
c (Å)	15.574(2)
α(deg)	90
β(deg)	90
γ(deg)	90
V ($Å^3$)	2834.44
Z	4
ρ(calc) (Mg/m^3)	1.546
μ (mm^{-1})	3.710
Absorption correction	Semi-empirical from equivalents
Final R indices [I>2σ(I)]	
R1[a]	0.0419
***w*R2**[b]	0.0976

[a] $R1 = \Sigma \| F_o | - | F_c \| / \Sigma | F_o |$

[b] $wR2 = (w(| F_o | - | F_c |)^2 / \Sigma w | F_o |^2)^{1/2}$

Table 4.2. Selected bond lengths (Å) and angles (°) for Hf[1,8-(N^{i}Pr)$_2$C$_{10}$H$_6$]$_2$ (**4.4**)

4.7	
	Bond lengths (Å)
Hf(2)-N(1)	2.060(6)
	Angles (°)
N(1)-Hf(2)-N(1)	91.0(2)
N(1)#1-Hf(1)-N(1)	119.40(19)
Hf(2)-N(1)-C(2)	123.5(5)
Hf(2)-N(1)-C(7)	119.3(5)
C(2)-N(1)-C(7)	116.9(6)

The synthesis of zirconium complexes with only one R_2DAN ligand can also be achieved. This is done by reacting R_2DAN ligands with two equivalents of n-BuLi followed by the addition of one equivalent of $ZrCl_4(THF)_2$ (Scheme 4.3).

Scheme 4.3

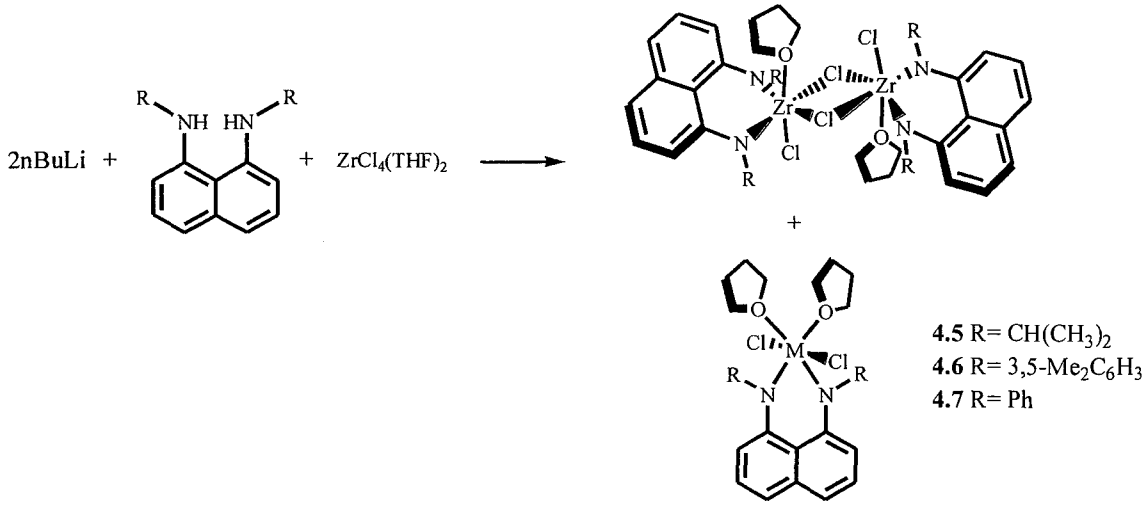

$Zr[1,8\text{-}(N^iPr)_2C_{10}H_6]Cl(THF)\mu\text{-}Cl]_2$ was isolated as a orange powder in 66.2% yield. The proton NMR for **4.5** shows two very broad signals at 1.52 and 1.78 ppm for the

CH_3 portion of the isopropyl groups. The broad signal could be an indication of a fluxional structure that is reminiscent of what was recently reported by Tabernero and al.[12] A monomer dimmer equilibrium could also be a reason for the broadening of the peaks in the NMR spectrum. $[Zr\{1,2C_6H_4(NCH_2tBu)\}Cl(THF)(\mu\text{-}Cl)]_2$ was attributed to two isomers of the product the first with *cis* oriented THF ligands and the other with the THF ligands in a *trans* orientation in this dimeric structure (**C**). The ^1H NMR spectra also show one septet at 5.67 ppm integrating for two protons and representing the ipso protons of the nitrogen substituent in the coordinated ligand. A second set of resonances is always observed in the crude product. This second set contains one sharp doublet at 1.24 ppm, a septet at 6.59 ppm and a series of aromatic resonances for a naphthalene ring. These signals correspond to **4.3**, the zirconium complex with two ligands. The formation of this side product can be minimized by performing the reaction in a more dilute solution but unfortunately the formation of this species can never be totally eliminated. Recrystallization of the crude product can also reduce the concentration of **4.3** but we can always observe traces of this product even after multiple recrystallizations. The formation of this type of complex has previously been observed by Lee and al.[16] when attempting to prepare $\{1,8\text{-}C_{10}H_6(NSiMe_3)_2\}ZrCl_2$ they obtained $\{1,8\text{-}C_{10}H_6(NSiMe_3)_2\}_2Zr$. This was observed with the smaller nitrogen substituents were used but when larger substituents are used such as in the $1,8\text{-}C_{10}H_6(NHSi(^i\text{-}Pr)_2$ ligand the mono substituted zirconium complex is observed ($\{1,8\text{-}C_{10}H_6(NSi(^i\text{-}Pr))_2\}ZrCl_2$).

An X-ray crystallography experiment on complex **4.5** confirmed that the complex was a dinuclear compound. Selected crystal data and structure refinement parameters and selected bond lengths and angles are presented in Tables 4.3 and 4.4. Figure 4.2 shows that

the zirconium centers in this complex are both distorted octahedral with the two amido nitrogens and the bridging chloride occupying the equatorial positions and the remaining chloride and one THF group in the axial positions. The Zr-N_{amido} bond are on average 2.0356Å which is a similar bond length that was observed in $\{1,8\text{-}C_{10}H_6(NSi(i\text{-}Pr)_3)_2\}ZrCl_2$ dimer that was reported in 1998 by Lee and *al.*[16] The Zr-Cl bond lengths are on average 2.679Å for the bridging chlorides and 2.4438Å for the terminal chlorides once again this is comparable to the ones in$\{1,8\text{-}C_{10}H_6(NSi(i\text{-}Pr)_3)_2\}ZrCl_2$. The nitrogen centers in this structure are planar with the sum of the angles surrounding them being 360°. The R_2DAN ligand in this structure is folded in a similar fashion to what we have observed in some of the tantalum complexes and in the tungsten chemistry that are presented in chapter 5 and 6. The angle formed by the N(1)-C(1)-C(10)-C(9)-N(2) and N(1)-Zr(1)-N(2) planes is 26.94°. The ligands bite angle in this complex are on average 84.60°. this is smaller than what is observed in **4.1** and also smaller than what was reported by Lee[16] for $\{1,8\text{-}C_{10}H_6(NSiMe_3)_2\}_2Zr$ and $\{1,8\text{-}C_{10}H_6(NSi(i\text{-}Pr)_3)_2\}ZrCl_2$ that had N-Zr-N angles between 90 and 95°.

Table 4.3. Selected Crystal Data and Structure Refinement Parameters for **4.5**, **4.6** and **4.7.**

	4.5	**4.6**	**4.7**
Empirical formula	$C_{44}H_{64}Cl_4N_4O_3Zr_2$	$C_{34}H_{40}Cl_2N_2O_2Zr$	$C_{30}H_{32}Cl_2N_2O_2Zr$
Formula weight	1021.23	670.80	614.70
Temperature (K)	202(2)	202(2)	203(2)
Wavelength (Å)		0.71073	
Crystal system	Monoclinic	Monoclinic	Monoclinic
Space group	C2/C	P2(1)	$P2_1/c$
a (Å)	24.789(3)	9.535(2)	17.975(6)
b (Å)	9.5513(12)	14.294(3)	9.537(4)
c (Å)	23.848(3)	12.766(3)	15.994(4)
α(deg)	90	90	90
β(deg)	116.822(2)	111.591(3)	90.152
γ(deg)	90	90	90
V ($Å^3$)	5039.0(11)	1617.8(6)	2741.8
Z	4	2	4
ρ(calc) (Mg/m^3)	1.346	1.377	1.489
μ (mm^{-1})	0.665	0.537	0.627
Absorption correction		Semi-empirical from equivalents	
Final R indices [I>2σ(I)]			
R1[a]	0.0591	0.0709	0.0559
***w*R2**[b]	0.1530	0.1490	0.1206

[a] $R1 = \Sigma \| F_o | - | F_c \| / \Sigma | F_o |$

[b] $wR2 = (w(| F_o | - | F_c |)^2 / \Sigma w | F_o |^2)^{1/2}$

Table 4.4. Selected Bond Lengths (Å) and Angles (°) for **4.5, 4.6** and **4.7**.

4.5		**4.6**		**4.7**	
		Bond lengths (Å)			
Zr(1)-N(1)	2.0128(2)	Zr(1)-N(2)	2.055(7)	Zr(1)-N(1)	2.038(5)
Zr(1)-N(2)	2.0188(3)	Zr(1)-N(1)	2.091(4)	Zr(1)-N(2)	2.048(6)
Zr(2)-N(3)	2.0317(3)	Zr(1)-Cl(1)	2.457(2)	Zr(1)-Cl(1)	2.747(2)
Zr(2)-N(4)	2.0789(2)	Zr(1)-Cl(2)	2.466(2)	Zr(1)-Cl(1)	2.461(2)
Zr(1)-Cl(1)	2.4508(3)	N(1)-C(1)	1.385(11)		
Zr(1)-Cl(2)	2.6647(3)	N(1)-C(11)	1.459(10)		
Zr(1)-Cl(3)	2.6856(3)	N(2)-C(17)	1.427(11)		
Zr(2)-Cl(2)	2.6307(4)	N(2)-C(9)	1.432(11)		
Zr(2)-Cl(3)	2.7350(3)				
Zr(2)-Cl(4)	2.4368(3)				
		Angles (°)			
N(1)-Zr(1)-N(2)	84.84(3)	N(2)-Zr(1)-N(1)	83.0(3)	N(1)-Zr(1)-N(2)	82.0(2)
N(3)-Zr(2)-N(4)	84.35(4)	C(1)-N(1)-C(11)	117.8(7)	Zr(1)-N(1)-C(6)	110.9(4)
Zr(1)-N(1)-C(1)	129.52(3)	C(1)-N(1)-Zr(1)	134.0(6)	Zr(1)-N(1)-C(7)	135.2(4)
Zr(1)-N(1)-C(11)	109.22(4)	C(11)-N(1)-Zr(1)	108.1(5)	C(6)-N(1)-C(7)	113.9(6)
C(1)-N(1)-C(11)	121.24(4)	C(17)-N(2)-C(9)	115.9(7)	Zr(1)-N(2)-C(13)	135.2(5)
Zr(1)-N(2)-C(14)	129.03(5)	C(17)-N(2)-Zr(1)	110.3(5)	Zr(1)-N(2)-C(22)	109.8(5)
Zr(1)-N(2)-C(14)	110.84(3)	C(9)-N(2)-Zr(1)	133.5(6)	C(13)-N(2)-C(22)	115.1(6)
C(9)-N(2)-C(14)	120.09(4)	Cl(1)-Zr(1)-Cl(2)	166.48(8)	Cl(1)-Zr(1)-Cl(2)	166.06(7)
Cl(1)-Zr(1)-O(1)	170.4(3)	N(2)-Zr(1)-O(2)	99.0(3)	N(2)-Zr(1)-O(2)	102.2(2)
N(2)-Zr(1)-Cl(2)	96.0(3)	N(1)-Zr(1)-O(1)	101.7(2)	N(1)-Zr(1)-O(1)	99.7(2)
N(1)-Zr(1)-Cl(3)	96.6(5)	O(2)-Zr(1)-O(1)	76.4(2)	O(1)-Zr(1)-O(2)	76.33(17)
Cl(3)-Zr(1)-Cl(2)	79.8(4)				

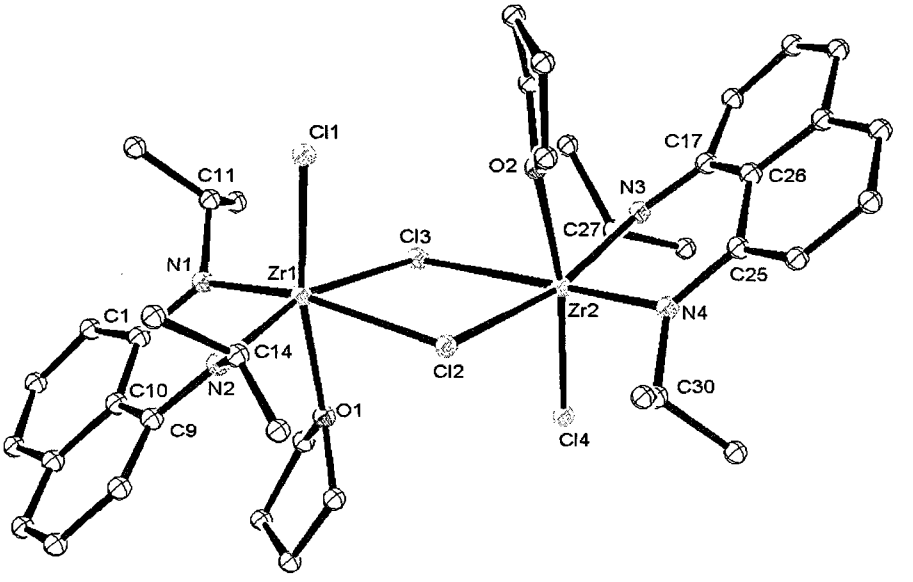

Figure 4.2. Molecular structure and partial atom-numbering schemes for **4.5**. Thermal ellipsoids are drawn at 20% probability. Hydrogen atoms have been omitted for clarity.

Carrying out a similar reaction with the diphenyl or the diaryl ligand also leads to the isolation of orange products. The ^{1}H NMR spectra of these products have much sharper peaks than those observed in **4.5**. For example the spectra of **4.6** had one peak at 1.72 ppm representing the methyl substituents on the aryl groups and the rest of the spectrum consisted of aromatic signals. The ^{13}C NMR spectra of this product demonstrated that we have a symmetric complex with only one resonance for the CH_3 groups and 6 peaks for the naphthalene backbone. Crystals suitable for X-ray diffraction experiments where obtained from a saturated toluene solution. Table 4.3 and 4.4 show selected crystal data and structure refinement parameters and selected bond lengths and angles for **4.6**. The results of the X-ray experiment show that the complex obtained is a mononuclear compound with an octahedral metal center (Figure 4.3). The complex has two chloride ligands in the axial

positions, forming a Cl-Zr-Cl angle of 166.48°(8), and two amido nitrogens and the THF ligands residing in the equatorial plane. The Zr-N_{amido} bond in this complex are on average 2.073Å and is very similar complex **4.5**. The Zr-Cl bonds are on average 2.462Å which is very similar to what was observed for the terminal chlorides in **4.5**. Both nitrogen centers are planar with the sum of the angles surrounding them being 359.9° and 359.7° respectively for N(1) and N(2). The ligand in this complex differs from that in **4.5** as it is very close to coordination with the Zr center in a planar fashion. The bite angle for the ligand in this complex is 83.0°(3) still much smaller than what was reported in the related silyl substituted product.[16]

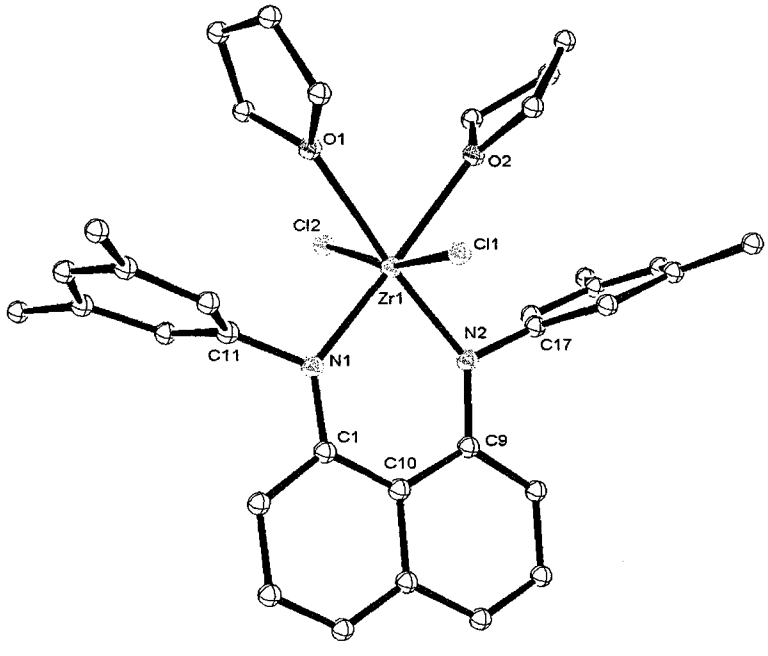

Figure 4.3. Molecular structure and partial atom-numbering schemes for **4.6**. Thermal ellipsoids are drawn at 20% probability. Hydrogen atoms have been omitted for clarity.

Complex **4.7** was also isolated as an orange solid in 69.5% yield. The ^{1}H NMR spectrum for this complex displayed only resonances for aromatic protons and coordinated THF. Further characterization using single crystal X-ray crystallography is summarized in Tables 4.3 and 4.4 and with Figure 4.4. As can be seen in Figure 4.4, compound **4.7** is a mononuclear complex. It appears that changing the nitrogen subtituents from 3,5-$(Me)_2C_6H_3$ to a less sterically demanding phenyl group is not a large enough difference to permit the formation of the dimeric product. The zirconium center in this complex is in an octahedral geometry with the two chlorides in the axial positions and the ligand N_{amido} and two THF groups in the equatorial sites. The Zr-N_{amido} bonds in this complex are similar to what was observed in **4.5** with an average of 2.043Å. The Zr-Cl bond are on average 2.604Å this is longer than what was observed in **4.5**, it is more similar to what was obtained for the bridging chlorides in complex **4.4**. Just like in the other zirconium complexes both nitrogen centers in **4.7** are planar and the ligand is not folded like in **4.5** but slightly twisted. The N-Zr-N angle is smaller in this complex than what we have observed in all the other complexes at 82.0°(2).

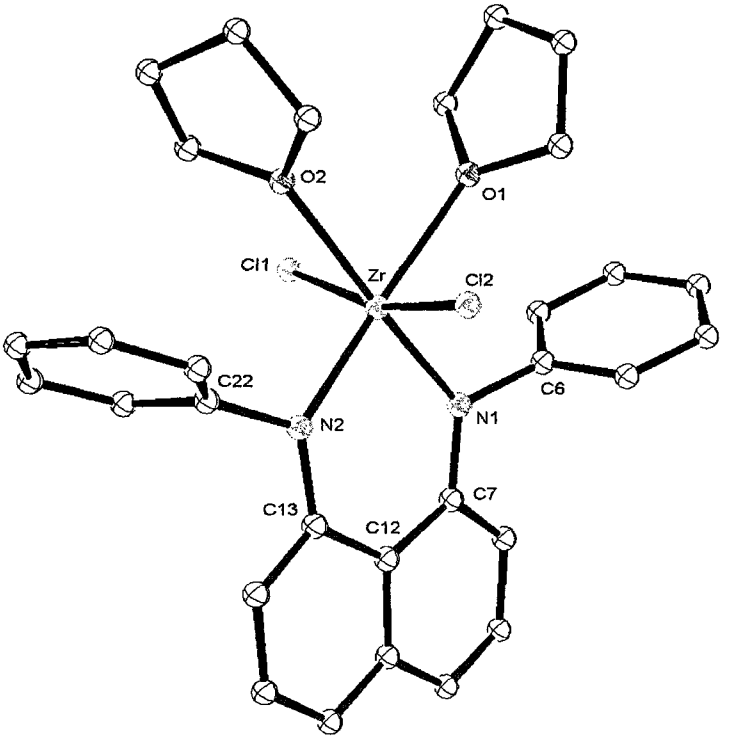

Figure 4.4. Molecular structure and partial atom-numbering schemes for **4.7.** Thermal ellipsoids are drawn at 20% probability. Hydrogen atoms have been omitted for clarity.

Another method to incorporate the R_2DAN ligands onto a zirconium center is by direct reaction of the parent ligand with a metal complex containing basic ligands that can be eliminated by proton transfer from the R_2DAN ligand. This method was employed using $Zr(NMe_2)_4$. The reaction of one equivalent of R_2DAN ligand with one equivalent of $Zr(NMe_2)_4$ led to the isolation of a yellow solid (Scheme 4.4). The ^{1}H NMR spectrum of this complex gave one doublet at 1.30 ppm integrating for 12 protons and one septet at 3.87 ppm integrating for two protons for the isopropyl groups. The single set of resonances for the isopropyl groups indicated a symmetric structure. This symmetrical structure was also supported by the presence of only one singlet at 2.70 ppm integrating for 12 protons and

representing the amide groups, this differs from the three signals that were observed in the ^{1}H NMR of [Zr{1,2-C_6H_4($NCH_2{}^tBu$)$_2$}(NMe_2)(μ-NMe_2)][12] at room temperature might be indicative of a monomer/dimer equilibrium. The ^{1}H NMR showed no trace of coordinated amine like was observed in [1,8-$C_{10}H_6$($NSiMe_3$)$_2$]Zr(NMe_2)($NHMe_2$)[17].

Scheme 4.4

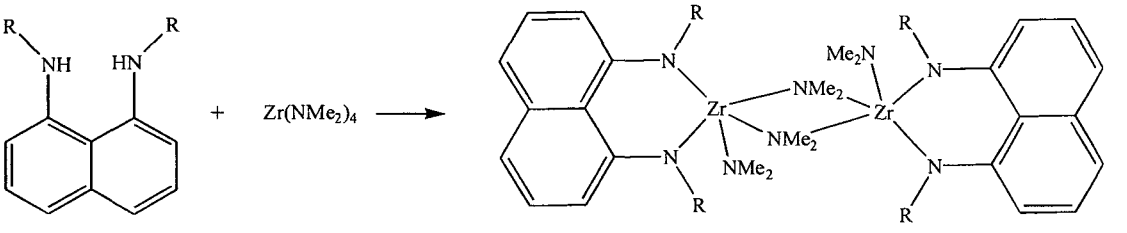

4.8 R= $CH(CH_3)_2$
4.9 R= 3,5-$Me_2C_6H_3$

The product of this reaction was further characterized by X-ray crystallography. Tables 4.5 and 4.6 provide selected crystal data and structure refinement parameters and selected bond lengths and angles for compound **4.8**. The structure obtained is a dinuclear species with two bridging amido groups. The zirconium centers are in distorted trigonal bipyramidal geometries with the axial positions being occupied by one of the briging amido and the other by of the ligand amido nitrogens. The equatorial positions are occupied by the other bridging amido, a terminal amido and the second ligand amido group. The Zr-N_{amido} bond lengths are of 2.156(9) and 2.032(8)Å respectively for N(1) and N(2) with the longest one being the one trans to the bridging amido. The Zr-N(2) bond length is very similar to what we have observed in the zirconium complexes presented above. The Zr-N_{amido} varying from 2.045(7)-2.382(1)Å with the longer bond lengths belonging to the bridging

groups as expected. The N(1)-Zr-N(2) angle in this complex is similar to what we observed for the zirconium complexes with a value of 84.3(3)° The nitrogen centers of the ligand are both planar with the sum of the angles surrounding them being 359.9°. The terminal amido nitrogen is also planar with the sum of the angles surrounding it being 360° while the bridging nitrogen centers are tetrahedral. Similar to what was observed in complex **4.5** the ligand in this molecule is folded with the angle between the N(1)-Zr-N(2) and N(1)-C(1)-C(6)-C(7)-N(2) planes being 49.15°

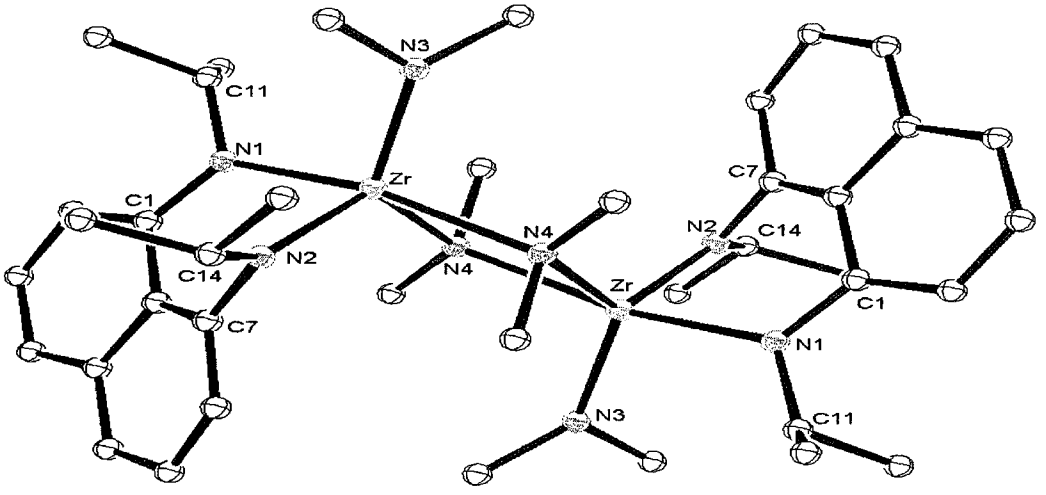

Figure 4.5. Molecular structure and partial atom-numbering schemes for **4.8.** Thermal ellipsoids are drawn at 20% probability. Hydrogen atoms have been omitted for clarity.

The preparation of $Zr(NMe_2)_2[1,8\text{-}(2,6\text{-}Me_2C_6H_3N)_2C_{10}H_6]$ can be achieved using the same method. From this reaction, compound **4.9** was also isolated as a yellow solid in high yield (83.4%). The ^1H NMR spectra of this product had two singlets integrating for 12 protons each, one for the NMe_2 groups and the other for CH_3 groups in the ligand. The presence of only two singlets suggested that this complex was fluxional.

Table 4.5. Selected Crystal Data and Structure Refinement Parameters for **4.8**

	4.8
Empirical formula	$C_{40}H_{64}N_8Zr_2$
Formula weight	839.43
Temperature (K)	203(2)
Wavelengths (Å)	0.71073
Crystal system	Monoclinic
Space group	P2(1)/n
a (Å)	10.6640(16)
b (Å)	19.4151(3)
c (Å)	10.6850(16)
α(deg)	90
β(deg)	109.981(4)
γ(deg)	90
V (Å^3)	2079.1(5)
Z	2
ρ(calc) (Mg/m^3)	1.341
μ (mm^{-1})	0.538
Absorption correction	Semi-empirical from equivalents
Final R indices [I>2σ(I)]	
R1[a]	0.0666
***w*R2**[b]	0.1787

[a] $R1 = \Sigma \| F_o | - | F_c \| / \Sigma | F_o |$

[b] $wR2 = (w(| F_o | - | F_c |)^2 / \Sigma w | F_o |^2)^{1/2}$

Table 4.6. Selected Bond Lengths (Å) and Angles (°) for **4.8**.

		4.8	
		Bond Lengths (Å)	
Zr-N(1)	2.156(9)	Zr-N(3)	2.045(7)
Zr-N(2)	2.032(8)	Zr#1-N(4)	2.263(9)
		Zr-N(4)	2.382(10)
		Angles (°)	
N(2)-Zr-N(1)	84.3(3)	C(17)-N(3)-C(18)	109.3(9)
C(1)-N(1)-C(11)	117.9(9)	C(17)-N(3)-Zr	117.5(6)
C(1)-N(1)-Zr	121.9(6)	C(18)-N(3)-Zr	133.2(8)
C(11)-N(1)-Zr	120.1(6)	C(20)-N(4)-C(19)	108.4(10)
C(7)-N(2)-C(14)	113.5(8)	C(20)-N(4)-Zr#1	119.7(8)
C(7)-N(2)-Zr	109.8(7)	C(19)-N(4)-Zr#1	95.3(7)
C(14)-N(2)-Zr	136.6(6)	C(20)-N(4)-Zr	116.0(8)
		C(19)-N(4)-Zr	111.4(7)
		Zr#1-N(4)-Zr	104.2(4)

Hafnium complexes can be prepared using the metathesis method. Reaction of one equivalent of $[1,8\text{-}(N^{i}Pr)_2C_{10}H_6]Li_2$ with $HfCl_4(THF)_2$ led to the formation of a yellow product which was characterized by NMR spectroscopy. The ^1H NMR spectrum for the product shows two doublets at 1.54 ppm and 1.73 ppm integrating for six protons showing that the CH_3 groups of the isopropyl groups are not equivalent. The ^1H NMR spectra also show the presence of one THF molecule per ligand suggesting that the complex would be a dimer with two bridging chlorides to give an octahedral hafnium center in analogy to the related zirconium structure (**4.3**). The ^{13}C NMR spectrum indicated a symmetric naphthalene backbone with only six aromatic signals.

Scheme 4.5

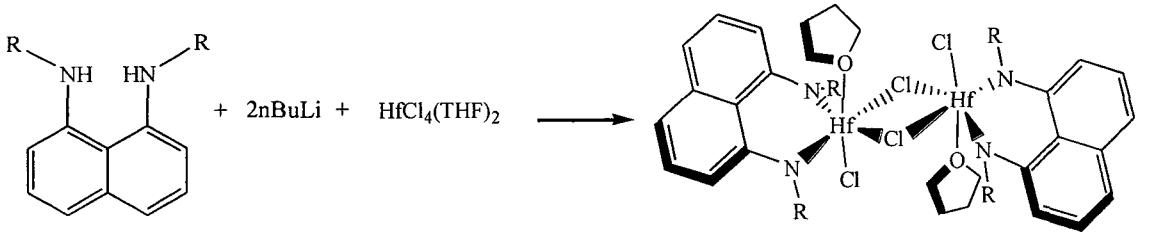

4.10 R= $CH(CH_3)_2$
4.11 R= 3,5-$Me_2C_6H_3$

Carrying out the same reaction with using an aryl substituted R_2DAN ligand led to the isolation of a yellow powder identified as **4.11** in 77.3% yield. The ^{1}H NMR spectrum for this product displayed only one peak for the aryl CH_3 groups. The ^{13}C NMR spectrum for this complex also suggests a symmetric structure. The one difference that is observed for this complex is the lack of signal for THF in both the proton and carbon spectra suggesting that the structure for this complex is different than what was proposed for complex **4.10.** This might be an indication that the hafnium center in this specific structure is in a tetrahedral geometry.

II. Conclusions:

A series of group 4 complexes bearing 1,8-diaminonaphthlene ligands was prepared. Crystallography experiments have shown that the R_2DAN ligand is flexible in coordination behavior and can be planar or folded. The nature of the nitrogen substituents have also been shown to influences the structural features of these complexes. Some substituents such as the isopropyl groups in complex **4.5** prefer to exist as dinuclear species while the aromatic

substituents led to the formation of monomeric complexes. These observations demonstrate the importance of the nitrogen substituents and the flexibility of the diaminonapthalene ligand.

III. Experimental Section:

General Methods. All manipulations were carried out in either a nitrogen-filled drybox or under nitrogen using standard Schlenk line techniques. Unless otherwise noted, solvents were sparged with nitrogen and then dried by passage through column of activated alumina using an apparatus purchased from Anhydrous Engineering. Deuterated benzene and toluene were dried by vacuum transfer from dried molecular sieve. $ZrCl_4$ and $HfCl_4$ where purchased from Strem and used without further purification. $TiCl_4$ was purchased from Aldrich and used without other purification. NMR spectra were run on either a Bruker Avance 300 MHz or a Bruker 500 MHz spectrometer with deuterated benzene or toluene as a solvent and internal standard. $HfCl_4(THF)_2$ and $ZrCl_4(THF)_2$ were prepared according to the literature methods[18].

Preparation of $TiCl_2[1,8\text{-}(N^iPr)_2C_{10}H_6]$ (4.1)

In a round bottom flask with a magnetic stir bar, $1,8\text{-}(HN^iPr)_2C_{10}H_6$ (201 mg, 0.83 mmol) was dissolved in ether. To this solution was added an ether solution of $TiCl_4$ (0.181 g, 0.95 mmol) followed by the addition of NEt_3 (324 mg, 3.2 mmol). The solution was allowed to stir at room temperature overnight fallowed by solvent removal under vacuum. The solid was extracted with toluene which was then evaporated under vacuum to afford a dark purple solid (100 mg, 34%).

^1H NMR (300 MHz, C_6D_6): δ 1.42 (d, 12H, $C(CH_3)_2$), 5.11 (sept, 2H, $CH(Me)_2$), 5.53 (d, 2H, Ar-H), 7.12-7.18 (m, 2H, Ar-H), 7.34 (d, 2H, Ar-H).

$^{13}C\{^1H\}$ NMR (75 MHz, C_6D_6): δ 19.5 (CH_3), 37.0 ($CH(Me)_2$), 103.9 ($C_{Ar}H$), 123.5 (C_{Ar}), 125.0 ($C_{Ar}H$), 125.6 ($C_{Ar}H$), 136.9 (C_{Ar}), 142.6 (C_{Ar}).

Preparation of $TiCl_2[1,8\text{-}(2,6\text{-}Me_2C_6H_3N)_2C_{10}H_6]$ (4.2)

In a round bottom flask equipped with a magnetic stir bar [1,8-(2,6-$Me_2C_6H_3N)_2C_{10}H_6$] (200 mg, 0.55 mmol) was dissolved in 10 ml of ether. To this was added 5 ml ether solution of $TiCl_4$ (113 mg, 0.60 mmol) followed by the addition of excess NEt_3 (228 mg, 2.25 mmol) . The reaction mixture was stirred at room termperature overnight and the resulting purple solution that was dried under vacuum. The solid obtained was extracted with toluene that was evaporated under vacuum to afford a purple solid. The purple solid is then washed with hexanes to give pure product (77 mg, 29%).

^1H NMR (300 MHz, C_6D_6): δ 2.04 (s, 12H, CH_3), 6.18 (d, 2H, Ar-H), 6.79 (s, 2H, Ar-H), 7.17-7.23 (m, 2H, Ar-H), 7.29 (s, 4H, Ar-H), 7.41 (d, 2H, Ar-H).

$^{13}C\{^1H\}$ NMR (75 MHz, C_6D_6): δ 21.0 (CH_3), 109.3 ($C_{Ar}H$), 122.2 (C_{Ar}), 125.4 ($C_{Ar}H$), 126.5 ($C_{Ar}H$), 126.8 (C_{Ar}), 128.9 ($C_{Ar}H$), 129.1 (C_{Ar}), 132.7 ($C_{Ar}H$), 141.2 (C_{Ar}), 147.8 (C_{Ar}).

Preparation of $Zr[1,8\text{-}(N^iPr)_2C_{10}H_6]_2$ (4.3)

In a vial equipped with a magnetic stir bar, 1,8-$(N^iPr)_2C_{10}H_6$ (200 mg , 0.83 mmol) was dissolved in 10 ml of ether. To this solution was added nBuLi (1.03 ml, 1.6 mmol) via syringe. This solution was stirred for 1h followed by the addition of $ZrCl_4(THF)_2$ (156 mg, 0.41 mmol). The reaction mixture was stirred overnight and then the solvent was removed under vacuum. The resulting solid was extracted with 30 ml of toluene and evaporated to dryness to afford an orange solid. The orange solid can be dissolved in THF precipitated by addition of hexanes to afford a pure product (174 mg, 74%).

^{1}H NMR (300 MHz, C_6D_6): δ 1.24 (d, 12H, $CH(CH_3)_2$), 6.59 (sept, 2H, $CH(Me)_2$), 7.00-7.11 (m, 2H, $C_{Ar}H$), 7.35-7.42 (m, 4H, $C_{Ar}H$).

$^{13}C\{^1H\}$ NMR (125 MHz, C_6D_6): δ 21.8 ($CH(CH_3)_2$), 47.5 ($CH(Me)_2$), 108.9 ($C_{Ar}H$), 121.7 ($C_{Ar}H$), 126.5 (C_{Ar}), 129.1 ($C_{Ar}H$), 129.9 (C_{Ar}), 147.9 (C_{Ar}).

Preparation of Hf[1,8-(N^iPr)$_2C_{10}H_6$]$_2$ (4.4)

In a round bottom flask equipped with a magnetic stir bar, 1,8-(^{i}PrNH)$_2C_{10}H_6$ (300 mg, 1.24 mmol) was dissolved in 30 ml of diethylether. To this solution was added nBuLi (1.55 ml, 2.48 mmol) and the mixture was stirred for 1 hour followed by addition of $HfCl_4$ (198 mg, 0.618 mmol). After stirring at room temperature overnight, the reaction mixture was filtered and dried under vacuum yielding a yellow solid that can be crystallized from saturated toluene solution at -20°C (209 mg, 78%).

^{1}H NMR (300 MHz, C_6D_6): δ 1.23 (d, 12H, CH_3) 3.96 (sept, 2H, CH), 6.57 (d, 2H, Ar-H), 7.11-7.35 (m, 4H, Ar-H)

$^{13}C\{^1H\}$ NMR (75 MHz, C_6D_6): δ 21.2 (CH_3), 47.7 (CH), 109.6 (CH_{Ar}), 120.7 (CH_{Ar}), 122.9 (C_{Ar}), 125.7 (CH_{Ar}), 138.3 (C_{Ar}), 147.9 (C_{Ar}).

Preparation of [$ZrCl_2$[1,8-(N^iPr)$_2C_{10}H_6$](THF)]$_2$ (4.5)

In a round bottom flask with a magnetic stir bar, 1,8-(^{i}PrNH)$_2C_{10}H_6$ (200 mg, 0.83 mmol) was dissolved in 15 ml of diethylether. To this solution was added nBuLi (1.05 ml, 1.7 mmol) and the solution was stirred for 1h. The solution was then added to $ZrCl_4(THF)_2$ (311 mg, 0.84 mmol) dissolved in 10 ml of diethylether. This reaction mixture was then stirred overnight at room temperature followed by filtration. The solvent was then removed

under vacuum to obtain an orange solid. This solid was crystallized at -20°C from a mixture of toluene and THF to afford orange crystal (259 mg, 66%).

^{1}H NMR (300 MHz, C_6D_6): δ 0.92 (br, THF), 1.52 (br, 6H, $CH(CH_3)_2$), 1.78 (br, 6H, $CH(CH_3)_2$), 4.10 (br, THF), 5.67 (br, 2H, $CH(Me)_2$), 6,83 (d, 2H, $C_{Ar}H$), 7.14 (s, 1H, $C_{Ar}H$,), 7.19 (s, 1H, $C_{Ar}H$), 7.24-7.31 (m, 2H, $C_{Ar}H$).

$^{13}C\{^1H\}$ NMR (75 MHz, C_6D_6): δ 19.2 (THF), 24.9 ($CH(CH_3)$), 46.9 ($CH(Me)_2$), 73.4 (THF), 111.1 ($C_{Ar}H$), 122.1 ($C_{Ar}H$), 125.1 ($C_{Ar}H$), 125.6 (C_{Ar}), 138.2 (C_{Ar}), 144.8 (C_{Ar}).

Preparation of $ZrCl_2[1,8\text{-}(2,6\text{-}Me_2C_6H_3N)_2C_{10}H_6](THF)_2$ (4.6)

In a round bottom flask equipped with a magnetic stir bar 1,8-(2,6-$Me_2C_6H_3NH)_2C_{10}H_6$ (200 mg, 0.55 mmol) was dissolved in 15 ml of diethylether. To this solution was added nBuLi (0.68 ml, 1.09 mmol) and the solution was stirred for 1h. $ZrCl_4(THF)_2$ (206 mg, 0.55 mmol) was then added to this solution. The reaction mixture was stirred overnight and the solvent was removed under vacuum. The resulting solid was extracted with toluene and dried under vacuum to obtain an orange solid that can be crystallized at -20°C from a saturated toluene (256 mg, 78%).

^{1}H NMR (300 MHz, C_6D_6): δ 0.89 (br, THF), 1.72 (s, 12, $CH(CH_3)_2$), 3.41 (br, THF), 6.25 (s, 2H, $C_{Ar}H$), 6.58 (s, 4H, $C_{Ar}H$), 6.98 (d, 2H, $C_{Ar}H$), 7.19 (t, 2H, $C_{Ar}H$), 7.24 (d, 2H, $C_{Ar}H$).

$^{13}C\{^1H\}$ NMR (75 MHz, C_6D_6): δ 14.9 (THF), 21.8 ($CH(CH_3)_2$, 73.4 (THF), 111.7 (C_{Ar}), 119.4 ($C_{Ar}H$), 122.1 (C_{Ar}), 127.0 ($C_{Ar}H$), 127.1 (C_{Ar}), 144.1 ($C_{Ar}H$).

Preparation of $ZrCl_2[1,8\text{-}(Ph)_2C_{10}H_6]$ (4.7)

In a round bottom flask equipped with a magnetic stir bar $1,8\text{-}(PhNH)_2C_{10}H_6$ (200 mg, 0.64 mmol) was dissolved in 20 ml of diethylether. To this solution was added nBuLi (0.81 ml, 1.3 mmol) and the solution was stirred for 1h. $ZrCl_4(THF)_2$ (242 mg, 0.64 mmol) was then added to this mixture. The reaction mixture was stirred overnight and then filtered and dried under vacuum to obtain an orange solid that was washed with hexanes to yield a clean product (294 mg 75%).

^1H NMR (300 MHz, C_6D_6): δ 1.13 (THF), 3.48 (THF), 6.41-6.64 (m, 4H. Ar-H), 6.73-6.82 (m, 6H, Ar-H), 7.02 (br, 2H, Ar-H), ($C_{Ar}H$), 7.33 (d, 2H, Ar-H), 7.65 (br, 2H, Ar-H).

$^{13}C\{^1H\}$ NMR (75 MHz, C_6D_6): δ 14.7 (THF), 72.4 (THF), 112.8 (C_{Ar}), 119.1 (C_{Ar}), 122.0 ($C_{Ar}H$), 124.1 ($C_{Ar}H$), 124.9 ($C_{Ar}H$), 127.1 ($C_{Ar}H$), 132.2($C_{Ar}H$), 139.2 (C_{Ar}), 144.2 (C_{Ar}),, 148.8($C_{Ar}H$).

Preparation of $ZrNMe_2[1,8\text{-}(N^iPr)_2C_{10}H_6]$ (4.8)

In a round bottom flask equipped with a magnetic stir bar $1,8\text{-}(^iPrNH)_2C_{10}H_6$ (300 mg, 1.24 mmol) was dissolved 25ml of toluene. To this solution was added $Zr(NMe_2)_4$ (330 mg, 1.24 mmol). The reaction mixture was stirred overnight at room temperature and then the solvent was removed under vacuum. The product obtained was washed with hexanes to yield a yellow powder (367 mg, 71%).

^1H NMR (300 MHz, C_6D_6): δ 1.30 (d, 12H, $CH(CH_3)_2$), 2.70 (s, 12H, $N(CH_3)_2$) 3.89 (sept, 2H, $CH(Me)_2$, 6.68 (d. 2H, Ar-H), 7.28-7.37 (m, 4H, Ar-H)

$^{13}C\{^1H\}$ NMR (75 MHz, C_6D_6): δ 24.5 $CH(\mathbf{C}H_3)_2$, 42.8 $N(CH_3)_2$, 53.0 $CH(Me)_2$, 111.6 ($C_{Ar}H$), 119.0 $C_{Ar}H$, 127.8 ($C_{Ar}H$), 128.1 (C_{Ar}), 139.9 (C_{Ar}), 149.5 (C_{Ar}).

Preparation of $ZrNMe_2[[1,8\text{-}(2,6\text{-}Me_2C_6H_3N)_2C_{10}H_6]$ (4.9)

In a round bottom flask [1,8-(2,6-$Me_2C_6H_3NH)_2C_{10}H_6$ (150 mg, 0.41mmol) was dissolved in toluene . To this solution was added $Zr(NMe_2)_4$ (0.112 mg, 0.42 mmol). The reaction mixture was stirred overnight fallowed by *in vacuo* solvent removal. The product obtained was an orange solid (186 mg, 83%).

^1H NMR (300 MHz, C_6D_6): δ 2.08 (s, 12H, CCH_3), 2.46 (s, 12H, NMe_2), 6.59 (d, 2H, Ar-H), 6.85 (br, 4H, Ar-H), 6.99 (d, 2H, Ar-H), 7.29 (t, 2H, Ar-H), 7.40 (d, 2H, Ar-H).

^{13}C NMR (300 MHz, C_6D_6): δ 22.1 (CH_3), 42.0 ($N(CH_3)_2$), 111.7 (C_{Ar}), 119.5 ($C_{Ar}H$), 120.5 ($C_{Ar}H$), 121.6 ($C_{Ar}H$), 122.0 (C_{Ar}), 127.0 ($C_{Ar}H$), 127.1 (C_{Ar}), 127.5 ($C_{Ar}H$), 142.4 (C_{Ar}) 143.5 (C_{Ar}).

Preparation of $HfCl_2[1,8\text{-}(N^iPr)_2C_{10}H_6](THF)$ (4.10)

In a round bottom flask 1,8-(^{i}PrNH)$_2C_{10}H_6$ (200 mg, 0.83 mmol) was dissolved in 15 ml of diethylether. To this solution was added nBuLi (1.05 ml, 1.68 mmol) and the solution was stirred for 1h. This solution was then added to $HfCl_4(THF)_2$ (387 mg, 0.83 mmol) dissolved in 10 ml of diethylether. The reaction mixture was then stirred overnight at room temperature. The reaction mixture was filtered and the solvent was removed under vacuum to obtain a yellow solid. The yellow solid was washed with 10 ml of hexanes to give the pure product (321 mg, 69%).

^{1}H NMR (300 MHz, C_6D_6): δ 0.79 (br, THF), 1.54 (d, 6H, $CH(CH_3)_2$), 1.73 (d, 6H, $CH(CH_3)_2$), 4.17 (br, THF), 5.39 (sept, 2H, $CH(CH_3)$, 6.85-6.82 (m, 2H, $C_{Ar}H$), 7.84 (d, 2H, $C_{Ar}H$), 7.20 (br, 2H, $C_{Ar}H$).

^{13}C NMR (300MHz, C_6D_6): δ 19.6 (THF), 23.1 ($CH(CH_3)$), 24.8 ($CH(CH_3)$), 48.5 ($CH(Me)_2$), 74.1 (THF), 113.6 ($C_{Ar}H$), 120.6 ($C_{Ar}H$), 125.0 ($C_{Ar}H$), 126.5 (C_{Ar}), 138.0 (C_{Ar}), 145.1 (C_{Ar}).

Preparation of $HfCl_2$[1,8-(2,6-$Me_2C_6H_3N)_2C_{10}H_6$] (4.11)

In a round bottom flask 1,8-(2,6-$Me_2C_6H_3N)_2C_{10}H_6$ (200 mg, 0.55 mmol) was dissolved in 15 ml of diethylether. To this solution was added nBuLi (0.68 ml, 1.09 mmol) and the solution was stirred for 1h. This solution was then added to a solution of $HfCl_4(THF)_2$ (0.253 mg, 0.55 mmol). The reaction mixture was stirred overnight and then the solvent was removed under vacuum. The resulting solid was extracted with toluene which was subsequently removed under vacuum. The yellow powder obtained can be washed with hexanes to obtain a pure product (259 mg, 77%).

^{1}H NMR (300 MHz, C_6D_6): δ 1.76 (s, 12H, CH_3), 6.26 (s, 2H, Ar-H), 6.67 (s, 4H, Ar-H), 6.92 (d, 2H, Ar-H), 7.19 (d, 2H, Ar-H), 7.32 (d, 2H, Ar-H).

^{13}C{^{1}H} NMR (125 MHz, C_6D_6): 22.2 (CH_3), 113.3 (C_{Ar}), 120.6 (C_{Ar}), 121.9 ($C_{Ar}H$), 126.3 (C_{Ar}), 126.7 ($C_{Ar}H$), 127.2 ($C_{Ar}H$), 129.2 ($C_{Ar}H$), 129.9 ($C_{Ar}H$, 139.4 (C_{Ar}), 142.9 (C_{Ar}).

References

[1] (a)Van der Linden, A.; Schaverien. C. J.; Meijboom, N.; Ganter, C.; Orpen, A. G. *J. Am. Chem. Soc.* **1995**, 117, 3008. (b) Fokken, S.; Spaniol, T. P.; Kang, H.-C.; Massa, W.; Okuda, J. *Organometallics,* **1996**, *15*, 5069. (c) Tjaden, E. B.; Swenson, D. C.; Jordan, R. F.; Petersen, J. L. *Organometallics* **1995**, *14*, 371. (d) Whitelaw, E. L.; Jones, M. D.; Mahon, M. F.; Kociok-Kohn, G. *Dalton Trans.* **2009**, 9020. (e) Zelikoff, A. L.; Kopilov, J.; Goldberg, I.; Coates, G. W.; Kol, M. *Chem. Commun.,* **2009**, 6804. (f) Kim, S. H.; Lee, J.; Kim, D. J.; Moon, J. H.; Yoon, S.; Oh, H. J.; Do, Y.; Ko, Y. S.; Yim, J-H.; Kim, Y. *J. Organomet Chem.* **2009**, 694, 3409. (g) Chmura. A. J.; Davidson, M. G.; Frankis, C. J.; Jones, M. D.; Lunnb, M. D., Chem. Commun. **2008**, 1293.

[2] (a) Guérin, F.; McConville, D. H.; Payne, N. C. *Organometallics* **1996**, *15*, 5085. (b) Guérin, F.; McConville, D. H.; Vittal, J. J. *Organometallics* **1996**, *15*, 5586. (c) Scollard, J. D.; McConville, D. H.; Vittal, J. J. *Organometallics,* **1995**, *14*, 5478. (d) Warren,T. H.; Schrock, R. R.; Davis, W. M. *Organometallics,* **1996**, *15*, 562. (e) Aoyagi, K.; Gantzel, P. K.; Kalai, K.; Tilley, T. D. *Organometallics,* **1996**, *15*, 923. (f) Horton, A. D.; de With, J. *J. Chem. Soc. Chem. Commun,* **1996**, 1375. (g) Horton, A. D.; de With, J.; van der Linden, A. J.; van de Weg, H. *Organometallics,* **1996**, *15*, 2672. (h) Tinkler, S.; Deeth, R. J.; Duncalf, D. J.; McCamley, A. *J. Chem.Soc. Dalton Trans.* **1996**, 2623. (i) Baumann, R.; Davis, W. M.; Schrock, R. R. *J. Am. Chem. Soc.* **1997**, *119*, 3830. (j) Scollard, J. D.; McConville, D. H.; Payne, N. C.; Vittal, J. J. *Macromolecules,* **1996**, *29*, 5241. (k) Scollard, J. D.; McConville, D. H. *J. Am. Chem. Soc.,* **1996**, *118*, 10008. (l) Mack, H.; Eisen, M. S. *J. Organomet. Chem.* **1996**, *525*, 81. (m) Skinner, M. E. G.; Toupance, T.; Cowhig, D. A.; Tyrrell, B. R.; Mountford, P. *Organometallics,* **2005**, *24,* 5586. (n) Blake, A. J.; Gillibrand, N. L.; Moxey, G. J.; Kays, D. L. *Inorg. Chem.* **2009**, 48, 10837. (o) Li, J.; Huang, S.; Weng, L.; Liu, D. *J. Organomet. Chem.* **2006**, 691, 3003. (p) Danièle, S.; Hitchcock, P. B.; Lappert, M. F.; Merle, P. G. *J. Chem. Soc. Dalton Trans.* **2001**, 13.

[3] Carone, C. L. P.; Fim, F. C.; Bisatto, R.; Jahno, V. D.; Lemos, C.; Basso, N. R. S.; Einloft, S.; Galland, G. B. *Journal of Applied Polymer Science*, **2008**, 110, 270.

[4] Gong, S.; Ma, H.; Huang, J.; *Dalton Trans.*, **2009**, 8237.

[5] Li, Y.; Gao. H.; Wu, Q. *J. Polym. Sci., Part A: Polym. Chem.* **2008**, 46, 93.

[6] Xie, G.; Qian, C. *J. Polym. Sci., Part A: Polym. Chem.* **2008**, 46, 211.

[7] Gong, S.; Ma. H.; Huang, J. *J. Organomet. Chem.* **2008**, 693, 3509.

[8] (a) Nomura, K.; Naga, N.; Takaoki, K. *Macromolecules* **1998**, *31,* 8009. (b) Nomura, K.; Naga, N.; Takaoki, K.; Imai, A. *Journal of Molecular Catalysis A: Chemical,* **1998**, 130, L209. (c) Nomuraa, K.; Oyab, K.; Imanishib. Y. *Polymer*, **2000**, 41, 2755.

[9] Lococo, M. D.; Lee, H.; Jordan, R. F. *Journal of Molecular Structure,* **2009**, 920, 363.

[10] Chisholm, M.H.; Hammond, C.E.; Huffman, J.C. *Polyhedron,* **1988**, 7, 2515.

[11] Polmano, M.; Mutikainen, I.; Leskela, M. Z. Kristallgr. **1996**, 211, 641.

[12] Tabernero. V; Cuenca. T.; Mosquera, M. E. G.; Ramírez de Arellano, C. *Polyhedron,* **2009**, 28, 2545.

[13] Cloke, F.G.N.; Hitchcock, P.B.; Love, J. B.; *J. Chem. Soc., Dalton Trans.* **1995**, 25.

[14] Lorber, C.; Donnadieu, B.; Choukroun, R.; *Organometallics,* **2000,** *19,* 1963.

[15] Freidrich, S.; Gade, L. H.; Scowen, I. J.; McPartlin, M. *Organometallics* **1995**, *14*, 5344.

[16] Lee, C. H.; La, Y-H.; Park, S. J.; Park, J. W. *Organometallics,* **1998**, 17, 3648.

[17] Lee, C. H.; La. Y-H.; Park. J. W. *Organometallics.* **2000**, 19, 344.

[18] Manzer, L. E. *Inorg. Synth.* **1982,** 21, 136.

Chapter 5

Tantalum Complexes Bearing 1,8-Diaminonaphthalene Ligands

I. Introduction

Exploring ligand-metal bonding and the associated impact in the stability and reactivity of metal complexes is a central theme in inorganic and organometallic chemistry. With d^0 early transition metal complexes, amido ligands have a well-established position and the role of such species in a host of small molecule transformations continues to stimulate interest in this area.[1,2] It remains important to explore new ligands in order to

reveal the fundamental and applied role and effects of the ligands in chemical transformation and catalysis.

The use of bis(amido) ligands to support high oxidation state tantalum complexes has become increasingly attractive to replace the less versatile cyclopentadienyl ligands. Some examples for bis(amido) ligands that have been employed to support tantalum include the o-phenylenediamine (PDA) (**A**)[3] and 1,8-$C_{10}H_6(HNSiMe_3)_2$ (**B**)[1(a)]. The PDA ligand resembles the disubstituted 1,8-diaminonaphthalene (R_2DAN) ligand (**C**) in bearing a dianionic charge but differs from the DAN ligand in the formation of a six-membered metallacyclic ring. One of the geometric effects of the larger ring size for R_2DAN should be a change in the steric impact of the N substituent. The α angle in **A** is larger than in **C** decreasing the steric protection for the metal that is offered by the ligand R groups. **B** on the other hand should have a very similar α angle to **C**, the difference in these two ligands will be in the electronic influences of the nitrogen substituents.

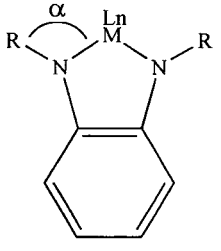

A

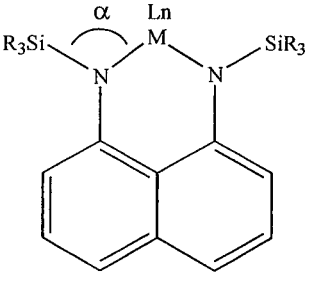

B

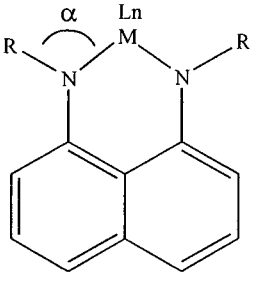

R= Alkyl or Aryl

C

One of our general interests, the design and implementation of rigid chelating ligands with delocalized π-electrons, led us to investigate the utilization of a family of diamido ligands, 1,8-$(RN)_2C_{10}H_6$ (**C**, R_2DAN^{2-}), in transition metal complexes.[4] In particular, we reported the reaction of 1,8-$(^iPrNH)_2C_{10}H_6$ with $TaMe_3Cl_2$ to produce an unusual

metallaaziridine complex, $\{[\kappa^3\text{-C,N,N-}(Me_2CN)(^iPrN)C_{10}H_6]TaCl_2\}_2$ (**E**).[3b] This species apparently arose from a σ-bond metathesis involving the ipso-CH function of the isopropyl substituents of the diamidonaphthalene ligand and elimination of methane from a Ta-Me function yielding this novel tridentate trianionic ligand, $[(Me_2CN)(Me_2CHN)C_{10}H_6]^{3-}$. This chapter reports the elaboration of this chemistry along two avenues. The first involves changing the N-substituents of the $1,8\text{-}(RN)_2C_{10}H_6$ ligand in an effort to control the reactivity of these groups when this scaffold is bonded to tantalum. The second explores the influence on the bonding and reactivity of the R_2DAN^{2-} through variation of the remaining ligands bonded to Ta. Through these efforts we demonstrate the versatility and flexibility of this ligand class in bonding with metal centers and the responsiveness of these species to the electronic demands of the metal center and conditions to provoke reaction and CH activation.

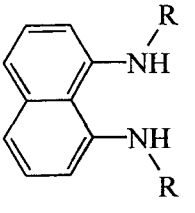

D

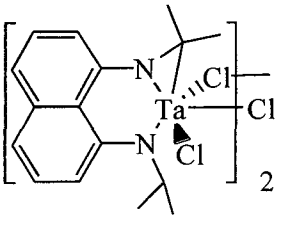

E

II. Results and Discussion

Synthesis and characterization of R_2DAN^{2-} complexes of Ta(V)

The introduction of the dianionic 1,8-diaminonaphthalene ligand, R_2DAN^{2-} into the coordination sphere of a metal complex can be achieved using two complimentary approaches. The first avenue involves the direct reaction of R_2DANH_2 with a metal complex possessing two basic ligands that are capable of undergoing a proton transfer

reaction. Elimination of the metal-bound ligand results in incorporation of dianion R_2DAN^{2-} into the metal coordination sphere. A second method involves a two step process that first deprotonates R_2DANH_2 with butyllithium to generate a dilithiated amido species, Li_2R_2DAN. A subsequent metathesis reaction between this reagent and a dichloro metal complex would incorporate the R_2DAN^{2-} ligand onto the metal center along with eliminatation of two equivalents of LiCl.

We found that $TaMe_3Cl_2$ was a readily accessible and functional starting material to demonstrate both approaches. The direct reaction of the N,N'-diaryl-1,8-diaminonaphthalene with $TaMe_3Cl_2$ produced two analogous species $TaCl_3$[1,8-$(RN)_2C_{10}H_6$] (**5.1** R= Ph; **5.2** R= 3,5-$Me_2C_6H_3$) as red-brown powders in good yields. (Scheme 5.1) The ^{1}H NMR spectra for these compounds provided the first indication for the formation of the symmetrical structures for **5.1** and **5.2** as represented in Scheme 5.1. In addition to the anticipated aromatic proton resonances, the spectrum for **5.2** displayed a singlet integrating for the 12 protons consistent with the four methyl groups on the N-Ar' substituents. The simple ^{13}C NMR spectra for both **5.1** and **5.2** also suggested a symmetrical structure for both species. Importantly, neither complex displayed spectroscopic indications of remaining Ta-Me functions suggesting that there had been exchange of Cl and Me groups bonded to tantalum during the reaction. This is an established phenomenon.[5]

Scheme 5.1

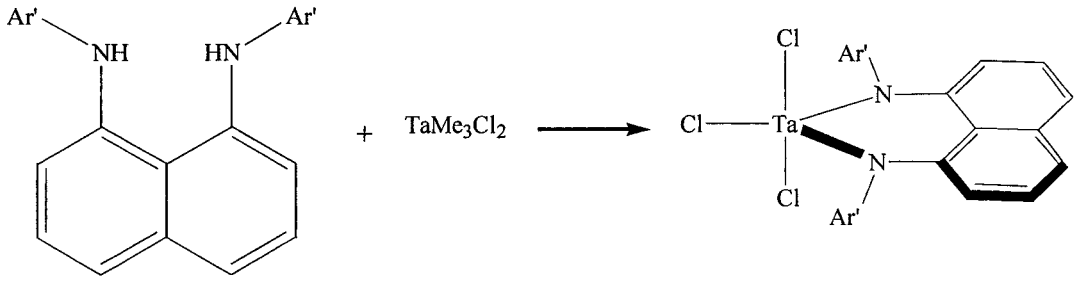

5.1 Ar' = Ph
5.2 Ar'= 3,5-$Me_2C_6H_3$

Details for the molecular connectivity and level of aggregation for **5.1** were revealed through X-ray crystallography (Table 5.1).[6] These results are displayed in Figure 5.1 and summarized in Table 5.2. Examination of Figure 5.1 indicated that the coordination geometry for **5.1** is derived from a distorted trigonal bipyramidal ligand array with two chloro ligands (Cl(2) and Cl(3)) in the axial positions (Cl(2)-Ta-Cl(3)= 169.0°(1)). The equatorial plane is defined by the remaining chloride (Cl(1)) and the N1 and N2 centers of the R_2DAN^{2-} ligand (Σ angles = 360°). The tau factor for this complex was calculated and once again was low due to the chelating ligand just like was observed in Chapter 3. The two nitrogen centers (N1, N2) for the R_2DAN ligand are planar (Σ N angles 359.9° and 358.3°) and these planes are coincident with the plane of the naphthyl group, which aligns the lone pairs of electrons on these centers for π overlap with their adjacent atoms. The Ta-N bond lengths in **5.1** average 1.91Å and are very similar to the ones we obtained for **E**.[4a] The Ta-Cl distances average 2.40Å they are slightly longer than the Ta-Cl bonds of the terminal chlorides in complex **E** but shorther than the briging chloride tantalum bonds in **E**.[4a] A distinctive feature for the coordination of the diamidonaphthalene ligand to the Ta

center is the planar orientation of the naphthyl moiety and the plane defined by N(1)-Ta-N(2). While this is similar to our observations with Ge(II)[7] and our reported pnictogenium cations,[8] this observation differs significantly from the previously reported tungsten[4b] and tin[9] complexes bearing this ligand. For example, in the W(VI) complex $W(=N^tBu)_2[1,8-(^iPr\ N)_2C_{10}H_6]$ the naphthyl moiety and the N(1)-W(1)-N(2) plane exhibit a fold angle of 122.6°.

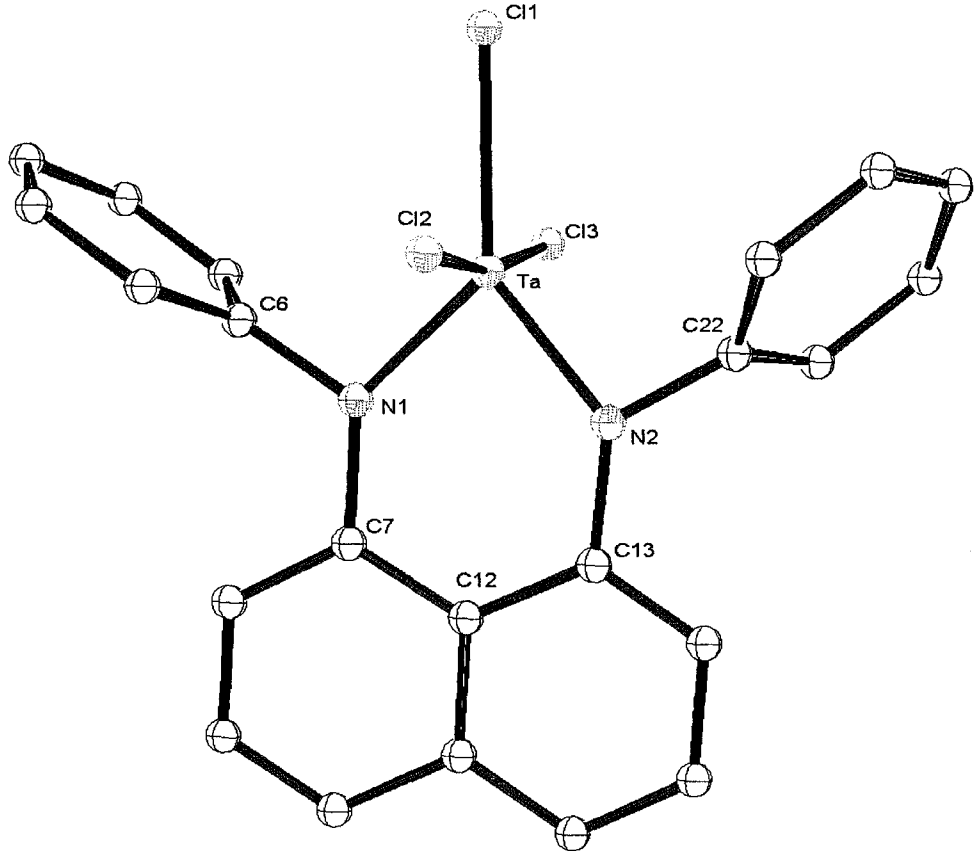

Figure 5.1. The molecular structure and atom numbering scheme for $TaCl_3[1,8-(PhN)_2C_{10}H_6]$ **(5.1)**. Co-crystallized hexane molecules and hydrogen atoms have been omitted for clarity.

Table 5.1. Selected Crystal Data and Structure Refinement Parameters for $TaCl_3[1,8\text{-}(PhN)_2C_{10}H_6]$ (**5.1**) and $TaMe_3[1,8\text{-}(PhN)_2C_{10}H_6]$ (**5.3**).

	5.1	**5.3**
Empirical formula	$C_{25}H_{23}Cl_3N_2Ta$	$C_{25}H_{25}N_2Ta$
Formula mass	638.75	534.42
Temperature (K)	203(2)	203(2)
λ (Å)	0.71073	0.71073
Crystal system	triclinic	triclinic
Space group	P-1	P-1
a (Å)	7.906(5)	10.5074(11)
b (Å)	12.406(8)	10.5509(11)
c (Å)	13.806(9)	11.9869(13)
α (deg)	70.028(7)	96.708(2)
β (deg)	85.467(7)	113.601(2)
γ (deg	78.172(7)	113.073(2)
V (Å^3)	1245.7	1059.64(19)
Z	2	2
ρ(calc) (Mg/m3)	1.703	1.675
μ (mm-1)	4.748	5.198
Absorbtion correction	Semi-empirical from equivalents	
final *R* indices [$I > 2\acute{o}(I)$]		
R1[a]	0.0581	0.0372
***w*R2**[b]	0.1138	0.1674

[a] $R1 = \Sigma \| F_o | - | F_c \| / \Sigma | F_o |$

[b] $wR2 = (w(| F_o | - | F_c |)^2 / \Sigma w | F_o |^2)^{1/2}$

Table 5.2. Selected Bond Lengths (Å) and Angles (°) for $TaCl_3[1,8\text{-}(PhN)_2C_{10}H_6]$ (**5.1**) and $TaMe_3[1,8\text{-}(PhN)_2C_{10}H_6]$ (**5.3**).

5.1		**5.3**	
	Bond lengths (Å)		
Ta-N(1)	1.892(8)	Ta-N(1)	2.064(7)
Ta-N(2)	1.931(9)	Ta-N(2)	1.954(7)
Ta-Cl(3)	2.393(3)	Ta-C(23)	2.120(10)
Ta-Cl(2)	2.396(3)	Ta-C(25)	2.153(11)
Ta-Cl(1)	2.414(3)	Ta-C(24)	2.181(10)
N(2)-C(13)	1.432(12)	N(2)-C(22)	1.397(10)
N(2)-C(22)	1.422(12)	N(2)-C(13)	1.420(10)
N(1)-C(7)	1.445(12)	N(1)-C(7)	1.430(9)
N(1)-C(6)	1.450(13)	N(1)-C(6)	1.430(10)
	Angles (°)		
C(7)-N(1)-C(6)	121.4(8)	C(7)-N(1)-C(6)	114.8(7)
C(7)-N(1)-Ta	136.1(7)	C(7)-N(1)-Ta	111.2(5)
C(6)-N(1)-Ta	102.4(6)	C(6)-N(1)-Ta	133.4(5)
C(22)-N(2)-C(13)	123.8(9)	C(22)-N(2)-C(13)	120.5(7)
C(22)-N(2)-Ta	99.9(6)	C(22)-N(2)-Ta	135.7(6)
C(13)-N(2)-Ta	134.9(7)	C(13)-N(2)-Ta	101.0(5)
N(1)-Ta-N(2)	85.3(4)	N(2)-Ta-N(1)	87.4(3)
Cl(3)-Ta-Cl(2)	169.04(10)	N(1)-Ta-C(24)	159.2(4)
N(2)-Ta-Cl(1)	141.7(3)	C(25)-Ta-C(23)	113.0(4)
N(1)-Ta-Cl(1)	133.0(3)	C(23)-Ta-N(2)	115.6(3)
		N(2)-Ta-C(25)	131.4(4)
τ	0.46	τ	0.46

The starting material $TaMe_3Cl_2$ also represented an excellent choice for exploring the second approach for introducing the R_2DAN^{2-} ligand (Scheme 5.2). The stoichiometric reaction of the *in situ* generated species $(R_2DAN^{2-})(Li^+)_2$ with one equivalent of $TaMe_3Cl_2$ led to the formation of $TaMe_3[1,8\text{-}(RN)_2C_{10}H_6]$ (R= Ph **5.3**; R= 3,5-$Me_2C_6H_3$ **5.4**) as dark

orange and red materials respectively. As with compounds **5.1** and **5.2**, complexes **5.3** and **5.4** displayed simple ^{1}H NMR spectra indicating symmetric structures. For example, both compounds provided one singlet for the Ta-bonded methyl groups.

Scheme 5.2

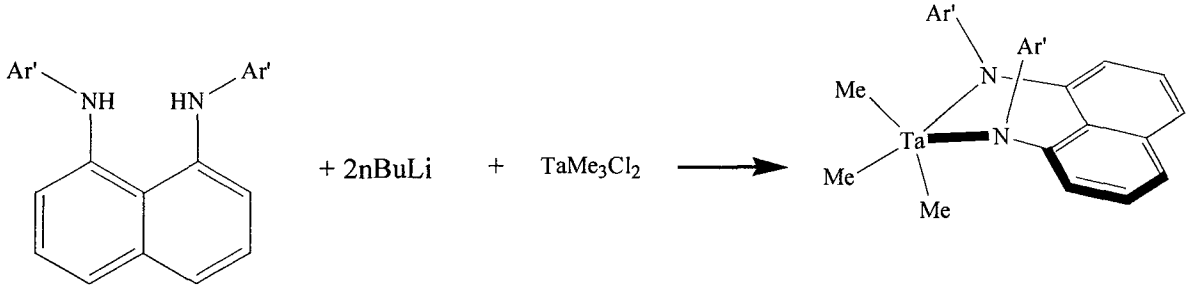

5.3 Ar' = Ph
5.4 Ar'= 3,5-$Me_2C_6H_3$

Single crystals suitable for X-ray analysis where obtained for **5.3** from a cooled solution of diethylether (Table 5.1). These results, summarized in Figure 5.2 and Table 5.2, not only establish the connectivity for this compound but allow for comparison of this trimethyl species with the trichloro complex **5.1**. Similar to compound **5.1**, the Ta center of **5.3** resides in a distorted trigonal bipyramidal coordination geometry. However, several key structural features of **5.3** contrast with those of **5.1**. Notably, in **5.3** the R_2DAN ligand is bonded to Ta through axial and equatorial sites leading to the pseudo-axial positions being defined by a methyl group and one of the nitrogen centers of the R_2DAN ligand (C24-Ta-N1 = 159.2(4)°). The equatorial positions are occupied by the remaining two methyl groups (C23, C25) and the second N center (N2) of the R_2DAN^{2-} ligand. The Ta-N bond lengths in **5.3** are slightly longer (~0.1Å) than those observed for **5.1**. Furthermore the axial Ta-N bond length is, as anticipated, slightly longer (Ta-N1 = 2.064(7)Å) than the equatorial Ta-

N2 bond at 1.954(7)Å. One of the most pronounced differences between the ligand binding in **5.3** compared to **5.1** is the orientation of the N-substituents relative the naphthyl plane. Importantly, while the two N centers in the $(PhN)_2C_{10}H_6^{2-}$ ligand are planar with the sums of the angle around N1 and N2 being 360.0 and 359.4°, it is quite clear that the ligand in **5.3** is not planar. It is the relative orientation of the ligand components that clearly differentiates the R_2DAN ligands of **5.1** and **5.3**. While $TaCl_3[1,8\text{-}(PhN)_2C_{10}H_6]$ (**5.1**) exhibited N planes that are coplanar with the naphthyl group, in the trimethyl complex **5.3**, only the plane for N1 is aligned with the napthyl moiety while the N2 plane is almost perpendicular to the naphthyl plane. This orients the phenyl group bonded to N2 vertical to the ligand plane. As a result, the ligand in **5.3** is not coordinated to the Ta center in a planar fashion and the observed fold angle between the naphthyl moiety and the N_1-Ta-N_2 plane is 61.4°. This feature is reminiscent of the reported tungsten[4b] and tin[4a] complexes with the R_2DAN^{2-} ligand. Furthermore, it is similar to structural features that have been observed in high valent group 4,[1g] Ta[10], Mo,[11,12] and W[13] species bearing N, N' – bis(trialkylsilyl)-o-phenylene diamide (PDA) ligands. In the case of the PDA complexes, the fold of the ligand about the N-N vector has been attributed to an increase in metal ligand interaction through a π donation from the phenylene component of the ligand into the metal orbitals.[4b,10,11] In order to better understand the origin of these structural differences, we have examined **5.1** and **5.3** computationally and the results of our analysis are presented below.

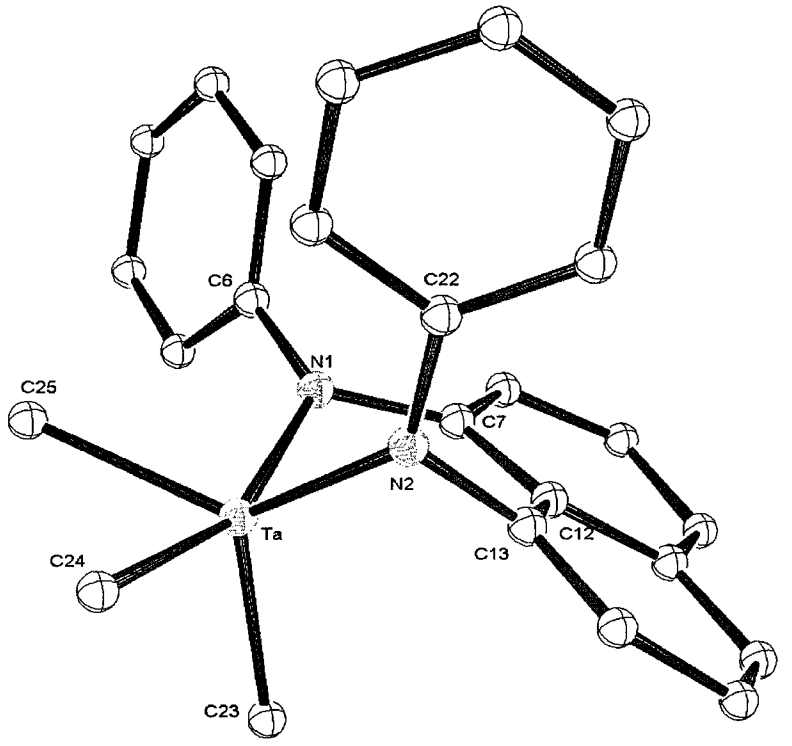

Figure 5.2. Thermal ellipsoid plot showing the molecular structure and atom numbering scheme for $TaMe_3[1,8\text{-}(PhN)_2C_{10}H_6]$ (**5.3**). Thermal ellipsoid are drawn at 20% probability. Hydrogen atoms have been omitted for clarity.

Similarly versatile Ta starting materials are represented by the two readily available Ta diethylamido species, $\{Ta(NEt_2)_2Cl_3\}_2$ and the mononuclear analogue $Ta(NEt_2)_2Cl_3(py)$.[14] These species allow for further investigation of the role of the tantalum ligand scaffold on R_2DAN^{2-} bonding. Both of these starting complexes undergo metathesis reactions with an equimolar ratio of $Li_2(R_2DAN)$ to yield the analogous products Ta $[1,8\text{-}(RN)_2C_{10}H_6](NEt_2)_2Cl$ (R = $(CH_3)_2CH$ **5.5**, 3,5-$Me_2C_6H_3$ **5.6**) (Scheme 5.3) which were isolated as orange/red solids in 63% yield. The structure of $Ta(NEt_2)_2Cl[1,8\text{-}(^iPrN)C_{10}H_6]$

(5.5) was initially proposed based on the ^1H NMR spectrum that displayed single sets of resonances for the two diethyl amido groups and for two isopropyl groups on the R_2DAN ligand. These observations differ from what Decams and *al.* had observed for the [1,8 - $C_{10}H_6(NSiMe_3)_2$]$Ta(NEt_2)_2Cl$ complex, in this case they observed two set of resonances for the diethyl amido and for the $SiMe_3$ groups indicating a non-symmetric structure[1a].

Significantly, the NMR data indicated that the ipso-CH signals of the isopropyl groups are intact in compound **5.5** and that both the ethyl CH_2 signals and the ipso-CH signals appeared as broad signals. These features point to two conclusions regarding **5.5**. First, in spite of the presence of basic amido sites within the tantalum complex, there is no reaction of these Ta-NR_2 groups with the isopropyl C-H bond. This contrasts with the reported reaction of [1,8-(^{i}PrNH)$_2C_{10}H_6$] and $TaMe_3Cl_2$ which involved the elimination of the isopropyl C-H bond and a Ta-Me group with formation of the metallaaziridine $[(Me_2CN)(Me_2CHN)C_{10}H_6]TaCl_2]_2$.[7] Second, complex **5.5** appeared to be fluxional on the NMR timescale at room temperature.

Scheme 5.3

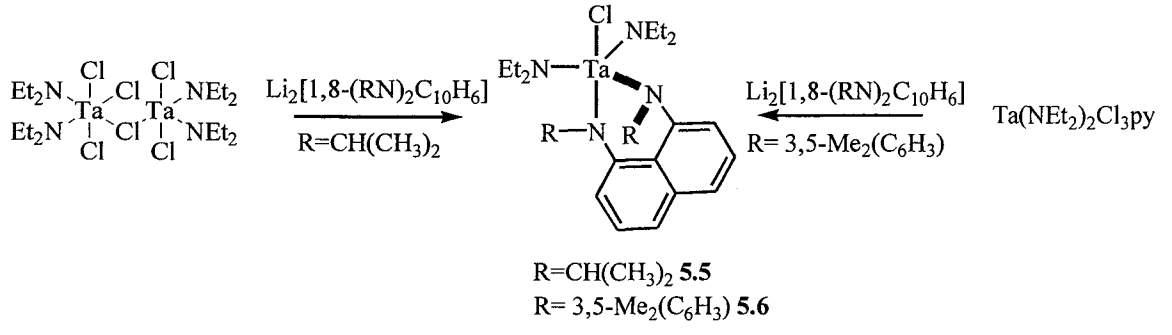

R=$CH(CH_3)_2$ **5.5**
R= 3,5-$Me_2(C_6H_3)$ **5.6**

The connectivity of **5.5** was firmly established by X-ray crystallography (Table 5.3) with the results summarized in Figure 5.3 and Table 5.4. In this complex the tau factor is of 0.89 supporting are assignment of trigonal bipyramidal geometry. The Ta core is reminiscent of **5.3** and, once again, the coordination geometry of the tantalum center can be described as a distorted trigonal bipyramidal with N(2) and Cl defining the axial positions (N(2)-Ta(1)-Cl(1) = 176.18(14)°). The sum of the angles in the equatorial plane, defined by N1, N3, and N4 is 360°. The Ta-N1 and Ta-N2 bond lengths of 1.983(5)Å and 2.084(5)Å are comparable to reported complexes. [15] The Ta-NEt_2 bond lengths are slightly shorter at 1.948(5)Å (Ta-N3) and 1.965(5)Å (Ta-N4). Within the chelating $^{i}Pr_2DAN$ ligand, nitrogen center N2 is planar while N1 deviates slightly from planarity (Σ angles N1= 355.9°). The plane of nitrogen N2 approaches alignment with the naphthyl plane. However, the mean plane for the N1 nitrogen makes an angle of 57° with the naphthyl plane. As a result the isopropyl substituent on N1 points away from the napthyl plane. The overall coordination geometry and the relative orientation of the R_2DAN ligand in **5.5** is similar to that observed in compound **5.3**.

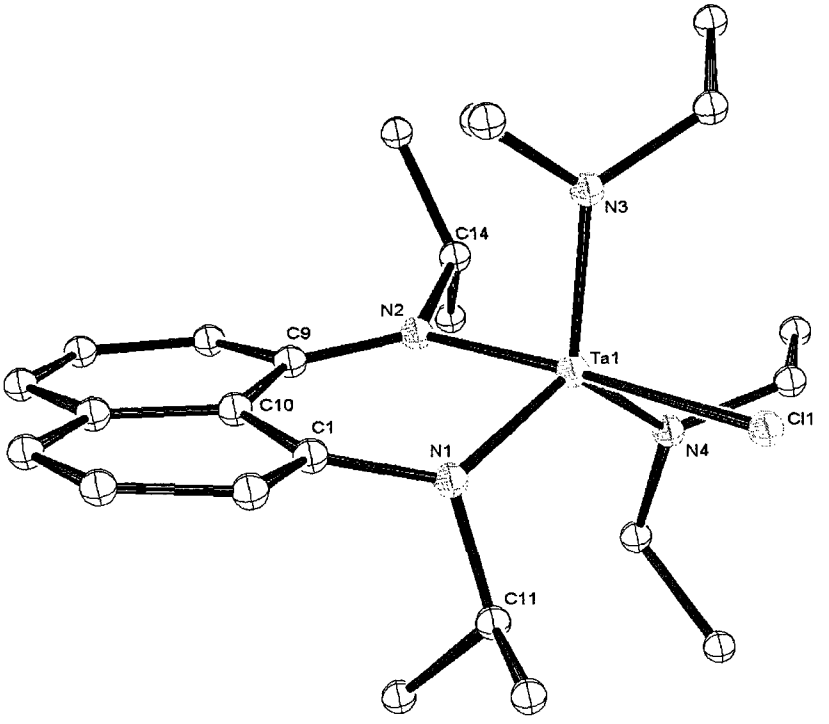

Figure 5.3. Thermal ellipsoid plot showing the molecular structure and partial atom numbering scheme for $Ta(NEt_2)_2Cl[1,8\text{-}(N^iPr)_2C_{10}H_6]$ (**5.5**). Thermal ellipsoid are drawn at 20% probability. Hydrogen atoms have been omitted for clarity.

Table 5.3. Selected Crystal Data and Structure Refinement Parameters for $Ta(NEt_2)_2Cl[1,8\text{-}(^iPrN)_2C_{10}H_6]$ (**5.5**) and $Ta(NEt_2)_2NMe[1,8\text{-}(^iPrN)_2C_{10}H_6]$ (**5.7**).

	5.5	**5.7**
Empirical formula	$C_{24}H_{40}ClN_4Ta$	$C_{26}H_{46}N_5Ta$
Formula mass	601.00	609.63
Temperature (K)	201(2)	293(2)
λ (Å)	0.71073	0.71073
crystal system	monoclinic	triclinic
Space group	P2(1)/n	P-1
***a* (Å)**	14.8426(12)	10.5712(12)
***b* (Å)**	11.4911(9)	10.6469(12)
***c* (Å)**	16.5518(13)	14.3310(17)
α (deg)	90	74.850(2)
β (deg)	113.9450(10)	73.189(2)
γ (deg	90	65.1710(10)
V (Å^3)	2580.1(4)	1383.0(3)
Z	4	2
ρ(calc) (Mg/m3)	1.547	1.464
***μ* (mm-1)**	4.381	3.995
Absorption correction	Semi-empirical from equivalents	
final *R* indices [$I > 2\sigma(I)$]		
R1[a]	0.0367	0.0446
***w*R2**[b]	0.0762	0.1065

[a] $R1 = \Sigma \| F_o | - | F_c \| / \Sigma | F_o |$

[b] $wR2 = (w(| F_o | - | F_c |)^2 / \Sigma w | F_o |^2)^{1/2}$

Table 5.4. Selected Bond Lengths (Å) and Angles (°) $Ta(NEt_2)_2Cl[1,8\text{-}(^iPrN)_2C_{10}H_6]$ (5.5) and $Ta(NEt_2)_2NMe[1,8\text{-}(^iPrN)_2C_{10}H_6]$ (5.7).

	5.5		5.7
	Bong lengths (Å)		
Ta(1)-N(1)	1.938(5)	N(1)-Ta(1)	2.064(18)
Ta(1)-N(2)	2.084(5)	N(2)-Ta(1)	2.04(3)
Ta(1)-N(3)	1.948(5)	N(4)-Ta(1)	1.899(10)
Ta(1)-N(4)	1.965(5)	N(5)-Ta	1.987(10)
Ta(1)-Cl(1)	2.468(2)	N(3)-Ta	2.086(10)
N(1)-C(1)	1.443(8)	N(1)-C(1)	1.405(15)
N(1)-C(11)	1.491(8)	N(1)-C(11)	1.50(2)
N(2)-C(9)	1.391(8)	N(2)-C(10)	1.418(15)
N(2)-C(14)	1.488(8)	N(2)-C(14)	1.45(3)
	Bond Angles (°)		
C(1)-N(1)-C(11)	116.9(5)	C(1)-N(1)-C(11)	116.3(17)
C(11)-N(1)-Ta(1)	110.3(4)	C(11)-N(1)-Ta(1)	108.1(10)
C(1)-N(1)-Ta(1)	128.7(4)	C(1)-N(1)-Ta(1)	135.2(15)
C(9)-N(2)-C(14)	118.9(5)	C(10)-N(2)-C(14)	117(2)
C(9)-N(2)-Ta(1)	130.9(4)	C(14)-N(2)-Ta(1)	118.9(13)
C(14)-N(2)-Ta(1)	109.8(4)	C(10)-N(2)-Ta(1)	123.8(16)
N(1)-Ta(1)-N(2)	83.5(2)	N(2)-Ta(1)-N(1)	81.9(7)
N(2)-Ta-Cl(1)	176.18(14)	N(3)-Ta-N(1)	172.1(5)
N(1)-Ta-N(3)	116.2(2)	N(2)-Ta-N(4)	116.6(6)
N(3)-Ta-N(4)	120.2(2)	N(4)-Ta-N(5)	125.9(5)
N(4)-Ta-N(1)	123.6(2)	N(2)-Ta-N(5)	117.5(6)
τ	0.89	τ	0.77

Computational Studies of Complexes 5.1, 5.3, and 5.5.

The fundamental electronic features that led to the observed structural differences for the trichloro complex **5.1** compared to the trimethyl compound **5.3** and the amido compound **5.5** were examined computationally using density functional theory. Optimizations of $[TaCl_3(1,8\text{-}(PhN)_2C_{10}H_6)]$ (**5.1**), $[TaMe_3(1,8\text{-}(PhN)_2C_{10}H_6)]$ (**5.3**) and $Ta(NEt_2)_2Cl[1,8\text{-}(N^iPr)_2C_{10}H_6]$ (**5.5**) using the B3LYP functional with a DGDZVP basis set yielded computed structures that were similar to the experimental X-ray structures of these species in terms of metal coordination geometry, ligand orientation and bond distances, thus supporting this approach. Our examination begins with a comparison of the electronic features of **5.1** and **5.3** and is followed by inclusion of compound **5.5**.

In the case of compound **5.1** the R_2DAN^{2-} ligand displayed a planar coordination. An electronic analysis was first carried out by examination of the interaction of the diamido ligand $((PhN)_2C_{10}H_6)^{2-}$ fragment orbitals with those of the $TaCl_3^{2+}$ fragment. The key donor orbitals of the ligand fragment are the four highest occupied fragment orbitals (HOFOs) shown in Figure 5.4. The HOFO and HOFO-1 are oriented for π interaction with the metal fragment and HOFO-2 and HOFO-3 are σ-type donor orbitals. The charge donation from each of these doubly-occupied orbitals to the $TaCl_3^{2+}$ fragment is indicated by the percentage values next to each HOFO in the figure. These represent the changes in the orbital populations upon the formation of the complex. In sum, 1.88 electrons are donated from the R_2DAN^{2-} fragment to the $TaCl_3^{2+}$ fragment giving a total bond order of 2.69. The donation from the ligand reduces the NPA (natural population analysis) charge on Ta in the $TaCl_3^{2+}$ fragment from +1.75 to +1.54.

The optimization calculation for the trimethyl species **5.3** also reflected the

orientation of the two amido moieties and the non-planar orientation of the R_2DAN^{2-} ligand that was obtained from X-ray analysis. Again, the interactions of the diamido fragment, $((PhN)_2C_{10}H_6)^{2-}$, and the metal fragment, $TaMe_3^{2+}$ were examined. The donor HOFOs for the ligand orientation represented in complex **5.3** are shown in Figure 5.4 and the energies of these orbitals are similar to those in **5.1**. The distortion from planarity changes the nature of the HOFOs to a mixture of σ and π overlap with the metal fragment. Again, the donor contribution from each orbital is shown by the percentage value of the change in electron population. Significant reduction in donation from the ligand HOFO and HOFO-2 are the most important differences from **5.1**. With the non-planar ligand orientation, the R_2DAN^{2-} fragment donates only 1.31 electrons to the $TaMe_3^{2+}$ fragment and this in turn leads to a reduced bond order between the fragments of 2.10. The reduced donation is also reflected by the higher NPA charge on the Ta center in **5.3** of +1.97 compared to **5.1**.

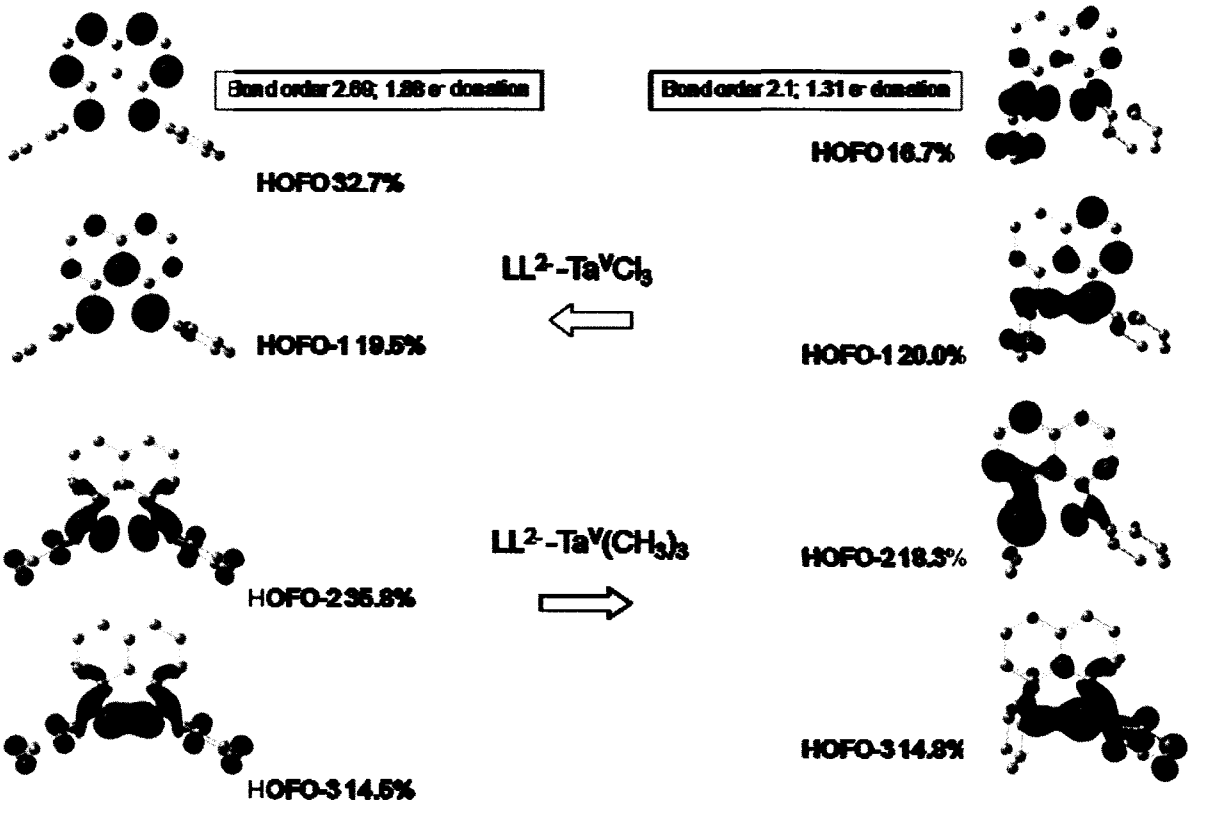

Figure 5.4. Representation of the ligand fragment donor molecular orbitals.

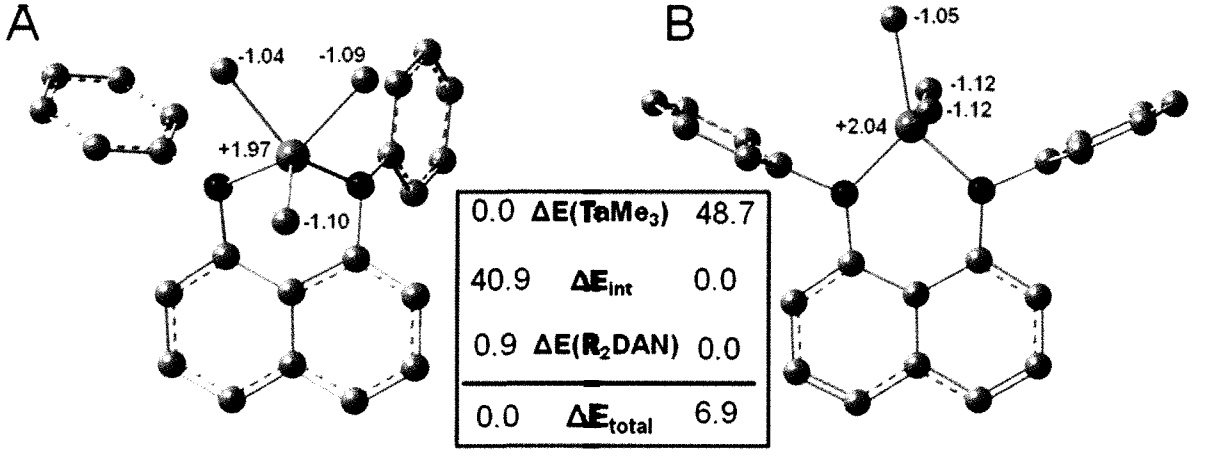

Figure 5.5. A comparison of energies (Kcal/mol) for the experimental structure of **5.3 (A)** and a proposed model structure **(B)**.

From this orbital interaction analysis it is clear that the degree of R_2DAN^{2-} donation and the ligand-metal fragment bond order is lower for the trimethyl complex **5.3** compared to the trichloro complex **5.1**. In order to more clearly determine the origin for these differences, the trimethyl complex, $[TaMe_3(1,8\text{-}(PhN)_2C_{10}H_6)]$ (**5 3**), was examined with different structural models. Specifically, the energy of the experimentally obtained structure for **5.3** (A), with a facial orientation of the Me groups, was compared to a model structure (B) that, analogously to complex **5.1**, positions the methyl ligands in a meridional array and a planar Ta-R_2DAN^{2-} is maintained. These two optimized structures are displayed in Figure 5.5 along with their relative electronic energies. The relative energies for the two R_2DAN^{2-} ligand fragments of these species are also included in this Figure. Interestingly, these results indicate that the planar geometry for the R_2DAN^{2-} fragment is slightly lower in energy (0.9 kcal mol^{-1}) than the non-planar orientation that was observed in the experimental structure of **3**. More importantly, the electronic interaction energy between the R_2DAN^{2-} and $TaMe_3^{2+}$ fragments is 40.9 kcal mol^{-1} more negative (stable) for the planar ligand configuration than for the non-planar configuration. However, the overall electronic energy of the non-planar structure of **5.3** is 6.9 kcal mol^{-1} lower in energy than the model structure with the planar ligand and meridional methyl moieties.

These results directed our attention to the features that stabilize the facial orientation of the methyl groups in $TaMe_3^{2+}$ compared to the meridional chloro ligands in $TaCl_3^{2+}$ as the driving force for the determining the overall structures of **5.3** and **5.1**. A comparison of the energies for the two orientations of the methyl substituents in $TaMe_3^{2+}$ revealed that the facial disposition, experimentally observed for **5.3,** is 48.7 kcal mol^{-1} lower in energy than a meridional orientation of these groups in the model complex. The ultimate origin of this

energy difference is revealed by examining the electrostatic interactions within the $TaMe_3^{2+}$ fragment. The C atoms of the methyl ligands in the $TaMe_3^{2+}$ fragment bear large negative charges (from -0.97 a.u. to -1.02 a.u.). The electrostatic repulsion between these negative moieties results in the meridionally-ligated $TaMe_3^{2+}$ lying 30.5 kcal mol^{-1} higher in energy than the facially-ligated $TaMe_3^{2+}$ fragment. This electrostatic component appears to be the major contributor to stabilizing the experimentally observed structure of **5.3**.

A similar examination can be made for $[TaCl_3(1,8\text{-}(PhN)_2C_{10}H_6)]$, **5.1**. In this case, the electronic energy of a model structure of **5.1** with non-planar R_2DAN^{2-} and facial chloro groups is 12.4 kcal mol^{-1} higher in energy than that of the experimentally observed structure. Similar to the $TaMe_3^{2+}$ fragment, the meridional $TaCl_3^{2+}$ fragment is 33.5 kcal mol^{-1} higher in energy than the computed facially ligated $TaCl_3^{2+}$ fragment. This indicates that the stabilizing energy for the observed structure of **5.1** must originate from a different interaction than for **5.3**. In fact, the major stabilizing feature for complex **5.1** turns out to be the electronic interaction energy between the R_2DAN^{2-} and $TaCl_3^{2+}$ fragments. This interaction is 42.4 kcal mol^{-1} more negative for the planar ligand configuration than for the non-planar configuration and arises from the stronger charge transfer interaction.

From these results we can conclude that the observed geometries of **5.1** and **5.3** are dictated by the balance between the energetics of the TaX_3^{2+} fragment and the TaX_3-R_2DAN interaction energy. The loss of energy in distorting the R_2DAN ligand from planarity is rather minor.

The similarity in the bonding array displayed by $[Ta(NEt_2)_2Cl(1,8\text{-}(^iPrN)_2C_{10}H_6)]$ (**5.5**) with the trimethyl compound **5.3** suggested that a similar electronic analysis of **5.5** should be carried out. Again the computed optimized structure for **5.5** at the B3LYP/DGDZVP level of theory was in line with the X-ray structure. The R_2DAN^{2-}

fragment of **5.5** displayed a set of donor HOFOs that correlated with the analogous fragment in **5.3**. The donation level of each fragment frontier orbital to the $Ta(NEt_2)_2Cl^{2+}$ fragment was very similar to what we observed in **5.3** with a total donation of 1.33 electrons, a bond order of 2.1 and a resulting NPA charge of +1.95 for the Ta(V) ion. Calculations on a model structure of **5.5** with planar R_2DAN^{2-} and *mer*-$Ta(NEt_2)_2Cl$ ligand arrangement gave an electronic energy that was 20.8 kcal mol^{-1} higher in energy than that of the experimentally observed structure. The energy required to reorganize to the meridional $Ta(NEt_2)_2Cl^{2+}$ orientation is the dominant component for this increased energy. This orientation was computed to be 53.1 kcal mol^{-1} higher in energy than the facial $Ta(NEt_2)_2Cl^{2+}$ fragment. Even though the planar R_2DAN^{2-} ligand would provide a more stabilizing interaction energy, by 17.5 kcal mol^{-1}, with the $Ta(NEt_2)_2Cl^{2+}$ fragment compared to the non-planar configuration, this is not adequate to overcome the favored *fac*-$Ta(NEt_2)_2Cl^{2+}$ configuration.

These results demonstrate that the ligand bonding configuration and the corresponding donation from the R_2DAN^{2-} ligand to the metal fragment is flexible. Furthermore, the ligand-metal interactions respond to the demands of the Ta(V) fragment which in turn is influenced by the nature of the ligands bonded to the TaX_3^{2+} fragment.

Reactivity and Transformations of $Ta(NEt_2)_2Cl[1,8\text{-}(NR)_2C_{10}H_6]$ (R = ^{i}Pr 5.5; R = 3,5-$Me_2(C_6H_3)$ 5.6)

The reactivity of compounds **5.5** and **5.6** provides an attractive avenue for exploring the stability and bonding of the R_2DAN^{2-} ligand coupled with the effects of metal coordination environment. Substitution of the chloro ligand with $LiNMe_2$ was examined as summarized in Scheme 5.4. The reaction of either **5.5** or **5.6** with $LiNMe_2$ proceeded to

introduce the dimethyl amido group on the tantalum center with elimination of LiCl and generated compounds **5.7** and **5.8**. The ^{1}H and ^{13}C NMR spectra of these reaction products appear similar to the corresponding starting materials with the addition, in each case, of resonances corresponding to the incorporated dimethyl amido protons.

Scheme 5.4

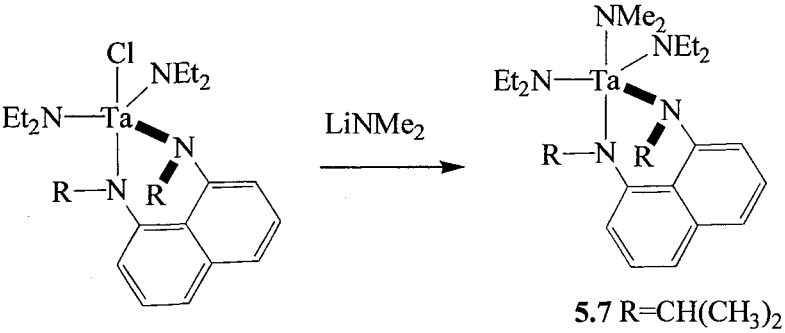

5.7 R=$CH(CH_3)_2$
5.8 R= 3,5-$Me_2(C_6H_3)$

Suitable crystals for single crystal X-ray diffraction analysis of $Ta(NEt_2)_2NMe_2$[1,8-($^{i}PrN)_2C_{10}H_6$] **5.7** where obtain from hexanes (Table 5.3). The results are summarized in Figure 5.6 and Table 5.4. Most striking is the similarity of **5.7** to the starting material **5.5** with the replacement of a chloro group with a dimethylamido ligand. The tantalum center remains in a distorted trigonal bipyramidal coordination geometry with the R_2DAN^{2-} ligand spanning axial/equatorial sites (N1-Ta-N3 = 172.1(5)°) and with N2, N4, and N5 defining the equatorial plane (Σ angles = 360°). The nitrogen centers of the R_2DAN^{2-} ligand are planar (Σ angles N1 = 359.6°, Σ angles N2 = 359.7°). The plane of nitrogen N1 approaches alignment with the naphthyl plane with the angle between these planes being only 21°. On the other hand, the mean plane for the N2 nitrogen makes an angle of 55° with the mean naphthyl plane. The net result is an R_2DAN^{2-} ligand geometry that is twisted and similar to

that obtained in compound **5.5**.

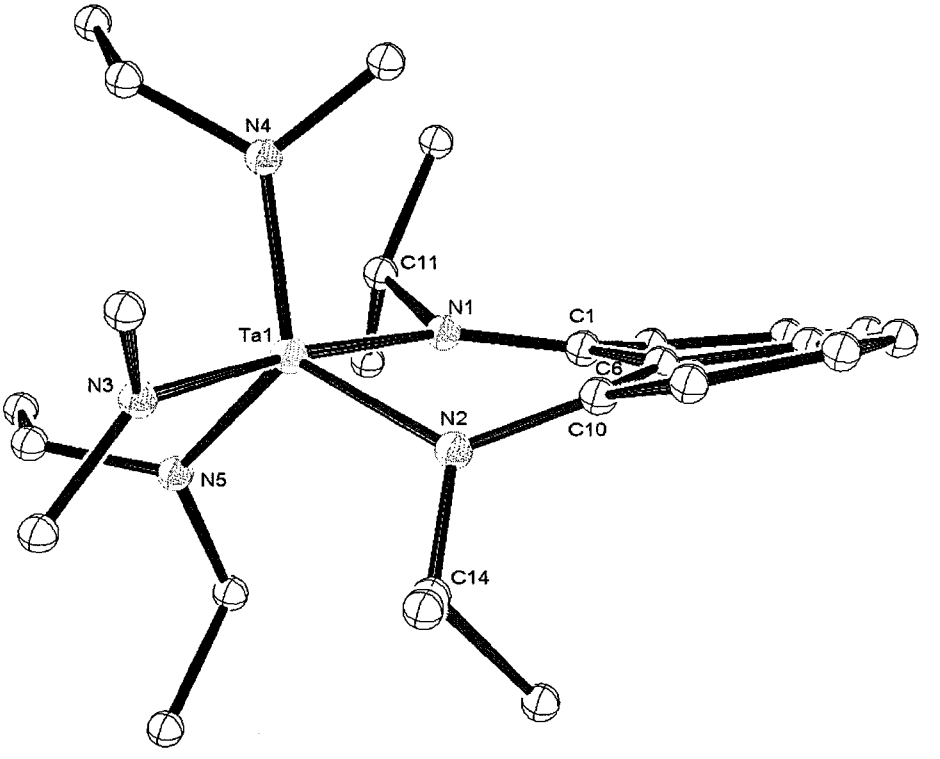

Figure 5.6. Thermal ellipsoid plot showing the molecular structure and partial atom numbering scheme $Ta(NEt_2)_2NMe_2[1,8\text{-}(^iPrN)_2C_{10}H_6]$ (**5.7**). Thermal ellipsoid are drawn at 20% probability. Hydrogen atoms have been omitted for clarity.

A notable feature of **5.7** is that the ^{i}Pr groups of the R_2DAN ligand remains intact in the formation of this compound. There is no deprotonation of the ispo-CH group even in the presence of three strongly basic amido ligands. This contrasts with the documented reactivity of the methyl groups in $TaMe_3Cl_2$ with $1,8\text{-}(^iPrNH)_2C_{10}H_6$ which ultimately led to metallaziridine.

These observations prompted our deployment of methyl lithium in a reaction with

$Ta(NEt_2)_2Cl[1,8\text{-}(^iPrN)_2C_{10}H_6]$ (**5.5**). The goal was to determine if this reaction would proceed by simple metathetical substitution of the chloro ligand with a methyl group or would involve transformation of the isopropyl CH group. From this reaction, an orange powder was obtained. Our previous experience with the appearance of the ^1H NMR spectrum for the tridentate trianionic metallaziridine ligand $(Me_2CN)(Me_2CHN)C_{10}H_6]^{3-}$ allowed us to identify compound **5.9** (Scheme 5.5) as the metallacyclic product. In particular, the spectrum for **5.9** displayed one intact ^{i}Pr group, exhibiting a doublet for the methyl moieties, and the methyl signals of the metallacycle appearing as a singlet with an integration value of six hydrogens. The remaining ^1H and ^{13}C NMR signals supported the structural assignment for $[(Me_2CN)(Me_2CHN)C_{10}H_6]Ta(NEt_2)_2$ (**5.9**).

Scheme 5.5

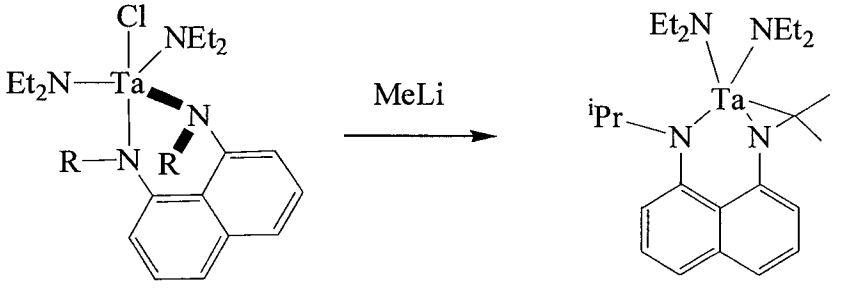

5.9 R=$CH(CH_3)_2$

III. Conclusions

1,8-Diaminonaphthalene has been employed in the preparation of a series of Ta(V) complexes. The influence of the ligand substituents and the ligand on the tantalum center was explored. The use of aromatic ligand sustituents prohibits CH activation and the

formation of metallaaziridine. The change of the tantalum bonded ligands from methyl to N-diethylamido and chloride groups also prohibits the CH activation but when the chloride is substituted for a methyl group CH activation is observed. These observations are indicative of the formation of a metallaziridine can occur by σ bond metathesis of the isopropyl CH bond and the Ta methyl group to eliminate methane. The computational studies on complex **5.1**, **5.3** and **5.5** have revealed that distortion in the ligand is a response to the demands of the Ta(V) fragment which in turn is influenced by the nature of the ligands bonded to the TaX_3^{2+} fragment.

IV. Experimental Section

General Methods. All manipulations were carried out in either a nitrogen-filled drybox or under nitrogen using standard Schlenk line techniques. Unless otherwise noted, solvents were sparged with nitrogen and then dried by passage through column of activated alumina using an apparatus purchased from Anhydrous Engineering. Deuterated benzene and methylene chloride were dried by vacuum transfer from dried molecular sieve. $TaCl_5$ was purchased from Strem and used without further purification. N,N-diethyltrimethylsilylamine was purchased from Aldrich and used without further purification. ^1H NMR spectra were run on either a Bruker Avance 300 MHz or a Bruker 500 MHz spectrometer with deuterated benzene or methylene chloride as a solvent and internal standard. Elemental analyses were carried out by Robertson Microlit Laboratories, Inc, Madison N.J or Midwest Microlab, LLC, Indianapolis, IN. Elemental analyses for compound **5.1, 5.2, 5.3** and **5.4** were not obtained due to the decomposition of the products during transportation. $[Ta(NEt_2)_2Cl_3]$[14], $Ta(NEt_2)_2Cl_3Py$[14], 1,8-$(2,6\text{-}Me_2C_6H_3NH)_2C_{10}H_6$, 1,8-$(NH^iPr)_2C_{10}H_6$ [16], $TaMe_3Cl_2$[17] were prepared according to the literature methods.

Preparation of $TaCl_3[1,8\text{-}(Ph)_2C_{10}H_6]$ (5.1)

A dark brown solution was formed after stirring 1,8-$(C_6H_5NH)_2C_{10}H_6$ (0.191 g, 0.64 mmol) and $TaMe_3Cl_2$ (0.201 g, 0.65 mmol) in 10 ml diethyl ether for 24 hours. The solvent was then removed from the reaction mixture and the solid is extracted with 4 ml toluene. Red crystals (0.151 g, 40%) were collected by crystallization from a mixture of toluene/hexanes at -20°C.

^1H NMR (300MHz, C_6D_6) 6.38 (d, 2H, CH_{Ar}), 7.02 (m, 6H, CH_{Ar}), 7.19(m, 2H, CH_{Ar}), 7.23(m, 2H, CH_{Ar}), 7.80 (m, 4H, CH_{Ar}).

$^{13}C\{^1H\}$ NMR (75 MHz, C_6D_6) 115.5 CH_{Ar}, 125.6 C, 126.6 C, 127.3 CH_{Ar}, 128.5 CH_{Ar} , 129.2 CH_{Ar}, 129.3 CH_{Ar}, 132.9 C, 134.2 CH_{Ar}, 135.5 C.

Preparation of $TaCl_3[1,8\text{-}(3,5\text{-}Me_2C_6H_3N)_2C_{10}H_6]$ (5.2)

$TaMe_3Cl_2$ (0.243 g, 0.82 mmol) and $1,8\text{-}(3,5\text{-}Me_2C_6H_3NH)_2C_{10}H_6$ (300 mg, 0.82 mmol) were dissolved in toluene and the reaction mixture was allowed to stir overnight at room temperature. The resulting red solution was dried by vacuum evaporation of the reaction solvent. A brown powder was obtained which was dissolved in hexanes and cooled to -20°C to give a red powder of **5.2** (269 mg, 51%)

^1H NMR (300 MHz, C_6D_6): 2.02 (s, 12H, CH_3), 6.45 (s, 2H, CH_{Ar}) 6.55 (s, 4H, CH_{Ar}), 7.18-7.27 (m, 4H, CH_{Ar}), 7.43 (d, 2H, CH_{Ar}).

$^{13}C\{^1H\}$ NMR (125 MHz, CD_2Cl_2) 21.6 CH_3,116.8 CH_{Ar}, 117.4 CH_{Ar}, 122.2 C_{Ar}, 123.6 CH_{Ar}, 126.5 C_{Ar}, 126.6 CH_{Ar}, 137.7 C_{Ar},139.5 CH_{Ar}, 141.3 C_{Ar}, 145.4 C_{Ar}

Preparation of $TaMe_3[1,8\text{-}(Ph)_2C_{10}H_6]$ (5.3)

In a vial, $1,8\text{-}(C_6H_5NH)_2C_{10}H_6$ (0.62 g, 2.0 mmol) was dissolved in 5ml diethyl ether and cooled to -30 ° C. To this solution was added methyllithium (2.9 ml of 1.4M in diethylether, 4.06 mmol) dropwise. The reaction mixture was maintained at –20 ° C and stirred for 30 min. $TaMe_3Cl_2$ (0.59 g, 1 mmol) that had been dissolved in 5 ml of diethylether was then added slowly to the reaction. This reaction mixture was allowed to stir for 1h at room temperature. The mixture was then filtered and the resulting dark red solution was cooled to -20 ° C. Dark orange crystals of **5.3** were obtained after several hours (0.31 g, 29%).

^{1}H NMR (300 MHz, C_6D_6): δ 1.20 (s, 9H, CH_3), 6.73(m, 2H, CH_{Ar}), 6.95(m, 4H, CH_{Ar}), 7.06(m, 2H, CH_{Ar}), 7.18(m, 6H, CH_{Ar}), 7.24 (m, 2H, CH_{Ar}).

$^{13}C\{^1H\}$ NMR (75 MHz, C_6D_6): δ 75.3 CH_3 , 120.1 CH_{Ar} ,123.9 CH_{Ar}, 125.2 CH_{Ar}, 125.8 CH_{Ar}, 126.4 C, 129.5 C, 130.2 CH_{Ar}, 137.0 C, 143.1 C , 146.4 CH_{Ar} .

Preparation of $TaMe_3[1,8\text{-}(3,5\text{-}Me_2C_6H_3N)_2C_{10}H_6]$ (5.4)

In a round bottom flask $1,8\text{-}(3,5\text{-}Me_2C_6H_3NH)_2C_{10}H_6$ (300 mg, 0.82 mmol) was dissolved in ether at room temperature. To this solution was added n-BuLi (1.02 ml of 1.6M in ether, 1.6 mmol) dropwise. The reaction mixture was allowed to stir for 1h. $TaMe_3Cl_2$ (0.243g, 0.82 mmol) was then added slowly to the reaction. The reaction mixture was then stirred for an additional three hours, filtered and the solvent was evaporated under vacuum to yield brown solid that was further purified by precipitation to yield pure **5.4** (208 mg, 89%).

^{1}H NMR (300 MHz, C_6D_6): δ 1.24 (s, 9H, Me), 1.98 (s, 12H, Me). 6.60 (s, 2H, CH_{Ar}), 6.80 (s, 4H, CH_{Ar}), 6.87 (d, 2H, CH_{Ar}), 7.15-7.27 (m, 4H, CH_{Ar}).

$^{13}C\{^1H\}$ NMR (75 MHz, C_6D_6): δ 21.4 ($C_{Ar}CH_3$), 73.6 ($TaCH_3$), 119.2 C_{Ar}, 123.8 CH_{Ar}, 123.9 CH_{Ar}, 126.5 C_{Ar}, 127.7 CH_{Ar}, 127.8 CH_{Ar}, 137.4 C_{Ar}, 140.3 CH_{Ar}, 144.4 C_{Ar}, 144.7 C_{Ar}.

Preparation of $Ta(NEt_2)_2Cl[1,8\text{-}(N^iPr)_2C_{10}H_6]$ (5.5)

In a round bottom flask $1,8\text{-}(^iPrNH)_2C_{10}H_6$ (0.50 g, 2.06 mmol) was dissolved in diethyl ether at room temperature. To this solution was added n-BuLi (2.58 ml of 1.6M in diethylether, 4.13 mmol) dropwise. The reaction mixture was allowed to stir for 1h. $[Ta(NEt_2)_2Cl_3]_2$ (0.89 g, 1.03 mmol) was then added to the reaction. This mixture was then

allowed to stir overnight, filtered through celite and the solvent was evaporated under vacuum. The resulting orange solid was crystallized from hexanes cooled to -20°C to yield **5.5** (0.782 g, 63%) as orange crystals.

^{1}H NMR (300 MHz, C_6D_6): δ 0.88 (t, 12H, NCH_2CH_3), 1.25 (d, 12H, $CH(CH_3)_2$), 3.62-3.44 (br, 8H, NCH_2CH_3), 4.67-4.24 (br, 2H, $CH(CH_3)_2$), 6.75-7.14 (m, 2H, Ar-H), 7.26-7.47 (m, 4H, Ar-H)

$^{13}C\{^1H\}$ NMR (75 MHz, C_6D_6): δ 13.8 (NCH_2CH_3), 21.7 ($CHCH_3$), 45.8 (NCH_2CH_3), 50.4 ($CH(CH_3)_2$, 55.3 ($CH(CH_3)_2$, 113.6 (C_{Ar}), 119.5 (C_{Ar}), 124.3 (C_{Ar}), 126.1 (CH_{Ar}), 128.9 (CH_{Ar}), 137.2 (CH_{Ar}).

Anal. Calcd for $C_{24}H_{40}N_4ClTa$: C 47.96, H 6.71, N 9.32 Found: C 47.69, H 6.43, N 9.16

Preparation of $Ta(NEt_2)_2Cl$ [1,8-$(3,5\text{-}Me_2C_6H_3N)_2C_{10}H_6$] (5.6).

In a round bottom flask 1,8-$(3,5\text{-}Me_2C_6H_3NH)_2C_{10}H_6$ (0.5 g, 1.36 mmol) was dissolved in diethyl ether at room temperature. To this solution was added n-BuLi (1.71 ml of 1.6M in diethylehter, 2.7 mmol) dropwise. The reaction mixture was allowed to stir for 1h. $Ta(NEt_2)_2Cl_3Py$ (0.697 g, 1.36 mmol) was then added to the reaction. This mixture was then allowed to stir overnight, filtered through celite and the solvent was evaporated under vacuum. The resulting red solid was recrystallized from hexanes cooled to -20°C to yield **5.6** (612 mg, 63%).

^{1}H NMR (300MHz, C_6D_6): δ 0.65 (t, 12H, NCH_2CH_3), 2.05 (s, 12H, $C_{Ar}CH_3$), 3.60 (q, 8H, NCH_2CH_3), 6.57 (s, 2H, Ar-H), 6.73 (br, 2H, Ar-H), 7.06-7,14 (br, 4H, Ar-H), 7.17-7.25 (m, 4H, Ar-H)

$^{13}C\{^1H\}$ NMR (75 MHz, C_6D_6): δ 13.0 ($NCH_2\mathit{C}H_3$), 21.5 ($C_{Ar}\mathit{C}H_3$), 45.6 ($N\mathit{C}H_2CH_3$), 117.1 ($\mathit{C}H_{Ar}$) , 117.5 (C_{Ar}) , 123.8 (C_{Ar}) , 125.7 (CH_{Ar}) ,126.5 (C_{Ar}), 126.7 (CH_{Ar}), 127.5 (CH_{Ar}), 129.5 (C_{Ar}) , 136.9 (C_{Ar}), 139.2 (CH_{Ar}).

Anal. Calcd for $C_{34}H_{44}N_4ClTa$: C 56.32, H 6.12, N 7.73 Found: C 56.53, H 6.21, N 7.59

Preparation of $Ta(NEt_2)_2NMe_2[1,8\text{-}(N^iPr)_2C_{10}H_6]$ (5.7)

In a round bottom flask compound **5.5** (0.18 g, 0.30 mmol) was dissolved in 40 ml of diethyl ether. To this solution was added $LiNMe_2$ (0.015 g , 0.30 mmol) and the reaction mixture was allowed to stir overnight. The reaction mixture was filtered and the solvent was removed under vacuum. Orange crystals of **5.7** (117 mg, 65%) were obtained by crystallization from hexanes cooled to -20°C.

^1H NMR (300 MHz, C_6D_6): δ 0.90 (t, 12H, $NCH_2C\mathit{H}_3$), 1.26 (d, 12H, $CH(C\mathit{H}_3)_2$) 3.35 (s, 6H, $NC\mathit{H}_3$), 3.39 (q, 4H, $NC\mathit{H}_2CH_3$), 3.68 (q, 4H, $NC\mathit{H}_2CH_3$), 4.16 (sept, 2H, $C\mathit{H}(CH_3)_2$), 6.96-6.99 (m, 2H, Ar-H), 7.34-7.38 (m, 4H, Ar-H)

$^{13}C\{^1H\}$ NMR (75 MHz, C_6D_6): δ 14.5 ($NCH_2\mathit{C}H_3$), 23.6 ($CH\mathit{C}H_3$), 46.4 ($N\mathit{C}H_3$), 48.6 ($N\mathit{C}H_2CH_3$), 51.6 ($C\mathit{H}(CH_3)_2$), 115.2 (C_{Ar}), 119.8 (C_{Ar}), 125.8 (CH_{Ar}), 128.8 (CH_{Ar}), 137.7 (CH_{Ar}), 147.7 (C_{Ar}).

Anal. Calcd for $C_{32}H_{42}N_5Ta$: C 51.22, H 7.62, N 11.49 Found: C 50.74, H 7.27, N 11.15

Preparation of $Ta(NEt_2)_2NMe_2[1,8\text{-}(2,6\text{-}Me_2C_6H_3N)_2C_{10}H_6]$ (5.8)

In a round bottom flask compound **5.6** (0.765 g, 1.05 mmol) was dissolved in 40 ml of diethyl ether. To this solution was added $LiNMe_2$ (0.057 g, 1.12 mmol) and the reaction mixture was allowed to stir overnight. The reaction mixture was filtered and the solvent

was removed under vacuum. Orange crystals of **5.8** (0.607g, 79%).were obtained by crystallization from hexanes and THF at -20°C.

^{1}H NMR (300 MHz, C_6D_6): δ 0.64 (t, 12H, NCH_2CH_3), 2.15 (s, 12H, $C_{Ar}CH_3$), 3.01 (s, 6H, $N(CH_3)_2$), 3.31 (q, 4H, NCH_2CH_3) , 3.81 (q, 4H, NCH_2CH_3), 6.58 (s, 4H, Ar-H$_r$), 6.71 (s, 4H, Ar-H), 7.14-7.30 (m, 4H, Ar-H)

^{13}C{^{1}H} NMR (75 MHz, C_6D_6): δ 14.4 (NCH_2CH_3), 21.7 ($C_{Ar}CH_3$), 46.1 (N(CH3)), 47.8 (NCH_2CH_3), 115.0 (C_{Ar}) , 119.6 (C_{Ar}), 124.8 (CH_{Ar}), 124.9 (C_{Ar}) , 125.2 (CH_{Ar}), 127.3 (CH_{Ar}), 128.2 (C_{Ar})137.9 (C_{Ar}) , 138.6 (CH_{Ar}), 151.3 (C_{Ar}) , 153.4 (CH_{Ar}).

Anal. Calcd for $[C_{36}H_{50}N_5Ta][THF]$: C 59.62, H 7.25, N 8.69 Found: C 60.69, H 7.49, N 8.24.

Preparation of $\eta^3C_{10}H_6(Me_2CN)(Me_2CHN)Ta(NEt_2)_2$ (5.9)

In a round bottom flask compound **5.5** (469 mg, 0.78 mmol) was dissolved in 30 ml of diethyl ether. To this solution was added MeLi (0.49 ml of 1.6M in diethylether, 0.78 mmol) and the reaction mixture was allowed to stir overnight. The reaction mixture was filtered and the solvent was removed under vacuum to give an orange solid. Orange crystals of **5.9** (224 mg, 51%) were obtained by crystallization from ether at -20°C.

^{1}H NMR (300 MHz, C_6D_6): 0.83 (t, 12H, NCH_2CH_3), 1.57 (d, 6H, $CH(CH_3)_2$), 2.16 (s, 6H, $C(CH_3)_2$, 3.02 (br, 8H, NCH_2CH_3), 4.47 (sept,1H, $CH(CH_3)_2$), 6.90-6.96 (m, 2H. Ar-H), 7.34-7.47 (m,4H, Ar-H)

^{13}C{^{1}H} NMR (75 MHz, C_6D_6): δ 16.7 (NCH_2CH_3), 21.8 (CH_3), 27.4 (CH_3), 42.6 (NCH_2CH_3), 52.6 ($CH(CH_3)_2$), 107.0 (CH_{Ar}), 109.1 (CH_{Ar}), 118.8 (CH_{Ar}), 125.3 (CH_{Ar}), 126.3 (CH_{Ar}), 126.7 (CH_{Ar}), 128.7 (CAr), 129.9 (CAr),139.1 (C_{Ar}), 145.3 (C_{Ar}).

Anal. Calcd for $C_{24}H_{39}N_4Ta$: C 51.06 , H 6.96 , N 9.92 Found: C 50.93, H 6.84, N 9.84

References

[1] (a) Decams, J. M.; Daniele, S.; Hubert-Pfalzgraf, G. L.; Vaissermann, J.; Lecocq, S. *Polyhedron*, 20, **2001,** 2405. (b) Ketterer, A. N.; Fan, H.; Blackmore, J. K.; Yang, X.; Ziller W. J.; Baik M-H.; Heyduk F. A. *J. Am. Chem. Soc.*, **2008**, 130, 13, 4364. (c) Ison, E. A.; Ortiz, C. O.; Abboud, K.; Boncella M. J. *Organometallics*, **2005**, 24, 26, 6310. (d) Ketterer, A. N.; Ziller, W. J.; Rheingold, L. A.; Heyduk, F. A. *Organometallics*, **2007**, 26, 22, 5330. (e) Ison, A. E.; Abboud, A. K.; Ghiviriga, I.; Boncella, M. J. *Organometallics*, **2004**, 23, 5, 929. (f) Cameron, M. T.; Ghiviriga, I.; Abboud, A. K.; Boncella, M. J.; *Organometallics*, **2001**, 20, 21, 4378. (g) Aoyagi, K.; Gantzel, K. P.; Kalai, K.; Tilley, T. D, *Organometallics*, **1996**, 15, 3, 923.

[2] For selected reviews see: (a) Britovsek, G. J. P.; Gibson, V. C.; Wass, D. F. *Angew. Chem. Int. Ed.* **1999**, *38*, 428 and references therein. (b) Arndtsen, B. A.; Bergman, R. G.; Mobley, T. A.; Peterson, T. H. *Acc. Chem. Res.* **1995**, *28*, 154 and references therein. (c) Berresford, D. J.; Bolm, C.; Sharpless, K. B. *Angew. Chem., Int. Ed. Engl.* **1995**, *34*, 1059 and references therein. (d) Negishi, E.; Takahashi, T. *Acc. Chem. Res.* **1994**, *27*, 124 and references therein. (e) Tilley, T. D. *Acc. Chem. Res.* **1993**, *26*, 22 and references therein.

[3] Tabernero, V.; Cuenca, T.; Mosquera, M. E. G.; Ramírez de Arellano, C. Polyhedron, **2009**, 28, 2545.

[4] (a) Bazinet, P.; Yap, G.P.A.; Richeson, D. S. *Organometallics.* **2001,** 20, 20, 4129. (b) Lavoie, N.; Ong,T.G.; I. Gorelsky, I. S.; Korobkov, I.; Yap, G.P.A. Richeson, D.S. *Organometallics*, **2007**, *26*, 26, 6586.

[5] Fowles, G. W. A.; Rice, D. A,; Wilkins, J. D. *J. Chem. Soc., Dalton Trans.* **1973,** 961.

[7] Bazinet, P.; Yap, G.P.A.; Richeson, D. S. *J. Am. Chem. Soc.* **2001,** *123,* 11162.

[8] Spinney. H. S.; Korobkov. I.; DiLabio. G. A.; Yap. G. P. A.; Richeson. D. S. *Organometallics* **2007**, *26,* 4972.

[9] Bazinet, P.; Yap, G. P. A.; DiaLabio, G. A.; Richeson, D. S. *Inorg. Chem.* **2005**, 44, 4616.

[10] Aoyagi, K.; Gantzel, P. K.; Tilley, T. D. *Polyhedron* **1996**, *15*, 4299.

[11] (a) Cameron, T. M.; Abboud, K. A.; Boncella, J. M. *Chem. Commun.* **2001**, 1224. (b) Ortiz, C. G.; Abboud, K. A.; Boncella, J. M. *Organometallics,* **1999**, *18*, 4253.

[12] Pindado, G. J.; Thornton-Pett, M.; Bochmann, M. *J. Chem. Soc., Dalton Trans.* **1998**, *393.*

[13] (a) Cameron, T. M.; Ortiz, C. G.; Abboud, K. A.; Boncella, J. M.; Baker, R. T.; Scott, B. L. *Chem. Commun.* **2000**, 573. (b) Wang, S. Y. S.; Vanderlende, D. D.; Abboud, K. A.; Boncella, J. M. *Organometallics* **1998**, *17*, 2628. (c) Wang, S. Y. S.; Abboud, K. A.; Boncella, J. M. *J. Am. Chem. Soc.* **1997**, *119*, 11990. (d) VanderLende, D. D.; Abboud, K. A.; Boncella, J. M. *Organometallics* **1994**, *13,* 3378.

[14] Chao, Y-W.; Wexler. P. A.; Wigley. D. E. *Inorg. Chem.,* **1989**, 28, 3860.

[15] Chisholm, M. H.; Huffman, J. C.; Tan, L-S. *Inorg. Chem.* **1981**, 20, 1859.

[16] Bazinet. P.; Ong. T-G.; O'Brien. J. S.; Lavoie. N.; Bell. E.; Yap. G. P. A.; Korobkov. I.; Richeson. D. S. *Organometallics,* **2007**, 26, 2885.

[17] Juvinall, G. L. *J. Am. Chem. Soc.*, **1964**, 86, 4202.

Chapter 6

Tungsten Bis(Imido) Complexes Bearing 1,8-Diaminonaphthalene Ligands

I. Introduction

Interest in imido transition metal complexes has grown tremendously in the past 30 years. Primarily due to their potential as catalysts for polymerization and metathesis reactions[1]. Imido ligands are common in high oxidation state chemistry due to there ability to donate up to six electrons to an electron deficient metal center. A key metric for this donation is the M-N-R angle as an indication of the degree of pi-donation to the metal. Dianionic imido ligands can

act as ancillary ligands or can be a reactive site in the complex. One example of a imido group used as supporting ligand are the well known Ziegler Natta catalysts[2]. Figure 6.1 shows an example of a titanium catalyst that processes a unreactive imido group[3]

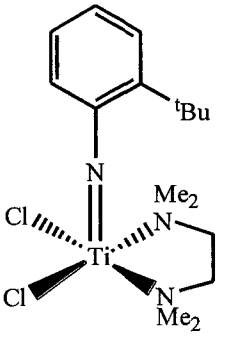

Scheme 6.1 on the other hand shows an example in which the imido ligand is a reactive site. In this example the reaction of the titanium complex with the isocyanate leads to the insertion of the isocyante in the Ti=N bond.[4]

Scheme 6.1

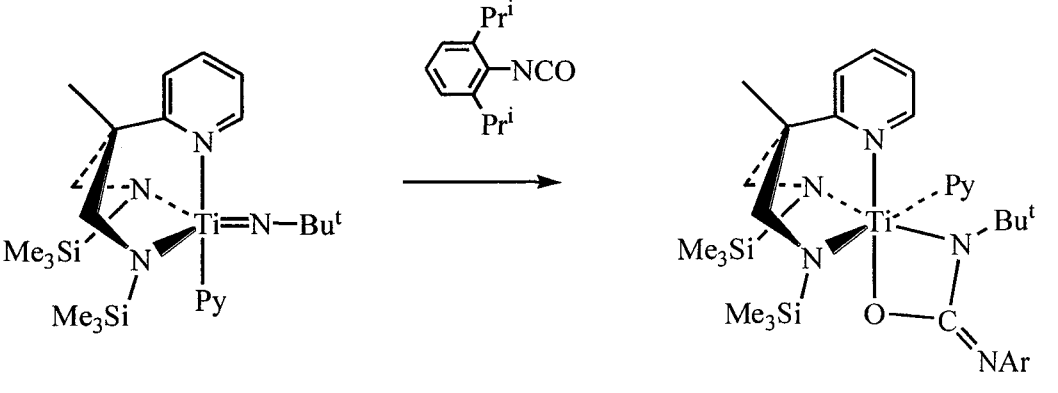

Amido ligands are also found throughout the literature and they have proven to be suitable for the stabilization of high oxidation state early transition metals. A primary incentive for the design and development of new ligand arrays centers on attempts to manipulate the structure, stability, and reactivity of coordination compounds. The nature of the ligand functional groups and the ligand framework essentially define these characteristics. As an example, β-diketiminates have a documented role as supporting ligands due to their strong metal binding in combination with their adjustable steric demands and their diversity of bonding modes.[5] We are interested in designing and implementing a new family of dianionic ligands that are reminiscent of the β-diketiminate scaffold in geometry and frontier orbital topology. This led us to an array that is built on the N,N'-substituted-1,8-diamidonaphthalene framework (R_2DAN), a rigid chelating ligand with delocalized π-electrons.[6,7] Among the significant differences between these two ligands are the dianionic charge and the naphthalene backbone of R_2DAN^{2-}. We anticipated that this first feature would allow the application of this ligand to metal complexes in their highest oxidation states and the second feature would lead to a more robust ligand relative to β-diketiminate.[8]

Additional inspiration for our investigations with R_2DAN^{2-} comes from the application of related chelating aromatic diamido ligands *N,N'*-bis(trialkylsilyl)-*o*-diamidobenzene ($(R_3Si)_2DAB^{2-}$) for the preparation of high-valent group 4,[9] Ta,[10] Mo, and W[11] species. While having the same ligand charge, the diamidobenzene and diamidonaphthalene species exhibit substantially different topologies which should markedly influence the reactivity of their respective metal complexes.

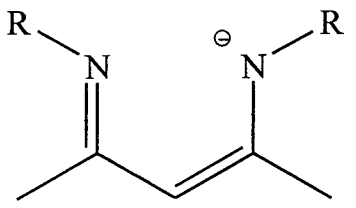

β-diketiminate

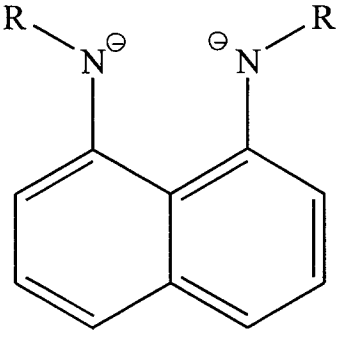

R_2DAN^{2-}

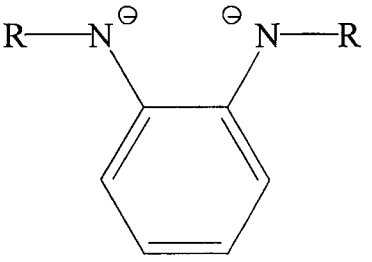

$(R_3Si)_2DAB^{2-}$

The success of the DAB ligands in supporting high oxidation state tungsten complexes has motivated use to explore are R_2DAN as a supporting ligands for tungsten imido complexes. This chapter reports the synthesis of tungsten imido complexes bearing R_2DAN ligands and the reactivity of these complexes.

II. Results and Discussion

N,N'-disubstituted-1,8-diamidonaphthalene (R_2DAN^{2-}) with R as either ^{i}Pr or 3,5-dimethylphenyl was readily introduced to the bis(imido) tungsten framework by reaction between the *in situ* generated dilithium salt, $Li_2[(RN)_2C_{10}H_6]$, and $W(=N^{t}Bu)_2Cl_2(py)_2$ as represented by Scheme 6.2.[6(a),12] The products of these reactions, $W(=N^{t}Bu)_2[1,8\text{-}(RN)_2C_{10}H_6]py_x$ (**6.1** R = ^{i}Pr, x = 0; **6.2** R = 3,5-$Me_2C_6H_3$, x = 1, **6.3** R_1=^{i}Pr R_2= 3,5-$Me_2C_6H_3$, x=0), were obtained in good yields as purple solids for **6.1** and **6.3** and a orange solid for **6.2**. Hydrocarbon soluble **6.1** exhibited a ^{1}H NMR spectrum with a broad signal (δ 0.9-1.8) corresponding to the 30 protons for the methyl groups of the combined ^{t}Bu and ^{i}Pr groups and a single septet at 3.95 ppm for the two protons of the ^{i}Pr moieties. The appearance of a single ^{i}Pr group in the ^{1}H NMR spectra of **6.1** suggests fluxionality on the NMR time scale. The

appearance of a single resonance for the methine groups suggested a symmetrical structure based on a tetrahedral ligand array. Compound **6.2**, while slightly less soluble, also provided ^{1}H and ^{13}C NMR spectra suggesting a symmetrical structure. In particular, the spectra displayed only two distinct signals attributable to the CH_3 groups of the 3,5-dimethylphenyl and the ^{t}Bu groups respectively. Furthermore, **6.2** provided NMR and microanalysis data confirming the presence of a single coordinated pyridine group that originated from the starting material. The formula for **6.2** is reminiscent of the W(IV) DAB complex $W(NPh)(CHCMe_3)(PMe_3)[(Me_3SiN)_2C_6H_4]$.[11(h)] The ^{1}H NMR for **6.3** shows one broad peak for the t-butyl groups and distinct resonance for each of the nitrogen substituents.

Scheme 6.2

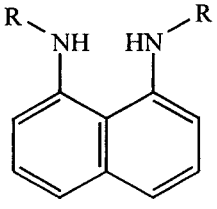

1. 2 BuLi / Et_2O
2. $W(N^tBu)_2Cl_2(Py)_2$

$W(=N^tBu)_2[1,8\text{-}(RN)_2C_{10}H_6]py_x$

6.1, R= ^{i}Pr, x = 0
6.2, R = 3,5-$(Me)_2C_6H_3$, x = 1
6.3, R1= ^{i}Pr, R2= 3,5$(Me)_2C_6H_3$, x= 0

The structure of **6.1** was confirmed through single crystal X-ray crystallography and Tables 6.1 and 6.2 show selected crystal data and structure refinement parameters and selected bond lengths and angles. For simplicity, discussion has been limited to only one of the two independent units of **6.1** in the unit cell. There are no significant differences in the bond lengths and angles between these two species. The distorted tetrahedral tungsten center possesses an approximate mirror plane of symmetry that bisects the $^{i}Pr_2DAN$ ligand and contains the C(8)-C(13) vector and the W(1), N(3), and N(4) centers. The two $W\text{-}N_{amido}$ bond lengths with an average bond length of 1.966Å are similar to related complexes.[11,13] The short

$W{=}N_{imido}$ bond lengths of 1.771(4) and 1.748(4)Å are consistent with W-N triple bonds.[14] A difference between the two imido ligands is reflected in the observed bend angles of 150.6(4)° and 169.4(4)°. Both N_{amido} nitrogen are planar with the sum of the angles surrounding them equal to 359.2° and 359.0° for N(1) and N(2) respectively.

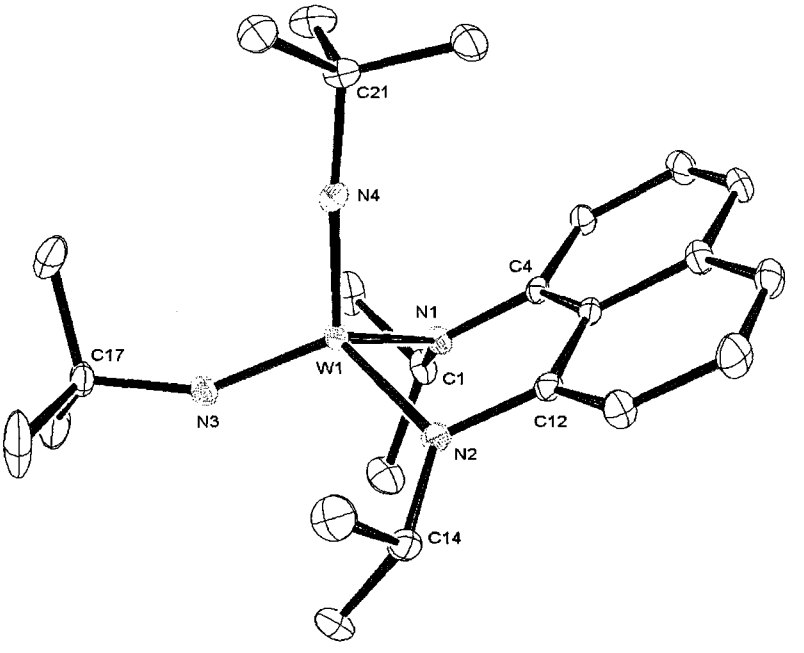

Figure 6.1. Thermal ellipsoid plot showing the molecular structure and partial atom numbering scheme for one of the independent molecules of **6.1**. For simplicity only one of the two independent units of **6.1** in the unit cell is shown. Thermal ellipsoid are drawn at 20% probability. Hydrogen atoms have been omitted for clarity.

Table 6.1. Selected Crystal Data and Structure Refinement Parameters for $W(=N^tBu)_2[1,8\text{-}(^iPrN)_2C_{10}H_6]$ (**6.1**)

Empirical Formula	$C_{24}H_{38}N_4W$
Formula weight	566.43
Temperature (K)	120(2)
Wavelength (Å)	0.71073
Crystal system	Triclinic
Space group	P-1
a(Å)	9.860(4)
b(Å)	14.171(5)
c (Å)	18.738(7)
α(deg)	98.619(6)
β(deg)	102.019(6)
γ(deg)	93.095(6)
V ($Å^3$)	2522.0(16)
Z	4
ρ(calc) (Mg/m^3)	1.492
μ (mm^{-1})	4.596
Absorption correction	Semi-empirical from equivalents
Final R indices [I>2σ(I)]	
R1[a]	0.0363
***w*R2**[b]	0.0893

[a] $R1 = \Sigma \| F_o | - | F_c \| / \Sigma | F_o |$

[b] $wR2 = (w(| F_o | - | F_c |)^2 / \Sigma w | F_o |^2)^{1/2}$

Table 6.2. Selected Bond Lengths (Å) and Angles (°) for $W(=N^tBu)_2[1,8\text{-}(^iPrN)_2C_{10}H_6]$ (**6.1**)

Bond lengths (Å)		Angles(°)	
W(1)-N(1)	1.949(4)	N(1)-W(1)-N(2)	92.83(17)
W(1)-N(2)	1.984(4)	C(4)-N(1)-C(1)	119.5(4)
W(1)-N(3)	1.771(4)	C(4)-N(1)-W(1)	107.1(3)
W(1)-N(4)	1.748(4)	C(1)-N(1)-W(1)	132.6(3)
N(1)-C(4)	1.411(6)	C(12)-N(2)-C(14)	119.4(4)
N(2)-C(12)	1.415(6)	C(12)-N(2)-W(1)	110.1(3)
		W(1)-N(3)-C(17)	150.6(4)
		W(1)-N(4)-C(21)	169.4(4)
		C(14)-N(2)-W(1)	129.5(3)
		N(4)-W(1)-N(3)	114.23(18)
		N(4)-W(1)-N(1)	108.07(18)
		N(3)-W(1)-N(1)	112.64(18)
		N(4)-W(1)-N(2)	111.05(18)
		N(3)-W(1)-N(2)	115.89(18)

Perhaps the most notable structural feature for **6.1** is the non-planar coordination of the $^iPr_2DAN^{2-}$ ligand. The fold angle of 122.6° between the naphthyl moiety and the N(1)-W(1)-N(2) planes positions the W atom *ca.* 1.14 Å out of the naphthyl plane. This feature causes the methyl groups on the ^{i}Pr substituents to be crystallographically distinct. This structural feature of **6.1** closely parallel what we have seen for lanthanides, zirconium and tantalum complexes in the previous chapters and is similar to the distortions observed in R_3SiDAB^{2-} complexes. However, the mononuclear structure of **6.1** is in contrast with the imido-bridged dimer observed for the closely the related bis(imido)Mo(Me_3SiDAB) species $[Mo(NPh)(\mu\text{-}NPh)(o\text{-}(Me_3SiN)_2C_6H_4)]_2$.[15] Furthermore, the structure of [N,N'-bis(trimethylsilyl)-6,6'-dimethylbipheny]-2,2'-diamido]bis(2,6-diisopropylphenylimido) tungsten(VI), displays a symmetrical albeit twisted biphenyldiamido ligand.[16]

The apparent ligand distortion observed for complex **6.1** was probed through DFT calculations (B3LYP) using both the SDD and LANL2DZ basis sets.[17] An optimization that began from a symmetrical C_{2v} structure for **6.1** possessing a planar $^{i}Pr_2DAN^{2-}$ ligand led to a C_s symmetric structure that represents a true energy minimum (all positive harmonic frequencies) and closely correlated with the experimentally obtained structure as shown in Figure 6.2 where we can see an overlay of the calculated structure and the experimental X-ray structure. From this calculation it is possible to see that the $W\text{-}N_{imido}$ and the $W\text{-}N_{amido}$ bond lengths are the same in the calculated and the experimental structure indicating that the structure obtained is not due to crystal packing effects. Furthermore, the low-symmetry structure was calculated to be approximately 15 kcal mol^{-1} more stable than the C_{2v} structure (Figure 6.3).[18]

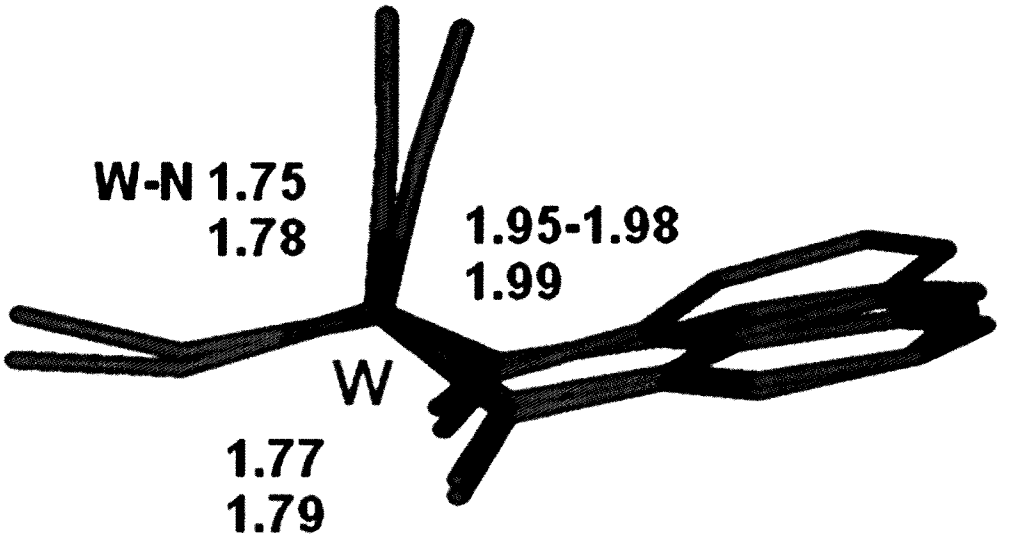

Figure 6.2. An overlay comparison of the experimental X-ray structure (black labels) and the calculated structures (at the B3LYP/SDD level) (blue labels) for compound **6.1**.

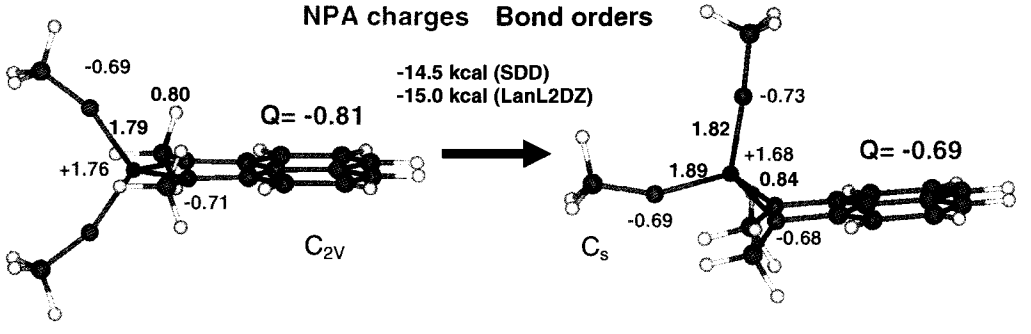

Figure 6.3. Calculation results for compound **6.1** with both C_{2v} and C_s symmetry. Calculated bond orders and NPA charges (Q= charge on the ligand) for the two structures are depicted in red and green labels respectively.

These results indicate that the observed structure for **6.1** is indeed the preferred minimum even in the absence of crystal packing forces. An analysis of the fragment orbital interactions for the R_2DAN^{2-} and $W(NR)_2^{2+}$ fragments in the complex indicates that the four highest occupied fragment orbitals (HOMO to HOMO-3) of the diamidonaphthalene ligand and the five lowest unoccupied fragment orbitals (LUMO to LUMO+4) of the $W(NR)_2^{2+}$ fragment are involved in covalent bonding for complex **6.1** (Figure 6.4). For the complex with C_{2v} symmetry, the donor HOMO-1 (π orbital) of the R_2DAN^{2-} ligand can interact with LUMO+4 of $W(NR)_2^{2+}$. The observed bend of the diamidonaphthalene ligand allows overlap between this donor orbital with low-energy, W 5d-based acceptor orbitals (LUMO and LUMO+2, (Figure 6.4), thus increasing the metal-ligand interaction through increased π donation from the amido N atoms to these two σ-type acceptor orbitals of the metal fragment (their electron populations increase from 18.0% (LUMO) and 6.5% (LUMO+2) for the C_{2v} structure to 25.3% and 14.8% for the C_s structure, respectively). This, in turn, reduces the W atomic charge, increases the bond order for the $W\text{-}N_{imido}$ linkages and leads to the observed differences in the two imido moieties. Related observations have been reported from computational investigations on diamidobenzene complexes.[19]

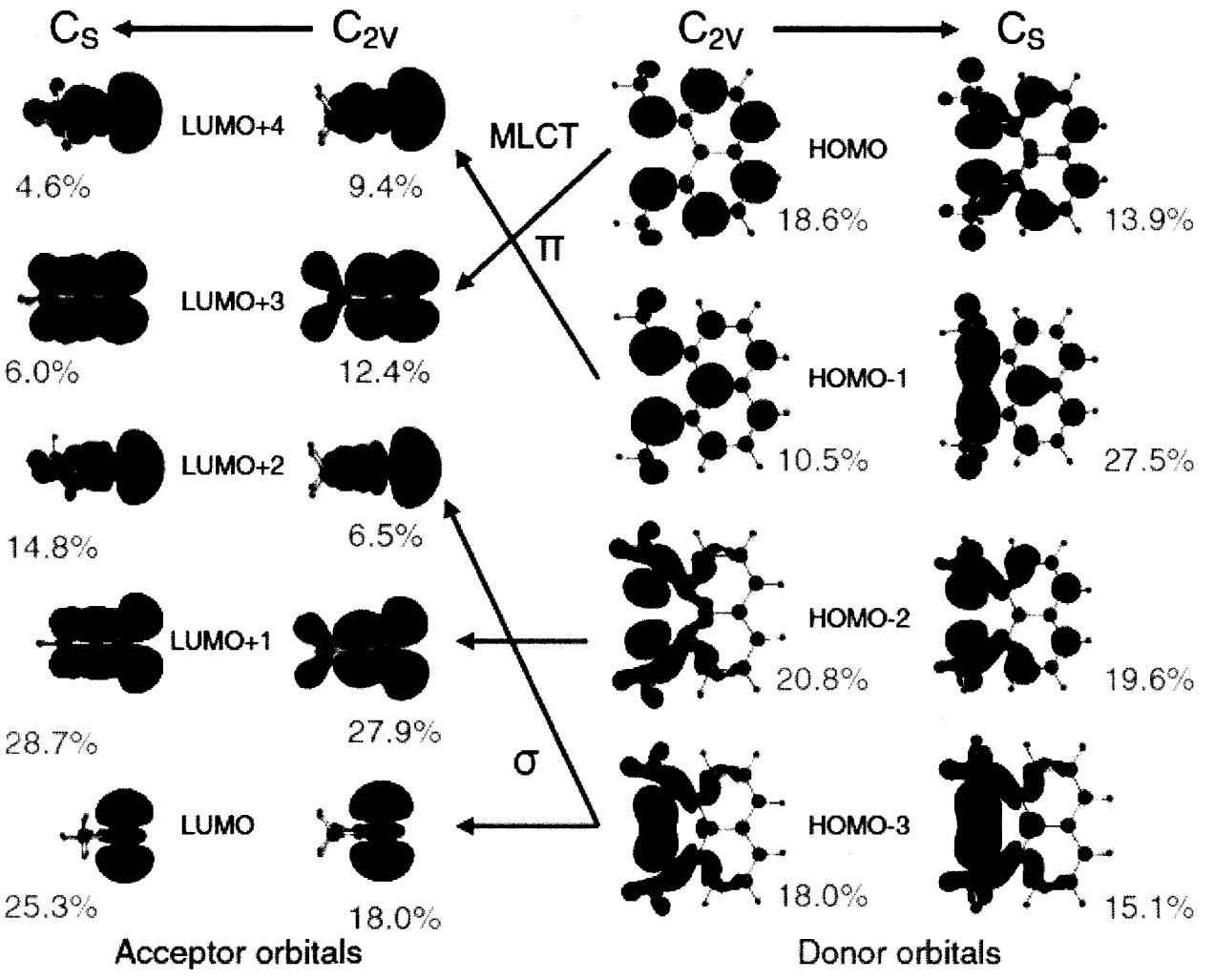

Figure 6.4. Frontier orbitals for the $(H_3CN)_2W^{2+}$ fragment (left) and the (CH3)2DAN2-ligand fragment (right) in C_{2v} and C_s symmetry. The populations of these fragment molecular orbitals in the complex are shown in green below the orbital. The major increase in ligand-to-metal donation involves HOMO-1 of $(CH_3)_2DAN^{2-}$ and increased overlap with LUMO (ε= -15.9 eV) and LUMO+2 (ε= -13.5 eV) of $(H_3CN)_2W^{2+}$. The B3LYP/LANL2DZ results are reported. The results from the B3LYP/SDD calculations are very similar. The red and blue arrows indicate σ and π donor-acceptor interactions in the complex with C_{2v} symmetry.

The computed electron distribution for **6.1** may presage the reactivity of this species. In particular, the increased electron density on the imido groups concomitant with the reduced NPA charges on the $^{i}Pr_2DAN^{2-}$ moiety and the W center in the observed (C_s) structure suggested the potential for increased reactivity of the imido ligands and prompted our exploration of addition reactions of **6.1** and **6.2** involving p-tolylisocyanate and phenyl-p-tolyl-carbodiimide as well as alkylation reactions of these compounds using Al_2Me_6. We began by examining the relative site selectivity, toward isocyanate, for the amido and imido functions of **6.1** computationally and experimentally. Possible ureato products of this reaction, $[(RN)C_{10}H_6(R'N)C(=O)NR]W(N^tBu)_2$ and $[C_{10}H_6(NR)_2]W(^tBuNC(=O)NR')(N^tBu)$, could arise from insertion into the $W\text{-}N_{amido}$ or addition to the $W{=}N_{imido}$ groups respectively. Optimizations of these products by DFT (B3LYP/SDD) generated structures that were confirmed to be true minima and with a ΔG preference for the amido insertion product between 6.4 and 15.8 kcal mol^{-1} depending on the isomer used in the computation.[20]

Treatment of either **6.1** or **6.2** with p-tolylisocyanate proceeded to yield the predicted ureato compounds $[(RN)C_{10}H_6(Ar'N)C(=O)NR]W(N^tBu)_2$ (Ar' = p-MeC_6H_4; R= ^{i}Pr **6.4**, 3,5-$Me_2C_6H_3$ **6.5**) (Scheme 6.3). The unsymmetrical nature of these species was demonstrated by the ^1H and ^{13}C spectra which in both cases displayed two unique N^tBu and two NR resonances. Definitive structural details of **6.4** and **6.5** were provided by single crystal X-ray diffraction studies. Tables 6.3 and 6.4 show selected crystal data and structure refinement parameters and selected bond lengths and angles. The results of these analyses unambiguously established the similarity of these products and the fact that they arose from the insertion of the isocyanate into amido W-N bond of the starting materials. These observations are consistent with the computational results and with the fact that amido-supported group 6 imido complexes generally undergo preferential reaction of isocyanate with the amido function,[11,13,21,22]

Scheme 6.3

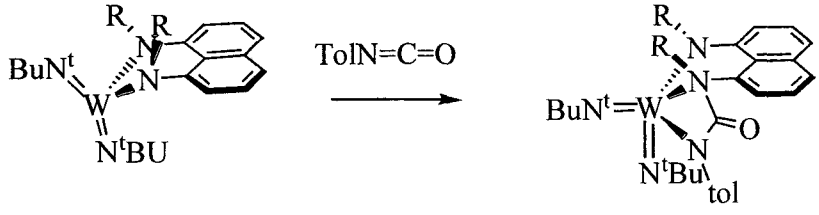

6.4, R= ^{i}Pr
6.5, R = 3,5-$(Me)_2C_6H_3$

Examining the structures of **6.4** and **6.5** (Figures 6.5 and 6.6) confirms the transformation of one of the original amido groups of the R_2DAN^{2-} ligand into an N,N'-ureato ligand. The coordination geometry of **6.4** can be described as a distorted square-based pyramidal with one of the NtBu imido groups (N5) in the axial position. The N^{t}Bu bond lengths of 1.752(5)Å and 1.748(5)Å are similar to the ones found in **6.1** (1.771(4)Å and 1.748(4)Å). The imido group are shown to be more similar in **6.4** than they were in **6.1**, one of the imido group is less bent than in the starting material with angle 163.7(4)° vs 150.6(4)° in the starting material and the second imido is slightly more bent with a angle of 167.6(4)° compared to the169.4(4)° in **6.1**. The W-N_{amido} bonds vary in lengths with the W(1)-N(1) being the shortest at 2.054(4)Å fallowed by the W(1)-N(3) with a length of 2.104(5)Å and finally the longest as expected, due to the isocyante insertion at this site, being the W(1)-N(2) with a value of 2.294(5)Å The structure obtained for **6.5** is very similar to what was obtained for **6.4.** The coordination geometry can again be described as distorted square-based pyramidal with one of the N^{t}Bu imido groups (N5) occupying the axial position. The imido W-N bond lengths are slight shorter (W(1)-N(4) 1.753(5)Å, W(1)-N(5) 1.739(5)Å) and more linear (average angle

167.4(4)°) than in **6.1**. The remaining W-N bonds span the anticipated range with W(1)-N(3) being the shortest amido linkage of 2.034(4)Å followed by W(1)-N(1) 2.129(5)Å and then the dative interaction W(1)-N(2) 2.300(5)Å.[21,23]

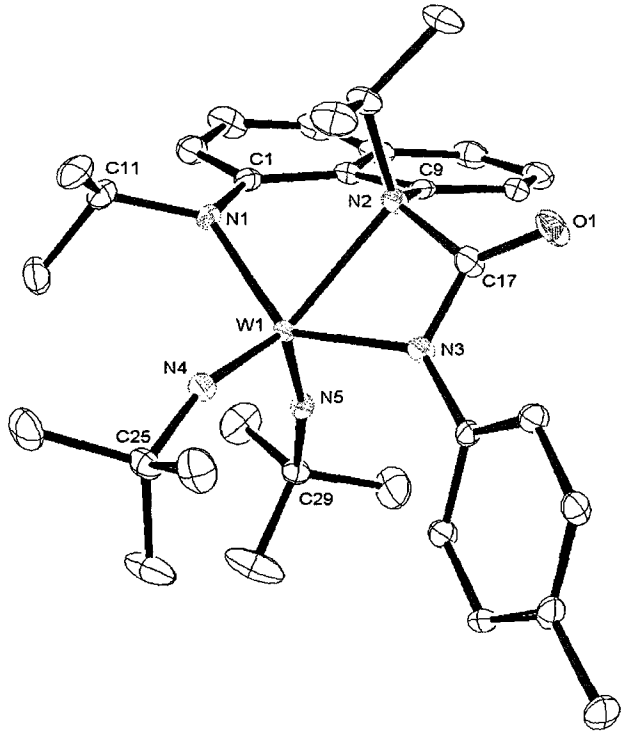

Figure 6.5 Molecular structure and partial atom-numbering scheme for **6.4**. Thermal ellipsoids are drawn at 30% probability. Hydrogen atoms have been omitted for clarity.

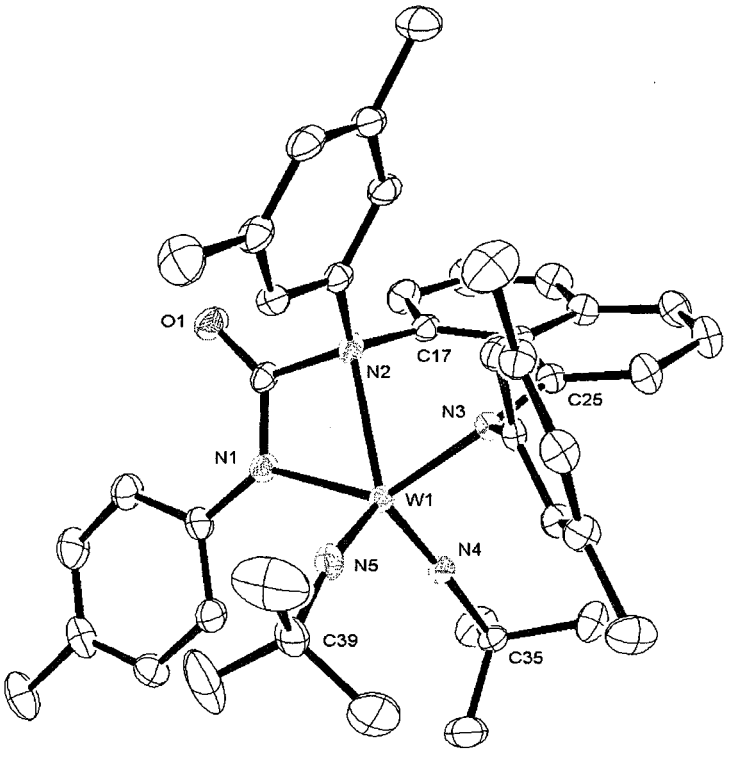

Figure 6.6. Thermal ellipsoid plot showing the molecular structure and partial atom numbering scheme for **6.5**. Thermal ellipsoids are drawn at 30% probability. Hydrogen atoms have been omitted for clarity.

Table 6.3. Selected Crystal Data and Structure Refinement Parameters for [(^{i}PrN)$C_{10}H_6$(Ar'N)C(=O)NR]W(N^tBu)$_2$ (**6.4**) and [(p-MeC_6H_4N)$C_{10}H_6$(Ar'N)C(=O)NR]W(N^tBu)$_2$ (**6.5**)

Empirical formula	$C_{64}H_{90}N_{10}O_2W_2$	$C_{42}H_{49}N_5OW$
Formula weight	1399.16	823.7
Temperature (K)	199(2)	213(2)
Wavelength (Å)	0.71073	071073
Crystal system	triclinic	monoclinic
Space group	P-1	P2(1)/C
a (Å)	10.757(3)	18.090(3)
b (Å)	17.465(5)	10.2206(14)
c (Å)	18.915(6)	22.508(3)
α(deg)	67.733(4)	90
β(deg)	74.304(5)	110.758(2)
γ(deg)	76.918(5)	90
V (Å^3)	3135.1(17)	3891.4(9)
Z	2	4
ρ(calc) (Mg/m^3)	1.482	1.406
***M* (mm^{-1})**	3.716	3.006
Absorption correction	Semi-empiriacal from equivalents	
Final R indices [I>2σ(I)]		
R1[a]	0.0337	0.0428
***w*R2**[b]	0.0855	0.0885

[a] $R1 = \Sigma \| F_o | - | F_c \| / \Sigma | F_o |$

[b] $wR2 = (w(| F_o | - | F_c |)^2 / \Sigma w | F_o |^2)^{1/2}$

Table 6.4. Selected Bond Lengths (Å) and Angle (°) for [(^{i}PrN)$_2$C$_{10}$H$_6$(Ar'N)C(=O)NR]W(N^{t}Bu)$_2$ (**6.4**) and [(p- MeC$_6$H$_4$N)C$_{10}$H$_6$(Ar'N)C(=O)NR]W(N^{t}Bu)$_2$ (**6.5**).

Bond Lenghts (Å)			
6.4		**6.5**	
N(1)-W(1)	2.052(4)	N(3)-W(1)	2.034(4)
N(2)-W(1)	2.294(5)	N(2)-W(1)	2.300(5)
N(3)-W(1)	2.104(5)	N(1)-W(1)	2.129(5)
N(4)-W(1)	1.752(5)	N(4)-W(1)	1.753(5)
N(5)-W(1)	1.748(5)	N(5)-W(1)	1.739(5)
N(1)-C(1)	1.417(7)	N(2)-C(17)	1.467(7)
N(2)-C(9)	1.465(7)	N(3)-C(25)	1.405(7)
Angles (°)			
N(1)-W(1)-N(2)	77.04(17)	N(2)-W(1)-N(3)	77.17(17)
N(2)-W(1)-N(3)	60.26(17)	N(2)-W(1)-N(1)	60.44(17)
W(1)-N(5)-C(29)	167.6(4)	W(1)-N(4)-C(35)	167.0(4)
W(1)-N(4)-C(25)	163.7(4)	W(1)-N(5)-C(39)	167.7(5)
C(1)-N(1)-C(11)	115.2(5)	C(25)-N(3)-C(27)	117.6(4)
C(1)-N(1)-W(1)	117.1(4)	C(25)-N(3)-W(1)	118.3(3)
C(11)-N(1)-W(1)	124.6(4)	C(27)-N(3)-W(1)	123.3(3)
C(9)-N(2)-C(17)	114.1(5)	C(17)-N(2)-C(9)	114.5(5)
C(9)-N(2)-C(14)	112.5(4)	C(17)-N(2)-C(8)	113.6(4)
C(17)-N(2)-C(14)	113.6(5)	C(9)-N(2)-C(8)	114.1(4)
C(9)-N(2)-W(1)	105.0(3)	C(17)-N(2)-W(1)	103.9(3)
C(17)-N(2)-W(1)	91.4(3)	C(9)-N(2)-W(1)	116.9(3)
C(14)-N(2)-W(1)	118.5(4)	C(8)-N(2)-W(1)	91.3(3)

A similar reaction was done with phenyl-p-tolyl-carbodiimide and compounds **6.1**, **6.2** and **6.3.** In all three cases a white solid was obtained from the reaction mixture. The proton NMR spectra of these white solids show that all three products are unsymmetrical. The ^{1}H NMR for **6.6** shows two singlets for the t-butyl groups on the imido moiety, four distinct doublets integrating for three protons each can be attributed to the isopropyl group of the ligand.

Compounds **6.7** and **6.8** also gave singlets integrating for nine protons representing the t-butyl groups for the imido ligands. Complex **6.7** displayed 2 singlets for the methyl groups on nitrogen substituents while **6.8** gave one singlet for the CH_3 group on the aryl nitrogen substituent and a doublet for the isopropyl group on the other nitrogen. X-ray diffraction experiments on compound **6.6** and **6.8** confirmed that the insertion of the carbodiimide occurred at the amido W-N bond (Figure 6.7 and 6.8).

Scheme 6.4

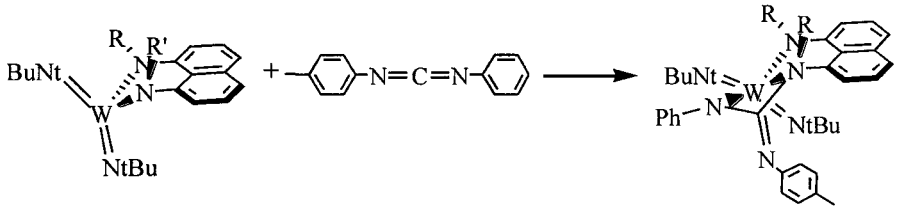

6.6, R and R' = $CH(CH_3)_2$
6.7, R and R' = 3,5-$Me_2C_6H_3$
6.8, R= $CH(CH_3)_2$ and 3,5-$Me_2C_6H_3$

Tables 6.5 and 6.6 present crystal data and structure refinement parameters and selected bond lengths and angles for **6.6** and **6.8**. The complexes can be described as distorted square based pyramidal geometry. The tungsten imido bond in **6.6** are 1.763(8)Å and 1.736(7)Å and 1.707(13)Å and 1.745(12)Å for complex **6.8**. The W-N_{imido} bond lengths for **6.6** very similar to what we saw in the starting material **6.1** (1.771Å and 1.748Å). Compound **6.8** on the other hand has slightly shorter W-N_{imido} bond lengths and are more of a triple bond character. One of the imido ligands in **6.6** is more linear than in the starting material 175.8(6)° versus 169.4(4)° in the starting material. The other imido group is bent with a angle of 158.3(8)° and very similar to one of the imido in the starting material (158.6(4)°. The imido angles in **6.8** are

in the same range as the starting material and **6.6** with the more bent imido being 158.0(15)° and the linear one being 171.1(13)°. W-N_{amido} bond for the ligands are 2.061(8) and 2.351(7)Å for **6.6** and 2.109(13) and 2.312(11)Å for **6.8.** In both these cases the longer W-N_{amido} is at the site of the carbodiiminde insertion which is indicative of a dative bond and are of similar lengths to the dative bond formed after the isocyanate insertion. The ligand nitrogen that did not react with the carbodiimide remains close to planarity with the sums of the angles surrounding them being 353.4° for **6.6** and 357.0° for **6.8.**

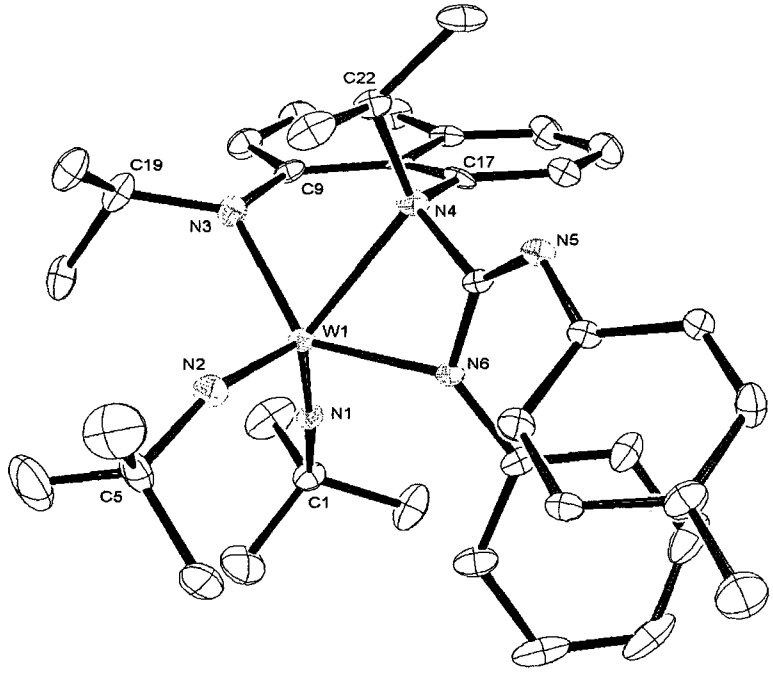

Figure 6.7. Molecular structure and atom-numbering scheme for **6.6.** Thermal ellipsoids are drawn at 30% probability. Hydrogen atoms have been omitted for clarity.

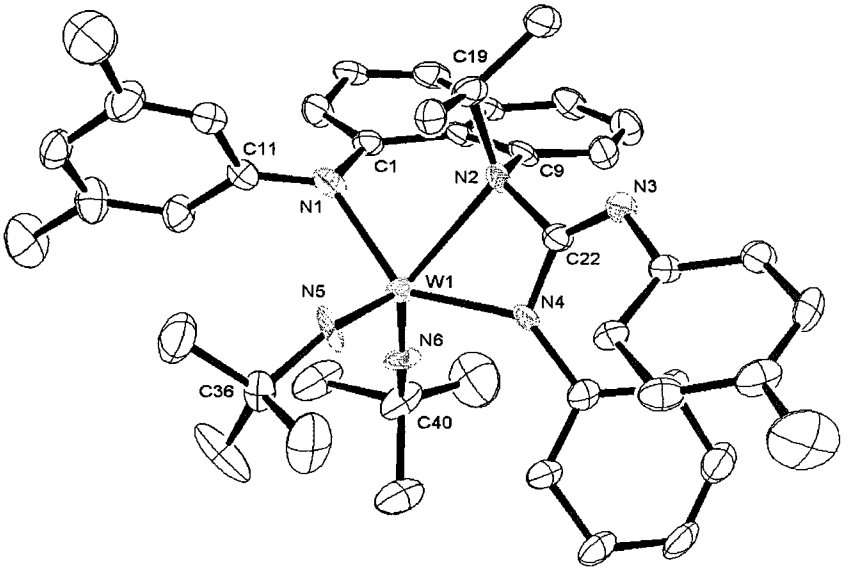

Figure 6.8. Molecular structure and atom-numbering scheme for **6.8**. Thermal ellipsoids are drawn at 30% probability. Hydrogen atoms have been omitted for clarity.

Table 6.5. Selected Crystal Data and Structure Refinement Parameters for (**6.6**) and (**6.8**)

Empirical formula	$C_{38}H_{50}N_6W$	$C_{43}H_{52}N_6W$
Formula weight	774.69	836.76
Temperature (K)	213(2)	200(2)
Wavelength (Å)	0.71073	
Crystal system	Monoclinic	Monoclinic
Space group	C2/c	C2
a (Å)	16.586(3)	25.02(3)
b (Å)	12.762(3)	14.954(16)
c (Å)	34.942(7)	12.153(13)
β(deg)	100.339(4)	108.372(16)
γ(deg)	90	90
V (Å^3)	7276(2)	4315(8)
Z	8	4
ρ (calc) (Mg/m^3)	1.414	1.288
μ (mm^{-1})	3.209	2.711
Absorption correction	Semi-empirical from equivalents	
Final R indices [I>2σ(I)]		
R1[a]	0.0587	0.0565
***w*R2**[b]	0.1502	0.1345

[a] $R1 = \Sigma \| F_o | - | F_c \| / \Sigma | F_o |$

[b] $wR2 = (w(| F_o | - | F_c |)^2 / \Sigma w | F_o |^2)^{1/2}$

Table 6.6. Selected Bond Lengths (Å) and Angle (°) for (**6.6**) and (**6.8**)

6.6		**6.8**	
	Bond Lengths (Å)		
W(1)-N(3)	2.061(8)	W(1)-N(1)	2.109(13)
W(1)-N(4)	2.351(7)	W(1)-N(2)	2.312(11)
W(1)-N(1)	1.734(7)	W(1)-N(5)	1.707(13)
W(1)-N(2)	1.763(8)	W(1)-N(6)	1.745(12)
W(1)-N(6)	2.086(7)	W(1)-N(4)	2.034(10)
N(3)-C(9)	1.401(12)	C(1)-N(1)	1.396(18)
N(4)-C(17)	1.486(10)	C(9)-N(2)	1.452(18)
	Angles (°)		
N(3)-W(1)-N(4)	76.4(3)	N(1)-W(1)-N(2)	78.1(4)
N(4)-W(1)-N(6)	59.5(2)	N(2)-W(1)-N(4)	60.0(4)
W(1)-N(2)-C(5)	158.3(8)	W(1)-N(5)-C(36)	158.0(15)
W(1)-N(1)-C(1)	175.8(6)	W(1)-N(6)-C(40)	171.1(13)
C(9)-N(3)-C(19)	117.3(8)	C(11)-N(1)-C(1)	122.7(13)
C(9)-N(3)-W(1)	112.2(5)	C(11)-N(1)-W(1)	120.1(10)
C(19)-N(3)-W(1)	123.9(7)	C(1)-N(1)-W(1)	113.9(10)
C(25)-N(4)-C(17)	112.7(7)	C(22)-N(2)-C(9)	115.6(12)
C(25)-N(4)-C(22)	118.2(6)	C(22)-N(2)-C(19)	115.7(12)
C(17)-N(4)-C(22)	112.0(6)	C(9)-N(2)-C(19)	109.71(12)
C(25)-N(4)-W(1)	88.2(5)	C(22)-N(2)-W(1)	90.0(8)
C(17)-N(4)-W(1)	100.9(4)	C(9)-N(2)-W(1)	103.3(8)
C(22)-N(4)-W(1)	121.9(6)	C(19)-N(2)-W(1)	121.1(10)

Compounds **6.1** and **6.2** both react with trimethylaluminum to alkylate the W center and to incorporate the resulting Me_2Al moiety into the complex via the diamidonaphthalene group. For example, treatment of a diethyl ether solution of **6.1** with ~5 equiv of Al_2Me_6 resulted in a pale yellow solution after 8 hours. The ^1H NMR spectrum of **6.9** indicated the incorporation of a $AlMe_3$ unit in the product. The spectrum displayed seven peaks ranging from -1.20 to 2,02 ppm integrating for either three or six protons each and summing to 21 protons indicating the presence of one ligand and one trimethyl aluminum unit. In the spectrum it can also be

observed that many of the peaks are broad signifying a fluxional structure. The ^{1}H NMR spectrum for **6.10** also indicated the presence of one ligand and one trimethyl aluminum unit with five singlets from -0.55 to 2.33 ppm for a total of 21 protons. Colorless crystals of these products were isolated from hexane and were subjected to X-ray diffraction analysis.

Scheme 6.5

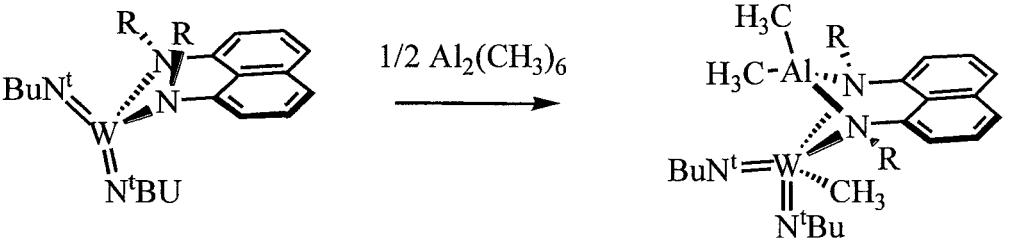

6.9, R= ^{i}Pr

6.10, R = 3,5-(Me)$_2$C$_6$H$_3$

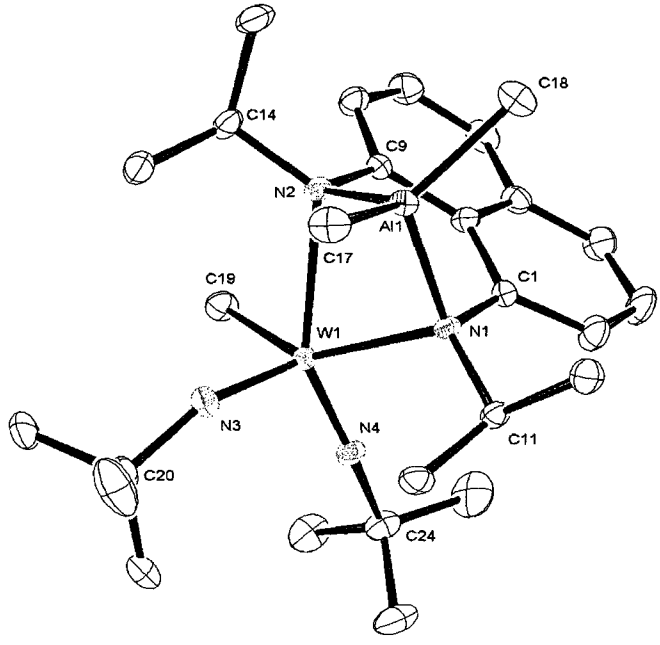

Figure 6.9. Molecular structure and atom-numbering scheme for **6.9**. Thermal ellipsoids are drawn at 30% probability. Hydrogen atoms have been omitted for clarity.

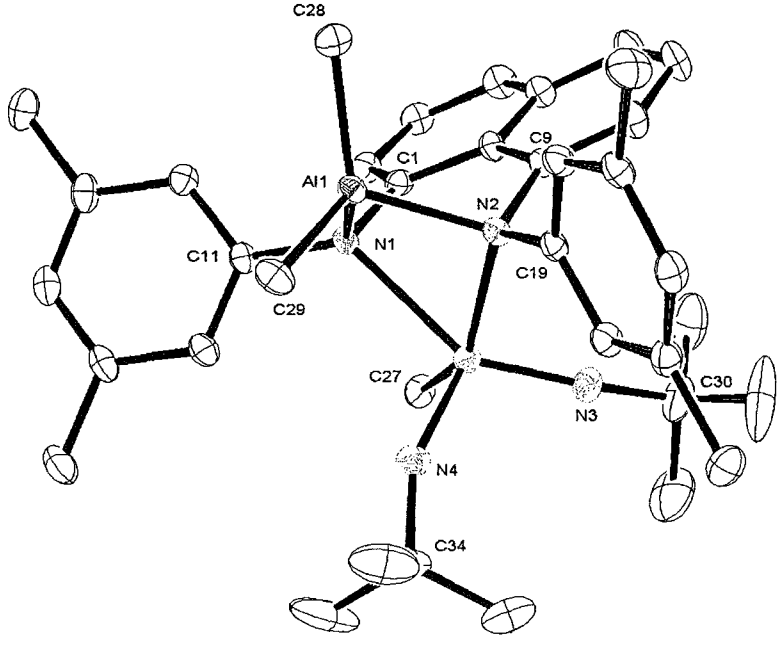

Figure 6.10. Molecular structure and atom-numbering scheme for **6.10**. Thermal ellipsoids are drawn at 30% probability. Hydrogen atoms have been omitted for clarity.

As shown in Figure 6.9, the bimetallic structure obtained for **6.9** consisted of a distorted square pyramidal W complex and a pseudo-tetrahedral Al center which are bridged by the R_2DAN^{2-} amido linkage. The imido center N(3) resides in the apical position and, while this group is less linear than the other imido group (C(20)-N(3)-W(1) 154.9(5)°, C(24)-N(4)-W(1) 175.7(4)°), both $W{=}N_{imido}$ bond distances remain short (W(1)-N(3) 1.755(5)Å, W(1)-N(4) 1.744(5)Å) and correspond to triple bonds thus providing an 18 electron configuration to W. The amido N centers are quaternary in compound **6.9** and, therefore, display longer W-N distances (W(1)-N(1) 2.237(5)Å, W(1)-N(2) 2.361(5)Å) than in the starting material. The longer W-N(2) bond distance is oriented *trans* to the imido-N(4) group. The coordination sphere of W is completed by a methyl group that originated from the Al starting material (W(1)-C(19) 2.172(6)Å). The approximately tetrahedral Al environment with average angles of 108.9(3)° consists of two methyl groups and the two bridging amido functions. The structure obtained for **6.10** was a complex that was very similar to **6.9** with a square pyramidal W center and a pseudo-tetrahedral Al center. The imido groups in **6.10** have $W{=}N_{imido}$ bond lengths of 1.756(4)Å. The tungsten imido angles of 155.7 and 169.7° are indicative of six electron donor imido ligand[24]. The $W\text{-}N_{amido}$ bonds in **6.10** are longer than in the starting material but are very similar to what we have observed for **6.9** (2.315(3) and 2.247(3)Å). The W(1)-C(27) bond is comparable to what was seen in **6.9** with a bond length of 2.168(4)Å.

Table 6.7. Selected Crystal Data and Structure Refinement Parameters for (**6.9**) and (**6.10**)

Empirical formula	$C_{27}H_{45}AlN_4W$	$C_{37}H_{51}AlN_4W$
Formula weight	638.52	762.65
Temperature (K)	200(2)	200(2)
Wavelength (Å)	0.71073	0.71073
Crystal system	Monoclinic	Triclinic
Space group	P2(1)/c	P-1
a (Å)	9.248(4)	10.6792(18)
b (Å)	21.027(9)	11.713(2)
c (Å)	15.445(7)	15.218(3)
α(deg)	90	84.744(3)
β(deg)	101.344(7)	78.196(8)
γ(deg)	90	75.125(3)
V (Å^3)	2942(2)	1799.2(5)
Z	4	2
ρ(calc) (Mg/m^3)	1.441	1.408
μ (mm^{-1})	3.976	3.264
Absorption correction	Semi-empirical from equivalents	
Final R indices [I>2σ(I)]		
R1[a]	0.0339	0.0270
***w*R2**[b]	0.1043	0.0736

[a] $R1 = \Sigma \| F_o | - | F_c \| / \Sigma | F_o |$

[b] $wR2 = (w(| F_o | - | F_c |)^2 / \Sigma w | F_o |^2)^{1/2}$

Table 6.8. Selected Bond Lengths (Å) and Angle (°) for (**6.9**) and (**6.10**)

6.9		**6.10**	
	Bond lengths (Å)		
N(1)-W(1)	2.237(5)	N(1)-W(1)	2.315(3)
N(2)-W(1)	2.361(5)	N(2)-W(1)	2.247(3)
N(3)-W(1)	1.755(5)	N(3)-W(1)	1.756(4)
N(4)-W(1)	1.744(5)	N(4)-W(1)	1.756(4)
C(19)-W(1)	2.172(6)	C(27)-W(1)	2.168(4)
N(1)-C(1)	1.444(8)	N(1)-C(1)	1.443(5)
N(2)-C(9)	1.439(7)	N(2)-C(9)	1.447(5)
Al(1)-N(1)	1.974(5)	Al(1)-N(1)	1.954(3)
Al(1)-N(2)	1.957(5)	Al(1)-N(2)	1.976(3)
Al(1)-C(18)	1.971(7)	Al(1)-C(28)	1.962(5)
Al(1)-C(17)	1.962(7)	Al(1)-C(29)	1.947(4)
	Angles (°)		
N(1)-W(1)-N(2)	69.07(17)	N(1)-W(1)-N(2)	68.65(11)
N(1)-Al(1)-N(2)	83.2(2)	N(1)-Al(1)-N(2)	81.80(14)
W(1)-N(3)-C(20)	154.9(5)	W(1)-N(3)-C(30)	169.7(4)
W(1)-N(4)-C(24)	175.7(4)	W(1)-N(4)-C(34)	155.7(4)
C(1)-N(1)-C(11)	114.2(5)	C(1)-N(1)-C(11)	116.0(3)
C(1)-N(1)-Al(1)	106.6(4)	C(1)-N(1)-Al(1)	112.7(2)
C(11)-N(1)-Al(1)	118.6(40	C(11)-N(1)-Al(1)	107.9(2)
C(1)-N(1)-W(1)	99.9(3)	C(1)-N(1)-W(1)	96.2(2)
C(11)-N(1)-W(1)	116.5(3)	C(11)-N(1)-W(1)	126.5(3)
Al(1)-N(1)-W(1)	98.3(2)	Al(1)-N(1)-W(1)	95.94(14)
C(9)-N(2)-C(14)	113.5(5)	C(9)-N(2)-C(19)	114.6(3)
C(9)-N(2)-Al(1)	109.2(4)	C(9)-N(2)-Al(1)	108.7(2)
C(14)-N(2)-Al(1)	116.5(4)	C(19)-N(2)-Al(1)	112.9(2)
C(9)-N(2)-W(1)	98.2(3)	C(9)-N(2)-W(1)	100.5(2)
C(14)-N(2)-W(1)	121.8(4)	C(19)-N(2)-W(1)	120.6(2)
Al(1)-N(2)-W(1)	94.84(19)	Al(1)-N(2)-W(1)	97.51(13)

The diamido bridged heterobimetallic species **6.9** and **6.10** contrast with recent reports of transmetallation reactions between trimethylaluminum and related Zr (IV) and Mo (VI) amido

species. For example, the o-diamidobenzene species, $(Mo(NPh)(o\text{-}(SiMe_3N)_2C_6H_4)(CH_2)_4$ and $(Mo(NPh)(o\text{-}(SiMe_3N)_2C_6H_4)(PhCCPh)$, reacted with Al_2Me_6 to undergo complete transfer of the diamido ligand to the Al and formation of a π-complex of the resultant $[Me_2Al(o\text{-}(SiMe_3N)_2C_6H_4)]^-$ with the Mo center.[25] Complexes of the type $(R\text{-}IAN)_2ZrNMe_2$, where IAN is a bidentate N,N' ligand formally of the β-diketiminate class, readily transmetallate to aluminum to give $(R\text{-}IAN)\text{-}AlMe_2$ and $Me_2Zr(NMe_2)_2$ as products.[26] In the case of products **6.9** and **6.10** the transfer reaction is apparently arrested at the formation of the diamido bridged Al/W complex.

Complexes **6.1** and **6.2** were found to be effective catalysts for the cyclotrimerization of aryl isocyanates (Scheme 6.6). Catalyst were placed into a round bottom flask in a 1% mole ratio to this was added the isocyanates. Table 6.9 summarizes the results obtained, the reaction was considered complete when all of the isocyanate was transformed into a white solid. The white powder was then washed with hexanes to obtain the isolated yield.

Scheme 6.6

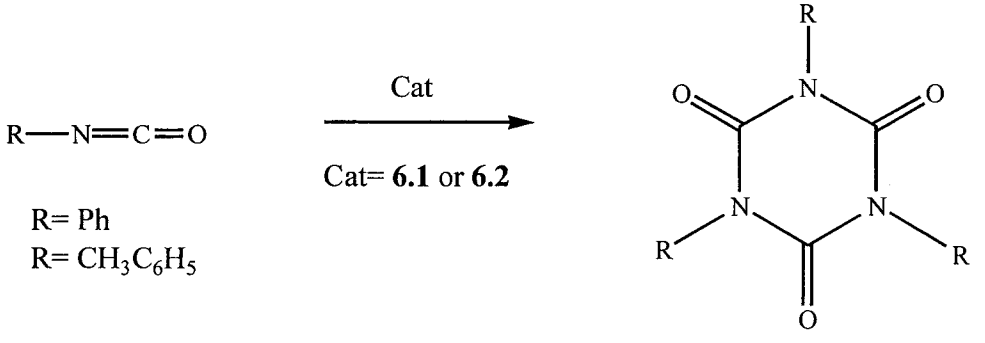

The data in Table 6.9 indicates that both **6.1** and **6.2** can catalyze the trimerization of phenyl isocyantes and p-tolyl isocyanate in good yield and in a relatively short time. The results show that catalyst **6.2** is slightly better then **6.1**, giving higher yields of transformation

in shorter time. This is possibly due to the difference in the nitrogen subtituents on the ligand. The isopropyl subtituents in **6.1** are less electron withdrawing than the aryl groups in **6.2** this can cause the nitrogen lone pair to be less donating to the tungsten center making it more electron deficient consequently being more electrophilic towards the carbodiimide.

Table 6.9. Yields and reaction times for the trimerization of phenyl and p-tolyl isocyanate using **6.1** and **6.2** as a catalyst

Catalyst	Phenyl isocyanate	p-tolyl isocyanate
6.1	79.8%(2min30sec)	75.0% (3min)
6.2	88.4% (1min10sec)	79.8% (1min)

Trimerization of other substrates such as diisopropyl carbodiimide, ethyl isocyanate, 2,6-dimethyl phenyl isocyanate and p-Tolyl isothiocyanate were attempted with no success.

III. Conclusions:

This first application of the N,N'-disubstituted-1,8-diamidonaphthalene framework (R_2DAN^{2-}) with a high-valent W(VI) metal center has been examined through structural, computational and reactivity studies. Computationally, the observed bonding features of this ligand array revealed the structural features that manifest themselves to allow for a flexible and increased ligand-to-metal π-electron donation. Computational and experimental analysis of the reactivity of these species with isocyanate and carbodiimide demonstrated insertion into one of the W-Namido bonds. Alkylation of the W centers of **6.1** and **6.2** with Al_2Me_6 and the incorporation of the Lewis acid $AlMe_2^+$ products through the diamidonaphthalene groups are consistent with the electron distribution of the starting

materials and reveal the ability of the R_2DAN^{2-} ligand to construct heterobimetallic species. Catalytic studies showed that **6.1** and **6.2** are effective catalyst for cyclotrimerization of aryl isocyanates.

IV. Experimental Section

General Methods. Reactions were performed using standard Schlenk techniques (N_2) or, alternatively, in a glovebox with a nitrogen atmosphere. Unless otherwise noted, solvents were sparged with nitrogen and then dried by passage through a column of activated alumina using an apparatus purchased from Anhydrous Engineering. Deuterated benzene was dried using activated molecular sieves. WCl_6 and 1,8-diaminonaphthalene were purchased from Aldrich and used without further purification. *N,N'*-Diisopropyl1,8-diaminonaphthalene and *N,N'*-bis(3,5-dimethylphenyl)-1,8-diaminonaphthalene were prepared according to a previously reported procedures.[6,12] $WCl_2(NtBu)_2Cl_2(Py)_2$ was prepared according to the literature.[24] NMR spectra were run on either a Gemini 200 MHz a Bruker 300MHz or a 500 MHz spectrometer with deuterated benzene as a solvent and internal standard. All elemental analyses were carried out by Guelph Chemical Laboratories, Ltd. in Ontario, Canada.

Preparation of $W(NtBu)_2[1,8\text{-}(^iPrN)_2C_{10}H_6]$ (6.1).

Addition of 1.6M nBuLi (5.3 mL, 8.46 mmol) to a solution of $1,8\text{-}(^iPrNH)_2C_{10}H_6$ (1.03 g, 4.23 mmol) in 30 mL of diethyl ether led to an immediate color change of the solution to green and then to brown with gas evolution. To this reaction mixture was added $W(NtBu)_2Cl_2(py)_2$ (2.35 g, 4.23 mmol), which was allowed to stir for 8 h. The solvent was then evaporated under vacuum, and the solid was extracted with hexanes that were removed under vacuum to yield **6.1** as a purple solid (1.70 g, 74%). The product can be crystallized from a saturated hexanes solution at -20°C.

^1H NMR (C_6D_6, 200 MHz,): δ 0.9–1.8 (br overlapping signals, 30 H, CH_3 from tBu and iPr groups), 3.97 (sept, 2H, $CHMe_2$), 6.53 (d, 2H, Ar-H), 7.15 (m, 4H, Ar-H).

$^{13}C\{^1H\}$ NMR (C_6D_6, 125 MHz): δ 25.4 (CH_3), 27.6 (CH_3), 33.8 (*C*H), 55.4 (CMe_3), 111.9 (CH), 122.4 (C), 127.8 (CH), 130.1 (CH), 138.5 (C), 151.4 (C).

Anal. Calcd for $C_{24}H_{38}N_4W$: C, 50.89; H, 6.76; N, 9.89. Found: C, 50.59; H, 6.91; N, 9.59.

Preparation of $W(NtBu)_2[1,8\text{-}(2,6\text{-}Me_2C_6H_3N)_2C_{10}H_6]$ py (6.2).

Using a procedure similar to the synthesis of **6.1** with 1.6 M nBuLi (1.35 mL, 2.17 mmol), 1,8-$(2,6\text{-}Me_2C_6H_3NH)_2C_{10}H_6$ (398 mg,1.09 mmol), and $W(NtBu)_2Cl_2(py)_2$ (603 mg, 1.09 mmol) produced compound **6.2** as an orange powder (716 mg, 86%).

^1H NMR (C_6D_6, 200 MHz): δ 1.07 (s, 18H, CCH_3), 2.11 (s, 12H, $CArCH_3$), 6.45–6.89 (m, 7H, Ar-H), 6.97 (s, 4H, Ar-H), 7.26–7.31 (m, 4H, Ar-H), 8.90 (d, 2H, py).

$^{13}C\{^1H\}$ (C_6D_6, 50 MHz): δ 21.49 (CH_3), 32.36 (CH_3), 67.91 (CMe_3), 116.18 (C_{Ar}), 121.13 ($C_{Ar}H$), 121.92 ($C_{Ar}H$), 123.43 ($C_{Ar}H$), 124.17 ($C_{Ar}H$), 126.31 ($C_{Ar}H$), 128.31 ($C_{Ar}H$), 137.62 (C_{Ar}), 137.91 (C_{Ar}), 138.35 ($C_{Ar}H$), 150.45 (C_{Ar}), 152.00 ($C_{Ar}H$), 156.48 (C_{Ar}).

Anal. Calcd for $C_{39}H_{47}N_5W$: C, 60.86; H, 6.16; N, 9.10 Found: C, 60.94; H, 5.80; N, 8.69.

Preparation of $W(NtBu)_2[1\text{-}(2,6\text{-}Me_2C_6H_3N)\text{-}8\text{-}(^iPrN)C_{10}H_6]$ (6.3)

Using a procedure similar to the synthesis of **6.1** with 1.6 M nBuLi (1.25 mL, 2.01 mmol), 1,8-$(^iPrN)(2,6\text{-}Me_2C_6H_3NH)C_{10}H_6$ (300mg, 0.98 mmol), and $W(NtBu)_2Cl_2(py)_2$ (560 mg, 0.98 mmol) produced compound **6.3** as a purple solid (433 mg, 66%).

^1H NMR (C_6D_6), 300 MHz): δ 1.27 (br s, 18H, CCH_3), 1.36 (d, 6H, $C(CH_3)_2$), 2.09 (s, 6H, $CArCH_3$), 4.05 (sept, 1H, $CH(Me)_2$), 6.58 (s, 1H, $C_{Ar}H$), 6.63 (d, 1H, $C_{Ar}H$), 6.76-6.96 (m, 3H, $C_{Ar}H$), 6.99-7.16 (m, 3H, $C_{Ar}H$), 7.20-7.28 (m, 1H,$C_{Ar}H$),

Reaction of $W(NtBu)_2[1,8\text{-}(^iPrN)_2C_{10}H_6]$ with $MeC_6H_4N{=}C{=}O$ (6.4).

To a solution of **6.1** $W(NtBu)_2[1,8\text{-}(^iPrN)_2C_{10}H_6]$ (0.320 g, 0.594 mmol) in 30 mL of ether was added $MeC_6H_4N{=}C{=}O$ (0.095g, 0.71 mmol). After the reaction mixture was stirred overnight, the volatiles were removed under vacuum and the resultant solid was redissolved in 10 mL of hexane. Insoluble solid was removed by filtration and the filtrate was cooled to -20 °C to afford microcrystals of **6.4** (0.211 g, 53%).

^1H NMR (C_6D_6, 500 MHz): δ 0.77 (s, 9H, CH_3), 1.20 (d, 3H, CH_3), 1.26 (s, 9H, CH_3), 1.45 (d,3H, CH_3), 1.63 (d, 3H, CH_3), 1.71 (d, 3H, CH_3), 2.08 (s, 3H, CH_3), 3.90 (br, 1H, CH), 4.63 (br, 1H, CH), 6.98 (d, 1H, Ar-H), 7.02 (t, H, Ar-H), 7.03 (d, 2H, Ar-H), 7.18 (d, 1H, Ar-H), 7.36 (t, 1H,

Ar-H), 7.49 (d, 1H, Ar-H), 8.02 (d, 2H, Ar-H), 8.17 (d, 1H, Ar-H).

$^{13}C\{^1H\}$ NMR (C_6D_6, 125 MHz): 18.3 (CH_3), 20.9, 21.6, 23.6, 26.0 (CH_3), 32.2, 33.1 (CH_3), 56.5, 58.0 (*C*H), 67.9(CMe_3), 67.6 (CMe_3), 111.2 (C_{Ar}), 119.3 ($C_{Ar}H$), 119.8 ($C_{Ar}H$), 122.4 (C_{Ar}), 124.8 ($C_{Ar}H$), 124.9 ($C_{Ar}H$), 127.1 ($C_{Ar}H$), 128.9 ($C_{Ar}H$), 129.5 ($C_{Ar}H$), 133.8 ($C_{Ar}H$), 136.8 (C_{Ar}), 137.7 (C_{Ar}), 143.0 (C_{Ar}), 152.4 (C_{Ar}), 156.9 (*C*O).

Anal. Calcd for $C_{32}H_{45}N_5OW$: C, 54.94; H, 6.48; N, 10.01. Found: C, 55.11; H, 6.61; N, 9.87.

Reaction of $W(NtBu)_2[1,8\text{-}(2,6\text{-}Me_2C_6H_3N)_2C_{10}H_6]$py with TolN=C=O (6.5).

Following a procedure similar to the synthesis of **6.4** using **6.2** $W(NtBu)_2[1,8\text{-}(2,6\text{-}Me_2C_6H_3NH)_2C_{10}H_6]$py (0.200 g, 0.26 mmol) and *p*-tolyl isocyanate (0.035 g, 0.26 mmol) produced compound **6.5** as a beige powder (0.117 g, 55%).

^1H NMR (C_6D_6, 200 MHz): δ 1.01 (s, 9H, CH_3), 1.10 (s, 9H, CH_3), 1.82 (s, 6H, CH_3), 2.09 (s, 3H, CH_3), 2.14 (s, 6H, CH_3), 6.24 (s, 2H, Ar-H), 6.65 (m, 3H, Ar-H) 7.15 (m, 7H, Ar-H), 7.57 (d, 1H, Ar-H), 8.25 (d, 2H, Ar-H), 8.56 (d, 1H, Ar-H).

$^{13}C\{^1H\}$ (C_6D_6, 50 MHz): δ 20.9 (CH_3), 21.0 (CH_3), 21.2 (CH_3), 31.9 (CH_3), 32.8 (CH_3), 67.6 (CMe_3), 67.7 (CMe_3), 115.0 ($C_{Ar}H$), 119.4 ($C_{Ar}H$), 119.9 (C_{Ar}), 121.9 (C_{Ar}), 122.7 ($C_{Ar}H$), 124.2 ($C_{Ar}H$), 125.6 ($C_{Ar}H$), 125.8 ($C_{Ar}H$), 126.9 ($C_{Ar}H$), 128.3 ($C_{Ar}H$), 128.7 (C_{Ar}), 129.0 ($C_{Ar}H$), 130.0 ($C_{Ar}H$), 134.0 (C_{Ar}), 135.7 (C_{Ar}), 136.6 (C_{Ar}), 138.2 ($C_{Ar}H$), 139.0 ($C_{Ar}H$), 142.9 (C_{Ar}), 145.5 (C_{Ar}), 151.9 (C_{Ar}), 156.6 (C_{Ar}), 157.8 (CO).

Anal. Calcd for $C_{42}H_{49}N_5OW$: C, 61.24; H, 6.00; N, 8.50. Found: C, 60.92; H, 6.23; N, 8.08.

Reaction of $W(N^tBu)_2[1,8\text{-}(N^iPr)_2C_{10}H_6]$ with TolN=C=NPh, (6.6).

To a solution of $W(N^tBu)_2[1,8\text{-}(NiPr)_2C_{10}H_6]$ (0.198 g, 0.368 mmol) in 30 mL of toluene was added sequentially TolN=C=NPh (0.077 g, 0.368 mmol). After the reaction mixture was stirred for 2 h, the solvent was evaporated under vacuum and washed with 3 x 3 mL hexane to afford the light yellow solid. The crude product was then purified by crystallization from ether at -20 °C. The crystals were filtered and dried under vacuum (0.185 g, 34%).

^1H NMR (C_6D_6): δ 0.57 (s, 9H, CH_3), 1.40 (d, 3H, CH_3, ^3J = 6.11Hz), 1.50 (d, 3H, CH_3, ^3J = 5.86Hz), 1.59 (s, 9H, CH_3), 1.70 (d, 3H, CH_3, ^3J = 5.86Hz), 1.88 (d, 3H, CH_3, ^3J =6.11 Hz), 2.00 (s, 3H, CH_3), 4.08 (br, 1H, CH), 4.70 (br, 1H, CH), 6.58 (t, 1H, Ar-H), 6.87 (m, 3H, Ar-H), 7.0-7.3 (m, 8H, Ar-H), 7.48 (t, 1H, Ar-H), 7.58 (t, 1H, Ar-H), 8.54 (d, 1H, Ar-H).

$^{13}C\{^1H\}$ NMR (125 MHz, C_6D_6): δ 18.3 (CH_3, toly), 20.8 (CH_3, iPr), 21.7 (CH_3, iPr), 23.99 (CH_3, iPr), 25.3 (CH_3, iPr), 31.9 (CH_3, ^{t}Bu), 33.7 (CH_3, ^{t}Bu), 56.2 (CH), 58.9 (CH),

67.1 (*C*), 67.5 (*C*), 111.8 (C_{Ar}), 119.2 (C_{Ar}), 120.8 (C_{Ar}), 121.8 (C_{Ar}), 122.3 (C_{Ar}), 122.5 (C_{Ar}), 123.0 (C_{Ar}), 124.8 (C_{Ar}), 127.4 (C_{Ar}), 128.3 (C_{Ar}), 129.1 (C_{Ar}), 130.0 (C_{Ar}), 131.0 (C_{Ar}), 137.1 (C_{Ar}), 138.3 (C_{Ar}), 145.0 (C_{Ar}), 147.5 (C_{Ar}), 150.1 (C_{Ar}), 151.7 (CN_3).

Reaction of $W(N^tBu)_2$[1,8-(2,6-$Me_2C_6H_3NH)_2C_{10}H_6$]py with TolN=C=NPh (6.7).

In a vial $W(N^tBu)_2$[1,8-(2,6-$Me_2C_6H_3NH)_2C_{10}H_6$]py (288 mg, 0.37 mmol) was dissolved in approximately 10 ml of diethylether p-tolylisocyanate (45mg, 0.37 mmol) was then added to the solution. The solution was stirred for 18 hours and the solvent was removed under vacuum to give a beige powder (266 mg, 80%). The product can be further purified by washing with hexane.

^{1}H NMR (C_6D_6, 200 MHz) δ 1.01 (s, 9H, CC**H**$_3$), 1.10 (s, 9H, CC**H**$_3$), 1.82 (s, 6H, C_{Ar}C**H**$_3$), 2.09 (s, 3H, C_{Ar}C**H**$_3$), 2.14 (s, 6H, C_{Ar}C**H**$_3$), 6.37-7.15 (m, 12H, CH_{Ar}), 7.57 (d, 2H, CH_{Ar}), 8.25 (d, 4H, CH_{Ar}), 8.56 (d, 2H, CH_{Ar}),

^{13}C{^{1}H} (C_6D_6, 50 MHz) δ 20.9 (CH_3, **C**C_{Ar} isocyanate), 21.0 (CH_3, **C**CAr), 21.2 (CH_3, **C**CAr), 31.9 (CH_3, t-Bu), 32.8 (CH_3, t-Bu), 67.6 (C, t-Bu), 67.7 (C, t-Bu), 115.0 (C_{Ar}), 119.4 (C_{Ar}), 119.9 (C_{Ar}), 121.9 (C_{Ar}), 122.7 (C_{Ar}), 124.2 (C_{Ar}), 125.6 (C_{Ar}), 125.8 (C_{Ar}), 126.9 (C_{Ar}), 128.3 (C_{Ar}), 129.0 (C_{Ar}), 130.0 (C_{Ar}), 134.0 (C_{Ar}), 135.7 (C_{Ar}), 136.6 (C_{Ar}), 138.2 (C_{Ar}), 139.0 (C_{Ar}), 142.9 (C_{Ar}), 145.5 (C_{Ar}), 151.9 (C_{Ar}), 156.6 (C_{Ar}), 157.8 (C_{Ar}).

Reaction of $W(NtBu)_2$[1-(2,6-$Me_2C_6H_3NH$)8-(NiPr)$C_{10}H_6$]py with TolN=C=NPh (6.8).

In a round bottom flask equipped with a magnetic stir bar $W(NtBu)_2$[1-(2,6-$Me_2C_6H_3NH$)8-(NiPr)$C_{10}H_6$]py (103 mg, 0.15mmol) was dissolved in 15 ml of ether. To this solution was added p-tolyl-carbodimide (34 mg, 0.16mmol).The reaction mixture was stirred overnight and the solvent was removed under vacuum fallowed by extractionwith toluene. The product obtained was washed with 15 ml of hexanes to afford an off white powder (95mg, 78%)

^{1}H NMR (200 MHz, C_6D_6): δ 0.95 (s, 9H, $C(CH_3)_3$), 0.96 (s, 9H, $C(CH_3)_3$), 1.47 (d, 6H, $CH(CH_3)_2$), 1.86 (s, 3H, CH_3), 2.28 (s, 6H, CH_3), 4.52 (sept, 1H, $CH(Me)_2$), 6.51-7.17 (m, 14H, CH_{Ar}), 7.67 (d, 2H, CH_{Ar}), 8.65 (br, 2H, CH_{Ar}).

Reaction of $W(NtBu)_2$[1,8-(^{i}PrN)$_2C_{10}H_6$] with Al_2Me_6 (6.9).

In a round-bottom flask equipped with a magnetic stir bar **6.1** (0.411g, 0.764 mmol) was dissolved in hexanes, trimethylaluminum (0.165g, 2.28 mmol) was added to this solution. The reaction mixture was stirred for 6 h and then dried under vacuum. The yellow solid was recrystallized from hexanes to give clear crystals (0.150 g, 31%).

^{1}H NMR (C_6D_6, 300 MHz, 50 °C): δ -1.20 (s, 3H, CH_3), 0.23 (s, 3H, CH_3), 0.41 (br s, 3H, CH_3), 0.91 (br s, 9H, *t*Bu), 1.28 (br, 3H, CH_3), 1.41 (s, 9H, *t*Bu), 1.78 (br, 6H, CH_3), 2.02 (d, 3H, CH_3), 3.86 (br m, 2H, CH) 6.86 (d, 1H, Ar-H), 6.96 (d, 1H, Ar-H), 7.32 (m, 4H, Ar-H).

$^{13}C\{^1H\}$ (C_6D_6, 75 MHz): δ -7.0 (br, CH_3,AlMe), -0.05 (br, CH_3, AlMe), 18.7 (CH_3, WMe), 21.4 (CH_3), 22.5 (CH_3), 25.7 (CH_3), 27.2 (CH_3), 31.5 (CH_3, *t*Bu), 32.2 (CH_3, *t*Bu), 66.7 (C, *t*Bu), 66.9 (C, *t*Bu), 112.1 (CH), 120.3 (C), 122.9 (CH), 124.3 (CH), 126.3 (C), 127.3 (CH), 127.4 (CH), 137.1 (CH), 147.0 (C), 148.0 (C).

Anal. Calcd for $C_{27}H_{47}AlN_4W$: C, 50.79; H, 7.42; N, 8.77. Found: C, 50.54; H, 7.65; N, 8.67.

Reaction of $W(NtBu)_2[1,8\text{-}(2,6\text{-}Me_2C_6H_3NH)_2C_{10}H_6]$py with $Al(Me)_3$ (6.10).

Using a procedure similar to the synthesis of **6.9** using **6.2** (0.330 g, 0.43 mmol) and trimethylaluminum (0.074 g, 1.03 mmol) produced compound **6.10** as light purple crystals (0.095 g, 28%).

^1H NMR (C_6D_6, 300 MHz): δ -0.55 (s, 3H, CH_3), -0.39 (s, 3H, CH_3), 0.73 (s, 3H, CH_3), 0.92 (s, 9H, *t*Bu), 1.50 (s, 9H, *t*Bu), 2.07 (s, 6H, CH_3), 2.33 (s, 6H, CH_3), 7.37–6.60 (m, 10H), 8.00 (s, 1H),8.37–8.29 (m br, 1H).

$^{13}C\{^1H\}$ (C_6D_6, 75 MHz) δ -9.17 (CH_3, AlMe), -7.96 (CH_3, AlMe), 21.6 (CH_3), 22.0 (CH_3, WMe), 22.8 (CH_3), 31.4 (CH_3, *t*Bu), 32.7 (CH_3, *t*Bu), 66.9 (C, *t*Bu), 67.8 (C, *t*Bu), 114.3 ($C_{Ar}H$), 115.3 ($C_{Ar}H$), 119.4 (C_{Ar}), 123.3 ($C_{Ar}H$), 124.2 ($C_{Ar}H$), 125.2 (C_{Ar}), 125.4 (C_{Ar}), 127.3 ($C_{Ar}H$), 127.4 ($C_{Ar}H$), 127.5 ($C_{Ar}H$), 129.0 (C_{Ar}), 137.1 (C_{Ar}), 139.4 (C_{Ar}), 139.6 (C_{Ar}), 145.2 ($C_{Ar}H$), 146.6 ($C_{Ar}H$),147.6 ($C_{Ar}H$), 149.0 (C_{Ar}).

Anal. Calcd for $C_{37}H_{51}AlN$ W: C, 58.27; H, 6.74; N, 7.35. Found: C, 57.85; H, 6.92; N, 7.15.

Cyclotrimerization results

General procedure for cyclotrimerization of isocyanate

Catalyst was weighed into a round bottom flask equipped with a magnetic stir-bar. To this was added isocyanate. The reaction mixture was stirred until everything became solid. The solid obtained was then washed with approximately 30ml of hexanes and then dried under vacuum. All products were characterized by ^{1}H NMR and Mass spectrometry

Phenyl isocyanate and 6.1

In a round bottom flask **6.1** was placed (0.024 g, 0,042 mmol) to this was added phenyl isocyante (0.5 g, 4.1 mmol). A white powder (0.399 g, 1.1 mmol, 80%) was isolated from the reaction mixture

Phenyl isocyanate and 6.2

In a round bottom flask **6.2** was placed (0.032 g, 0,042 mmol) to this was added phenyl isocyante (0.5 g, 4.1 mmol). A white powder (0.442 g, 1.24 mmol, 88%) was isolated from the reaction mixture

p-tolyl isocyanate and 6.1

In a round bottom flask **6.1** was placed (0.023 g, 0,040 mmol) to this was added p-tolyl isocyante (0.5 g, 3.76 mmol). A white powder (0.375 g, 0.94 mmol, 75%) was isolated from the reaction mixture.

p-tolyl isocyanate and 6.2

In a round bottom flask **6.2** was placed (0.029 g, 0.038 mmol) to this was added p-tolyl isocyante (0.5 g, 3.76 mmol). A white powder (0.399 g, 1.0 mmol, 80%) was isolated from the reaction mixture.

Computational Details. DFT calculations with the B3LYP functional were carried out using the Gaussian 03 (revision D.01) suite of programs. Spin-restricted treatment was used for all closedshell species. The basis sets SDD and LANL2DZ were employed. In the case of complex **6.1**, a symmetrical *C*2V structure was prepared and used as the staring point in optimizations with both SDD and LANL2DZ basis sets. Both cases resulted in the same minimum structure of lower (*Cs*) symmetry that was similar to the experimentally obtained crystal structure. Frequency calculations on the optimized structures were used to compare the thermodynamic stability of the *C*2V and *Cs* structures. Atomic charges were calculated by natural population analysis (NPA) as implemented in Gaussian 03. Mayer bond orders were obtained using the AOMix-L program. The analysis of molecular orbitals (MOs) in terms of fragment orbital (FO) contributions and calculations of the FO overlap matrices and FO populations were carried out using the AOMix-CDA program. The converged wave functions were tested to confirm that they represent to the true ground state. Three possible ureato products of the reaction of complex **6.1** and *p*-tolyl isocyanate were prepared with GaussView and were used as the starting points in the optimization calculations for these species using the SDD basis set. In all cases, the default optimization conditions were employed. Frequency calculations on these optimized structures were used to confirm that the computed structures were indeed minima and in the calculation of the relative thermodynamic stabilities of these species.

Structural determination of 6.1, 6.4, 6.5, 6.6, 6.8, 6.9 and 6.10.

Single crystals were mounted on a thin glass fibre and held using viscous oil. They were subsequently cooled to data collection temperature. Crystal data and details of the measurements are summarized in table 6.1, 6.3, 6.5 and 6.7. Data were collected on a Bruker AX SMART 1k CCD diffractometer using 0.3° ω-scans at 0, 90, 180° in Φ. Unit-cell parameters were determined from 60 data frames collected at different sections of the Ewald sphere. Semi-empirical corrections based on equivalent reflections were applied (Blessing, R., *Acta Cryst.*, **1995**, A51, 33-38). The structures were solved by direct method, completed with difference Fourier synthesis and refined with full-matrix least-squared procedures based on F^2. All non-hydrongen atoms were refined with anisotropic displacement parameters. All hydrogen atoms were treated as idealized contributions. All scattering factors and anomalous dispersion factors are contained in the SHELXTL 5.1 program library (Sheldrick, G. M. AXS, Madison, WI, 1997).

References:

[1] (a) Boncella, J. M,; Wang, S-Y. S.; VanderLende, D. D.; Huff R. L.; Abboud, K. A.; William M. Vaughn, W. M. *Journal of Organometallic chemistry,* **1997**, 530, 59. (b) Huff, L. R.; Wang, S-Y. S.; Abboud, A. K.; Boncella, J. M. *Organometallics,* **1997**, *16,* 1779. (c) Ward, B. D.; Dubberley, S. R.; Gade, L. H.; Mountford, P. *Inorganic Chemistry*, **2003,** 42, 16, 4961. (d) Montford, P.; Gade, L.H. *Coordination Chemistry Reviews,* **2001**, 216, 65.

[2] Bolton, P. D.; Mountford, P. Adv. Synth.Catal. **2005**, 347, 355.

[3] Nielson, A. J.; Glenny, M. W.; Rickard, C. E. F.; *J. Chem. Soc. Dalton Trans.* **2001**, 232.

[4] Gade, L.H.; Mountford, P. *Coordination Chemistry*, Reviews 216-217, **2001**, 65.

[5] For recent reviews of β-diketiminates and their metal complexes see: Bourget-Merle, L.; Lappert, M. F.; Severn, J. R. *Chem. Rev.* **2002**, *102,* 3031. Gibson, V. C.; Spitzmesser, S. K. *Chem. Rev.* **2003**, *103*, 283; Dechy-Cabaret, O.; Martin-Vaca, B.; Bourissou, D. *Chem. Rev.* **2004**, *104*, 6147.

[6] (a) Bazinet, P.; Yap, G. P. A.; DiLabio, G. A.; Richeson, D. S. *Inorg. Chem.* **2005**, *44*, 4616. (b) Bazinet, P.; Yap, G. P. A.; Richeson, D. S. *J. Am. Chem. Soc.* **2003**, *125*, 13314. (c) Bazinet, P.; Yap, G. P. A.; Richeson, D. S. *Organometallics* **2001**, *20*, 4129. (d) Bazinet, P. Yap, G. P. A.; Richeson, D. S. *J. Am. Chem. Soc.* **2001**, *123*, 11162.

[7] For selected applications of R_2DAN^{2-} see: (a) Danièle, S.; Drost, C.; Gehrhus, B.; Hawkins, S. M.; Hitchcock, P. B.; Lappert, M. F.; Merle, P.G.; Bott, S. G. *J. Chem. Soc., Dalton Trans.* **2001**, 3179. (b) Lee, C. H.; La, Y.-H.; Park, J. W. *Organometallics* **2000**, *19*, 344. (c) Nomura, K.; Naga, N.; Takaoki, K. *Macromolecules* **1998**, *31*, 8009. (d) Galka, C. H.; Trösch, D. J. M.; Rüdenauer, I.; Gade, L. H.; Scowen, I. J.; McPartlin, M. *Inorg. Chem.* **2000**, *39*, 4615. (e) Hellmann, K. W.; Galka, C. H.; Rüdenauer, I.; Gade, L. H.; Scowen, I. J.; McPartlin, M. *Angew. Chem. Int. Ed. Engl.* **1998**, *37*, 1948.

[8] An example of a W(VI) β-diketiminate complex can be found in Tonzetich, Z. J.; Jiang, A. J.; Schrock, R. R.; Müller, P. *Organometallics* **2006,** *25,* 4725.

[9] Aoyagi, K.; Gantzel, P. K.; Kalai, K.; Tilley, T. D. *Organometallics* **1996**, *15*, 923.

[10] (a) Pindado, G. J.; Thornton-Pett, M.; Bochmann, M. *J. Chem. Soc., Dalton Trans.* **1998**, *393.* (b) Aoyagi, K.; Gantzel, P. K.; Tilley, T. D. *Polyhedron* **1996**, *15*, 4299.

[11] For selected recent examples see: (a) Hayton, T. W.; Boncella, J. M.; Scott, B. L.; Abboud, K. A.; Mills, R. C. *Inorg. Chem.* **2005**, *44*, 9506. (b) Cameron, T. M.; Gamble, A. S.; Abboud, K. A.; Boncella, J. M. *Chem. Commun.* **2002**, 1148. (c) Mills, R. C.; Abboud, K. A.; Boncella, J. M. *Chem. Commun.* **2001**, 1506. (d) Mills, R. C.; Wang, S. Y. S.; Abboud, K. A.; Boncella, J. M. *Inorg. Chem.* **2001**, *40*, 5077. (e) Cameron, T. M.; Abboud,

K. A.; Boncella, J. M. *Chem. Commun.* **2001**, 1224. (f) Cameron, T. M.; Ortiz, C. G.; Ghiviriga, I.; Abboud, K. A.; Boncella, J. M. *Organometallics* **2001**, *20*, 2032. (g) Cameron, T. M.; Ghiviriga, I.; Abboud, K. A.; Boncella, J. M. *Organometallics* **2001**, *20*, 4378. (h) VanderLende, D. D.; Abboud, K. A.; Boncella, J. M. *Organometallics* **1994**, *13*, 3378. .

[12] Bazinet, P.; Ong, T.-G.; O'Brien, J. S.; Lavoie, N.; Bell, E.; Yap, G. P. A.; Korobkov, I.; Richeson, D. S. *Organometallics* **2007**, *26*, 2885.

[13] Ward, B. D.; Orde, G.; Clot, E.; Cowley, A. R.; Gade, L. H.; Mountford, P. *Organometallics* **2005**, *24*, 2368. Ward, B. D.; Orde, G.; Clot, E.; Cowley, A. R.; Gade, L. H.; Mountford, P. *Organometallics* **2004**, *23*, 4444.

[14] (a) Nugent, W. A.; Mayer, J. M. *Metal-Ligand Multiple Bonds*; Wiley: New York, 1988. (b) Wigley, D. E. *Prog. Inorg. Chem.* **1994**, *42*, 239.

[15] Ortiz, C. G.; Abboud, K. A.; Boncella, J. M. *Organometallics* **1999**, *18*, 4253.

[16] Mills, R. C.; James M. Boncella, J. M.; Abboud, K. A. *Acta Cryst.* **2001**, *E57*, m218.

[17] Gaussian 03, Revision D.01, M. J. Frisch, *et al*, Gaussian, Inc., Wallingford CT, 2004.

[18] (a) Gorelsky, S. I.; Ghosh, S.; Solomon, E. I. *J. Am. Chem. Soc.***2006**, *128*, 278. (b) Gorelsky, S. I. AOMix software for molecular orbital analysis, www.sg-chem.net.

[19] Galindo A.; del Rıo D.; Mealli C.; Ienco A.; Bo C. *J Organomet. Chem.* **2004**, *689*, 2847. Galindo, A.; Ienco, A.; Mealli, C. *Comments Inorg. Chem.* **2002**, *23*, 401. Galindo, A.; Ienco, A.; Mealli, C. *New J. Chem.* **2000**, *24*, 73.

[21] Lam, H. W.; Wilkinson, G.; Hussain-Bates, B.; Hursthouse, M. B. *J. Chem. Soc., Dalton Trans.* **1993**, 781.

[22] For an example of cycloaddition of isocyanates with tungsten imides see: Legzdins, P.; Phillips, E. C.; Rettig, S. J.; Trotter, J.; Veltheer, J. E.; Yee, V. C. *Organometallics* **1992**, *11*, 3104.

[23] Rische, D.; Baunemann, A.; Winter, M.; Fischer, R. A. *Inorg. Chem.* **2006**, *45*, 269.

[24] Bolton, P. D.; Mountford, P., *Adv.Synth.Catal.* **2005**, 347, 355.

[25] Ison, E. A.; Abboud, K. A.; Ghiviriga, I.; Boncella, J. M. *Organometallics* **2004**, *23*, 929.

[26] Cortright, S. B.; Coalter III, J. N.; Pink, M.; Johnston, J. F. *Organometallics* **2004**, *23*, 5885.

Chapter 7

Conclusions

The main focus of the work described in this thesis was to explore the application of N, N'-disubstituted diaminonaphthalene as a supporting framework for diverse element centers. In particular, this thesis describes the use of this frame to prepare and explore the reactivity of carbene centers and of high oxidation state early transition metal and lanthanide complexes. The role of N-substituents and their potential to tune reactivity was also examined. The results presented throughout this work have demonstrated the versatility and flexibility of the R_2DAN scaffold.

Stable, free carbenes were obtained using the DAN framework. The identity of the nitrogen substituents controlled whether free carbenes or eneteramines were obtained. Furthermore, the dimerization of some of these perimidine-based carbenes with gentle heating was demonstrated. The architecture of perimidine-derived carbenes was significantly expanded upon by bridging two perimidinium precursor units followed by the deprotonation of these salts to give a bis(carbene) with a metaxylyl bridging unit. The bis(carbene) chemistry was further elaborated by bridging a perimidium salts and an imidozolium salt to target a linked mixed carbene. When an orthoxylyl bridging unit was used, an unusual enentetramine was obtained. This species apparently arose from the carbene coupling reaction of the perimidine- and imidazole-based carbene centers.

The synthesis of lanthanide complexes bearing R_2DAN ligands was achieved by reaction of dilithiated R_2DAN ligands with lanthanide halides to produce a colorful series of complexes. The characterization of these species relied heavily on X-ray crystallography which revealed that many of these complexes were "ate" species with lithium counter cations or had not completely eliminated LiCl. Interestingly, the R_2DAN ligands in these complexes commonly display a folded coordination motif that demonstrated the flexibility in the coordination of the R_2DAN ligands

Stabilization of high oxidation state group IV metal centers was achieved using the R_2DAN ligand. One of the results of these efforts was a demonstration of the importance of the nitrogen substituents on the structure of the complex. With larger nitrogen substituents the isolated complexes tend to be mononuclear while when smaller substituents are employed dinuclear species were obtained. The ability of the R_2DAN

ligand to undergo flexibility in coordination behaviour was again highlighted from these investigations.

N, N'-disubtituted1,8-diaminonaphthalene was also employed in the preparation of a series of Ta(V) complexes. These results demonstrated the importance the nitrogen substituents as well as the key role played by the other ligands bonded to the Ta center. The use of aromatic substituents on R_2DAN prohibited a previously observed CH activation/metallaaziridine formation. The variable coordination geometry/behavior of the R_2DAN ligand in some of these complexes was analyzed computationally. These results further highlighted the flexibility in coordination for this ligand and the ability of R_2DAN to accommodate the demands of the metal/ligand fragment to which it is coordinated. The influence of other ligands bonded to Ta on the CH activation/metallaziridine reactivity of R_2DAN was also explored by changing the identity of the tantalum bonded ligands from chloro to methyl and N-diethylamide.

The R_2DAN ligands were successfully used to support bis(imido) tungsten (VI) complexes. Again, structural and spectroscopic studies revealed the folding of the coordinated ligand along the N,N vector. The folding of the ligand was studied computationally and these results demonstrated that this folding increased ligand-to-metal π-electron donation. Reactivity of the tungsten complexes with isocyanate, carbodiimide and trimethyl aluminum revealed that the reactive site can be the ligand N_{amido}-W. The complexes have also been shown to be active catalyst for trimerization of isocyanante.

Overall, this work demonstrated the rich coordination behavior and reactivity for the R_2DAN ligand framework. These results have substantially added to the chemistry of

this ligand as both a supporting species and as a site for reaction. In addition, these results have prompted broader considerations on factors that influence ligand metal bonding, catalytic reactivity and stabilization.